Mechanisms of Elasticity in Elastic Proteins

Submitted by Ellen Marie Green, to the University of Exeter as a thesis for the degree of Doctor of Philosophy in Physics, June 2012.

I certify that all material in this thesis which is not my own work has been identified and that no material has previously been submitted and approved for the award of a degree by this or any other University.

..... Ellen Green

Abstract

This thesis investigates the mechanical properties of the elastic proteins isolated by cyanogen bromide digestion from lamprey cartilages and compares them with the mammalian protein, elastin. Thermomechanical testing and measurements of the effects of hydrophobic solvents on mechanics are used to determine the energetic and entropic contributions to the mechanical properties and the role of solvent interactions. Raman microspectrometry is shown to be a valuable tool in determining the secondary structure of the proteins, their interactions with water and molecular-level effects of mechanical strain. The supramolecular structure of the proteins matrices are investigated using nonlinear microscopy and X-ray diffraction.

The mechanical properties of fibrous elastin agreed with those previously reported with elastic moduli in the region of 0.2-0.4 MPa. Elastic moduli decrease by approximately 25% with increased temperature, which was accompanied by a small decrease in hysteresis loss. In agreement with earlier findings, an entropic mechanism of elasticity became dominant only at high temperatures with a major contribution from interactions with solvent water. The lamprey proteins can be divided into two broad groups, the 'soft' branchial and pericardial cartilages resembling elastin, with linear stress-strain behaviour over a range of strains, elastic moduli in the range 0.13 MPa to 0.35 MPa, breaking strains of up to 50% and low hysteresis. Annular and piston proteins showed a very different response having much higher elastic moduli (0.27 MPa to 0.75 MPa), higher breaking strains and large hysteresis. Similarities between elastin and the lamprey matrix proteins extended to their thermomechanical behaviour with a decrease in elastic moduli and a drive towards entropic elasticity at high temperatures, although the annulus and piston were less thermally stable.

Raman spectroscopy was able to detect differences between the various proteins

and between elastin fibres and fragmentation products. Although no vibrational modes associated with cross-linking of the fibres could be identified, the secondary structure of dehydrated fibrous elastin was significantly different from α-elastin. The former differed from previous experimental measurements, but was close to the theoretical predictions with 36% β-structures, 46% unordered and 18% α-helix. α-Elastin contained 29% β-structures, 53% unordered and 18% α-helix. Strains of up to 60% in ligament fibre bundles resulted in no significant shifts in peak positions or in secondary structure. Polarization measurements revealed that the peptide bonds and several of the bulky side-chains re-orientated closer to the fibre axis with strain. Heating nuchal elastin fibres to 60°C to increase the energetic component of the elasticity was associated with a 30% increase in the proportion of β-structures in the amide I band, a 50% increase in the amide III band, and a 50% reduction in the signal from bound water.

The Raman spectra of the lamprey matrix proteins are similar both to each other and when compared to fibrous elastin. Only small differences could be detected in side-chain modes consistent with reported biochemical differences. Decomposition of the amide I band indicated that the secondary structures were also very similar to that of elastin, with a preponderance of unordered structures which probably confer the high degree of conformational flexibility necessary for entropy elasticity. Piston and annular proteins, like elastin, showed a strong interaction with water, suggesting a greater role of hydrophobic interactions in their mechanics compared to the branchial and pericardial proteins.

Elastin is well known to exhibit autofluorescence. However, only the branchial protein has been reported to autofluoresce. This study shows that all four lamprey matrix proteins investigated exhibit strong autofluorescence which was subsequently exploited to image these tissues using multiphoton microscopy.

Microscopic investigations revealed that the architecture of lamprey proteins differ from that of elastin. Nuchal elastin forms bundles of fibres running predominantly parallel to the direction of applied force. The arrangement in lamprey cartilage is very different forming honeycomb structures, which in the case of annular and piston cartilages, is surrounded by a dense sheath of matrix material. Dye injections

revealed that the branchial and pericardial form open systems whereas in piston and annular cartilages a closed system exists. These variations in architecture are reflected in their different mechanical properties and in vivo functions.

Acknowledgements

Throughout the course of my PhD I have received the very kind help of many people, who have contributed to this thesis in different ways. There are too many to mention individually, but it gives me great pleasure to be able to give special thanks a number of people in particular.

I must first extend my sincerest thanks to Prof. Peter Winlove, for giving me the opportunity to work in the Biophysics Laboratory, both as a research technician and as a PhD student. I would like to thank him for introducing me to the wonders of elastin and for sharing his enthusiasm on this and many other subjects, which has provided me with constant motivation. I am indebted to Peter above all for his excellent guidance, support, endless patience and friendship over the years, without which completion of this thesis would not have been possible.

I am also thankful to other members of the Biophysics Group, both past and present, including Dr. James Bell for constructing the MATLAB routine used for polarization analysis and for his encouragement in writing this thesis. I would also like to thank Dave Colridge for his help with all things IT related and Dr. Jessica Mansfield for her assistance with the multiphoton microscope. I am also grateful to Dr Clare Thorn for her valued friendship over the years and for listening patiently to my frustrations and concerns.

Special thanks to Dick Ellis for his friendship, encouragement and support as well as his endless knowledge and skills which have been invaluable in the design and construction of equipment essential for this project.

I am very grateful to Matt, Kevin and Nick, the highly skilled engineers of the mechanical workshop for the excellent work they always produce that make research projects like this possible.

I would also like to thank Dr Michail Isupov of the Biocatalysis Centre for his assistance with X-ray diffraction measurements.

On a personal note, I would like to express my sincere thanks to my husband, George and my children, Tom and Emily, for their understanding and patience during the course of my PhD and especially during the past months whilst I have been writing my thesis, often at the expense of my family's needs.

Last but by no means least, I would like to thank my parents for their boundless love, support and encouragement in all I have strived to do. I thank them for their never failing belief in me and for raising me with the attitude of never giving up when things become difficult. Sadly they are no longer here to share my joy at completing this thesis but I hope I have still made them both proud.

Contents

List of Figures

List of Tables

Chapter 1

Introduction and Background

1.1 Introduction

Long-range elasticity is an essential requirement for many biological tissues and is normally associated with entropy changes arising from the ability to adopt a wide range of energetically similar conformational states that is common amongst random, cross-linked polymers [24, 25, 26]. Long-range elasticity is therefore an unusual property in proteins whose functions generally arise from the existence of well defined secondary structures and highly ordered supramolecular assemblies [27]. Despite this, a small family of extracellular matrix proteins has evolved amongst mammalian and non-mammalian species alike, that have the ability to deform reversibly over large strains [25, 28]. These so called elastic proteins are unique both in their physical properties and structurally. These unusual properties are believed to be essential to the mechanical properties of the elastic proteins and also involved in other processes including self-assembly and matrix organization. Despite this some aspects of the relationship between molecular structure and the physical properties of these proteins are still not completely understood [29]. This research project concerns the structural bases of the mechanical properties of elastic proteins. We first focus on some of the unresolved issues concerning the molecular basis of elastin's elasticity and then apply the same protocols to the family of lamprey matrix proteins. In the introductory chapter we discuss the necessary background to understand the remainder of the thesis. Firstly we describe the extracellular matrix and some of its major constituents, which is followed by a short section outlining the roles of elastic

proteins. A comprehensive description of elastin, its structure, formation and properties, both physical and mechanical is then given. The effects of ageing and disease on the elastic fibre is then discussed which leads onto a section dedicated to lamprey and the structure of their cartilagenous endoskeleton. Comparisons are made to mammalian elastin with regard to their ultrastructure, amino acid composition, cross-linking and physical properties. We finish the introductory chapter by giving a brief account of elastin-based biomaterials.

1.2 General Introduction to the Extracellular Matrix

All organisms rely on connective tissue in one form or another to provide structural support, both at the cellular level and the whole tissue level. Connective tissue is the structural component of tissues consisting of a limited number of cells embedded in, or glued together, by an extensive, non-living extracellular matrix (ECM) and is responsible for providing integrity to tissues. The composition of connective tissue, including cell type and matrix material, is far from uniform, being highly dependent on location in addition to functional requirements. Connective tissues is one of four major tissue types found in mammals, the others being epithelium, muscle and nervous tissue, with the primary functions of organization, maintenance of shape and providing additional strength [30]. Connective tissue can be further divided according to the organization and concentrations of their extracellular matrix components [31] these being: i) loose connective tissue which serves to hold epithelium and organs in place, ii) dense connective tissue, as found in bone, ligaments and tendon, iii) reticular connective tissue having a supporting roles for many organs including the lymphatic system and bone marrow and, iv) special connective tissue. This research project is primarily concerned with a form of special connective tissue known as elastic connective tissue. Elastic connective tissue is found wherever elasticity is an essential requirement, has a mechanical role in tissues like the major blood vessels and ligaments and, as its name suggests, has a large elastic fibre content.

Extracellular matrix is considered to be all the material located outside cells. It is a complex, composite material which surrounds and supports cells found within the connective tissue and to this end, is vital to survival of most organs. The composition

of the ECM is highly tissue-dependent but in general the ECM is composed of a combination of water, ions, proteins and macromolecules. The cells are responsible for production, organization and maintenance of the ECM components. The various components of the ECM are depicted schematically in figure 1.1. The ECM is a three-dimensional, tissue specific, structure displaying enormous variation in both architecture and physical properties, being highly adapted to specific functional requirements [32], although many aspects regarding the synthesis and turnover of many of the individual components are still poorly understood. This diversity in form can be seen in bone and teeth, for example, where strength and rigidity is required and the ECM becomes heavily calcified, whereas in the basement membrane its structure is that of a flexible membrane. In tissues exposed to high tensile forces, such as ligament, rope-like structures dominate. Although the major role of the ECM is mechanical, providing a combination of support and flexibility, this is not its only function. The ECM, being a system of predominantly insoluble proteins interacting dynamically with cells and other matrix components, has the capacity to act as an anchorage site and to co-ordinate cellular activities [33], or to buffer against changes in the extracellular microenvironment and to aid in the retention of water.

Diversity in function is reflected by a highly complex architecture which is essentially an interacting assembly of insoluble fibrous proteins, collagen and elastin, providing strength and resilience respectively, surrounded by a viscous gel rich in large macromolecules, including proteoglycans, glycosaminoglycans and glycoproteins that fill the extrafibrillar spaces. The matrix fibres may be bound to cell surface receptors mediated by the adhesive extracellular matrix proteins fibronectin and laminin. The relative amounts and organization of these components is directed by tissue type whilst function is dependent on close interactions between all components [34].

Collagen and elastin are the two principle structural proteins found in the ECM and despite differences in their structure, chemistry and function these two proteins share several characteristics. Both are large, cross-linked, self-assembling proteins consisting of multiple domains, but each has a different function. Elastin, a major

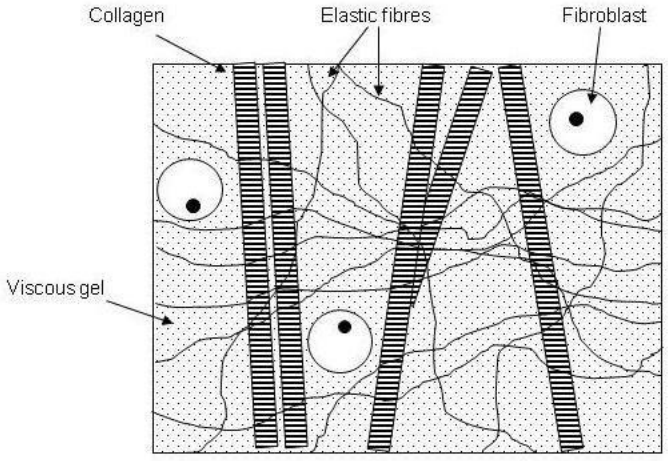

Figure 1.1: Schematic diagram to represent the major components of the extracellular matrix including the structural proteins, elastin and collagen, cells and the surrounding viscous gel composed of water, ions and proteoglycans.

contributor to the work of this thesis, will be discussed in detail in section 1.5 whilst collagen and other matrix molecules are briefly described first for completeness.

1.2.1 Collagen

The collagens are the most abundant of all mammalian proteins forming a major component of tissues such as bone, tendon, skin, cornea and cartilage [35]. This protein is frequently found in conjunction with elastin in composite materials to form an intricate network where collagen, being largely inextensible, provides tensile strength while elastin provides flexibility and distributes loads evenly throughout the tissue. This arrangement is encountered in tissues such as skin, blood vessels and cartilage. In other tissues, such as tendon, collagen occurs in almost pure form where strength is paramount.

The collagens constitute a family of more than twenty one different types, each of which differs in both structure, amino acid composition and function. The collagens can be separated into several families, the most common ones being; the fibril-forming collagens and network-forming collagens, which in turn assemble into higher order structures such as fibres and membranes respectively. The most frequently occurring collagens found in connective tissue are types I, II, III and V, all being fibrous in form. These collagens have a hierarchical organization taking the form of long, relatively rigid structures achieved by the twisting together of three

collagen subunits, or $\alpha-$chains, to produce a characteristic right-handed triple helix structure, typically 300 nm in length, 1.5 nm in diameter and stabilized by inter-chain non-covalent bonds. Several collagen molecules then interact extracellularly and become arranged in a highly regular manner to form micro-fibrils with an average diameter of approximately 4 nm which, in turn, are then twisted together to form collagen fibres with a diameter of 20-500 nm [36]. This arrangement is only made possible by careful alignment followed by stabilization of collagen molecules through non-covalent bonds. The collagen fibre formed as a result is further stabilized by covalent cross-links in order to provide strength and stability. Cross-link formation is beyond the scope of this thesis. However, additional information can be found in a number of excellent reviews and references therein [37, 38, 39].

Formation of the tightly coiled helix, or super-coil, is reliant on the presence of numerous glycine and proline residues. Glycine makes up approximately one third of all the amino acid residues comprising the collagen molecule. They are spaced regularly along the length of each α-chain (every third residue). Being the smallest amino acid, glycine permits tight packing of the three peptide chains to form a superhelix which confers rigidity to the molecule. Stability of the triple helix is provided primarily by the presence of hydrogen bonds between the α-chains as well as by electrostatic interactions between neighbouring residues. All collagens have high glycine, proline and hydroxyproline content and they are all largely insoluble due to the high degree of cross-linking at the hydroxylysine residues. The interaction between collagen and other matrix macromolecules is strong and, by binding to neighbouring cell surface receptors, cellular activities and regulation can be influenced. In this way collagen can exhibit a profound impact on processes such as cell proliferation, differentiation and migration.

In addition to the fibrous proteins, collagen and elastin, the other major components of the ECM are glycosaminoglycans and proteoglycans which are the macromolecules that form the highly viscous gel-like ground substance in which the fibrous proteins are embedded. This viscous gel has important roles both in providing support and resistance to applied forces as well as permitting the rapid movement of small molecules between the blood and tissues.

1.2.2 Proteoglycans and Glycosminoglycans

Proteoglycans and their constituent glycosaminoglycans are high molecular weight macromolecules that form fundamental components of the extracellular matrix. They have a number of important functions including regulation of water movement through the extracellular matrix, control of cellular activities, proliferation and migration and interaction with other matrix components, often influencing tissue mechanics.

Proteoglycans (PG) are complex macromolecules constituting a special class of glycoproteins which tend to be of greatly extended form and occupy a large volume compared to their molecular weight and entrap large quantities of water. This property is very important in tissues where PG's exert a cushioning role under compression, as seen in cartilage. These macromolecules are all heavily glycosylated, the basic unit consisting of a 'core protein' with one or more glycosaminoglycans (GAGs) covalently attached [40].The proteoglycan monomer itself is unbranched, but molecules such as aggrecan are attached onto hyaluronan filaments forming a complex macromolecule with a molecular weight of approximately 3.5 x 10^6Da [40]. Not only does the number of attached GAG chains vary, but also the length of these chains, as does the arrangement of the sulphate and carboxyl groups. These factors are important because they provide this group of macromolecules with enormous variations in structure responsible for their corresponding diversity of functions [41].

Glycosaminoglycans are a small family of polymers formed by the linking of numerous, long, un-branched disaccharide repeat units containing sulphate and carboxylate groups. Furthermore, due to the presence of carboxyl and/or ester groups on the disaccharide units, GAG's are highly negatively charged [42] and are also extremely hydrophilic providing them with the ability to form hydrated gels even at very low concentrations and occupy a large percentage of the total volume. Together, these factors lead to formation of a swelling pressure which, in many tissues, aids in resisting compressive forces. GAGs are primarily situated either of the surface of cells or PG's where they exert their many physiological functions, often by interacting with matrix proteins. Within the ECM the principle GAGs are chondroitin sulphate and dermatan sulphate.

1.2.3 Cellular component of the extracellular matrix

Within the non-living matrix are a small number of cells which differentiate into specialized cell types each with a different function. The differentiation process itself is dependent upon extracellular matrix components as is cell movement, re-arrangement, remodelling and repair. Fibroblasts are the most abundant cell type found in elastic connective tissue and are, in general, responsible for the local production and maintenance of the major extracellular matrix components including elastin and collagen fibres, as well as the proteoglycans and the glycosaminoglycans. Fibroblasts are also involved in the wound healing processes. In cartilage and bone fibroblasts are modified resulting in the formation of chondroblasts and osteoblasts respectively, but again they have a major role in ECM matrix production.

The main focus of this particular research has been on the elastic proteins that constitute a major part of the ECM in elastic tissues and are discussed in the following section.

1.3 Elastic Proteins

1.3.1 Long-range Elasticity

The term 'elastic' can have several alternative meanings the first of which relates to Hooke's Law. This states that deformability of an object is directly proportional to the magnitude of the force applied, and, provided that the elastic limit for the material is not exceeded, then the object will return to its original size once the applied force is removed [32]. Recovery of the object to its original state is a passive process which utilizes the elastic-strain energy or entropy stored in the system following deformation. Alternatively, 'elastic' can refer to the property of 'stretchiness' which refers to the fact that many rubber-like materials can be stretched to high deformations with very little applied force [25]. Materials that display long-range elasticity can be described as 'pliant' with low elastic moduli and the ability to be greatly deformed without rupture. These flexible materials, found to occur naturally, tend to be versatile but possess very complex structures which are often poorly understood in relation to function.

For any tissue to exhibit long-range elasticity, several essential requirements must

be met by the elastic protein. Firstly they must be able to undergo large deformations repeatedly without breakage which relies on the polymer chains being long. This accommodates a large number of possible spatial arrangements which can be rapidly re-arranged in response to any applied stress. Secondly, individual monomers from which the polymeric chains are composed must be both highly flexible and mobile thus permitting un-hindered re-arrangements of the chain. The tissue must be able to recovery completely to its original state following removal of the applied force with minimal energy loss. This is achieved by cross-linking to form a permanent network that is capable of distributing the stress throughout the system and reducing the likelihood of over-stretching [32, 25, 24, 28, 43]. The ability of tissues to undergo long-range elasticity is largely provided by a small family of elastic proteins which are discussed next in the section that follows.

1.3.2 The Family of Elastic Proteins

Elastic proteins are a diverse family of extracellular matrix proteins that are widely distributed amongst both mammalian and non-mammalian animal species [24, 28, 43, 26].

One of the most extensively studied elastic proteins is the mammalian protein known as elastin. This protein provides passive elastic stretch within tissues such as the skin and also acts dynamically allowing elastic expansion and recoil in the major arteries which serves to accommodate high pressure pulses, store energy and smooth blood flow [25]. Long-range elasticity also occurs in the form of return springs. This can be seen in molluscs, for example, where opening of the bivalve mollusc shell is controlled by the protein abductin acting antagonistically to the abductor muscle [44, 45]. Resilin is an extremely elastic and resilient protein found in insects where it attaches the wings to the thorax and forms the jumping mechanisms of fleas acting as an energy store. Perhaps a more unusual function of elastic proteins can be seen in byssal threads which serve to attach bivalve mussels to rocks in wave swept shores [25, 28, 46]. These, like most elastic proteins, function as elastomers when hydrated in water or other aqueous media, whereas spiders produce a whole range of elastic proteins (silks) that have evolved to function in air. Each of the silks

has different mechanical properties according to their particular functional requirements [47, 48, 49]. Whilst these are just a few of the many functional roles that elastic proteins serve, it seems reasonable to assume that the remarkable diversity in functions observed in this family of proteins will be accompanied by just as broad a spectrum of elastic properties, molecular structures, chemical compositions and physical properties in order to achieve the numerous combinations of extensibility (strain at rupture), resilience (energy recovered on elastic recoil) and strength (stress at rupture) required [25].

As stated previously, all elastic proteins share the property of elasticity which, regardless of its exact definition, is an extremely unusual property of any protein whose functions usually arise as a result of rigid secondary structures and supramolecular organization. Elastic protein research has revealed that these proteins all have unusual structures and it is these characteristics that are believed to be responsible for their varied mechanical properties.

It is somewhat surprising that research conducted so far has revealed very little evidence to suggest that elastic proteins share any homology in amino acid sequence which can be accountable for their shared property of elastic recoil. However, most of these elastomers do in fact adopt similar flexible secondary structures e.g. β-turns, as a result of the presence of blocks of repeating amino acid sequences within the polymer chain [28]. It can be concluded from this that there is no one universal design responsible for elasticity and that the various elastic proteins have evolved over millions of years to meet these requirements in very different ways. Although technological advances have led to greater understanding in some areas of protein elasticity, it has also led to even more questions being raised that have yet to be answered [43].

1.4 Mechanical Properties of Elastic Proteins

There are essentially two main categories of structural proteins: i) Those that display rubber-like elasticity e.g. elastin and ii) those that show little rubber-like elasticity but have high tensile strength e.g. collagen.

As near perfect elastomers, elastic proteins such as elastin, show the same characteristics as rubber, with the main function of efficient energy storage. Rubber-like proteins have a combination of high resilience, low stiffness (modulus of elasticity) and high extensibility, whereas collagen and other non-rubber-like proteins have a very different combination of material properties. Byssal threads, which serve to attach bivalve mussels to rocky substrates in wave-swept environments, have material properties somewhere between those described above. This material is complex in form possessing different properties at opposite ends of the fibre, one end being stretchy and the other being stiff. Overall, these threads are considered to be tough, being highly extensible, having high strength and low resilience [46, 50, 51, 52]. Likewise spider silks display a remarkable range of mechanical properties, ranging from rubber-like to almost inextensible, depending on their functional requirements [48, 49, 53]. Perhaps the most extensively studied are the 'stretchy' viscid silks which form the catching spiral of the orb web and the tougher dragline silks that form the safety line and the frame of the orb web. Table 1.1 lists some of the material properties relating to the elastic proteins discussed above, with rubber and steel as a comparison.

Material	Elastic Modulus (MPa)	Tensile strength (MPa)	Extensibility	Resilience (%)
Elastin[a]	1.1	2	1.5	90
Collagen[b]	1.5×10^3	50-100	0.13	90
Abductin[c]	4.7	-	-	82-97
Mussel byssus, distal[d]	8.7×10^2	75	1.09	28[f]
Mussel byssus, proximal[d]	16	35	2.0	53[f]
Spider dragline silk[e]	1×10^4	1.1×10^3	0.3	35
Spider viscid silk[e]	3	500	2.7	35
Resilin[e]	2	3	1.9	92
High tensile steel[c]	2×10^5	1.5×10^3	0.008	-
Synthetic rubber[e]	1	50	5-10	-

[a] Aaron and Gosline (1981)
[b] Fung (1993)
[c] Alexander (1966)
[d] Bell and Gosline (1996)
[e] Gosline et al (2002)
[f] Waite et al (2001)

Table 1.1: Comparative material properties for elastin (bovine ligament), other representative biological materials, rubber and steel. References used for data are [a]Aaron and Gosline [54], [b]Fung [55], [c]Bell and Gosline [50], [d]Gosline et al [25] and [e]Waite et al [46].

The particular mechanical properties of any elastic protein will depend largely on the amount of cross-linking and the length of the flexible regions of the polymer

chain [38]. Given that some elastic proteins, for example spider silks, function only in air whilst others require hydration, it would not be unexpected that their individual mechanisms of elasticity also differ. What is clear is that each of the elastic proteins found in nature has a near perfect design, evolved and 'fine tuned' over millions of years [32].

1.5 Elastin

Elastic fibres are complex structures forming an integral component of the extracellular matrix which, despite being extensively studied for several decades, are still incompletely understood. The purpose of the the following sections is to give a detailed account of the composition, synthesis, ultrastructure and biochemistry of these fibres in relation to current understanding, followed by a description of the major models of elastin elasticity. The final section describes the possible roles of elastic fibres in disease.

1.5.1 Evolutionary Aspects

In all vertebrates, with the exception of the Agnatha (or jawless fish) such as lamprey and hagfish, elasticity is provided by the rubber-like protein, elastin, which is one of the most unusual proteins known to exist, both regarding its physical properties and its unique chemical composition [56]. Life itself in these vertebrates relies on elastin which has an essential role to play in the elastic properties of tissues including the blood vessels, ligaments, skin and lungs. There still remains considerable debate over the evolutionary origin of elastin, although there is some evidence to suggest that the matrix proteins found in the primitive vertebrates may provide an evolutionary link, having diverged from the vertebrate line 500 million years ago. Elastin may have evolved as a necessity with the emergence of high pressure circulatory systems, but tropoelastin, and in particular the cross-linking domains, have remained exceptionally well conserved over the past 5.8 million years despite an increase in hydrophobicity. An overall increase in hydrophobicity would suggest some kind of adaptive advantage. Chalmers et al [57] hypothesised that increased

hydrophobicity is associated with i) enhanced mechanical performance, ii) yielding thermally independent behaviour or, iii) promoting self-aggregation of tropoelastin [57]. However, after performing mechanical and thermal swelling tests on elastins of different hydrophobicities, it was concluded that none of the hypotheses could be either accepted or rejected.

Similarities do exist between lamprey matrix proteins and that of elastin both in biochemical composition [5, 11] and in the presence of hydrophobic repeat sequences [58, 59]. A major aim of this present study has been to establish whether similarities exist in their mechanical properties and supramolecular composition.

1.5.2 Elastin's Biological Role

Elastin is normally found in association with other complex structures known as microfibrils, which together form elastic fibres. It is these structures that have the ability to undergo long-range, reversible deformations under normal physiological load, thus providing the elastic properties and high resilience seen in numerous tissues [25, 56, 60, 61]. There is no doubt that the major role of elastin is to provide elasticity. However, this is by no means its only function, with some evidence to suggest that elastin is also involved in cell signalling which promotes activities including cell proliferation, differentiation and migration [62, 63]. The work contained in this thesis will however concentrate on aspects relating to elastin's elasticity.

1.5.3 The Ultrastructure of Elastin

Initial identification of elastin proved extremely difficult for many years sinsce elastin reacts with histological stains also associated with collagen [29]. Since this time stains regarded as being selective for elastin, or elastin-like materials, have become widespread, making identification easier in composite materials. The most popular stains include Verhoeff's, Weigert's-resorcin-fuchsin and orcein [64, 65].

The ultrastructure of elastic fibres has conventionally been investigated using classical techniques such as electron microscopy and X-ray diffraction. The following account gives an overview of the fine structure of elastic fibers based on the literature, although more detailed information can be found in a comprehensive review by Pepe

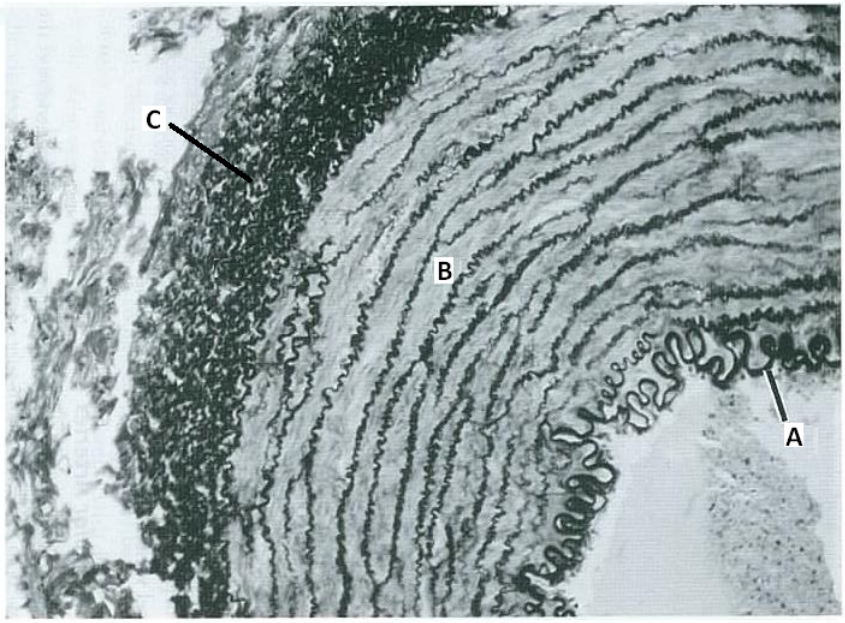

Figure 1.2: Histological section (mag x 130) through the wall of a canine major artery stained with Verhoeff stain (black) for the selective determination of elastin fibres. (A) is the elastic membrane composed of predominently elastin fibres; (B) is the tunicia media consisting of alternating layers of smooth muscle cells and elastic lamellae or fibres; and (C) the tunicia externa which is dominated by elastin. This image is reproduced from Eurell and Frappier [66].

et al [67]. The results from early microscopic studies led investigators to believe that elastic fibres have an amorphous elastin core, lacking structure, surrounded by fibrillin-rich micrifibrills [8, 68, 69]. However, this view is not unanimous, with other researchers reporting elastin as having a fibrillar structure. These studies have demonstrated individual water-swollen elastin fibres to have a diameter ranging from 5-8 μm [70] aligned parallel to the long axis of the fibre, which themselves can be composed of even finer fibrils, typically 1-3μm in diameter [70, 71]. These ultra fine fibres have frequently been seen to aggregate to form thicker structures [72, 73, 67] which in some tissues can twist together into rope-like structures [74, 75]. Electron microscopy also revealed that elastin fibres, isolated from bovine nuchal ligament, had a characteristic beads-on-a-string [76, 77] appearance and showed higher level ordering typically being arranged into bundles lying parallel to the axis of the ligament [70]. Other techniques such as negative staining electron microscopy of sonicated elastin fibres [77], freeze fracture electron microscopy and scanning force microscopy [78] have also revealed a fibrous structure. Fibrillar organization is not exclusive to elastic fibres as similar structures have also been observed in α-elastin and synthetic elastin-like peptides [79, 80, 81], coacervates [82] and tropoelastin [83].

Although evidence from electron microscopy indicates some order in elastin, caution is required in the interpretation of micrographs because features observed may be artefacts induced through harsh sample preparations and extensive drying. The need for caution was confirmed by a study conducted by Quinerelli and coworkers who, in an attempt to resolve issues regarding the amorphous or ordered nature of elastin, compared electron micrographs of elastin fragments prepared by placing them onto carbon coated grids and by the traditional method of embedding in epoxy resin [84]. The results revealed a fibrous structure for the elastin suspensions prepared on carbon grids and an amorphous appearance for those prepared by epoxy embedding. This would suggest that the method of preparation does have a significant effect on ultrastructure.

At the molecular level, early X-ray diffraction studies by Gotte et al revealed the presence of limited order in elastin [85] which was confirmed a few years latter by Seraffini-Fracassini [86] and similarly by Ali et al [87]. Observations from this later study showed two broad diffraction rings consistent with spacings of 0.45 and 0.93 nm, which disappeared at strains in excess of 60% extension of the original length. Despite these results being inconsistent with earlier findings of Serafini-Fracassini [86, 77], they do compare favourably with the early works of Cox and Little [68] who identified bands at 0.45 and 0.78 nm. This study again observed no change in d-spacing at high strains (100-150%) but at low strains an additional sharp ring was detected corresponding to a spacing of 4.5 nm.

NMR has only had limited success in probing the structure of elastin, as this technique is not well suited to the large size of tropoelastin or the flexible nature of its backbone structure. Studies on hydrated elastic fibres have revealed the dominance of kinetically free peptide chains [88] whilst Flemming et al [89] showed that cross-linking of elastin imposed a large constraint on chain movement.

1.5.4 The Elastic Fibre

It is beyond the scope of this thesis to go into extensive detail regarding processes involved in elastic fibre formation, but further information is available in a number of comprehensive reviews [56, 60, 90, 91, 92] and references therein. Unlike collagen,

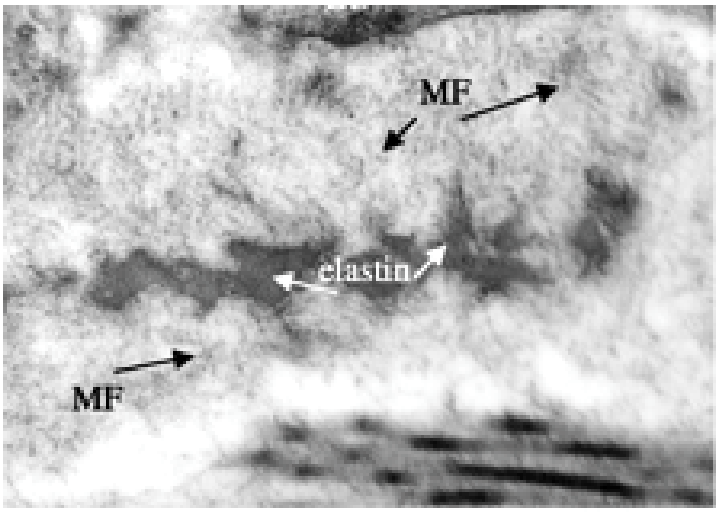

Figure 1.3: Transmission electron micrograph showing developing elastic fibres cultured from bovine nuchal ligament fibroblasts. Amorphous elastin forms a central mass that becomes surrounded and interspersed with fibrillin-rich microfibrils (MF) [4]

there is no information currently available on the precise organization of the elastin fibre at the molecular or fibrillar level and as a result this remains as an outstanding problem. This section discusses the structure of the elastic fibre, the individual components and their arrangement.

Ultrastructural studies have begun to reveal the structural complexity of mature elastic fibres, but large gaps still remain in our current understanding regarding their hierarchical assembly. The transmission electron micrograph in Figure 1.3 shows elastic fibres cultured from bovine nuchal fibroblasts [4]. Mature fibres are composite structures composed of two morphologically and chemically distinct components; fibrillin-rich microfibrils and a central elastin core [8, 69, 93]. Elastin is the dominant component comprising approximately 90% by mass [62, 94, 95] and are surrounded by and interspersed with microfibrils. The composition of elastic fibres shows little variation, but the organization of these fibres differs according to the tissue in which they are found and their functional requirements. For example, in the aorta, elastic fibres are arranged into sheet-like structures (2.5 μm thick) forming concentric rings of elastic lamellae that surround the blood-filled lumen, allowing them to withstand multi-directional forces. In the lungs, elastin forms a delicate network of elastic fibres providing vital support for alveolar junctions and openings of alveoli [96], whilst in ligaments and tendons elastin forms bundles of long fibres parallel to the direction of force, as described by Pasquali-Ronchetti et al [78] using freeze-fracture

techniques. The wavy, fibrillar structure observed by light microscopy as shown in Figure 1.2 demonstrates limited organization, but at the ultrastructural level this is less apparent. Elastin and fibrillin-rich microfibrils will be discussed in greater detail in the sections that follow, whilst comprehensive reviews of the elastic fibre can be found in recent publications by Wagenseil [97] and Kielty et al [93].

1.5.4.1 Microfibrils

Microfibrils are supramolecular structures that are widely distributed in elastic and non-elastic tissue alike. These complex structures are frequently found in blood vessels, skin, lung as well as in non-elastic tissue of the kidney and ciliary zonules of the eye. Like many other of the ECM proteins, microfibrils are large multi-domain structures that are able to interact with other matrix molecules. Advances in molecular biology and associated techniques over recent years have led to a rapid increase in knowledge regarding their structure and composition which have been found to vary with age, location and disease.

Within developing elastic fibres, fibrillin-rich microfibrils are thought to appear before the amorphous elastin component [93]. In the mature elastic fibre microfibrils form approximately 10% of the total mass, although their number decreases with age. Their number and arrangement is also tissue specific and is ultimately directed by cellular as well as local environmental factors such as direction of force. Some researchers suggest that microfibrils play an important role in the formation of elastin fibres by acting as a scaffold for elastin deposition, assisting in its organization and in the assembly of tropoelastin molecules [60, 93, 95, 98], although this opinion is not accepted by all. Nonetheless, there is some evidence to suggest that microfibrils aid in the facilitation of crosslink formation by interacting with the enzyme lysyl oxidase [97]. The presence of microfibrils embedded within the amorphous elastin is suggested to aid nucleation of elastin but considerably less is understood regarding the function of the many microfibrils that form a sheath on the outer surface of elastic fibres. Although microfibrils have a critical role in the formation of the elastic fibre this is not their sole function. Proteoglycans interact with microfibrils, and in turn influence levels of hydration, cell signaling, molecular sieving and transport within

the ECM [93, 99]. The fibrillins are also known to be involved in the activation of certain growth factors [100] and thereby have a responsibility for regulatory roles in both development and signaling. Deficiencies in microfibril formation and mutations have been associated with several genetically acquired diseases resulting in impaired microfibril function and loss of tissue integrity. This topic is discussed in greater detail in section 1.5.8.

It has proved difficult to isolate the microfibrillar component of elastic fibres without the use of denaturing solvents or by using sodium hydroxide. Some success has been achieved by the use of gentle, but more lengthy, sequential procedures using a combination of guanidine and collagenase. Characteristically, the end product of these procedures is a protein fraction with a significantly different amino acid composition and staining properties to elastin. Characteristic features include relatively high numbers of polar residues including cystine, histidine, serine, threonine and methionine residues which are either completely absent from elastin or found in minimal amounts [99]. Cysteine residues account for 70-80 per 1000 residues and it is this high cysteine content that is responsible for the large number of disulphide (cysteine) links detected in microfibrils [99], thus accounting for their resistance to solubilization [101]. Other differences in amino acid composition are the lower levels of residues including glycine, valine and alanine whilst hydroxyproline is completely absent.

Much research has been undertaken in an attempt to probe the structure of fibrillin-rich microfibrils using techniques such as X-ray diffraction, electron microscopy and more recently Raman spectroscopy. A general conclusion is that the microfibrils are in themselves complex. They have a diameter of 10-14 nm, are unbranched and are frequently arranged into small bundles that run parallel to the elastic fibre [98, 102, 103, 104] with a characteristic appearance reminiscent of 'beads-on-a-string' and an average axial periodicity of 56 nm [105]. Their size, complexity and insolubility have, like elastin, made microfibrils difficult to characterize. Although microfibrils are composed of several different glycoproteins, the dominant components take the form of long, flexible, fibrillins -1 and -2 [98, 106, 107] which Kielty and co-workers described as multidomain glycoproteins [98, 4]. Cleary and

colleagues also made significant progress in discovering the existence of other macromolecules known as microfibril-associated glycoproteins 1 & 2 (MAGP) in bovine ligament [108]. MAGP located on the surface of microfibrils has been shown to bind to tropoelastin and may be involved in cross-linking and fibre formation [109].

Microfibrils themselves have been shown to possess elastic properties which, in organisms that possess low pressure circulatory systems, are believed to confer resilience [110]. Whether the same is true of organisms that express elastin is less certain. Some research has indicated that microfibrils have an elastic modulus of 0.2-1.1 MPa [111, 112] which is the same order of magnitude as that of elastin. This would suggest that they do not have a significant reinforcing role [113], but instead that their intrinsic elasticity allows them to extend alongside elastin of the elastic fibres. Spina and co-workers [114] have a different opinion based on similar tests on an elastin-glycoprotein composite (from porcine thoratic aorta) from which the authors concluded that the composite material is stiffer than pure elastin alone. Whether this can be explained as the sum of the contributions of the two components, or whether their interaction is sufficiently intimate as to alter molecular mechanisms of elasticity has yet to be established. This view is shared by others in this field. For example, mechanical tests on isolated zonular filaments have revealed an elastic modulus two orders of magnitude greater than first observed at 78-96 MPa [106], implying that microfibrils are significantly stiffer than elastin and in some tissues may participate in reinforcing roles. This is an area of continued debate which will require additional experiments in an attempt to resolve the conflicting opinions on how microfibrils contribute to the mechanical properties of elastic fibres.

Wright and co-workers [115] performed mechanical tests on zonular filaments from which it was discovered that microfibrils have a characteristic J-shaped stress-strain curve, with elastic moduli of 0.1-0.14 MPa, as well as a sizeable time-dependent stress-relaxation response. At low strains individual fibres or small bundles of microfibrils undergo minimal re-arrangement as shown by the non-linear portion of the stress-strain curve. However, as strain is increased, so the microfibrils become taut and/or more closely packed and stress increases in a more or less linear manner. These changes in packing of microfibrils under increased strain are confirmed by

X-ray diffraction [106].

1.5.4.2 Elastin Component of Elastic fibres

Elastin, the main component of elastic fibres, is an extremely durable protein with a very low turnover [92, 94]. This protein displays truely remarkable elastic properties, as seen by the impressive performance of aortic elastin which, in the average human life time (70-80 years), has to withstand in excess of 2.2 x 10^9 stress-relaxation cycles without permanent damage or failure [116]. It is the highly hydrophobic and cross-linked nature of elastin are regarded to be responsible for its durability. There is great variation in the distribution of elastin depending on both tissue type and function. For example, elastin constitutes 30-57% dry weight of major blood vessels, 50% of ligaments, 3-7% of lung, 4% of tendon and only 2-5% of skin [91, 101]. Elastin's ability to repeatedly deform in a dynamic manner is ultimately due to conformational changes that occur at the molecular level. On the other hand, in tissues such as skin, (where the primary function is to avoid over-extension), the architecture of the elastic fibre network is very different and consequently elastin has a much more passive role, requiring a significantly lower content.

1.5.4.3 Tropoelastin

Mature elastin is the most insoluble vertebrate protein known and this leads to difficulty in its characterization. However, this situation improved when it was realized that synthesis of mature elastin relies on the assembly and cross-linking of soluble precursor molecules known as tropoelastin. During the 1960's a breakthrough in elastin research occurred with the realization that crosslink formation could be prevented by feeding animals with a copper-deficient diet leading to the discovery of tropoelastin and its successful isolation in 1969 [117]. Tropoelastin, the only naturally occurring soluble form of elastin, is synthesized by several cell types including fibroblasts, chondrocytes and smooth muscle cells. Other soluble forms of elastin include α-elastin, β-elastin and κ-elastin, all of which are the end products of elastin fragmentation (α-elastin will be discussed further in section 1.5.5.1). Despite this

breakthrough, tropoelastin still remained difficult to isolate in significant quantities even from elastin-rich tissues such as ligamentum and thoracic aortae, which has led to the widespread use of elastin peptides, elastin fragments and structural predictions in expanding our knowledge regarding this complex protein [14, 118, 119].

The tropoelastin gene has been highly conserved during evolution having undergone very few changes over the past 5.8 million years. The primary transcript for tropoelastin is a 40 kb sequence that possesses large introns and small exons at a ratio of 20:1 [60, 120, 121]. This gives rise to a 60-70 kDa protein in humans that is coded for by a single gene containing 34 exons located on chromosome 7 [122, 123]. Alternative splicing of the primary tropoelastin transcript results from consistent splitting of the intron-exon boundary [124] which results in the production of several different isoforms, the role of which remains unclear [121]. The human tropoelastin gene has been fully characterized. It is one of the largest genes in the whole human genome [124]. The number of exons shows variation between species [125] and in the human gene, exons 34 and 35 were sequentially lost over the course of evolution. Exon 34 is associated with long hydrophobic domains whilst exon 35 is a site of potential cross-linking. The reason for loss of these two exons in primates is unclear. However, it has been suggested that this loss may be associated with changes in arterial wall function [126, 127]. Further insight may be gained by investigating elastin from other sources, such as inter-vertebral disc, to establish whether elastin from these sources have the same deletions. An important characteristic of tropoelastin is its amphiphilic nature with alternating hydrophobic and hydrophilic domains that are organized in a cassette-like manner [122, 124, 128]. These domains are thought to be functionally distinct, although there is some evidence to suggest that they are not entirely independent of each other, but instead interact so that changes in the hydrophilic cross-linking regions effect the hydrophobic domains also [128]. A schematic diagram to illustrate the structure of the tropoelastin molecule is given in figure 1.4.

Hydrophobic domains are rich in non-polar amino acids and are frequently described as being flexible, giving rise to elastin's elasticity. In contrast, the cross-linking domains are believed to be more rigid α-helical structures rich in polar

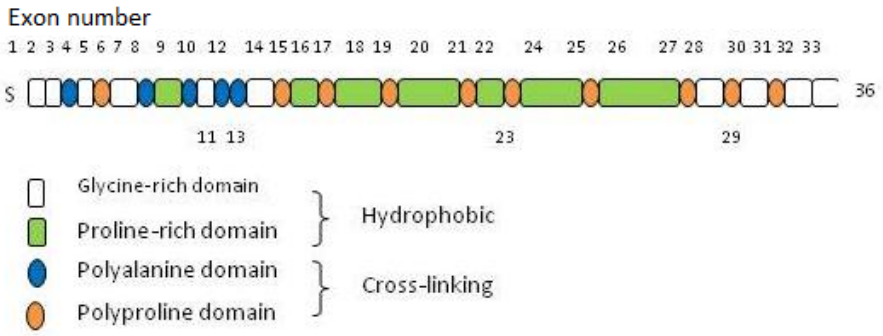

Figure 1.4: Cartoon to illustrate the cassette-like organization of the tropoelastin gene into alternating hydrophobic and hydrophilic cross-linking domains. The hydrophobic domains are believed to represent the flexible structures able to undergo large deformations while the hydrophilic domains are the sites for cross-linking of the tropoelastin monomers (based on [90]). The corresponding exon number is shown above each domain.

amino acids [120, 129]. There is some variation in amino acid sequence within the hydrophobic domains, but that of the cross-linking domains shows much less variation.

1.5.4.4 Amino Acid Composition

Given elastin's unique physical properties, it comes as no surprise that tropoelastin also has a unique amino acid composition. Because of its extreme insolubility much of the analysis has been based on soluble fragments and therefore interpretation should be treated with some degree of caution as elastin fragments are known to be very heterogeneous. More complete chemical characterization was only made possible following the isolation of tropoelastin and the development of procedures for highly purified elastin preparations usually involving the use of pancreatic elastase.

The pioneering work of Sandberg et al in the 1970's and 1980's confirmed that the amino acid composition of tropoelastin resembles that of insoluble elastin [117, 130, 131]. The major difference was found to be the absence of desmosine/isodesmosine cross-links and therefore a significantly greater contribution from lysine in tropoelastin. Another unusual feature of tropoelastin compared to most other proteins is that it is not glycosylated. Elastin has been identified in 28 different species from which characterization of the tropoelastin gene has revealed significant homology in amino acid sequence, details of which can be found in a recent review by Chung et al [125]. Table 1.2 compares the amino acid composition of mature ligamentum

Amino Acid Residue	Microfibrils (a)	Ligamentum Elastin (b)	Tropoelastin from aorta of copper-deficient pigs (c)
Hydroxyproline	-	8.1	9.3
Aspartic acid	114	5.8	3.5
Threonine	55.9	9.3	13.1
Serine	62.2	8.7	9.6
Glutamic acid	114	15.4	14.5
Proline	63.5	115.5	113.9
Glycine	110	328.1	306.2
Alanine	65.1	227.0	233.1
Cystine	48.2	-	-
Valine	56.3	131.6	129.2
Methionine	15.6	0.0	-
Isoleucine	47.7	23.9	17.3
Leucine	68.6	59.4	51.0
Tyrosine	36.0	5.9	16.8
Phenylalanine	37.7	30.1	30.4
Desmosine	-	29.3	-
Lysine	45.0	10.1	46.6
Histidine	15.4	3.3	-
Tryptophan	-	0.0	-
Arginine	45.2	5.8	4.8

(a) Ross. R. (1969) J. Cell. Biol, **40**
(b) Jacob. M.P. and Robert. L. (1989) Ealstin and Elastase. CRC Press.
(c) Sandberg L.B. and Wolt T.B. (1982) Methods in Enzymology, **82**

Table 1.2: Amino acid composition for mature ligamentum nuchal elastin, tropoelastin and microfibrils. The data are based on previously published work of Ross and Bornstein [8], Jacob and Robert [9] and Sandberg and Wolt [10]. The numbers given are residues per thousand.

elastin, tropoelastin and microfibrils.

Biochemical analysis has revealed that hydrophobic domains dominate the tropoelastin molecule, having a high proportion of glycine (33%), valine (10-14%) and proline (13%) residues which frequently form hydrophobic repeat sequences composed of 4-8 residue long peptides [124]. Typical sequences include PGVGVA, PGVGV, GGLGV and PGGV and, although similar repeat motifs occur in all elastins, the exact sequences may differ between species. Repeat sequences of varying length are frequently found in proteins where they have a tendency to form a particular conformation such as β-strand or α-helix [132]. However, the purpose of these repeat motifs in elastin is not certain, although their conservation over millions of years suggests that they have an important role, possibly providing a mechanism of elasticity or assisting self-assembly of the protein [133]. In contrast, the hydrophilic domains are dominated by alanine and lysine residues which participate in cross-linking. These, like the hydrophobic domains, contain repeat motifs which are typically in the form of AAAAYKAA, and tend to be very well conserved. As far back as the 1970's it had been recognized that tropoelastin contains 40 lysine residues of which

35 are involved in crosslink formation accounting for the exceptionally high degree of cross-linking in mature elastin [122].

In some respects elastin's amino acid composition shares features with that of collagen, having around one third of all its amino acids being glycine. However, in elastin these glycine residues are randomly distributed as opposed to being regularly spaced at every third position. An extensive study by Sage and Gray [134] analysed elastin taken from the major blood vessels of a wide range of vertebrates and demonstrated that some variation in amino acid composition exists between species, although they all possess several distinguishing characteristics. All the elastins have desmosine/isodesmosine cross-links, they have a high proportion of hydrophobic residues and few hydrophilic residues, they are both glycine-rich and proline-rich [94, 125], as well as having no methionine residues. Despite the inter-species variation, there is very little difference in amino acid composition of elastin from the various tissues taken from the same species [134]. The unique amino acid composition of elastin makes it one of nature's most hydrophobic proteins, which has important implications for secondary structure, its ability to coacervate and also its mechanical properties. Phylogenic studies suggest that the amino acid composition of the earliest elastins were very similar to that of present day mammals. This does not mean that elastin has not changed during the course of evolution. On the contrary, elastin appears to have become progressively more hydrophobic with time, possibly associated with a corresponding increase in mechanical loads. A good example of this is seen in the circulatory systems which have gradually changed from being open, low pressure systems (typically 30 mm Hg) to sophisticated high pressure circulations as seen in present day mammals and birds (120-150 mm Hg) [63].

1.5.4.5 Secondary Structure

The secondary structure of a protein refers to the local conformations formed as a result of folding of the peptide chain, which is ultimately dictated by the primary amino acid sequence. Amino acids with small side-chain groups generally allow greater rotation of the backbone and therefore permit greater flexibility. In turn,

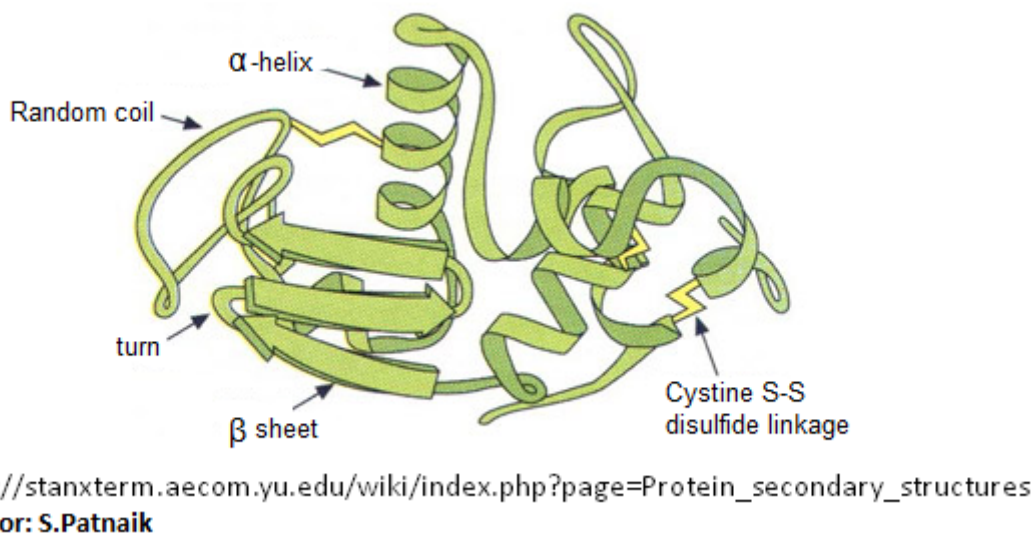

Figure 1.5: Schematic diagram representing the major secondary structures found in elastic proteins.

interactions between amino acid side groups and the backbone of a single peptide chain, or between more than one chain also influences the overall flexibility of the protein. This structure is not static; macromolecules constantly experience rearrangement as the local environment changes. There are a number of well defined secondary structures that can be formed in proteins, some of which are described below as they are an important element in the work reported in this thesis.

The α-helix is a compact, rod-like secondary structure frequently found in proteins. In elastin, α-helices are right-handed being stabilized by the formation of hydrogen bonds between the carboxyl oxygen of one amino acid residue and the hydrogen of the amino group of a residue four amino acids further down the chain [27]. Because of this, any interaction with other parts of the peptide backbone must occur through interactions of the side-chain groups. The distance between each of the turns is 3.6 residues. In elastin the α-helices have been established as being right handed and tend to be confined to the hydrophilic cross-linking domains forming regions that offer little flexibility [135].

β-structures display a greater variation in form than α-helical structures and can be present as strands, turns, spirals or sheets, all of which are considered to be more extended and flexible than the α-helix. Which particular form of β-structure, or combination of β-structures, dominates is highly dependent on the protein in question and evidence to date indicates that elastin is composed of mainly β-turns,

which may eventually form β-spirals. The β-turn is described as a short loop consisting of normally 4 amino acid residues that separate two β-strands (parallel or anti-parallel). During the course of evolution a proline residue has been conserved in the second position of the repeat sequence so as to allow the polypeptide backbone to change direction. Proline residues are described as helix-breakers and for this reason are not located in the amino acid sequences of the cross-linking domains of elastin where α-helices dominate. Glycine, which lacks a bulky side chain, is restricted to the fourth position where it is able to provide flexibility. In this way, β-turns allow the polypeptide chain to fold back on itself and tend to be located towards the surface where hydrogen bonding with solvent water can occur. Stabilization of these structures occurs via side-chain interactions between adjacent β-strands. In elastin the β-turns form a major contribution to the structure of the hydrophobic domains where they are likely to play an essential part in extension and flexibility. The β-spiral has been proposed to be important in elastin elasticity and is formed by the joining of several consecutive β-turns, which serve to act as spacers between each turn of the spiral. Regions of polypeptide chain between the turns have a high degree of conformational freedom [136]. The importance of β-spirals will be discussed in greater detail in section 1.5.7.4 where they are related to possible mechanisms of elasticity.

Polyproline II (PPII) is another frequently encountered structure common to many proteins particularly when present in aqueous solutions [135, 137]. It is essentially an extended left-handed helix and, as its name suggests, is rich in proline residues [137, 138]. Although proline is fundamental to PPII formation there still remains considerable confusion over the mechanisms involved. Urry and co-workers [136] proposed that hydrophobic repeat sequences, such as VPGVG, VPGG and APGVGV, are central to the formation of β-spirals (see section 1.5.7.4) whereas Tamburro's group [137] suggest that these hydrophobic domains are involved in formation of PPII. PPII has been detected in elastin, although in the past this structure has frequently been mistaken for unordered regions [139, 140]. The reason for this confusion arises because PPII does not take the form of either classical β-structures or that of α-helix. Circular dichroism has been a particularly sensitive technique

for investigating PPII in proteins and recent studies have shown that it does indeed take the form of a distinct, highly flexible structure that may have important roles in providing flexibility, cell motility and signal transduction processes [140]. Several researchers have indicated that PPII may also play an important role in elastin elasticity [141, 142]. The dynamic nature of PPII is most likely due to the fact that this structure lacks intramolecular hydrogen bonding. However, there is some evidence that this conformation interacts with water molecules which serve to stabilize the structure [139]. The absence of hydrogen bonds is also why PPII structures are not detected in conventional techniques such as NMR.

Based on the primary amino acid sequences, predictions can be made regarding the secondary structure composition of any protein. For elastin, Debelle and coworkers predicted for human tropoelastin 10% α-helix, 35% β-structures and 55% unordered structures [14]. The same group measured 10% α-helix, 45% β-structures and 45% undefined for bovine elastin fibres [15]. Similarly, it was predicted that the alanine-rich cross-linking domains take the form of α-helices which is supported by the presence of two lysine residues separated by two or three alanine residues.

A number of experimental techniques have been employed over the past 40 years or more in an attempt to explore the secondary structure characteristics of insoluble elastin, tropoelastin, elastin fragments and synthetic elastin-like polypeptide sequences. Techniques such as circular dichroism (CD) [143], infrared spectroscopy (IR) and Raman spectroscopy have all been employed with some success, although there still remain gaps in current understanding [17]. From these investigations it was concluded that elastin is predominantly disordered, although there do exist short regions of local order. This has also been confirmed for elastic fibres by Raman spectroscopy [21, 144]. Vrhovski et al [143], using CD, estimated 3% α-helix, 62% β-structures and 33% other structures. However, this is not consistent with similar studies applied to the hydrophobic exons 3, 7 and 30 of human tropoelastin, which predicted a substantial contribution from PPII structures [140]. These finding are not conclusive and further information relating to the secondary structure composition of elastin is given in section 2.2.2.3 where the amide I and amide III bands are discussed in some detail.

Tropoelastin is composed of a large number of both proline and glycine residues located within the hydrophobic domains. Glycine residues lack side chains and consequently promote a high degree of conformational freedom, thus contributing to disorder. Proline on the other hand, has a methylene group attached which results in disruption of the hydrogen bonding network, therefore preventing helix formation and reducing conformational freedom. It is this glycine-rich and proline-rich combination of elastin that has been proposed as one possibility for sustaining structural disorder in elastin [133, 145].

Some additional studies on elastin fragments have demonstrated that the contribution made by α-helices can be influenced by changes in the local environment, for example, by raising the temperature [15, 143, 146] or by exchanging water for trifluoroethanol (TFE) [135, 147, 148]. Many of these studies have focused on tropoelastin or other soluble elastin fragments. However, a similar effect may be expected for insoluble elastin fibres although the interpretation would be much more complex.

Despite the large number of investigations that have been conducted, few firm conclusions have been reached and substantial speculation regarding the molecular structure of elastin still exists. Elastin's unique amino acid composition, its amphiphilic nature and the frequent occurrence of hydrophobic repeat sequences have all prompted a general trend towards the reductionist approach in recent years. This has included the use of synthetic elastin-like peptide sequences and studies on individual domains [119, 149, 150, 151, 152]. There is general agreement from these studies that there does exist a high degree of conformational freedom for elastin in aqueous solutions, but caution is required when relating these observations to the native protein. This will be pursued in connection with new results from the current research.

1.5.4.6 Cross-linking

For elastin to behave as an elastomer the long polymer chains must be flexible and conformationally free, except at the regions where the chains are stabilized by cross-links [153].

Partridge and co-workers performed pioneering investigations on the cross-linking

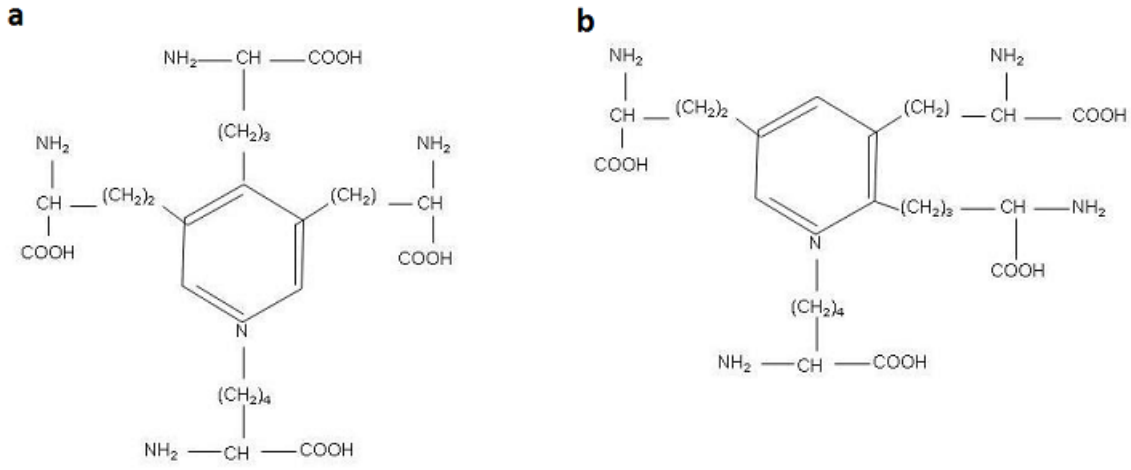

Figure 1.6: Schematic representation of a) desmosine and b) isodesmosine which form the major form of cross-links in elastin. Tropoelastin molecules aggregate via coacervation are cross-linked through the action of lysyl oxidase in the extracellular space. Oxidation of lysine residues results in the formation of allysine which then under goes spontaneous condensation with another allysine or lysly residue to form desmosine / isodesmosine cross-links.

of tropoelastin in the 1960's [154] which led to the discovery that, in addition to the presence of disulphide bridges, tropoelastin monomers are also joined by covalent lysyl-derived desmosine and isodesmosine cross-links, unique to elastin. Because of their occurrence in elastin alone, the number of desmosine/isodesmosine residues can provide an indication of the amount of the protein present in a tissue. For elastin it has been estimated that per 1000 residues there are 1.5 desmosines and 1.0 isodesmosines [155]. Figure 1.6 shows the structure of desmosine and isodesmosine cross-links. Since the initial discovery of desmosine/isodesmosine, several additional amino acids known to have potential cross-linking capabilities have been identified. However, all the cross-linking structures detected have so far been confirmed to be lysine derivatives.

It is well known that copper is required as a co-factor for the catalytic action of lysyl oxidase and animals fed with a copper-deficient diet produce elastin fibre defects [117]. Lysyl oxidase is also involved in collagen cross-linking in a broadly similar manner. The initial step involves the oxidation of three out of every four lysine residues to form aldehydes (allysine) [37] catalyzed by lysyl oxidase (LOX) [156], after which all subsequent reactions are believed to occur spontaneously [63]. Deamination is subsequently followed by the condensation with other lysines, either modified or unmodified, resulting in the formation of desmosine or isodesmosine,

although it is possible for other types of cross-links to be formed if the lysine-derived aldehydes react with a lysine to form a Schiff base. This does not occur with great frequency and desmosine/isodesmosine cross-links are dominant. Most evidence indicates that two polypeptide chains are connected at each cross-link site with two residues from each of the chains being involved [157]. However, there remains a certain degree of uncertainty regarding the number of chains involved as discussed by Brown-Augsburger et al [158], who suggested the possibility of cross-linking of three as opposed to two polypeptide chains. It is beyond the scope of this thesis to describe in great detail the reactions involved in cross-link formation, but additional information can be found in [37, 38, 39, 157, 159]. The minor differences in elastin cross-link formation are, i) there is no hydroxylysine involved, ii) histidine is only a minor component and therefore unlikely to be involved and iii) the final products are desmosines and isodesmosine, which are not present in collagen [37]. A self-assembly process, known as coacervation, is also important in crosslink formation and will be discussed further in section 1.5.4.7.

Cross-links are formed in the α-helical, alanine-rich domains of the tropoelastin molecule [122] and are normally derived from four lysine residues [131], which occur as pairs separated by two or three alanine residues. Of the 40 lysine residues present in tropoelastin, all but five take part in crosslink formation which results in the occurrence of lysine-derived cross-links every 65-70 amino acid residues [56]. It is also possible, in principle, for proline-rich domains of tropoelastin to be involved in cross-linking, but the end product is neither desmosine nor isodesmosine[37, 160, 161]. It was reported by Wise and co-workers [162] that crosslink formation shows some specificity, which highlights the importance of tropoelastin self-assembly and coacervation in aligning monomers for correct fibre formation.

1.5.4.7 Coacervation

Following excretion into the extracellular space, tropoelastin is rapidly aligned, aggregated and cross-linked [163]. The fact that tropoelastin is able to self-aggregate is remarkable and many of the precise mechanisms involved are still incompletely understood. There is, however, general agreement that a process referred to as

coacervation is essential in elastic fibre formation by concentrating tropoelastin molecules and ensuring they are correctly aligned in preparation for cross-link formation [82, 90, 143, 164].

Coacervation is an entropy-driven, endothermic process that has been likened to that of nucleation [129, 165] and is initiated in vitro by an inverse temperature transition. At room temperature tropoelastin is soluble, but on raising the temperature towards physiological values a phase separation of the solution occurs resulting in the formation of an opaque protein-rich phase (the coacervate) at the bottom and a clear solution at the top [163, 166] with no stage in between [167]. Over a short timescale this process is fully reversible on cooling the solution. However, if left in the phase separation stage for prolonged periods then fibre formation is permanent with further aggregation to form bundles of fibres [82, 168, 169]. Coacervation is sensitive to even minor changes in local environmental conditions including temperature, pH, ionic strength, protein concentration and the presence of glycosaminoglycans [137, 143, 166, 170, 171]. In addition, Tamburro's group has recently shown that low concentrations of trifluoroethanol (TFE) has the effect of substantially lowering the temperature required for coacervation to occur, despite the fact that TFE has little effect on conformation [172]. It comes as no surprise that the optimum conditions for coacervation coincide with normal physiological conditions of the extracellular matrix which translate to a temperature of 37°C, pH 7.0-8.0 and 150 mM NaCl [143].

The coacervate forms parallel filaments that, when viewed microscopically, these are similar to the small fibres of mature elastin and small bundles of fibrils [82]. Volpin and co-workers [173] made a similar observation using optical diffraction techniques confirming the presence of 5 nm fibrils. Tropoelastin is the only naturally occurring soluble form of elastin. However, coacervation has also been seen to occur using chemical fragmentation products including α- [92] and κ- elastin as well as synthetic elastin-like peptides [133, 174, 175] and individual hydrophobic domain sequences [150]. Coacervation of these elastin-like peptides again yielded fibrous structures resembling elastic fibres within the coacervate that could be detected by light and electron microscopy.

Hydrophobic repeat sequences have been proposed to play an important part, in particular GVGVP, GGVP and GVGVAP [91]. Studies on the self-assembly properties of peptide sequences based on elastin's domain structures have revealed that these somewhat simplified polypeptides can mimic elastin's ability to self-assemble through hydrophobic interactions [79, 133, 163, 168] and that the precise organization, location and number of these hydrophobic sequences also affect coacervation [151, 164]. At low temperatures ($< 20°C$) the tropoelastin molecules are shielded from the surrounding water molecules making them fully soluble, but as temperature is increased the solution becomes cloudy as elastin aggregates and the coacervate forms [163]. At this stage the tropoelastin molecules become increasingly ordered as hydrophobic interactions form due to the disruption of clathrate water (structured water) surrounding the non-polar domains as hydrogen bonds are broken [91, 164]. Coacervation is therefore an unusual event since elevated temperatures normally result in denaturation and loss of order in proteins. This results in a net increase in order within the protein, but the system as a whole experiences increased entropy (disorder) due to the release of water molecules [143, 165, 174]. In vivo, in addition to the hydrophobic domain's coacervation may also be regulated by microfibrils and cell-surface glycosaminoglycans including chondroitin sulphate and heparan sulphate [164].

An extensive study conducted by Chalmers et al [57] showed that the hydrophobicity of elastin increased during the course of evolution. Given the importance of hydrophobic interactions in the process of coacervation it would seem reasonable to suggest that the temperature at which coacervation occurs should also decrease over the same time scale, but as yet this has not been confirmed.

1.5.4.8 Elastogenesis

As previously stated in section 1.5.4, elastic fibres are complex assemblies made up of two structurally distinct components, a central core of amorphous elastin and surrounding fibrillin-rich microfibrils. The formation of competent elastic fibres, referred to as elastogenesis, is a very complex process involving the careful co-ordination of numerous events including alignment and coacervation of tropoe-

lastin monomers, deposition onto microfibrils and cross-linking, each of which are intricate mechanisms in themselves [164]. Despite extensive research in this field the precise stages of fibre formation and the role of each of the principle components still remain to be clarified [176, 177], although recent live imaging studies have expanded current understanding [97].The schematic diagram shown in Figure 1.7 illustrates two of the most popular representations of fibre formation.

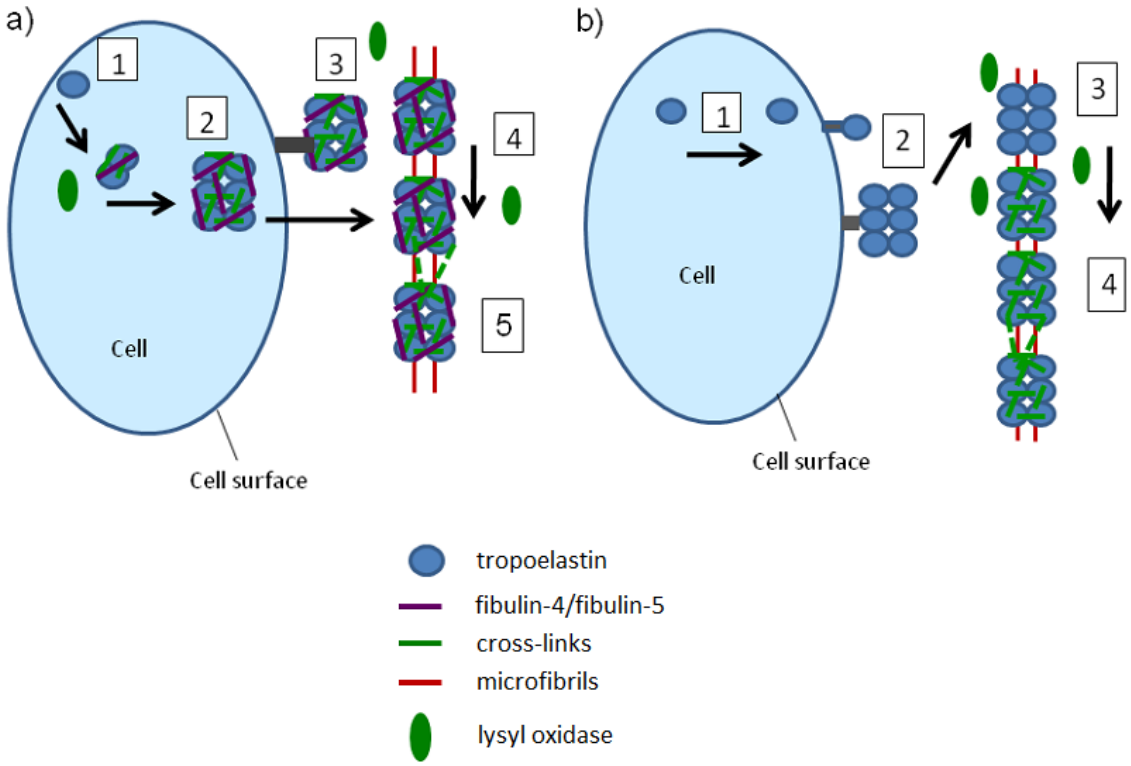

Figure 1.7: Schematic diagram to illustrate two most common models representing elastic fibre formation. Model a) 1. Tropoelastin is synthesized and begins to assemble forming small aggregates within the cell. There is some evidence to suggest that assembly may be assisted by fibulin-4 / -5. Lysyl oxidase promotes cross-linking between the tropoelastin monomers 2. Aggregates attach to the cell surface where they remain until more tropoelastin accumulates. 3. Elastin aggregates are transported to nearby microfibrils onto which they begin to align and coalesce. 4. More tropoelastin molecules aggregate and self-assemble onto microfibrils. 5. Additional cross-links formed between tropoelastin molecules result in the formation of an insoluble elastic fibre. This schematic diagram is adapted from Wagenseil and Mecham [97]. Model b). (classical opinion) 1. Newly synthesized tropoelastin is transported to the extracellular space. 2. Tropoelastin attaches to the cell surface and forms small aggregates via coacervation. 3. Elastin interacts with microfibils which act as a scaffold and aids alignment of tropoelastin. 4. Lysyl oxidase facilitates crosslink formation to form elastic fibres [8, 93].

There are currently several alternative explanations for the role of tropoelastin in elastic fibre formation as supported by various research groups. One opinion still widely accepted [93] is that tropoelastin synthesized by the cell interacts with mi-

crofibrils in the extracellular space which then act as a scaffold for elastin deposition and further assist in fibre formation by aligning the elastin prior to cross-linking. Additional elastin deposition ultimately results in the majority of the microfibrils being displaced to the periphery of the developing fibre. The need for microfibrils to act as a scaffold is supported by the fact that microfibrils are always present in elastic tissues during early stages of fibre formation [69].

Other researchers support an alternative view that microfibrils are not initially required for aggregation of tropoelastin, but instead tropoelastin monomers self-assemble and become properly aligned on the cell surface, facilitated by the action of fibulin-4 or fibulin-5. They are cross-linked by the action of lysyl oxidase and remain attached to the cell surface whilst more newly synthesized tropoelastin adheres to form larger aggregates. These aggregates are then transported to the microfibrils onto which they continue to assemble and eventually form an insoluble elastic fibre. Dynamic imaging studies by Kozel et al [178] lend some support for this model. The composition of the elastic fibre is far from static. Newly formed fibres tend to be rich in microfibrils, but the ratio of microfibrils to amorphous elastin declines as the fibre matures [179, 180]. This observation supports the opinion that microfibrils become freed from elastin following fibre formation and, therefore, that the latter do not contribute significantly to mechanical properties.

Despite doubts concerning the exact underlying mechanisms behind elastic fibre formation, it is known that the majority of formation occurs, in humans at least, during late fetal and early neonatal stages, after which elastin synthesis is dramatically reduced and ceases by puberty. After this point further synthesis does not normally occur except if damage to fibres should occur [60], which in later life can result in a number of pathological conditions.

1.5.5 Soluble Elastins

There are several soluble forms of elastin, being tropoelastin, α-elastin and κ-elastin. Tropelastin is the only naturally occurring soluble form of elastin and was described in detail in section 1.5.4.3. The main problem associated with the use of tropoelastin for research purposes is that it is extremely difficult to isolate in significant quantity.

Because of this α-elastin and κ-elastin have frequently been used.

1.5.5.1 α-elastin

α-elastin is the partial hydrolysis product of purified elastin and was first produced in 1955 by Partridge et al [166]. It comprises a heterogenous mixture of elastin fragments with molecular weights in the region of 68-75 kDa and has been shown to have an amino acid composition very similar to that of insoluble elastin, being dominated by glycine, proline, valine and alanine residues [72].The major difference between α-elastin and tropoelastin is that the former has cross-link residues present whereas the latter does not. Despite its high hydrophobicity, α-elastin is readily soluble in cold water. This is thought to be due to intramolecular interactions occurring between the non-polar regions of the polypeptide chain which have the effect of minimizing exposure of the hydrophobic domains. Preparation of α-elastin involves repeated boiling in 0.25M oxalic acid [166] which is described in greater detail in section 2.1.1.4. This form of soluble elastin has been used extensively in structural studies and optical spectroscopies and X-ray diffraction show that α-elastin displays limited order in its substructure [147, 181] like mature insoluble elastin. It has also been found that in polar solvents α-elastin is largely unordered in secondary structure. However, in less polar solvents such as TFE, regular α-helices are formed [147, 182, 183, 184].

κ-elastin is another soluble form of elastin and, like α-elastin, is again a fragmentation product of purified elastin fibres. This preparation relies on treatment with potassium hydroxide as opposed to oxalic acid but was not used in this study.

1.5.6 Physical and Mechanical Properties of Elastin

Physical characteristics of purified elastin include its pale yellow colour and a strong blue-white autofluorescence when viewed under ultraviolet (UV) light [92]. For elastin to exhibit rubber-like behaviour it must be fully hydrated in water, or other polar solvents otherwise elastin becomes brittle and hard [185, 186]. The reason for this is that, unlike rubber, which is composed of long hydrocarbon chains, elastin

is not self-lubricating and therefore is dependent on water to exert a plasticizing effect by disrupting the inter chain hydrogen bonds and increase conformational entropy [187]. The consequence of this is that elastin's mechanical properties are very sensitive to hydration levels with the elastic modulus increasing dramatically to a point where the glass transition phase (T_g) is rapidly reached in the dehydrated state. The glass transition temperature refers to the temperature at which flexibility of the polymer chain is so reduced that the material is said to become glassy [32]. Above T_g a polymer is said to act as an elastomer whereas below this point it would characteristically be brittle. Samouillan showed that the T_g of elastin in the dehydrated state is in the region of 200°C which falls in the fully hydrated state to around 30°C [188]. All the evidence indicates that water is essential for elastin's elasticity [187], but there still remains debate as to where in the peptide chain water interacts and how it interacts [120]. Some evidence suggests that water does not exert its effect on elastin directly, but interacts indirectly through the hydration shell [189]. Debelle and Alix [120] added to this by describing the elastin-water system as being 'tri-phasic' involving; elastin polypeptide chains, tightly bound hydration water and free or bulk water which causes swelling of the protein.

Temperature is known to have a significant effect on the water content of elastin which at 2°C is 0.76g water/g protein and decreases to 0.46g water/g protein at 37°C. This decrease of almost 50% in water contribution at higher temperatures is associated with a decrease in swollen volume [190, 191]. In arterial elastin water content has also been shown to be dependent on glycoprotein content.

In the native tissue, mechanical properties are closely linked to those of all the interacting components, such as collagen, and therefore changes associated with disease or ageing are very difficult to interpret since each of the individual components responds differently to applied stresses.

The mechanical properties of elastic fibres have been a subject of extensive investigation for several decades. The elastic modulus is determined from the slope of the stress-strain curve and is used as a measure of a materials stiffness. Lillie and Gosline [192] found that the stress-strain curve for elastin is best described as linear up to strains of around 70% with an elastic modulus of purified porcine aorta in

the range 0.13 to 0.65 MPa, whilst that of single elastic fibres isolated from bovine ligamentum nuchae has been estimated at 0.40 to 1.20 MPa [193] or 0.30-0.60 MPa [194]. At the molecular level, a recent study using AFM has shown that individual tropoelastin molecules are both highly extensible, with an elastic modulus of 3KPa, and show no measurable hysteresis [195]. The authors suggest that tropoelastin is responsible for elastin's extraordinary elasticity by acting as a near perfect spring. Elastic fibres are quite remarkable in their unique ability to undergo millions of reversible stress-strain cycles during their lifetime without failure and can withstand extensions of between 100 and 220% of their original length [55] with minimal force [193].

Further information can be gained from the hysteresis loop area of the loading/unloading curves which provides a measure of the material's energy storage efficiency. The energy used in extension is the area under the loading curve and the energy recovered on recoil is the area under the unloading curve. The area between these two curves, the hysteresis, represents the energy lost and is important for elastomers where energy storage is frequently fundamental to their efficient function. As a general rule, the larger the hysteresis the less energy is returned to the system on relaxation, therefore indicating less efficient energy storage. Elastic fibres typically have very small hysteresis losses making them very well suited to their dynamic role in blood vessels where efficient energy storage is crucial [196].

The mechanical properties of elastin as discussed above relate to the purified protein. However, in vivo mechanical properties are closely linked to all of the interacting components. In blood vessels, for example, collagen fibres interact with elastic fibres, resulting in non-linear (J-shaped) stress-strain behaviour. Initially, when collagen fibres are unstretched and elastin alone is extended, stiffness is low. At higher strains collagen fibres begin to bear some of the load causing them to straighten, becoming aligned with the direction of force, thus causing the material to become stiffer. Therefore, whilst elastic fibres permit extension of the tissue with minimal force, the interacting network of collagen fibres provides some rigidity and prevents over-extension.

Similarly, in native tissue, water content is effected by the presence of glycopro-

teins. This has been shown experimentally where elastin treated with collagenase, to remove glycoproteins, results in a decrease in water contribution, although the precise reason for this is still uncertain [114]. It is possible that glycoproteins serve to constrain the elastin network in some way or alternatively glycoproteins may alter the hydrophobic or electrostatic interactions with elastin. The tensile tests of Spina et al [114] also show a slower viscoelastic response and a 50% reduction in the circumferential elastic modulus of glycoprotein-depleted arterial elastin. For normal functioning of some tissues it is important that the relaxation phase is controlled and it may be that glycoproteins assist with this. The close association of elastin with interacting extracellular matrix components and their effect on mechanical properties make changes associated with disease or ageing very difficult to interpret since each of the components respond differently to applied stresses.

A major characteristic of elastin is its ability to undergo large reversible deformations with minimal force. The associated properties of low stiffness and high resilience are typically likened to that of rubber and several attempts have been made to explain elastin's elasticity based on the same principles. The following section discusses some of the most important features regarding elastin's molecular structure that may account for these fundamental mechanical properties. Understanding how natural elastomers are designed and behave could provide us with additional information for use in the development of novel biomaterials that could be used in a number of applications.

1.5.7 Models of Elastin Elasticity

The diversity of elastic properties displayed by elastic proteins can be related to difference in their molecular mechanisms of elasticity. The two fundamental elements that determine the driving force of elastic recoil in any elastic protein are i) the energy component and ii) the entropy component [32, 43] which are illustrated in Figure 1.8. The basic elastic mechanism exhibited by stiff materials is frequently referred to as energy elasticity. This arises from changes in internal energy when an applied force distorts the material resulting in displacement of atoms. The driving force for recovery in these materials is determined by the need to return to a state

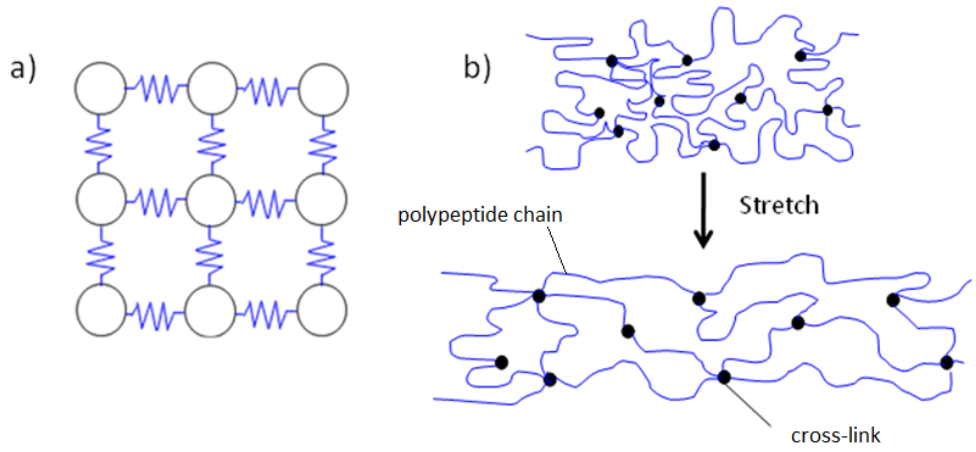

Figure 1.8: Cartoon representing a) energy elasticity and b) entropy elasticity

of minimum energy on removal of the applied load. The forces between the atoms tend to be strong making them difficult to deform and therefore these materials are stiff. On the other hand, the fundamental driving force behind extensible materials, like elastin, is said to be entropy driven whereby stretching the material leads to a decrease in entropy (reduction in the number of conformational states available) which acts as the spontaneous driving force to return to a state of maximum entropy (or minimum order). In these materials recovery is driven by the difference in entropy between the strained and un-strained states. Entropy elasticity relies on a highly disordered molecular structure, although the precise molecular basis underlying entropy elasticity of elastin is still incompletely understood and remains a subject of considerable controversy. Because of this a number of simplistic models have been proposed which either consider elastin to be isotropic and lacking structure, or where elastin is regarded as anisotropic and having some level of structural order [91]. One important feature shared by all these models is that elastin elasticity is primarily entropy-driven, whereby stretching causes a decrease in entropy which acts as a driving force for a return to the relaxed state of maximum entropy. The following sections give a brief account of several of the most important models.

1.5.7.1 Random Chain Model

As far back as the 1930's several models were proposed in an attempt to explain the elasticity of rubber, but these models failed to account for entropic elasticity

and spatial requirements.The first real progress was made by Mayer in 1932 [197], who had a clear understanding of the need for flexible bonds linking the individual monomers thus accounting for conformational freedom. A little later, this conept was expanded into the well recognised governing theories of rubber elasticity as proposed by Flory [198] and Treloar[199]. The proposed model suggested that rubber is composed of a network of kinetically free, random chains of variable length and lacking short- or long-range order, that are in constant motion and favour a state of high entropy where disorder is greatest. As the rubber is stretched the peptide chains are pulled further apart resulting in a decrease in the number of available conformational states so that the random network goes from a state of high entropy to a state of lower entropy. On removal of force this state of decreased entropy then acts as the main driving force for spontaneous recoil. The presence of permanent cross-links is essential allowing for macroscopic deformations of the network. If no cross-links existed then the material would instead act as a viscous liquid [176].

This model has been used with great success in interpreting the elastic behaviour of many rubber-like materials and since elastin exhibits physical characteristics very similar to those of rubber, it seemed reasonable to use this model in an attempt to explain elastin's elasticity (figure 1.9a). This was done by Hoeve and Flory in 1974 [52] with thermomechanical experiments on elastin fibres swollen in a mixture of ethylene glycol and water. From these investigations it was concluded that elastin swelling was independent of temperature and that elastin forms a network of random chains held together by cross-links which, when stretched, leads to a decrease in entropy, driving the system back to a state of maximum entropy. This study has since been criticized for the use of complex mixtures, which are difficult to interpret because of differential partitioning of solvents in the intrafibrillar space [200, 201]. Despite disagreements over the experimental procedures, there is general agreement that internal energy changes make only minor contributions with elasticity being dominated by entropy changes. The requirements of random kinetically free chains are largely true of water swollen elastin [196]. The condition of being random is supported by recent investigations into elastin's secondary structure composition [14, 15, 21] and flexibility is achieved through the use of small side-chain groups.

However, one criterion not met by elastin is that there should be a negligible change in internal energy. Elastin is a highly hydrophobic protein which, when stretched, there may be a change in free energy caused by changes in the water interactions associated with the hydrophobic residues.

There are several lines of evidence to support the random chain model for elastin elasticity including, thermoelasticity measurements with internal energy contributing between 10-26% only to recoil force [52, 200, 201], optical isotropy as revealed by polarized light microscopy [193] and the high mobility of elastin's polypeptide chains [119, 137]. Likewise, NMR studies also provide some evidence in support of rubber-like elasticity by indicating a high degree of disorder and a lack of both β-sheet and α-helix [202]. A further piece of evidence to support the random chain model comes from a calorimetry study by Andrady and Mark [201] which has shown that entropy provides the main route for elasticity. However, this view is far from conclusive and, despite elastin sharing a number of similarities with rubber, several investigations suggest elastin displays some degree of order, both at the ultrastructural level [76, 78] and at the molecular level [146, 147, 165, 203, 204, 205].

The main argument against the random chain model is that it does not explain why elastin is not self-lubricating like rubber [92, 206]. This led to the development of several alternative models, all of which assume some order and consist of two-phase systems having separate hydrophobic domains that largely exclude water separated by rigid cross-linking domains.

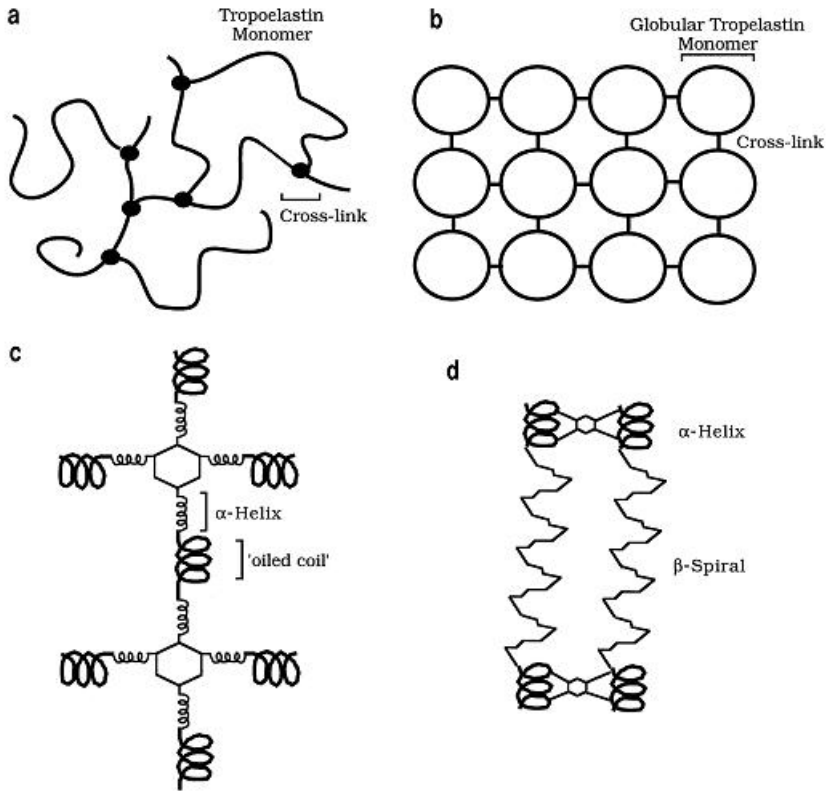

Figure 1.9: Schematics representing the four major models of elastin elasticity. a) Random coil model. b) Liquid drop model. c) Oiled-coil model and d) the fibrillar model [91]. More detailed explanations are given in the main text of this thesis.

1.5.7.2 Liquid Drop Model

This model was first proposed by Weis-Fogh and Andersen in 1970 [207] as an alternative to the random chain model. Water swollen elastin is depicted as oil droplets (tropoelastin) which are interconnected by cross-links and surrounded by water (figure 1.9b). The principle behind this model is that stretching of elastin distorts the spherical droplets to form ellipsoids. The larger surface area increases exposure of hydrophobic groups in the protein core to surrounding water molecules, accounting for the large change in enthalpy as observed by Weis-Fogh and Anderson by means of calorimetry, which would act as the primary driving force to the relaxed state. The liquid drop model has been criticized by Hoeve and Flory[52] who suggested that the change in enthalpy was due to dilution effects on swelling that occurs on stretching elastin in the presence of excess solvent. This was later confirmed by thermoelasticity measurements of Andrady and Mark in 1980 [201]. However, some

support for the involvement of hydrophobic interactions in elastin's elasticity within open systems has come from the work of Gosline and co-workers [185, 24] although they disagreed with the structural principles of this model. Likewise, Debelle [15] supported the cross-linked globular domain structure of elastin but rejected the proposed hydrophobic mechanism. Given the complexity of elastin networks it seems unlikely that such a simple model could account for the mechanisms of elasticity.

1.5.7.3 Oiled Coil Model

The oiled coil model was proposed by Gray et al [122] as an alternative to the liquid drop model with which it shares some similarity including the hydrocarbon-water interactions. The main difference is that tropoelastin is predicted as being fibrillar as opposed to globular (figure 1.9c). The fibrillar units are thought to be composed of rigid α-helical cross-linking regions that alternate with flexible hydrophobic GVPG repeats ('oiled coils') to form a broad left-handed coil structure. Within this coil the proline and valine residues are buried in the core whilst the small glycine residues are exposed to the water environment. As the chains are stretched so the coil begins to be opened up and as a result the hydrophobic core is exposed to surrounding water. This leads to a decrease in entropy of the system which then acts as the restoring force to the relaxed state. The failing of this model is that high mobility of the peptide chains observed by CD and NMR [140, 145, 202] cannot be accounted for, leading Urry and co-workers to propose the fibrillar model.

1.5.7.4 Fibrillar or Librational Entropy Model

The fibrillar model was proposed by Urry and co-workers [205] following extensive work using synthetic polypeptide sequences based on the hydrophobic domains of elastin. This model proposes that elasticity arises from repetitive β-spirals. The β-spirals are formed from regular, consecutive β-turns which act as spacers between the turns of the β-spiral (figures 1.9d and 1.10). The β-turns are stable structures composed of repeat sequences such as APGVGV, VPGVG and VPGG that have been reported to be present in tropoelastin [136, 175]. The β-spirals are believed

to be dynamic, loose, coils filled with water that are able to participate in low-amplitude, high-frequency rocking motions (librations) and if several of these spiral structures then combine they form structures referred to as twisted filaments and hydrophobic interactions are optimized further [208]. Stretching of the spiral results in a reduction in amplitude of these librations, which decreases the entropy to provide the restoring force for elasticity.

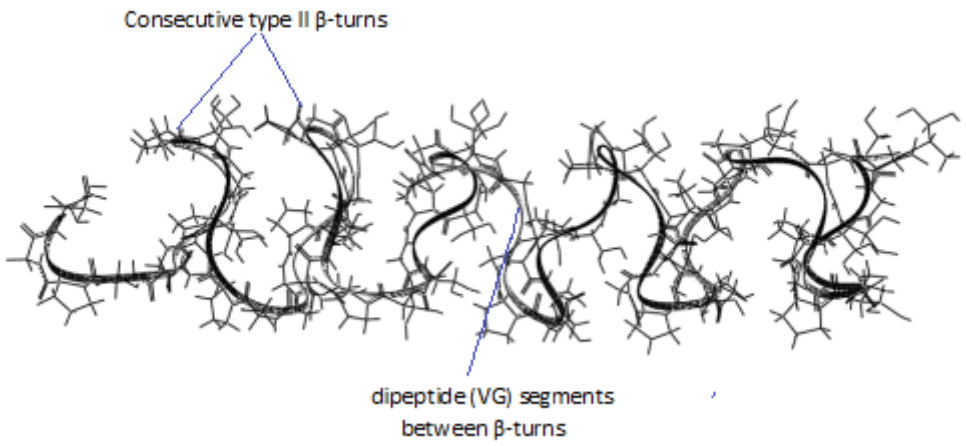

Figure 1.10: Schematic representation (reproduced from Li and Daggett [206]) of the β-spiral as proposed by Urry [136, 175]. The β-sprial is composed of consecutive type II β-turns between which are dipeptide (VG) segments. The β-turns act as spacers between each turn of the spiral structure.

This model has been well supported by investigations using polypeptide repeats [136, 205] but the major criticisms arise from the requirement of tandem XPGXG repeats which have not been found in human tropoelastin and fixed chain lengths which are not supported by NMR [202]. Although this model cannot be discounted, Tamburro and co-workers pointed out that this particular repeat sequence is also unstable [142], a fact which was also confirmed independently by Li et al [206, 209]. In addition, there is also some criticism over the fact that β-spirals would introduce regions of order within the elastin molecule which does not agree with birefringence experiments where elastin has been shown to display isotropy [193, 54].

An alternative model was later proposed by Tamburro et al [119] which again highlighted the importance of flexible and dynamic β-turns. The underlying difference between the two models was the location of these structures which, in the Tamburro model, was predicted to be within the more labile glycine-rich GXGGX sequences. Furthermore, Tamburro and co-workers hypothesized that there exist two

states; folded or quasi-folded (β-turns) and extended or semi-extended (β-sheets and / or PPII), where these structures inter-convert dynamically [56] forming the basis of elastin's elasticity. The system is regarded as being predominantly unordered and composed of freely fluctuating peptide chains with the restoring force arising from a decrease in entropy.

Both the Urry and Tamburro models are based on elastin-like synthetic peptide sequences and therefore the relevance of these investigations with regard to understanding the native protein has to be questioned. The structural predictions of Debelle differed significantly from those of both Urry and Tamburro and gave support for the liquid drop model of Weis-Fogh and Andersen. Rather than demonstrating the presence of numerous type II β-turns the resulting architectural model indicated large numbers of distorted β-structures and the importance of water in elastin's conformation [120].

Many of these models are over simplistic and although none should be completely disregarded, no single model provides a conclusive explanation of the molecular basis of elastin elasticity and the conformational changes involved. From the experimental data currently available it appears that the fibrillar/librational entropy-based models are most plausible as they combine regions of disorder (required for rubber-like elasticity) with limited regions of structural order, mainly in the form of β-structures. It is well known that coacervation of tropoelastin, α-elastin, and peptide sequences based on the hydrophobic regions all result in fibre formation and therefore can be associated with an increase in order. The fibres formed have also been shown to consist primarily of loose β-turns which is in agreement with the fibrillar model. Entropic mechanisms are preferred in biological systems as they permit durable, extensible proteins that rely on reduction in the number of accessible states available of deformation [28].

1.5.8 Effects of Ageing and Disease

Ageing is often associated with a reduction in elasticity which can be manifested in the skin, in a decline in respiratory function and in vascular complications [116]. Because elastin has to withstand vigorous mechanical activity repeatedly throughout

the organisms life time, it is particularly prone to age-related damage including the accumulation of lipids, proteins and calcium [210, 211]. It is currently believed that failure or modification of the elastic fibres is related to a 100-120 year maximum life expectancy in humans [212].

Cutaneous ageing refers to the changes in the skin which appear visibly as wrinkles and sagging. This is normally associated with loss of existing collagen and elastin fibres as well as degeneration or alteration of elastic fibres [213]. The heart and associated blood vessels work dynamically, relying heavily on the elastic fibres for smoothing blood flow and energy storage with each pump of the heart. It comes as no surprise that changes in these functions impose a high risk of heart failure. It is still uncertain as to the exact cause of decline in vascular performance. However, although elastic fibres are involved, it is likely that modifications to the overall extracellular matrix organization plays a significant part in changing mechanical properties. Ageing also has a dramatic effect on the pulmonary system with lung function being compromised due to deterioration of the elastic fibres, reduced elasticity and associated difficulties in breathing [116].

Some of the most serious consequences of ageing involve changes in the mechanical properties of major blood vessels. Normal arterial function relies on a combination of collagen's and elastin's mechanical properties, with any change having potentially serious consequences. Ageing is associated with increased cross-linking. However, it is now apparent that similar complications are also associated with glycation [214]. Non-enzymic glycation of collagen and its association with diabetes has been extensively studied, but elastin, because it has fewer possible glycation sites, has received much less attention [215]. Despite this, elastin should not be discounted as a potential target for non-enzymic glycation, since duration of the reaction is equally important. By this criterion, elastin may be considered as being susceptible to glycation as it has a very slow turn-over rate. This has been supported by an investigation by Winlove et al [216] whereby it was shown that purified elastin does incorporate glucose, resulting in increased stiffness of the tissue which may ultimately have serious implications for cardiovascular function. This initial investigation was conducted in vitro and further studies are required in vivo to establish

how elastin glycation, through ageing or diabetes, affects elasticity.

Elastic fibres are able to bind readily to various lipids even after treatment with hot alkali. It is thought that elastin's extreme hydrophobicity may, in part, contribute to its uptake of lipids which may be modified further by altering the calcium content [217, 218]. Blood vessels typically contain in the region of 1-2% lipids where they are thought to interact with the elastic lamellae, but this figure has been shown to increase dramatically to 30-40% in individuals suffering from atherosclerosis [219]. In addition, Partridge and Gems [210] have shown that elastins from normal and atherosclerotic plaques also differ in their amino acid composition. Atherosclerosis is known to effect a large number of individuals in the western world today, but elastin and the associated microfibrils are also now known to be closely associated with a number of other diseases.

It is beyond the scope of this thesis to provide an extensive account of all the possible diseases associated with the elastic fibre system. There are many diseases, both acquired and inherited, which affect elastic fibre structure, assembly or number in humans and it stands to reason that the tissues most severely affected are those that are considered to be elastin-rich. Table 1.3 below lists some of the relevant diseases as well as their broad effects on both elastic fibre components and the individual per se. Additional information can be found in extensive reviews [101, 220, 221]. Many of the defects are genetically acquired and as such may effect any system in which the elastic fibre plays a central role, displaying a broad spectrum of phenotypes. On the whole, genetic disorders of the elastic fibre can be split in accordance with the affected component being either (i) mutations of the elastin gene and (ii) those affecting the microfibrils.

There are several known genetic disorders that have now been associated with modifications of the elastin gene, leading to structural modification and impaired function, which clearly can have a considerable impact on the well-being of the individual concerned. Many elastin gene mutations are lethal in utero because the period of greatest growth coincides with times of greatest elastin synthesis and deposition. In attempting to increase our understanding of these diseases and the mutations involved we may also be able to better understand both elastin fibre

Disease	Effect on Elastic Fibres	Symptoms
Cutis laxa	Loss of elastic fibres and increased fragmentation	Inelastic, loose folds of sagging skin. Also associated with pulmonary emphysema and urinary / gastrointestinal diverticula
Wrinkly skin syndrome	Elastic fibres are reduced in number and in length	Reduced elastic recoil of fibres and numerous musculoskeletal defects
DeBarsy syndrome	Under developed and fragmented elastic fibres	Loose, sagging and inelastic skin as well as mental abnormalities and dwarfism
Pseudoxanthorma	Build-up of calcified elastic fibres in mid-dermis of skin	Inelastic skin, plaques and cardiovascular defects
Marfan syndrome	Mutations to microfibrils and in particular fibrillin-1	Multiple effects on skeletal system, vascular system and skin. Typicallytall stature with disproportionally long arms and legs
Supravalvular aortic stenosis	Mutations of elastin gene and deficiency in elastic fibres that are both thickened and irregular	Narrowing of major blood vessels due to excess elastin deposition

Table 1.3: Some heritable connective tissue diseases, their major symptoms and effects on elastic fibres.

formation and function.

Cutis laxa is generally considered to be an autosomal recessive or autosomal dominant condition, although there are also known cases of this disorder with no known genetic basis. The autosomal dominant cases have been found to be linked to mutations in the elastin gene [222, 223] and are accompanied by a reduction in number of elastic fibres as well as fragmentation of existing fibres. This in turn can impair the function of elastin in the lungs and lead to fewer microfibrils in the dermis. The lack of elastic fibres may be explained by several alternative mechanisms. Translational and post-translational modifications may result in either elastin degradation or alternatively, due to changes in gene expression, resulting from faulty formation during the pre-translational stages. There appears to be some variation in the characteristics displayed by individuals with cutis laxa, but in all cases the skin appears prematurely aged, occurring as loose sagging folds of skin, with reduced elasticity and resilience [220].

Wrinkly skin syndrome is a relatively rare autosomal recessive disorder which,

like cutis laxa, is the result of modifications to the elastic fibres. Again numbers of fibres are reduced and in appearance the fibres tend to be irregular or fragmented, which consequently leads to reduced elasticity. Characteristic features of this disease include fine wrinkles covering the abdomen and dorsa of hands and feet, as well as increased palmar and plantar creases and prominent veins on the chest [224].

Another condition sharing some similarities to cutis laxa is known as DeBarsy syndrome. This again is an autosomal recessive disease with typical physical characteristics including loose folds of sagging skin. However, unlike cutis laxa, this disorder is frequently accompanied by other complications including mental problems, cataracts and even dwarfism [221]. In this case elastic fibres are not degraded, but synthesis of new fibres is very low and aggregation of fibres can also occur.

Pseudoxanthoma elasticum (PXE) is yet another disorder of elastic connective tissue. It is typically an autosomal recessive disorder, although there have been reported cases of the autosomal dominant form as well. There is some variation in the age of onset and also in the expression of PXE. Typical characteristics include small lesions of the skin which thicken in time to form inelastic plaques, sagging skin on the face and changes to the eyes and sometimes blood vessels [225]. Ocular changes usually refer to angioid streaks (greyish streaks radiating outwards), regular hemorrhaging of the eye and impaired vision. Defects to vasculature normally affect arteries and tend to develop as a consequence of coronary occlusion, hemorrhages and / or gastrointestinal bleeding [101]. Modifications to the elastic fibres include aggregation, fragmentation and calcification. There is also some evidence that amorphous elastin in PXE individuals is replaced by substantial quantities of granular material which, unlike elastin, does not stain positively with Verhoeff's stain. As yet it is still unclear as to whether PXE results from abnormalities in the synthesis and / or the cross-linking of elastin or due to breakdown of existing elastin both of which could have serious implications on the function of elastic fibres.

Supravalvular aortic stenosis (SVAS) is a genetic disorder effecting approximately 1 in every 13,000 live births [226]. SVAS is primarily the result of point mutations in the elastin gene and affects the aorta and other major blood vessels including the pulmonary, carotid and cerebral arteries often leading to narrowing of the lumen

through excess elastin deposition and poor control of cellular proliferation [220]. Microscopic observations have shown a deficiency in elastic fibres that are abnormal in appearance, being both thickened and irregular, as well as collagen deposits and the presence of enlarged smooth muscle cells.

Marfan syndrome is one of the most common heritable connective tissue disorders affecting approximately 1 in every 10,000 individuals worldwide [220, 227, 228] with around 25% having no known previous family history of the disease. Marfan syndrome can manifest itself as abnormalities in many different systems including the skeleton, cardiovascular system, the eyes, the pulmonary system and the skin [227, 229] Although the symptoms vary, this disorder generally results in tall stature with arms, legs, fingers and toes being especially over-grown compared to the rest of the body. Ocular defects may also occur which are usually associated with dislocation of the lens and myopia (short sightedness). Some of the most serious complications involve defects to the vascular system including the heart. Within the heart the mitral valves are most frequently affected which can lead to collapse and leaking. Aortic aneurysm and dissection together make the greatest contribution to premature death in Marfan syndrome patients [230]. The aorta becomes increasingly dilated which triggers weakening and eventually stiffening of the blood vessels and, as a consequence, can lead to rupture of the ascending aorta wall. Histological investigations have shown Marfan syndrome to be associated with a reduced number of fragmented elastic fibres [231], few smooth muscle cells and collagen and glycosaminoglycan deposits [227]. A biochemical investigation revealed that elastin extracted from the aorta of Marfan syndrome individuals had significantly reduced levels of desmosine and isodesmosine (50% of that in controls) and elevated lysine residue levels, indicating that cross-linking is reduced in major blood vessels of these individuals and therefore may be a possible explanation for the aortic weakness observed in Marfan's syndrome patients. The cause of lowered levels of desmosine/isodesmosine levels is not known, but it has been suggested that inadequate oxidation of lysine residues could be responsible or alternatively, a modified conformation of elastin may result in misalignment of lysine residues therefore reducing the number of functional cross-links [231]. Marfan syndrome individuals also

have defective microfibrils and in particular the fibrillin-1 gene [226, 228, 232, 233] which is crucial for maintenance of functional elastic fibres. The difficulty is in detection of these mutations mainly because they rarely occur more than once. As discussed previously, microfibrils have many important functions including elastogenesis, maintenance of tissue integrity, anchorage and support. As a consequence any mutation that affects the biochemistry or structure of microfibrils is highly likely to have a knock-on effect to any system in which they participate. This may help to explain why the physical expression of Marfan syndrome can be so varied.

1.6 Lamprin

The previous sections have provided an account of the structure and function of the vertebrate elastic protein, elastin. The relationship between elastin and the family of matrix proteins isolated from the cartilagenous endoskeleton of lampreys is unclear and it is a major aim of this project to shed light on this relationship in terms of their physical properties and molecular structure.

Lamprey matrix proteins have been relatively well studied but despite this our current understanding of their biochemistry and mechanisms of elasticity is far from complete. It is known, however, that this family of proteins does in fact share several characteristics in common with vertebrate elastin; they are all resistant to digestion with hot alkali and cyanogen bromide [234], they are highly hydrophobic and extensively cross-linked [235], they stain positively with Verhoeff's and other elastin stains [236] and they self-assemble [58]. The following section gives an overview of lamprey in general, their evolutionary link to elastin-containing species, and the skeletal components relevant to this project which will then be discussed in relation to their biological function, ultrastructure, biochemistry and physical properties.

1.6.1 Introducing Lamprey

The agnathans are the earliest known vertebrates dating back to around 500 million years ago [237]. The only remaining agnathans, or jawless fish, today are hagfish (Hyperotreta) and lamprey (Hyperoartia), which together form the higher group

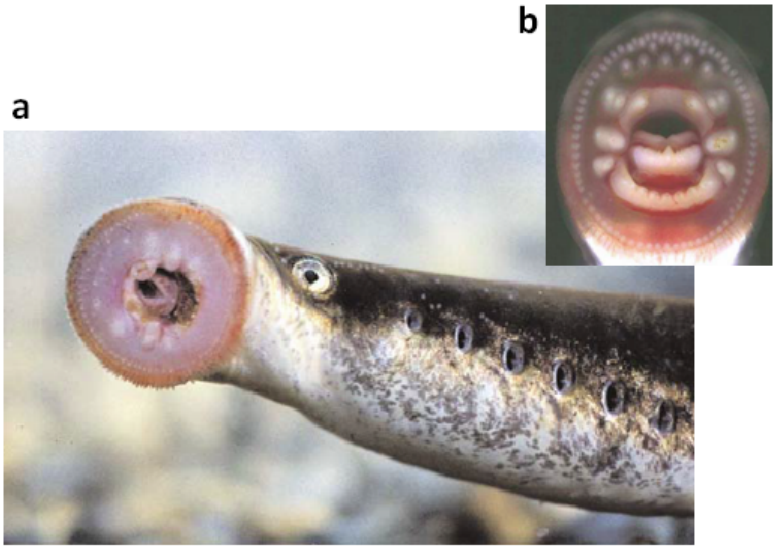

Figure 1.11: Photographic images of adult river lamprey (fluviatillis), (a) showing the general physical characteristics, large eyes, gill slits and broad disc-shaped mouth equipped with rings of teeth, and (b) enlarged image of mouth cavity showing arrangement of teeth on the oral disc. (Images are reproduced from [239])

of cyclostomes based on the structure of their mouth-parts (i.e. their tongue) and water pumping mechanism [238].

The overall appearance of lamprey is very similar to that of eels, being long, slender and lacking scales, instead being covered by a thin layer of mucus. They are also characterized by the absence of jaws or paired fins. The mouth parts are primitive in form, being slit-like when closed but forming a broad disc-shape when opened, equipped with rings of rasping teeth and a lip that acts as a powerful sucker used to attach to its host. The tongue is also well adapted to the lamprey's largely parasitic lifestyle being both rough, and endowed with additional teeth designed to scrape the flesh of its victim. Other unusual features of lamprey include the presence of a single nostril located on the upper surface of the head, seven gill openings on each side of the body and large eyes on either side of the head and a soft cartilagenous endoskeleton. Most vertebrates loose their notochord in the early stages of development but lamprey maintain the presence of a notochord for their entire life acting as a support for the spinal cord.

There are some 50 different species of lamprey with the three most common to British waters being the brook lamprey (Lamperta planeri), the river lamprey (Lamperta fluviatillis) and the sea lamprey (Petromyzon marinus). The brook lamprey differs from the other species in that it spends all its life in freshwater. The river

lamprey spends the majority of its life in coastal waters and migrates to freshwater to spawn during the spring and autumn months. The sea lamprey is the largest of the British species growing up to one metre in length and, as its name suggests, spends long periods of time feeding in salt waters from where it migrates during spring and summer. All lamprey construct 'nests' in the gravel substrates into which they lay large numbers of eggs. The young larvae then drift downstream until they reach slower flowing waters which act as 'nursery' grounds where they are able to feed on rich supplies of algae and bacteria. Depending on the species, the young lamprey remain in these 'nursery' sites for anything between three to eight years before undergoing profound changes and transforming into young adults able to migrate to feeding waters. It is at this stage that the lamprey develop a sucker-like mouth, a rasping tongue, and teeth as well as changes to their respiratory and digestive systems [240]. Such dramatic changes equip the young lamprey for a predominantly parasitic lifestyle feeding on the blood and other body fluids of host species. The adult phase is relatively short lived and it is uncommon for mature lamprey to live in excess of two years.

Although all lamprey are armed with a powerful sucker and rasping teeth, they are not all parasitic. In fact, approximately half of all known species are non-parasitic, including the brook and river lamprey, which often feed on small invertebrates. Parasitic adults attach to their host by means of powerful suckers and then use their many sharp teeth to cut through the flesh by a rasping motion until they are able to suck the hosts blood on which they feed.

1.6.2 Lamprey and Evolutionary Perspectives

The agnathans are the most primitive of all known vertebrates. The majority of these disappeared during the late Devonian period with the sole survivors being the lampreys and hagfishes putting these animals in a unique position with the potential to shed light on issues such as the morphology and physiology of ancestral vertebrates as well as development from jawless to jawed vertebrates. The fossil record of these animals is very limited due to the lack of mineralized components although several well preserved fossils have now been discovered [241, 242]. The family of novel

matrix proteins that comprise the cartilagenous structures of the lamprey skeleton are also of particular interest as it has been suggested that these proteins may be the evolutionary precursors to elastin, diverging from the mammalian line approximately 500 million years ago [237]. This opinion is not universally accepted and several attempts have been made to trace the evolution of elastin lineage both through vascular tissues [134] and cartilage [58] neither of which proved conclusive. Following a short section describing the elements of the lamprey endoskeleton an account of similarities between this group of proteins and elastin will be discussed.

1.6.3 The Skeleton of Lamprey

Lamprey are unusual in the fact that there is a total absence of mineralization from the internal supporting structures of the lamprey's body, which instead is composed entirely of non-collagenous cartilage [243, 244]. The exact nature and composition of lamprey cartilage has been for many years the source of debate. Typically vertebrate cartilage has a high collagen, proteoglycan and water content. However, the cartilaginous structures forming the endoskeleton of lamprey [5, 236] and hagfish [245] are unique, with collagen not making a major contribution. Although collagen is almost totally absent from the endoskeleton, at least five types of collagen have been identified within other lamprey tissues including the notochord, the dermis and the body wall [246, 247]. The lamprey endoskeleton can be divided into several distinct, specialized structures each having a different function as shown in the photograph and schematic illustrations in Figures 1.12 and 2.1. This study focuses on the annular cartilage, the piston cartilage, the branchial basket and the pericardial sac. The annular cartilage is a ring structure located in the mouth cavity where it supports the mouth parts including the suckers and teeth and serves as a site of muscle attachment. The piston is a cylindrical structure which forms the skeleton of the rasping tongue. The branchial cartilage forms a delicate basket-like structure that supports the gill openings onto which, at its rear end, is attached the pericardial sac, a bag-like structure that surrounds and supports the heart [248, 243]. For a comprehensive description of the lamprey anatomy please refer to a book by Hardisty [243]. Each of these structures has a different function, requiring different

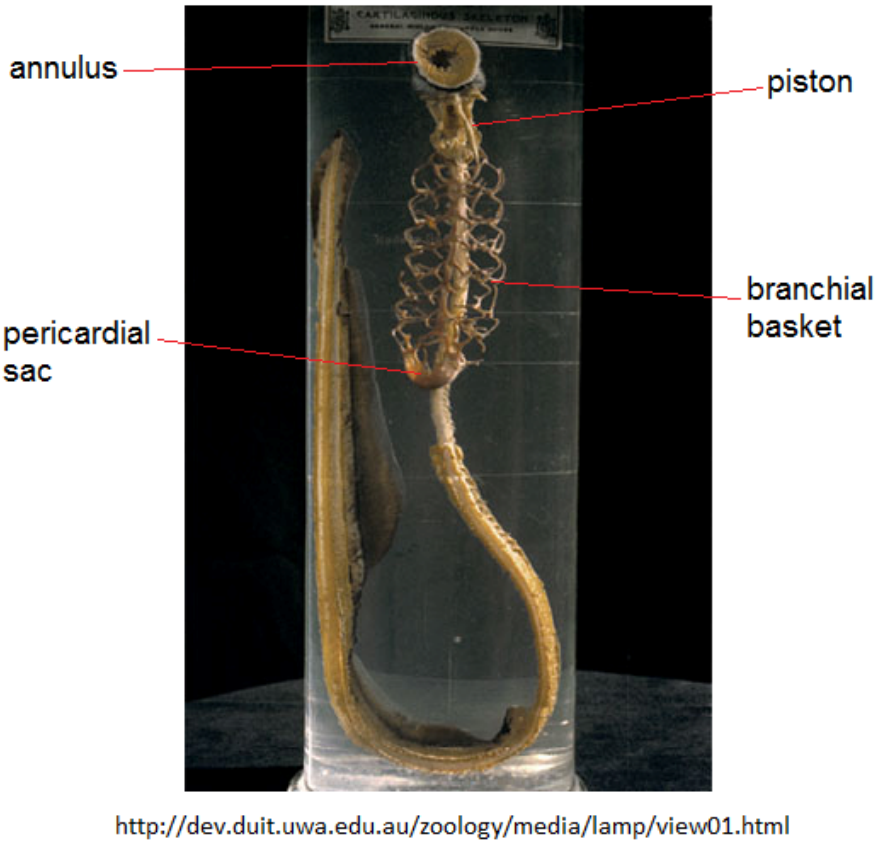

Figure 1.12: Image to show the complete skeleton of the sea lamprey (Petromyzon marinus) after all the surrounding soft tissue and organs have been removed.

mechanical properties. The annular and piston cartilages for example have relatively static roles in situ where large extensions and flexibility are not essential. On the other hand the branchial cartilage and pericardial sac experience both extensive and repeated deformations. The branchial structures undergo repeated dynamic compression and recoil during each respiration cycle whilst the pericardial sac, which encases and supports the heart, has to accommodate repeated pulsatile action with each heart beat. This differs from the pericardial sac in humans which completely encases the heart and does not undergo repeated expansion and recoil. It does not seem unreasonable that the differing functions of each of the skeletal structures are also reflected in differences in their ultrastructure, biochemical composition and material properties.

Unlike other vertebrates, no elastin-containing fibres have been detected in any lamprey tissue including blood vessels [249]. The circulatory system of lampreys is a low pressure system (30-60 mm/Hg) where the blood vessel walls are composed primarily of microfibrils [110, 250, 251]. DeMont and Wright [110] and Davison et al

[251] independently confirmed that these microfibril-rich blood vessels are able to exhibit mechanical properties very similar to those of higher vertebrates. The absence of elastin has been confirmed by biochemical investigations although the presence of other fibres similar in appearance to elastin has been observed microscopically.

1.6.4 Ultrastructure of Lamprey Cartilage

Several extensive ultrastructural studies have been conducted by Wright and coworkers during the 1980's which have provided the basis of our current understanding of the ultrastructure of lamprey cartilages [11, 236, 245, 252]. The nature of lamprey cartilage is unique and has been the subject of debate over the past 50 years or more with early investigations suggesting they are a form of hyaline cartilage, true cartilage or chondroid. However, more recent studies by Wright have demonstrated that these tissues are in fact a new, novel form of cartilage that is unique to lamprey [11, 236, 252].

There is a high degree of similarity in the ultrastructure of each of the lamprey cartilages with all consisting of both cellular and extracellular matrix components. The dominant cell type is that of chondrocytes which are frequently found in small clusters separated by seams of matrix material, characterized by the absence of collagen fibrils and an abundance of branched matrix fibres [5]. Although each of the lamprey cartilages is composed of the same basic components, their organization shows some variation [236].

On a structural basis the four cartilages can be divided into two distinct groups based on the classification of Cole [253]; the flexible branchial and pericardial cartilages in one group ('soft' cartilages) and the more rigid annular and piston cartilages in another ('hard' cartilages). The branchial and pericardial cartilages tend to be highly cellular with clusters of 2-10 cells surrounded by narrow bands of matrix material, whereas the annular and piston cartilages have fewer cells, more extensive matrix material [252] and the presence of canal-like structures (80-600μm in diameter) which are thought to protect underlying vasculature [254]. In all these tissues the cells located within the core begin to degenerate over time and the spaces formed become filled with matrix granules and proteoglycan-rich fibrous material.

The high proteoglycan content may be of particular importance in the branchial and pericardial cartilages as this could enhance flexibility in these tissues, required for continuous compression and recoil [252]. Similar to many other vertebrate elastic tissues, the branchial cartilage and pericardial sac are seen to contain small quantities of lipid droplets which tend to be restricted to the peripheral regions. The annular and piston cartilages can be separated into three separate regions based on the size and shape of the chondrocytes as well as the organization of the matrix fibrils [236, 252]. The outer perichondrial region consists of a high percentage of small, elongated chondrocytes (involved in matrix production) surrounded by numerous, densely packed, branched matrix fibrils that lack any specific orientation. In the subperichondrial region the cells become slightly enlarged and more circular and in the innermost core the cells are largest and polygonal in shape and structural fibrils are fewer in number and less densely packed. Electron microscopy has also shown that there are fewer organelles associated with the cells of the central domains which can be explained by the fact that these cells are less active in the production of matrix material [236, 252].

Although the lamprey cartilages are generally described as being non-collagenous, microscopy investigations have revealed limited amounts of collagen fibres forming a highly vascular perichondrial sheath on the outer surfaces which are often associated with the presence of fibroblasts and microfibrils [236]. This layer is particularly thick on the inner surface of the pericardial sac where it comes into contact with the heart thus providing additional support [254]. Evidence to support the absence of collagen from the majority of the tissue includes, the presence of dense matrices composed of randomly arranged, branched fibrils (15-40 nm in diameter) which display no cross-banded periodicity [236], the absence of methionine and only a minor contribution made by hydroxyproline [5, 11]. Light microscopy has also revealed that like elastin, the matrix of all the lamprey cartilages stain positively with Verhoeff's which has in the past been regarded as being specific to elastin. The mode of Verhoeff's staining is unclear [255]. However, it may be linked to hydrophobic domains and in particular where they form β-turns and/or β-sheets, which may account for positive staining of lamprey cartilages.

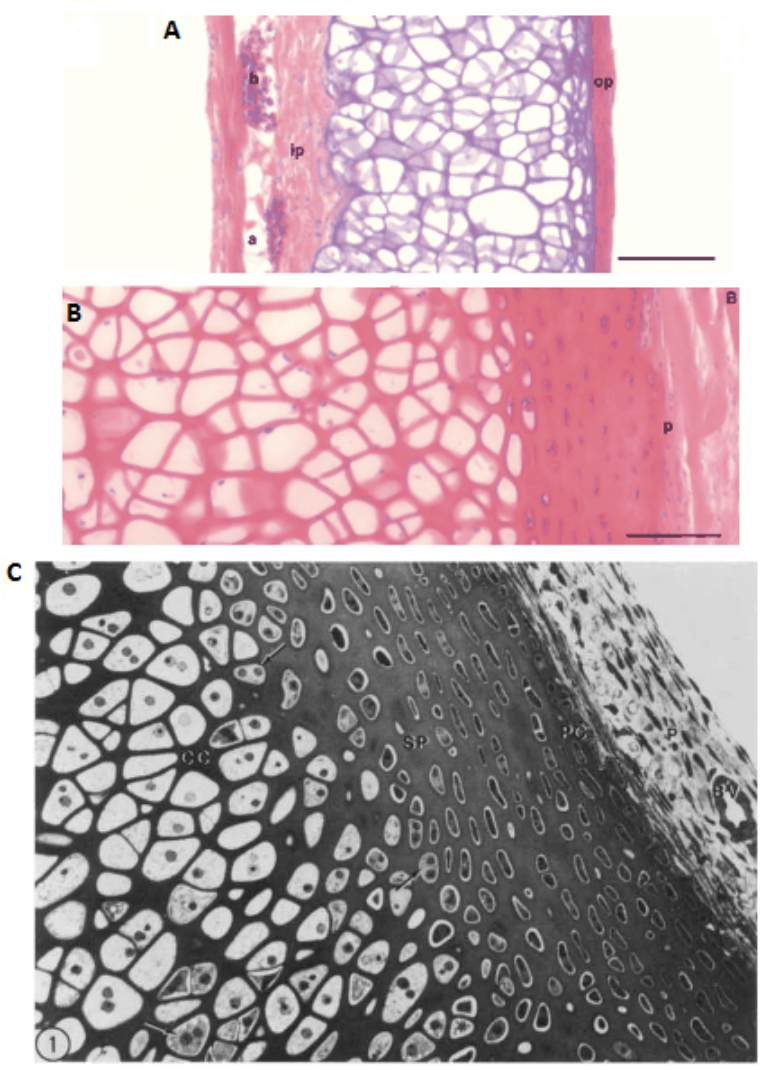

Figure 1.13: Histological sections from intact a) pericardial cartilage, b) and c) annular cartilage. Sections shown in a) and b) were stained using the standard haematoxylin and eosin method and the scale bar represents $100\mu m$. The pericardial and annular cartilages have a distinctive layer of collagen fibrils forming a perichondrial sheath (shown in pink on image (a)), on their outer surfaces. This layer is particularly dense on the outer surface of the pericardial cartilage. The annular cartilage is divided into three distinct regions according to shape and size of the chondrocytes; the perichondrial, sub-perichondrial and central zones. The central regions consist of large hypertrophied chondrocytes surrounded by thin seams of matrix material. Towards the outer edges chondrocytes become progressively smaller and oval in shape. Images (a) and (b) are reproduced from [254] and image (c) from [236].

It is only in recent years that characterization of lamprey cartilages has begun to attract the attention of the scientific community. It is the aim of the following section to detail what is known regarding the biochemistry of this family of matrix proteins.

1.6.5 Amino Acid Composition

Initial biochemical studies focused on the matrix protein isolated from the annular and piston cartilages which has subsequently led to the full characterization of this protein, referred to as lamprin [5, 58], forming 44-51% of the cartilage dry weight. However, similar analysis of branchial and pericardial cartilages has been less extensive and only partial characterization of these proteins is as yet available. Despite the incomplete biochemical information, the branchial and pericardial proteins are regarded as a second group of closely-related proteins sharing significant similarities in both structure and biochemistry. Table 1.4 compares the amino acid composition of the several lamprey cartilage matrix proteins and fibrous elastin from bovine ligamentum nuchae.

Amino Acid Residue	Elastin Fibers[1]	Annular Cartilage[2]	Branchial Cartilage[3]	Pericardial Cartilage[3]
Hydroxyproline	8.1	1.4	22	17
Lysine	3.3	7.3	13	12
Histidine	0.5	38	14	13
Arginine	5.8	17	29	30
Aspartic acid & asparagine	11.6	21	66	70
Threonine	9.3	31	14	14
Serine	8.7	27	43	46
Glutamic acid & glutamine	15.4	38	60	61
Proline	115.5	96	109	102
Glycine	328.1	282	323	313
Alanine	227.0	156	169	176
Valine	131.6	79	30	33
Isoleucine	23.9	20	15	16
Leucine	59.4	119	31	33
Tyrosine	5.9	53	47	50
Phenylalanine	29.3	14	16	12
Cysteine	0	0	0	0
Methionine	0	0	0	0

1 Jacob & Robert (1989)
2 Wright et al (1983)
3 Robson et al (1997)

Table 1.4: Similarities in amino acid composition between the various lamprey matrix proteins as well as for bovine ligamentum elastin as a comparison. Amino acid compositions are expressed as residues per 1000 residues. Data have been reproduced from previously published work of Jacob and Robert [9], Wright et al [11] and Robson et al [5].

All the matrix proteins show some differences in amino acid composition although it is reasonable to group the annular and piston cartilages together and the branchial and pericardial into another group. The annular and piston are rich in the very hydrophobic residues including glycine, leucine and alanine as well as the small amino

acid, proline. They are also moderately rich in the hydrophobic amino acids valine and tyrosine and also histidine. The second group have high numbers of hydrophobic residues, and in particular glycine and alanine, although the levels of valine, leucine and histidine are lower. This group is also distinguished by the high number of hydroxyproline residues (17-22 residues) [5] compared to approximately 10 residues in elastin fibres and only 1-2 in annular and piston cartilages [11]. In addition, all the lamprey matrix proteins differ from elastin in having histidine residues, substantially more tyrosine and many more polar residues including threonine, serine, arginine, glutamine and asparagine. One biochemical characteristic all these proteins share is the absence of any methionine or cysteine residues. Based on hydrophobicity indices, we calculated that elastin, annular and piston cartilages are the most hydrophobic, all having a similar percentage of hydrophobic residues (61-62%), whilst that of the branchial and pericardial cartilages is lower (approximately 46%). There is also a difference in the number of small amino acid residues. Small amino acids include glycine, proline, alanine, serine, threonine, aspartate and asparagine the total of which is greatest in elastin, branchial and pericardial cartilages all being within the range of 721-726 residues. In the annular and piston cartilages this number is less at around 613 residues. This may be important in the conformations adopted by the various proteins, as small residues have greater conformational freedom being less constrained by bulky side chains.

1.6.6 Lamprin Monomer

Mature lamprin, like elastin, is a cross-linked, hydrophobic, highly insoluble protein. Lamprin has previously been hydrolyzed resulting in the formation of at least three soluble monomers showing some variation in both amino acid composition and size. This has been taken to suggest the existence of multiple lamprin genes [235]. Each of the variants of the protein is able to self-assemble, forming low molecular weight polypeptides of either 10 or 12 kDa [58]. The same authors [58] also established that the lamprin genes, of sea lamprey at least, have either seven or eight exons and that all lamprin genes are alternatively spliced at exon 4. The authors proposed that multiple lamprin genes may have evolved to meet the need for large quantities

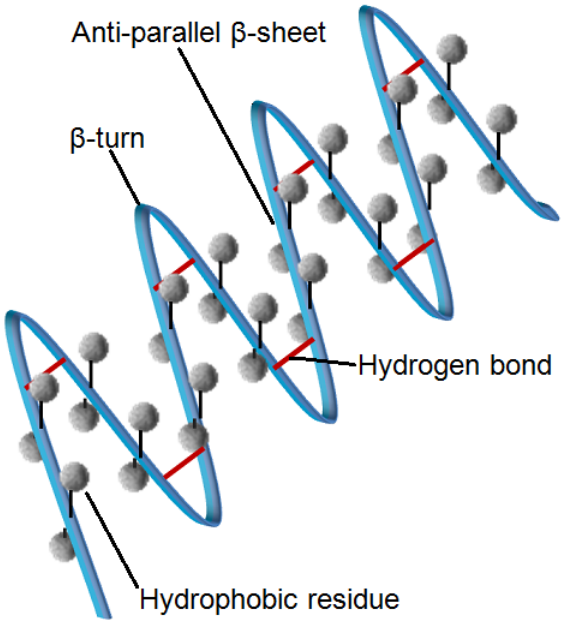

Figure 1.14: Schematic diagram representing the arrangement of structures involved in 'lego-like' stacking of lamprin. The peptide chain is arranged into anti-parallel β-sheets and β-turns, as proposed for the GGLGY repeat motif. This results in the formation of an essentially flat structure onto which hydrophobic residues can protrude from both the upper and lower surfaces. Many similar structures can then stack together in a 'lego-like' manner to facilitate self-assembly of lamprin monomers.

of the relatively small protein, lamprin, which in larger proteins like elastin may be synthesized by single-copy genes. All of the proteins also showed a strong similarity in amino acid composition to that of insoluble elastin.

Mechanisms underlying the assembly of the monomers to form a stabilized insoluble protein are not fully understood, although it is likely to involve the hydrophobic residues, and in particular the repeat sequences, with the ability to stack in a manner likened to that of lego [58]. A 'lego-like' stacking arrangement has previously been described for silk fibroin [256], which consequently led Robson and co-workers to propose a similar mechanism of self-assembly involving the GGLGY repeat motif of lamprin, where anti-parallel β-sheets are interspersed with β-turns. Such a structural arrangement would permit hydrophobic residues to be exposed on both upper and lower surfaces of an otherwise flat structure [58]. Figure 1.14 shows a schematic representation of the arrangement of structures for 'lego-like' stacking.

1.6.7 Repeat Sequences of Lamprin

As discussed previously, hydrophobic repeat sequences are frequently encountered

Protein	Repeat Sequence
Elastin	VPGG, VPGVG, APGVGV
Lamprin	GGLGY, VGGLG
Silk moth chorion protein	GGLGY
Abductin	GGFGGMGGGX
Byssal thread	GPGGG
Spider dragline silk	GPGQQ, GPGGY, GGYGPGS
Spider flagelliform silk	GPGGX

Alanine,A Proline,P Glycine,G Valine,V Leucine,L
Serine,S Glutamine,Q Tyrosine,Y Phenylalanine,F
Methionine,M X, any amino acid residue

Table 1.5: Representation of some of the most frequently encountered hydrophobic repeat sequences found in elastic proteins. Although differing in exact sequence, these repeat motifs are likely to form similar flexible secondary structures.

within the amino acid sequences of many elastic proteins and suggest the presence of regular structures. Lamprin is no exception and, although this protein has a unique amino acid composition, the occurrence of the pentapeptide motif GGLGY within the hydrophobic domains was confirmed by Keeley and co-workers [58]. It occurs twice as a single sequence and a further six times in tandem and comprising around 35% of the mature protein [257]. This sequence is also found in silkmoth chorion protein [258], whilst similar sequences are found in other proteins including elastin [56], spider silks [53] mussel byssal thread [259] and others. Some of these sequences are shown in table 1.5

It appears that the lamprin repeat sequences have been conserved for a period of approximately 500 million years following the divergence of the agnathans from the main vertebrate line. This would imply that these motifs have an important functional role. All of the matrix proteins sharing similar repeat sequences also have several other characteristics in common; they all have the ability to self-aggregate forming fibrillar structures and they are all rich in β-turns and β-sheets. There is overall agreement that these repeat motifs and β-structures have important roles to play in the self-assembly process and both Robson [58] and Debelle [204] have

proposed similar structural models involving the aligning, followed by interlocking or stacking of hydrophobic amino acid side chains located within the β-turns and antiparallel β-sheets in a 'lego'-like manner to form stable fibrillar structures [58]. In solid form GGLGY sequences consist of β-structures as well as some extended PPII helices. However, Bochicchio and co-workers [59] showed that, in solution, synthetic GGLGY repeats contain increased amounts of PPII which co-exist with β-turns and β-sheets to form a flexible combination of conformations. Their experimental data supports the earlier proposed interdigitization models of Keeley and Robson with the addition of interaction by PPII helices.

1.6.8 Cross-linking

One of the main criteria for elastic proteins is that they must be cross-linked in order to form a network that is able to distribute applied forces throughout the system and also permit rapid recoil, thus providing strength and elasticity. Research into lamprin cross-linking has so far been limited, although it has been established that no desmosine/isodesmosine cross-links can be detected [11]. Early investigations by Koob and Eyre [260] instead proposed the existence of pyridinoline based cross-links in lamprey branchial cartilage. Fernandes and Eyre [234] later confirmed this result and in addition demonstrated that although both lysyl pyridinoline and hydroxypyridinoline were found to be present, the lysyl pyridinolides dominated at a ratio of 7:1. Pyridinoline cross-links are not uncommon in structural proteins and in fact are characteristic of the major fibrillar collagens [37]. This is particularly intriguing as the same investigation also revealed that both lysyl pyridinolines and hydroxylysyl pyridinolines were absent from the more rigid lamprin based annular and piston cartilages.

Biochemical characterization of annular and piston cartilages indicates the presence of lysine residues which, although approximately half that found in branchial and pericardial cartilages, should still be available to participate in cross-linking. Disulphide bonds, another form of linking mechanism employed in collagen, are not possible in lamprin due to the total absence of cysteine residues. Although lamprin is rich in tyrosine residues, dityrosine cross-links, as found in resilin, again are not

detected in lamprin [58]. It is possible that covalent interactions alone are able to link lamprin monomers into an insoluble matrix although this has not yet been confirmed and therefore the issue of cross-link formation is still largely unresolved.

Our understanding of the physical properties of these proteins and their supramolecular assembly will undoubtedly be restricted until further biochemical studies have been conducted in order to establish the nature of the lamprin cross-links.

1.6.9 Properties of Lamprey Matrix Proteins

1.6.9.1 Physical Properties

It was reported earlier that purified elastin is cream to pale yellow in colour and characteristically autofluorescent when irradiated with a UV source (500 nm wavelength). The physical appearance of all the purified lamprey matrix proteins is very similar to that of elastin and Robson et al [5] showed that lamprey branchial cartilage also autofluoresced when irradiated with light at a wavelength of 500 nm, whereas the annular and piston proteins did not. The lysyl-pyridinoline cross-links are known to autofluoresce under ultraviolet illumination which may explain the positive autofluorescence [5]. Autofluorescence of lamprey branchial cartilage is shown in figure 1.15.

Like elastin, lamprey annular and pericardial cartilages have a high water content, being in the region of 77-81% of the total wet mass [254]. However, the tissues used in this investigation were not digested to remove cells, collagen and any other components and as a result the amount of water associated with the protein itself has not been established. High water content is believed to play an important part in the elastic behaviour of elastin and therefore it is highly plausible that the same is true for this family of lamprin-like proteins.

The remarkable mechanical properties of elastin and their relation to its physical properties and molecular composition have already been discussed in section 1.4. However, investigations involving the lamprey cartilage proteins have been very limited. A single study by Courtland et al [254] determined the equilibrium moduli for undigested lamprey annular and pericardial cartilages, with mean values of 0.71 MPa and 2.87 MPa respectively, although these values showed some variation with

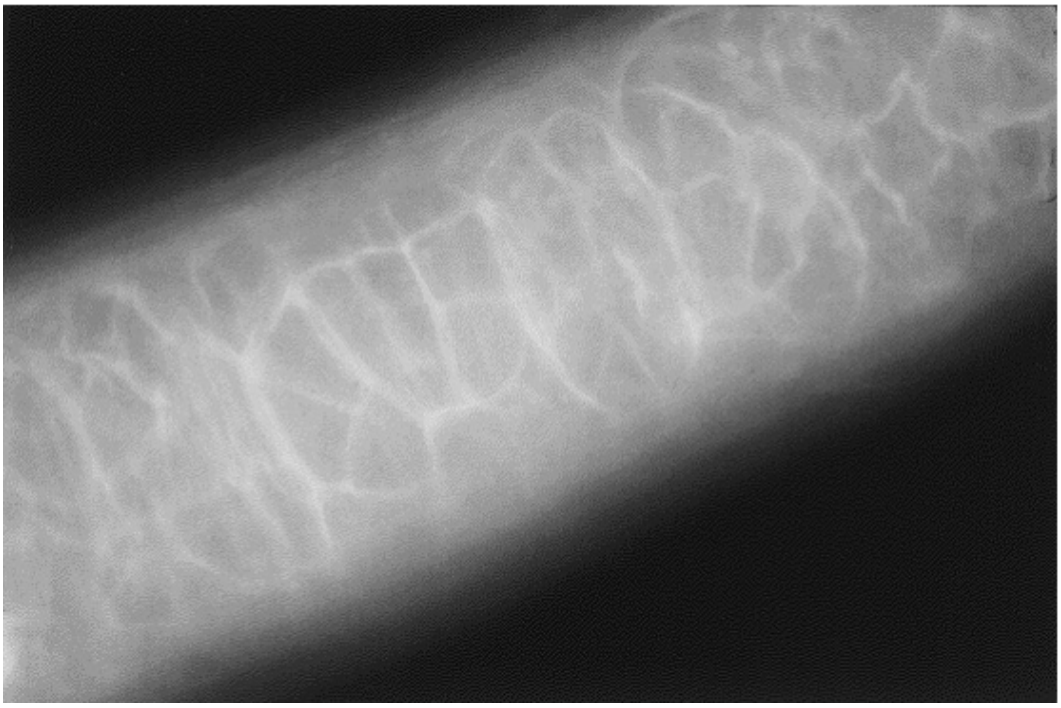

Figure 1.15: A light microscopy image of lamprey branchial cartilage to illustrate autofluorescence of this tissue when irradiated with light at a wavelength of 500 nm . This image is the work of Robson et al [5].

age indicating that the tissues became progressively stiffer (1.18 MPa and 4.85 MPa respectively). The mean modulus for elastin is around 1.0 MPa which is comparable to that of intact annular cartilage but lower than that of pericardial tissue, possibly being accounted for by the surrounding layer of dense collagen fibres in intact tissue. The same study also demonstrated that the lamprey annular and pericardial cartilages are highly viscoelastic, showing time-dependent stress responses to loading, with complete relaxation taking 120 minutes or more. It was suggested by the authors that these long relaxation times indicate low tissue permeability, the reason for which is not clear. There is some evidence to suggest that low permeability may be related to the tissues physiological function, but how this is influenced by tissue structure is not fully understood. It is difficult to relate these material properties to the mechanical properties of the proteins themselves and in the light of this we pursued a more extensive set of mechanical and thermomechanical tests on the four isolated proteins following extraction with cyanogen bromide.

1.6.9.2 Structural Properties

The structural properties of lamprin and lamprin-like proteins from lamprey carti-

lages are poorly understood. The only study that has addressed this issue in any detail is that of Bochicchio and co-workers [59] where conformational analysis of the repeat sequence, GGLGY, of lamprin revealed that PPII, β-turns and β-sheets may co-exist. The results from this investigation showed that the proportion of each of these structures showed variation depending on whether this sequence was in solution or occurred in solid form. The GGLGY repeat sequence forms around 35% of the protein which, when found in solution was concluded to have a highly flexible conformation.

It is a major aim of this current research to determine, by vibrational spectroscopy, the secondary structure of these proteins which, until now, has only been speculated on. This additional structural information together with an increased understanding of their mechanical properties, may assist in the future development of new, novel biomaterials. The following section will briefly discuss the importance of biomaterials, give some examples of elastin-based materials and finally outline the potential benefits of the development of similar materials based on the family of lamprey matrix proteins.

1.7 Elastic Biomaterials

Materials science has in the past focused on the use of materials such as polymers, ceramics and metals. This began to change in the early 1980's when biological materials were introduced into this field of research. By the 1990's biomaterial research had expanded considerably resulting in numerous potential applications, however, they also introduced enormous complexity [261]. Despite the fact that natural, or biological materials, are assembled from a limited number of elements, they are able to form complex structures with a huge range of physical and mechanical properties which have been 'finely tuned' throughout the course of evolution. Biological materials have an enormous range of densities, strengths and stiffnesses with elastic moduli values ranging between 0-001 and 100 GPa. Despite recent advances in technology, levels of complexity associated with biological materials, including their self-assembly, architecture and multiple functions present enormous challenges

to materials scientists in development of new biomaterials. The field of biological materials can itself be divided into several categories i) materials found to occur naturally, ii) biomimetics, which are synthetic materials based on natural materials, and iii) biomaterials that are specifically designed to interact with existing biological systems [261]. This is a rapidly expanding and highly complex area of research and the following section is merely aimed at giving a brief overview of biomaterials with emphasis on elastin-based materials. More detailed information can be found in comprehensive reviews by Meyers [261], Ratner [262], Daamen [118], Martino [263], Chow [264], Li [265] and Nivison-Smith [266].

The nature of biomaterials can take many forms depending on the function for which they are intended. Many of these materials are developed with the view to forming substitutes for biological materials that are able to maintain, restore or even enhance tissue performance/function. Natural materials have the advantage of being bioactive, biodegradable and possess desirable biological properties. However, they are frequently of limited supply, have naturally occurring structural limitations, display large variability, and promote immunogenicity. The development of synthetic biomaterials can address some of these important issues with the potential of being finely tuned to meet specific functional requirements. Disadvantages of synthetic biomaterials include failure to adequately mimic the architecture or bioactivity of the native material and poor interaction with other biological systems. No matter what the source, natural or synthetic, there are many factors that need to be considered before selection or design of a material can occur. Such considerations include the desired mechanical properties, molecular structure, chemical composition, ultrastructure, physical characteristics and degradation time all of which are essential if the biomaterial is to serve its intended function.

1.7.1 Tissue-Engineering

Tissue-engineering is a vast area of research in itself and it is beyond the scope of this thesis to go into any great detail. Therefore the section that follows is intended only to give a brief insight into its potential in elastic tissue repair. For many years tissue-engineering has been regarded as a promising technique for the fabrication

of functional constructs with bio-properties (biological and mechanical) that mimic the native material. The possibility of applying tissue-engineering to elastic tissue repair has naturally been considered for some time, but progress has so far been limited. Despite this, research into this field has continued, fuelled by the possibility of fabricating tailor-made scaffolds that could be used to treat vascular disease or injury.

One approach has been the development of synthetic, 3-dimensional scaffolds that are able to adhere to and regulate cell migration and differentiation as well as synthesize matrix material and direct tissue regeneration. In order to be fully functional, such synthetic constructs must fulfill several requirements, including bio compatibility, appropriate porosity, interaction with invading cells and producing the desired biological response. One major problem experienced in the development of synthetic scaffolds has been the release of degradation products from the polymers used, which in addition to being potentially toxic can also impair function due to reduction in cell attachment and growth as well as decreased elastin synthesis.

A more recent approach has been the development of biological scaffolds for tissue regeneration, utilizing naturally occurring extracellular matrix proteins and other components. This area of research is as yet in its early stages but has the definite advantage of reduced inflammatory response and permitting cell signalling that would be essential in the natural environment. In this respect, the issue of matrix stabilization has to be addressed in a way that avoids alteration of the ECM biochemical or other characteristics by irradiation or similar techniques.

1.7.2 Elastin-Derived Biomaterials and Their Applications

Elastin is known to be a very stable protein, with low turnover and little degradation in healthy individuals. However, injury, increasing age or disease can lead to a reduction in the number of fully functional elastic fibres and impair tissue function. Consequently the need for elastin-based biomaterials has expanded in an attempt to meet the need to replace damaged tissues or provide a scaffold onto which functional extracellular matrix can grow. Some important features of elastin-based materials that make them well suited for the development of biomaterials are their ability to

self-assemble, their long-range extensibility and their durability [118].

The use of insoluble elastin as a potential biomaterial has been severely limited due to it's extreme insolubility as well as problems associated with the transmission of disease. Despite this, several investigations have looked into the potential use of these materials as skin and vascular grafts [267]. In recent years the use of soluble elastin derivatives has become increasingly popular. These may include elastin peptides, fragmentation products and recombinant tropoelastin. The major advantage of using soluble elastin derivatives is that they have desirable intrinsic physical and cell-interactive properties, overcome immune-compatibility complications associated with native tissues, and have the potential to be fabricated into a number of physical forms, including fibres, 3D scaffolds or hydrogels.

Urry and co-workers have made some progress in the development of biomaterials using synthetic peptide sequences based on important amino acid sequences known to occur in elastin including the VPGXG elastin repeat [268, 269, 270, 271]. Many of these peptide sequences are able to self-assemble, coacervate and display mechanical properties very similar to those of the native protein. Tamburro's group have also investigated the structural properties of synthesized glycine-rich sequences, but further investigations would be required to determine their mechanical properties [263]. As well as developing synthetic materials based on the amino acid sequence of single proteins, it is now also possible to form hybrid structures by co-polymerization of sequences from several parts of the elastin sequence, or by combining with elements of other proteins. This has been successfully achieved for synthetic polymers based on the elastin-like sequences combined with spider silk sequences [272], therefore adapting the material's mechanical properties as a result.

Hydrogels are a relatively new form of biomaterial that can take the form of sheets or tubes. They are formed by cross-linking elastin-based peptides to create flexible structures with a range of mechanical properties and porocities which can be modified by adding other proteins, altering the environmental conditions or changing the cross-links [273, 266]. There are a number of benefits to be gained from incorporating elastin into hydrogels, such as the generation of bio-compatible 3D-scaffolds able to support cell growth, differentiation and interaction. Both tropoelastin and

α-elastin have been successfully incorporated into hydrogels to produce materials with mechanical properties very similar to that of native elastin and having the unique ability to absorb 10-1000's times their weight in water [274]. For tissue engineering purposes, some hydrogels can be injected as a solution into the body where they rapidly form a hydrogel that is able to act as a scaffold into which cells are able to grow and interact [264].

Soluble elastins can also be electrospun to form fine fibres [275]. These fibres, ranging from 100 nm to several micrometers in diameter, can then be used in the production of complex 3D- scaffolds which are becoming increasingly popular for tissue engineering applications [276]. Like hydrogels, properties of these scaffolds, such as porocity, can be modified to meet a particular requirement. Another advantage of electrospun elastin fibres is that they can facilitate cellular attachment and have the unique ability to retain intrinsic elastic properties of tropoelastin. Cardiovascular disease is a serious problem worldwide being one of the major causes of premature death, and the potential use of electrospun elastin fibres in treatment of vascular damage looks promising.

Skin grafts are typically used in wound healing and as a treatment for severe burns for which it is common to graft on skin taken from other areas of the patient's body (autograft), from another person (allograft), or from another species (xenograft) [277]. These grafts often have limited success due to complications including organ rejection, transmission of disease and poor compatibility. In an effort to overcome some of these difficulties several alternatives have been expressed including the use of decellularized tissue, which remove the problems of immunological response [118]. Elastin is particularly well suited for this purpose being able to withstand the required extraction treatments [266]. The most promising applications for decellularized tissues are as replacements for arteries, bladder and skin [118]. The main restriction to the use of decellularized tissue is that it is derived from animal tissue and therefore availability of purified material, shape and size are limited.

Purified elastin is prepared from naturally occurring tissue that has been subjected to one of several standard purification procedures to produce an end product that is pure elastin, free from any contaminants. The elastic fibres can be used

to construct scaffolds of various size and shape with properties being modified by the addition of other proteins, e.g. collagen, glycosaminoglycans or incorporating cross-links.

Elastin has a unique structure, chemical composition and mechanical properties which can be incorporated into biomaterials. By exploring similar properties relating to the family of lamprin-like protein it may be possible to exploit these proteins in the development of new, novel biomaterials to provide even greater diversity.

1.8 Synopsis of Thesis

This thesis is structured as follows. **Chapter Two** describes materials, the experimental methods developed and apparatus constructed in this project. It also discusses the methods for determination of secondary structure from Raman spectra whose development constituted a large part of the early work of the thesis. **Chapter Three** describes studies on elastin. Although the molecular structure of elastin has been established, with evidence for alternating hydrophobic and cross-linking domains, exactly how the molecules are organized within the higher-order structure is still not fully understood. One of the principle aims of this study is to address this question using Raman spectroscopy. As previously stated in section 1.5.7, elastic recoil of elastin is driven primarily by entropic factors, although there is some evidence to suggest that enthalpic contributions are also important [24, 200]. As a result several models have been developed to describe this behaviour. In order to select between these models, additional experimental data are required in a number of areas. Some of this will be addressed by means of mechanical testing by investigating the effect of temperature and exposure to different solvents. Raman spectroscopy is used to investigate molecular organization within the elastin fibre and how this changes under conditions of applied load, dehydration, and the effect of solvent interactions and increased temperature. In view of uncertainties that remain concerning the similarity of elastin networks that exist within different tissues and the structural effects of methods of purification, an additional objective of the present study is to compare ligament and aortic elastin isolated by a number of different procedures

described in section 2.1.1. To investigate the differences between elastin fibres and isolated molecules, α-elastin is also analysed by Raman spectroscopy. Structural investigations using various microscopy techniques are included in this present study in an attempt to relate differences observed in mechanical behaviour to the tissues overall morphology, whilst X-ray diffraction is performed on each of the proteins to detect structure at the molecular level. Differential scanning calorimetry is used to determine thermal transitions for each of the proteins in the dehydrated state.

Chapter Four describes work undertaken on lamprey proteins. Much less is known about lamprin and closely-related lamprin-like proteins both in terms of their molecular structure and mechanical properties. In an attempt to better understand the molecular composition, organization and changes associated with applied strain, a large part of this study is directed at applying the same procedures used to investigate the molecular bases of elastin elasticity and the effects of mechanical stress, to this family of proteins.

Chapter Five summarizes the main outcomes and conclusions from the work undertaken in this thesis.

Chapter 2

Materials and Methods

This chapter aims to describe in some detail the materials and methods of purification used in this current study as well as the experimental method by which results were obtained. This chapter begins by describing the tissue sources and the procedures used to isolate the proteins from the intact tissue. This is followed by a section on Raman spectroscopy in which we outline the basic concepts, instrumentation used, experimental set-up and methods of data analysis. This chapter then introduces the principles of mechanical testing, describes the purpose-built apparatus used and the experimental protocols. We then move on to structural investigations describing protocols used for light microscopy observations including, dye injections and autofluorescence, multiphoton microscopy and scanning electron microscopy. Towards the end of this chapter we describe the set-up available for X-ray diffraction measurements. Finally, we conclude Chapter two by describing the system and experimental procedures used for differential scanning calorimetry measurements used to detect the second order glass transition temperature for each of the proteins under investigation.

2.1 Tissue Preparation

2.1.1 Isolation and Purification of Samples

Mature elastin, due to its unique chemical composition and highly cross-linked structure, is generally regarded as the most insoluble vertebrate protein known. The majority of available protocols for extraction or purification of elastin depend on the protein's resistance to attack by protein solvents as well as hydrolysis with

weak acids and alkali [278] or repeated autoclaving [166]. These particular methods of extraction are harsh and therefore only suitable for use on tissues containing large amounts of elastin such as thoratic aorta and ligamentum nuchae. Several alternative purification techniques have since been proposed by various researchers in an attempt to obtain a more 'pure' and less degraded product, as indicated by its amino acid composition. Ross and Bornstein [8], for example, isolated elastin by extraction with cyanogen bromide (CNBr) and by incubation with collagenase. Some of these 'milder' techniques have the disadvantage of producing preparations that can be contaminated by other proteins, but they are still often used in tissues where elastin content is low. The particular method selected depends very much on the required outcome, such as the degree of purity, the presence / absence of microfibrils, or the need to avoid excessive peptide bond cleavage. Elastic fibres are incorporated into the surrounding connective tissue which is highly complex being composed of a combination of other proteins, proteoglycans, fatty tissue and cellular components. For most purposes, elastin can be isolated by the solubilisation and then subsequent removal of the other connective tissue constituents. Comprehensive reviews of the main procedures employed for the isolation of elastin are given in Daamen et al [279] and Mecham et al [280]. The richest sources of elastin are the thoratic aorta and the ligamentum nuchae of grazing animals and it is these tissues that are the most commonly used for isolation of large quantities of elastin. In tissues where less elastin is present, such as in the lung, purification is more problematical [281].The following section outlines the standard procedures used for the isolation of elastin fibres adopted in this project.

2.1.1.1 Protocol 1. Lansing Method [1]

This procedure was used for the majority of investigations in this project where insoluble elastin was required because previous studies have shown that although there is some peptide bond cleavage and therefore a small amount of damage to the elastin network [192, 282] as a result, only limited amino acid alteration occurs leaving a relatively pure product [279, 281]

Bovine nuchal ligament and porcine thoratic aorta were obtained from a local abattoir, and were dissected free from adhering fatty tissue and other connective

tissue. Aortic tissue was prepared by removing surrounding adventitia then cutting it carefully into rings approximately 10 mm in length, taking care to avoid intercostal arteries. Ligamentum tissue was cut into strips measuring approximately 10 mm in width and 30 mm in length. Tissue was then placed into a beaker with $\geq$10 volumes of 0.1M NaOH (Fisher Chemicals), placed into a water bath at 95°C and heated for a period of 45 minutes. Following heating the tissue was allowed to cool to room temperature before being transferred to a refrigerator (at 4-8°C) and repeatedly washed in distilled water until a pH of 7.0 was reached. The tissue remaining after purification was either frozen at -20°C or stored in 0.15 M NaCl (Fisher Chemicals) with the addition of a small quantity of sodium azide to prevent bacterial growth.

2.1.1.2 Protocol 2. Collagenase Digestion With and Without Dithioerythritol (DTE)

This protocol involves extraction of the tissue with 6M GuHCl (guanidine-hydrochloride) which eliminates soluble collagen, proteoglycans and glycoproteins. The tissue is then further treated with collagenase to remove any remaining insoluble collagen. At this stage in the extraction the product that remains contains both amorphous elastin and microfibrils and an additional extraction with DTE (dithioerythritol) is required to remove the microfibrillar component. The method used is based on the original procedure of Ross and Bornstein [8] and further modified by Spina et al [283] to produce a final product free of peptide bond cleavage.

Porcine thoratic aorta were stripped of adventitia and cut into rings approximately 10 mm in length taking care to avoid the intercostals. All the thoratic rings were then placed over glass rods in order to prevent collapse, washed in physiological strength saline and sequentially extracted in; 80% ethanol, 100% ethanol, 2:1 and 3:1 chloroform/methanol and finally diethyl ether to delipidate the tissue. The next stage was performed to remove proteoglycans which involved completely immersing all the samples in 6M GuHCl (Sigma-Aldrich) made up in phosphate buffered saline (PBS) and extracting them for a period of 24 hours at room temperature whilst gently stirring. This process was repeated a further three times. Half of the rings were then extracted twice more under the same conditions and finally washed in PBS (Sigma-Aldrich). For the remaining half of the samples an

additional step was required in order to remove the microfibrillar component. The rings were placed into screw capped tubes with a solution containing 6M GuHCl, 10 mM ethylenediaminetetra-acetic acid disodium salt (EDTA), 50 mM DTE (Sigma-Aldrich) in PBS. This was then degassed and extracted for a period of 24 hours at 37°C under a nitrogen atmosphere whilst gently shaking on an orbital shaker. Again this process was repeated twice more before the samples were washed in PBS. All samples were then treated for the removal of collagen by the following procedure. Tissue samples were transferred to 200-300 ml of 10 mM $CaCl_2$ in 0.1M Tris buffer (Fisher Chemicals) at pH 7.50, degassed at room temperature and left to equilibrate overnight at 4 ° C whilst gently stirred. Following equilibration all the samples were incubated in one volume of this same buffer with the addition of collagenase (EC 3.4.24.3)(Sigma-Aldrich) at a concentration of 1/300 w/w enzyme to substrate ratio at 37 ° C for a period of 24 hours. Fresh buffer was then added and all samples incubated for an additional 24 hours at a 1/600 enzyme to substrate ratio. The collagenase is normally purified from elastase activity by passing it through an elastin column. However, we adapted the process as follows: The buffer solution was made up as specified with the addition of 1/300 or 1/600 of the original weight of the sample of collagenase. A small quantity of powdered elastin was then added to this buffer and incubated at 37°C overnight. The following day the solution was inspected for the presence of elastin. If no elastin powder was visible then the same process was repeated with the addition of more powdered elastin. At the point when a small amount of elastin remained following incubation, the buffer was centrifuged (3000 rpm for 10 minutes) and the insoluble residue discarded before proceeding. All samples were then washed in fresh Tris buffer (pH 7.50) containing 6M GuHCl. Finally the samples were washed repeatedly in 2M NaCl, followed by distilled water and frozen at -20°C until required.

2.1.1.3 Protocol 3: Extraction with Cyanogen Bromide

This method of isolation is based on that of Fernandes [234]. Extraction of the protein relies on the fact that cyanogen bromide hydrolyzes the peptide bond at the C-terminus of methionine residues and because elastin, unlike most proteins, has no methionine residues it remains insoluble whilst other non-elastin components are

digested.

Once samples were dissected free of adventitious tissue they were placed into a solution of 70% formic acid (analytical reagent grade)(Fisher Chemicals) with the addition of cyanogen bromide (CNBr)(Sigma-Aldrich) made up to a concentration of 50 mg/ml. The solution was then bubbled gently with nitrogen for 5 minutes after which all containers were sealed. This preparation was left shaking gently for 18-24 hours at room temperature after which solid residues were transferred to 10 volumes of distilled water and heated at 100°C for 5 minutes to remove any adhering collagen. Finally the insoluble material was repeatedly washed in distilled water and left to soak overnight before storing at 4°C with the addition of sodium azide or alternatively frozen at -20°C until required.

2.1.1.4 Protocol 4: Preparation of α-elastin by Partial Hydrolysis with Oxalic Acid

Due to the extensive covalent cross-linking of elastin, solubilisation can only occur by breaking of the peptide bonds. One of the most frequently used methods is that of Partridge et al [166] which results in the formation of two soluble entities, a- and β-elastin. The average molecular weight of α-elastin is 60-85 kDa whereas that of β-elastin elastin is approximately 5.5 kDa [166]. The following section describes the method we used to produce α-elastin.

Porcine aorta was dissected free of adhering fats and cut into rings whilst avoiding the intercostals and treated with hot alkali following the Lansing procedure in section 2.1.1.1 above. After repeated washing in distilled water the rings of tissue were dried in an oven at 60°C until completely dry and ground with a pestle and mortar. The ground, purified elastin was then transferred into a round-bottomed flask fitted with an air condenser and containing 8 volumes of 0.25 M oxalic acid (Fisher Chemicals). The mixture was heated on a steam bath at 100°C for 1 hour before being rapidly cooled in ice and centrifuged at 3000 rpm for 10 minutes. The supernatant was then carefully poured off and set aside whilst the remaining insoluble residue was re-suspended in 0.25 M oxalic acid and washed in the centrifuge. After washing, the solution was added to the supernatant from the previous spin and set aside. This cycle of heating and centrifugation was repeated a further 4 or

5 times until all the elastin powder had completely dissolved to leave a clear yellow solution. The solubilized elastin was then dialysed in tubing with a molecular cut-off of 12-14,000 daltons (Medicell International Ltd, size 2) against distilled water at 4°C until free of oxalate at pH 7.0. The remaining product was then concentrated in the dialysis tubing by the addition of a thin layer of polyethylene glycol (PEG, average molecular weight of 20000), transferred to vials and frozen at -20°C until required. Alternatively, to produce a dry, powdered form of α-elastin, the concentrated solution was freeze dried for a period of approximately 24 hours until dry, transferred to suitable sealed containers and stored until required.

2.1.1.5 Protocol 5: Isolation of Lamprey Cartilage Structures.

The routine procedure for the isolation of lamprey matrix material involves cleaving of the methionine residues in the surrounding tissue with cyanogen bromide. This method of extraction is successful because the family of matrix proteins forming the lamprey endoskeleton, like elastin, has no or very few methionine residues and therefore remains intact.

Whole river lamprey (Lamperta fluviatilis) were decapitated behind the last gill slit and autoclaved for 20 minutes at 12 psi followed by gross dissection of muscle and flesh. The remaining tissue was treated as described in section 2.1.1.3 above, after which the insoluble cartilagenous structures were stored in a refrigerator until required. The cartilagenous components that remain intact following treatment with cyanogen bromide are shown in figure 2.1 and are as described by Robson et al [5].

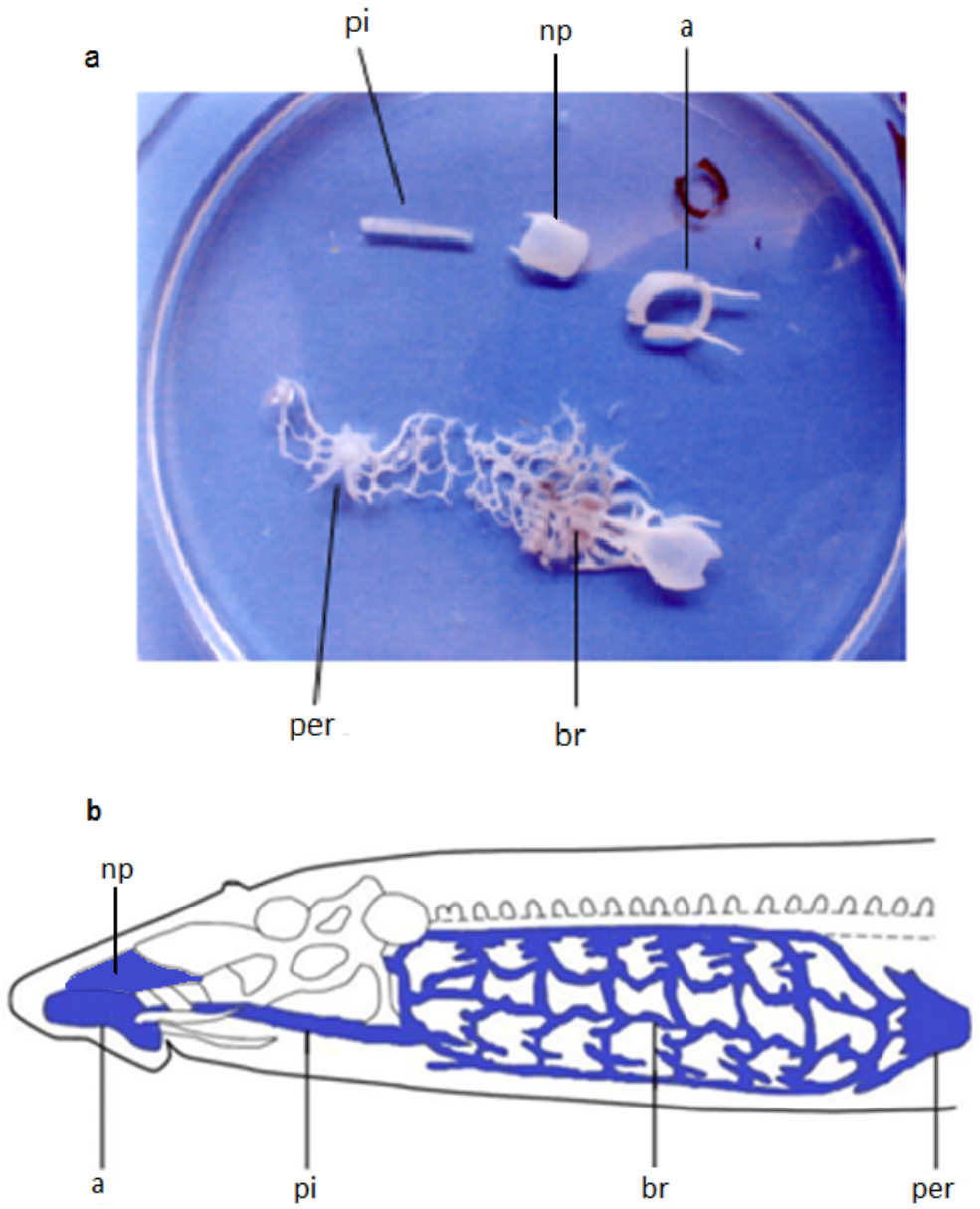

Figure 2.1: Image of a) the insoluble lamprey matrix material after extraction with cyanogen bromide (see section 2.1.1.3) and b) schematic diagram of the lamprey skeleton based on [254]. The arrows indicate the four structural elements of interest in this study; the piston (pi), the annular disc (a), the branchial basket (br) pericardial sac (per) and nose plate (np)..

2.2 Raman Spectroscopy

In this section a brief outline of the major advantages and disadvantages of Raman spectroscopy compared to other techniques of structural analysis is given. This is followed by a short section on the principles underlying the Raman effect. A major objective of this study was to detect changes in protein structure following the application of mechanical strain as well as by altering the local environment. We therefore describe the Raman spectrum of proteins, explain the methods used for

processing the data and analysis of complex bands within the spectrum in order to gain information on secondary structure composition and water interactions. Finally we describe the various experimental conditions employed.

2.2.1 Why Use Raman Spectroscopy?

Raman spectroscopy is a technique that provides information about molecular vibrations. Despite its discovery in the 1920's Raman spectroscopy has only become popular as an analytical tool in more recent years due to rapid advances in technology, which as a result led to greatly improved instrumentation that could be used in most laboratories without the need for highly trained experts. Raman spectroscopy is frequently used in conjunction with infrared (IR) spectroscopy to provide complementary information, since these techniques are sensitive to different aspects of molecular structure. Vibrations that are strong in IR tend to be weak in Raman and vice versa. Raman spectroscopy has several advantages that make this technique attractive compared to other analytical techniques. These advantages include:

1. rapid spectral acquisitions
2. the provision of both quantitative and qualitative information
3. the provision of complementary information to techniques such as infrared spectroscopy
4. the need for little or no sample preparation
5. the need for only small sample volumes
6. the process is non-destructive
7. there is minimal interference from water, eliminating the requirement for sample dehydration. This is particularly important when studying biological materials.
8. that spectral acquisition is possible through glass

These advantages together with technological advances have made Raman spectroscopy an invaluable analytical tool, with diverse applications in the pharmaceutical industry, forensics, materials science, chemistry, geology and in the clinical

detection of certain diseases. Raman spectroscopy, as promising as it is, still has a number of associated disadvantages including:

1. strong interference from intrinsic fluorescence
2. a weak Raman signal
3. sample damage caused by intense laser radiation
4. the difficulties of peak attribution in complex spectra

2.2.2 Fundamentals of Raman Spectroscopy

The phenomenon of Raman scattering was first observed experimentally more than 80 years ago (in 1928) by Sir Chandrasekhra Venkata Raman using focused and filtered sunlight as the source of incident light, a telescope as a collector and the eye as a detector. From these experiments he discovered that when monochromatic light interacts with molecules, the scattered light contains a small component which is frequency shifted. These shifts in frequency correspond to specific molecular vibrations, the combination of which are specific for each type of molecule. In recent years there have been enormous developments in Raman spectrophotometers which has led to renewed interest in this technique. In the early 1960's laser sources were developed which transformed the field of Raman spectroscopy by providing monochromatic light sources of high intensity and small beam size, meaning that sample volumes could be reduced significantly. Commercial systems soon became available as important analytical and research tools in many laboratories due to advances in imaging, digital acquisition, filters, holographic gratings, improved detectors and computer technology.

Raman spectroscopy is a form of vibrational spectroscopy and is frequently used in conjunction with infrared (IR) spectroscopy. Raman differs from IR in that information is derived from scattering of light whereas IR is a light absorption process. These techniques provide valuable and complementary information regarding molecular structure and vibrational modes. Vibrations that are strong in Raman spectroscopy tend to be much weaker in IR, and vice versa.

When high power monochromatic light is focused onto a molecule it can either pass through unchanged, or can interact with the molecule in a number of ways un-

dergoing absorption (as in IR), reflection or scattering. These interactions can lead to excitation of the molecule which temporarily raises the energy of the molecule to a higher energy 'virtual' state. Relaxation from this virtual state by release of a photon occurs almost immediately because it is an unstable state, and if the molecules return to exactly the same energy level from which they were excited then the emitted photon's energy (and also wavelength) is unchanged from that of the incident photon. This is referred to as elastic scattering (or Rayleigh scattering) and forms the dominant process. However, if on relaxation the molecule returns to a higher or lower vibrational state, then the emitted photon has less (Stokes) or more (anti-Stokes) vibrational energy respectively, which is associated with a corresponding frequency shift to longer or shorter wavelengths. The intensity of inelastic (Raman) scattering is much weaker (typically 10^{-6} the incident light intensity) [284] than elastic scattering and most frequently occurs as Stokes scattering. Figure 2.2 shows schematic energy level transitions involved for Rayleigh scattering, Raman scattering and infrared absorption processes. The selection rules differ for Raman and IR, with Raman requiring a change in the polarizability of the vibrating molecule, whilst IR depends on a change in the electric dipole of the molecule. Because of this, the Raman activity and IR activity of a given vibrational mode can differ significantly.

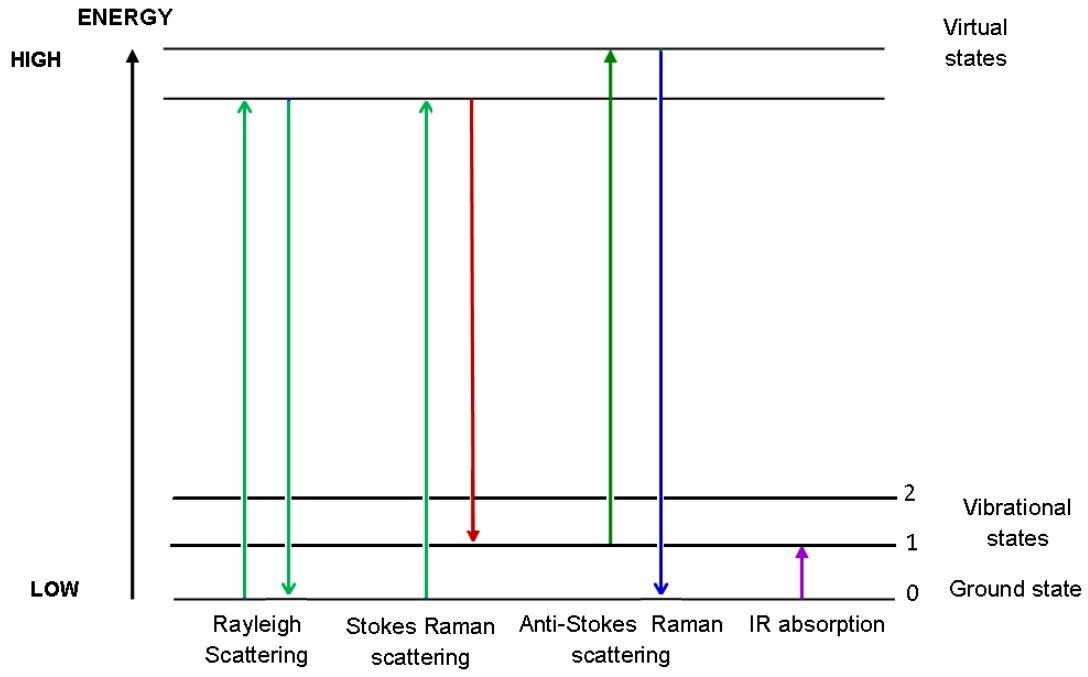

Figure 2.2: Energy diagram for Rayleigh scattering (elastic), Stokes and anti-Stokes Raman scattering (inelastic) and infrared absorption

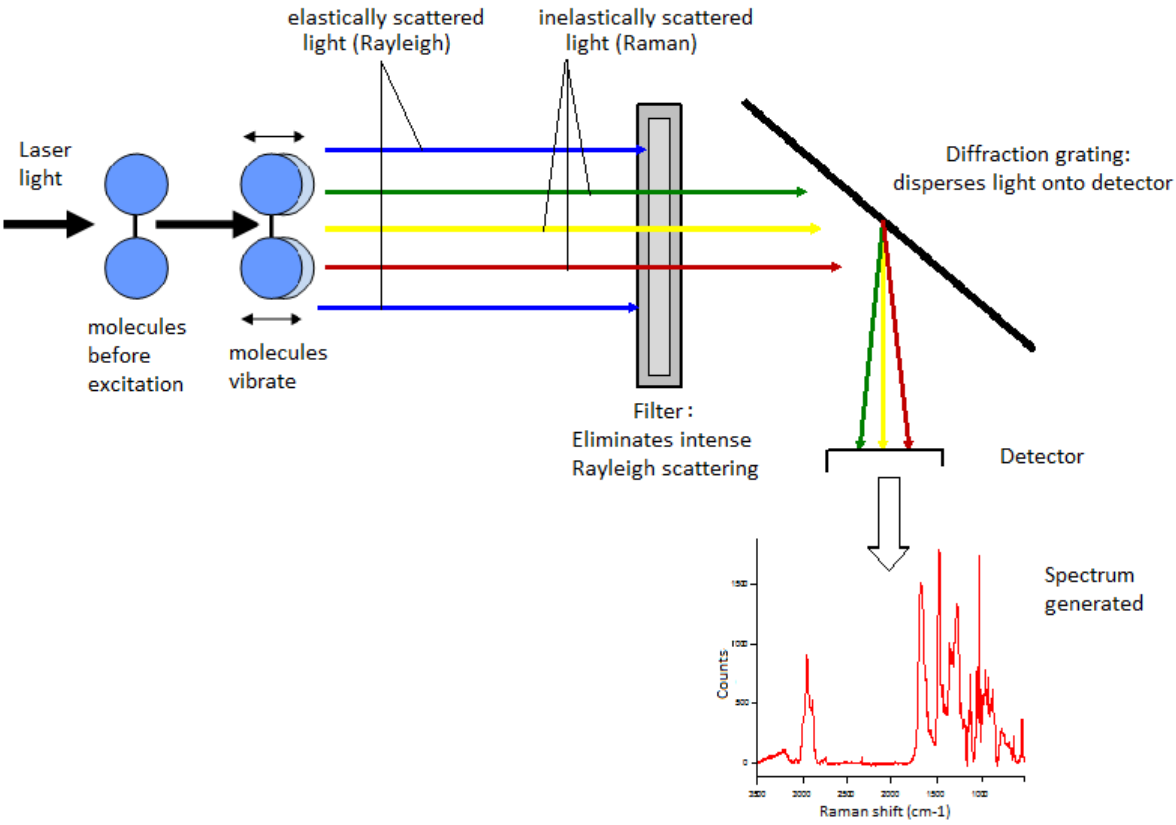

Figure 2.3: Diagrammatic representation of the basic concept of spontaneous Raman scattering: When laser light interacts with a material some of the light is scattered. Of this scattered light ≥99% has the same frequency as the incident light (Rayleigh scattering), whilst only a small fraction has a different frequency (Raman scattering) resulting from small changes in molecular configuration, or in vibrations. Notch or edge filters remove Rayleigh scattered light and the diffraction grating disperses the Raman scattered light onto a detector, which generates the Raman spectrum.

Raman scattered light can be collected by a spectrometer and viewed as a spectrum, which is a plot of scattered light intensity as a function of the energy difference between the incident and scattered photons, measured in wavenumbers (cm^{-1}). This is shown schematically in Figure 2.3. The positions of Raman peaks are independent of the excitation wavelength, but the greater the number of Raman scattering events for a particular vibrational mode, the greater the peak intensity will be [284]. In addition, the more energy that is needed to produce a disturbance within a molecule the larger the Raman shift will be. The energy is used to initiate a change in the conformational shape of the molecular bonds by initiating molecular vibrations such as stretching or bending. Molecules cannot be regarded as static, but instead undergo continuous movements. Chemical bonds associated with each molecule have a unique set of molecular vibrations which are highly dependent on the molecu-

lar structure, environment, degree of hydrogen bonding and atomic mass and can involve a change in either bond length (as in 'stretching') or a change in bond angle. Stretching motions can be symmetric or asymmetric, whilst bending (often referred to as deformations) can be further divided into wagging, twisting, rocking and scissoring motions. Some of these molecular vibrations are shown schematically in Figure 2.4. Each of these molecular vibrations occurs at a specific frequency and therefore provides a highly specific 'fingerprint' for each molecule. In this way a Raman spectrum of groups of molecules is able to provide information on molecular structure, composition and conformation.

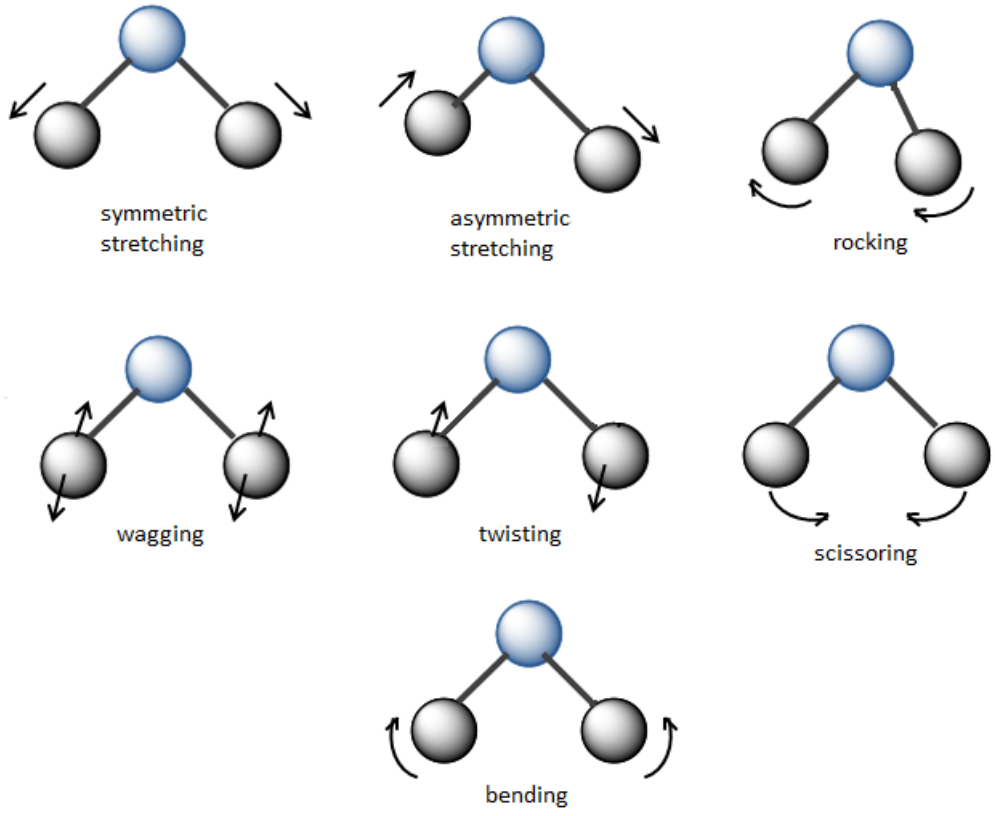

Figure 2.4: Schematic representation of various types of molecular vibrations detected by Raman spectroscopy.

2.2.3 The Protein Spectrum

Proteins are large, complex molecules consisting of numerous amino acids resulting in highly complex Raman spectra which are difficult to interpret. Nevertheless, investigations into protein structure using Raman spectroscopy have been performed for more than three decades leading to the recognition of several specific spectral characteristics. These include the protein backbone vibrations arising from amide

I and amide III bands [285]. These bands generally give rise to intense peaks that are dominant in the protein spectrum.

The amide I band originates from C=O stretching and appears in the Raman spectrum at around 1600-1700 cm^{-1} [286]. This band is known to be very sensitive to conformational changes and has traditionally been used to provide a measure of secondary structure compositions in proteins. The amide III band occurs at 1200-1300 cm^{-1}, represents N-H in plane deformations and again can be used to interpret protein structure, but this mode is generally regarded as being less sensitive to conformation than the amide I band. Another amide band frequently identified in proteins and other biological samples is the amide II band, which arises mainly from N-H bending with some contribution from C-N and C-C stretching. This amide band is generally much weaker than the amide I or amide III bands and occurs between 1510-1580 cm^{-1}. The amide I and amide III bands are particularly useful, being conformation-sensitive, and they therefore provide structural information from the protein backbone vibrations. However, the vibrations of the side-chains can also provide additional information on the amino acids and the side-chain environment [287]. Figure 2.5 illustrates the basic structure of the amide (peptide) bond and its interaction with the α-helix, β-turn and β-sheet. Another region of considerable interest is the broad band between 3000-3600 cm^{-1} which provides information on rearrangements of the water hydrogen-bond network under varying conditions [7].

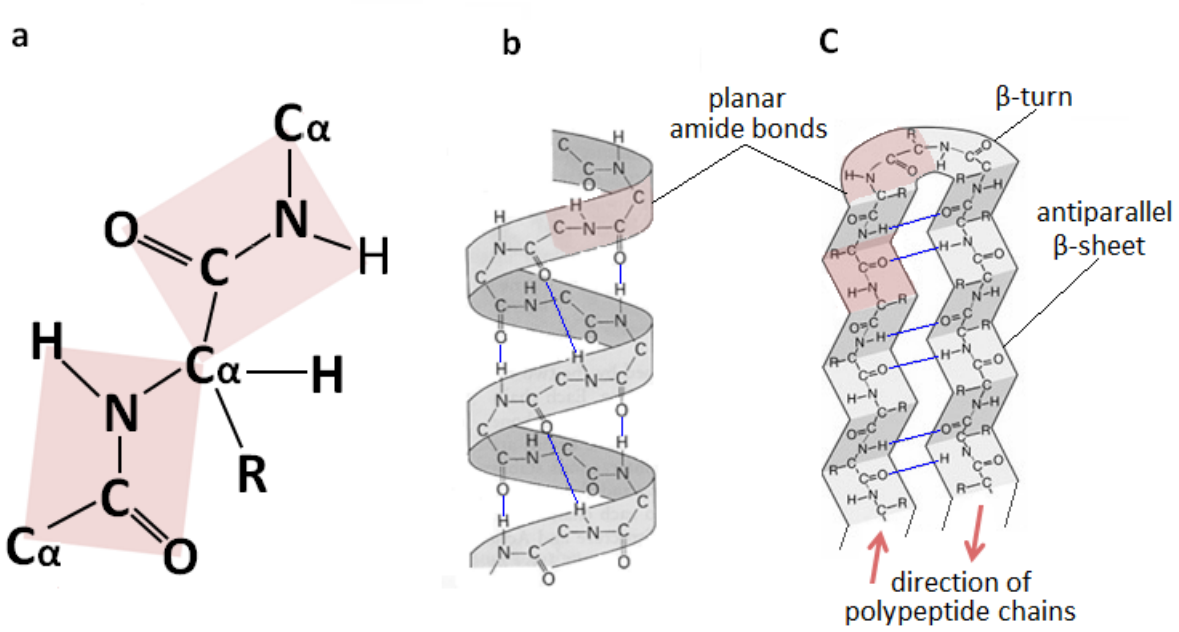

Figure 2.5: Models representing the arrangement of (a) the amide (or peptide) bond, (b) right-handed α-helix and (c) the β-turn and antiparallelβ-sheet. The shaded areas illustrate the interaction of the planar amide bond with each of these secondary structures whilst hydrogen bonds between C=O and N-H groups that serve to stabilize the structures are represented by blue lines. Images adapted from [288].

Raman spectra are both qualitative and quantitative and so it follows that information can be deduced both from peak positions and also from the relative peak intensities. Peak intensity varies relative to concentration, but is also dependent on other factors such as the nature of the bond vibration. For example, a stretching mode is more intense than an angular deformation. In addition, bonds which stretch in phase are more intense than those that stretch out of phase [289].

One of the main problems associated with Raman spectroscopy of biological samples is that of fluorescence. However, this problem can be significantly reduced by the use of near infra-red lasers [290], since fluorescence decreases rapidly at longer excitation wavelengths. Another problem frequently encountered in biological samples is that of heating caused by high power lasers and therefore the possibility arises of burning, leading to permanent sample damage. This is especially problematic for dark-coloured materials with a tendency to absorb much of the incident energy which has the end result of localized heating effects.

2.2.4 Instrumentation

In order to acquire Raman spectra with macroscopic spatial resolution the sample

must be placed at the focal point of a focused laser. This is achieved quite easily by coupling a research grade optical microscope to the Raman spectrometer. Excitation is accomplished by directing monochromatic laser light onto the sample using an epi-illuminated microscope set-up whereby the objective lens both focuses and collects the scattered light, which is then directed through a notch / edge filter to suppress unwanted elastically scattered light. Inelastically scattered light then passes to a diffraction grating allowing the beam to be split into constituent wavelengths which are finally directed to a CCD. The resulting Raman spectrum is a plot of intensity against Raman shift /cm^{-1}(the difference in wave number between the incident and the observed frequency) with peak positions being related to the vibrational mode at a particular frequency. A labeled schematic diagram of the Raman microspectrometer setup used is shown in figure 2.6. A major advantage of the Raman microspectrometer over classical Raman systems is that the focal volume is very small (typically around 10 μm^3), which also assists in reducing the influence of Raman scattering from the surroundings.

Spectra were obtained using a Renishaw Raman Systems RM1000 spectrometer (Renishaw, Wooton-Under-Edge, UK) equipped with a near infrared diode laser, emitting at 785 nm and giving a laser power at the sample of $<$ 200 mW. This wavelength was chosen to minimize interference from tissue fluorescence. A variety of objective lenses were available for use of which the 40$\times$ / 0.55 NA or 50$\times$ / 0.50 NA objectives were employed, giving a sampling area $<$10 μm^2. A photograph of the Renishaw Raman system is shown in figure 2.7. Spectra were generally acquired over the range 4000 to 500 cm^{-1} using 100% power for 3 successive scans with 20 s exposure per detector pixel to give an overall exposure time of approximately 15 mins per scan. This level of radiation was found not to affect the structure of the samples. The exceptions to this were for dehydrated lamprey samples where laser power was reduced to 10% in order to prevent sample damage. For each sample a minimum of 8-10 measurements were made at separate locations. Prior to each set of measurements a frequency calibration was performed against the 521 cm^{-1} line of silicon.

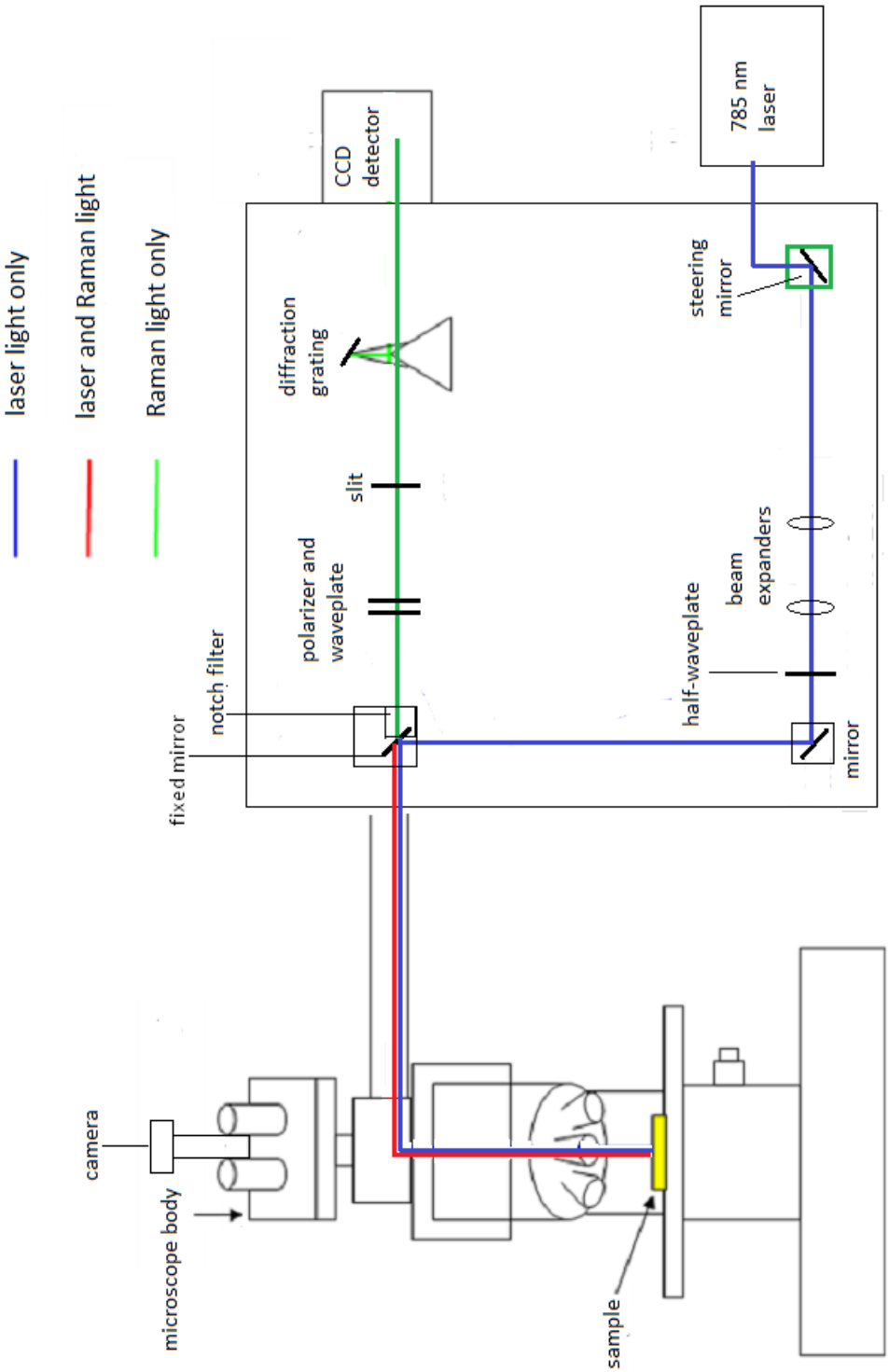

Figure 2.6: Schematic diagram of the Raman instrumentation used for spectral acquisition. The excitation source was provided by a 785 nm NIR diode laser in order to minimize fluorescence. Laser light was focused onto the sample using a conventional microscope. Backscattered light was collected by high numerical aperture objective lenses, passed through a holographic notch filter which separated elastically scattered light from inelastically scattered light and onto a diffraction grating (1200 lines/mm) before the Raman scattered light was finally passed on to a CCD. The instrument was also fitted with a polarizer and waveplate before the entrance slit of the spectrometer to permit polarization measurements to be made.

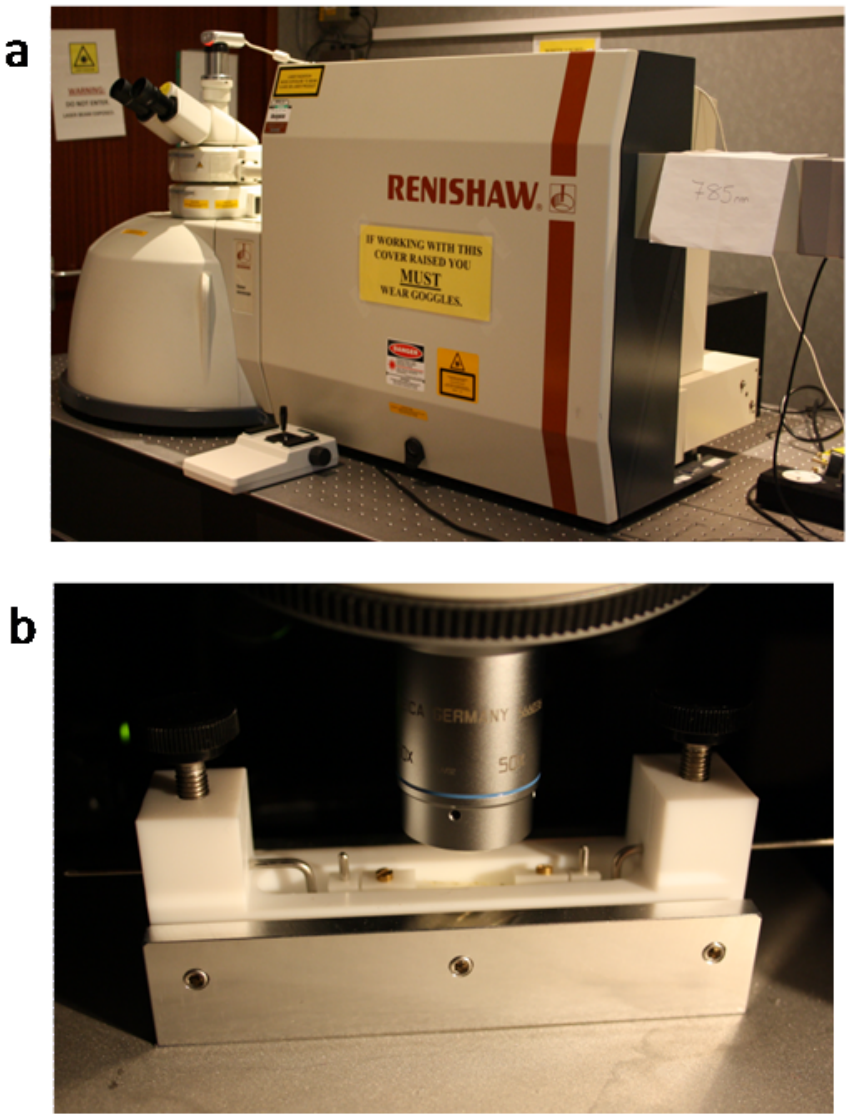

Figure 2.7: Images of the Raman system and sample set-up used for spectral acquisitions. a) Photograph of the Renishaw RM1000 Raman system equipped with a 785 nm laser source. b) A purpose constructed apparatus employed for the acquisition of Raman spectra in various bathing solutions or under a prescribed strain.

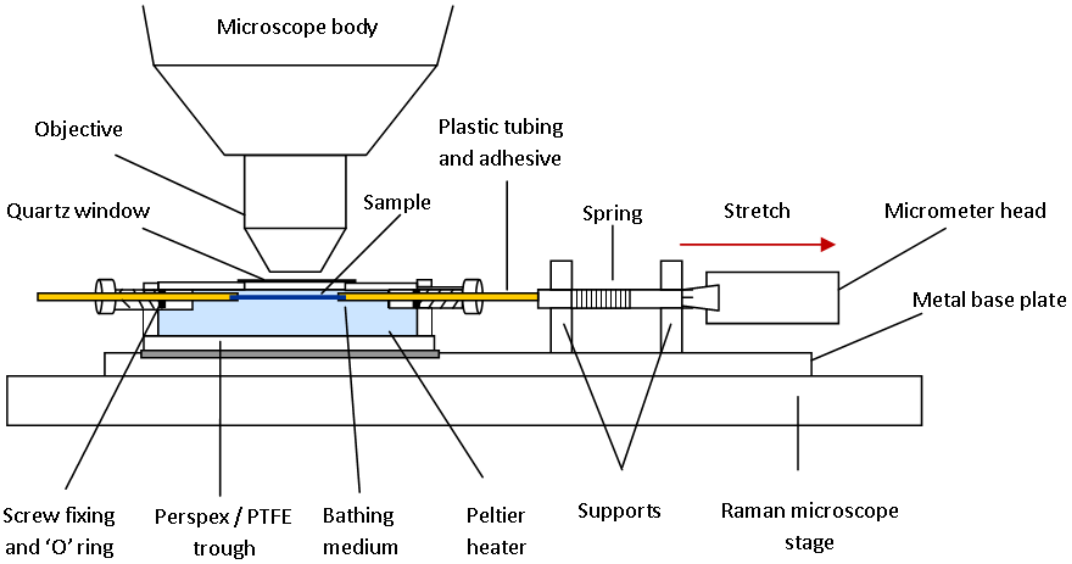

Figure 2.8: Schematic representation of the purpose built stretching apparatus for use in the Raman microspectrometer

2.2.5 Sample Set-Up

For measurements on hydrated samples, small bundles of fibres from nuchal ligament, thin rings of aortic elastin or strips of lamprey cartilage were attached with Kwik Cast adhesive (World Precision Instruments Ltd, UK) to nylon supports in a Perspex/PTFE trough (approximate dimensions 3.0 × 0.5 × 0.5 cm in depth), fitted with a quartz coverslip. Samples could then be immersed into a given solution and could be subjected to graded strains of up to 100% using an attached micrometer head. The temperature of the bathing solution was thermostatically controlled in the range 20-60°C using a Peltier heater (Dura Tec high power heat pump, 71watt heat capacity). Two additional series of measurements involved replacing water with deuterium oxide (Sigma-Aldrich) or TFE whilst held at constant 20% extension. For the TFE measurements a trough constructed from PTFE was used and samples were mounted using PTFE clamps so as to avoid dissolving the adhesive. In a final set of measurements, samples were mounted in deionised water, strained by 60% of the original length and allowed to dehydrate whilst extended for a period of approximately 72 hours. Figure 2.8 shows a schematic diagram of the custom built apparatus and Figure 2.7 the actual instrument.

The polarization of Raman scattered light can provide additional, valuable information regarding molecular orientations. We measured this by acquiring polarized spectra for all combinations of polarization of the incident and scattered radiation as shown in figure 2.9. We corrected for the polarization sensitivity of the instrument using an isotropic film of α-elastin deposited on an aluminized cover slip. Polarization (parallel or perpendicular) of the incident laser light was achieved by changing the direction of a half wave plate, whilst the insertion of a polarizer before the entrance slit permitted detection of the polarized scattered light. The use of an additional half wave plate inserted into the incident laser path allowed the four measurements to be acquired sequentially on the same point in the sample eliminating the need for physical sample rotation.

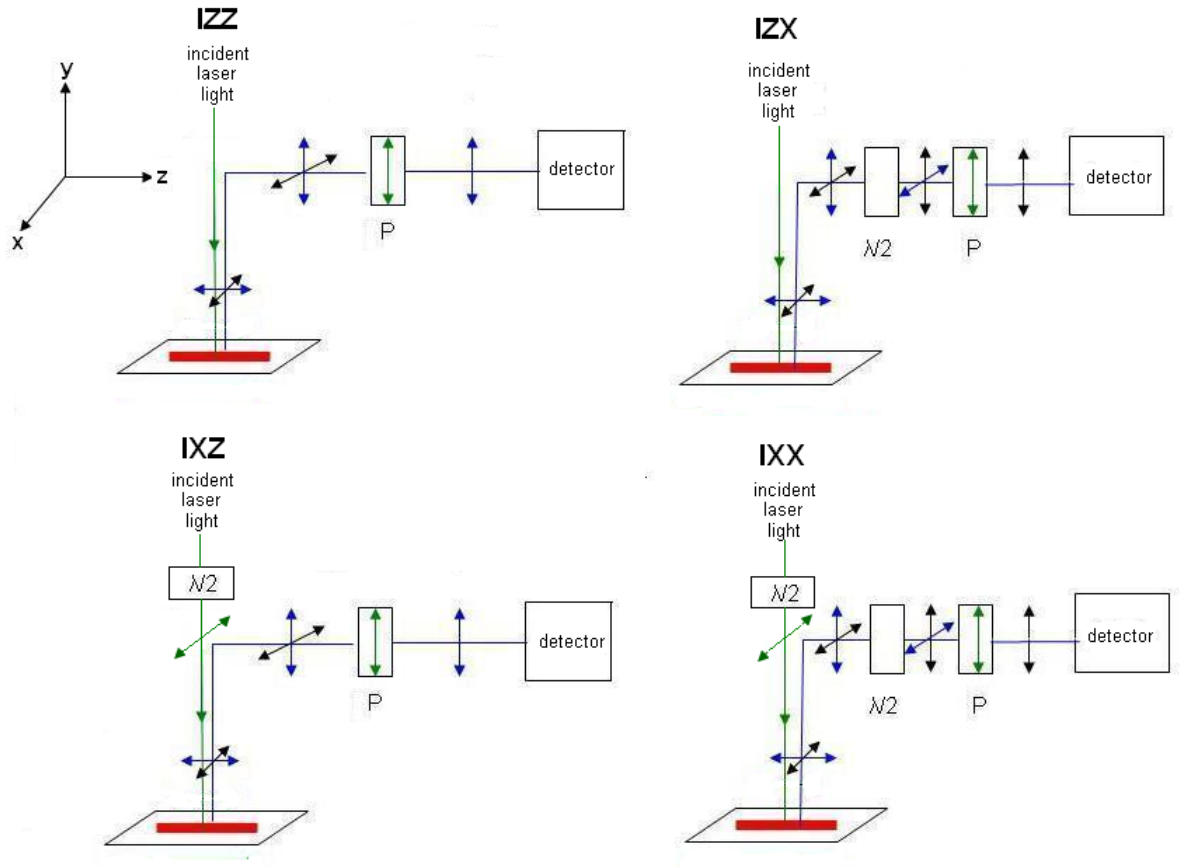

Figure 2.9: Schematic diagram representing the combinations of polarization of the incident and scattered radiation. The sample was not physically rotated, instead a half wave plate was inserted into the incident laser path to allow measurements to be made sequentially on the same point of the sample. By acquiring spectra from the four combinations of polarization shown, it was possible to calculate the polarization ratio for selected spectral features.

2.2.6 Raman Spectroscopy Data Analysis

2.2.6.1 Amide I and Amide III Band Analysis

Qualitative analysis of secondary structure composition within proteins has been discussed and debated for some time. Of particular importance are the amide I and amide III bands which have traditionally been deconvolved into several component peaks representing the vibrational modes of the individual secondary structures (α-helix, β-turn etc), to provide an estimate of secondary structure composition. A number of alternative methods involving spectral decomposition have been developed and with this goal in mind we conducted a comparative analysis of several methods which will be discussed in detail in the following section.

Between 60 and 200 spectra obtained as described in sections 2.2.4 and 2.2.5 were averaged using Grams/A1 software (Thermo Galactic) which was also used for second derivative analysis. Peak fitting was done using WiRE^{TM} 2.0 (Renishaw, Wootton-Under Edge, UK). Extracting structural information from the peak fitting poses two interrelated problems: i) correction for background arising from fluorescence and other sources and ii) attributing peaks to particular structural motifs. The first step of data manipulation to remove background fluorescence involved fitting a cubic spline baseline to the whole spectrum, passing through points where no peaks were expected. This process can be seen in Figure 2.10. For hydrated samples a water and quartz spectrum was subtracted prior to applying the baseline and this is shown in Figure 2.11. Processes such as smoothing of raw data were kept to a minimum by using large numbers of individual spectra.

We first investigated the Reference Intensity Profiles (RIP) Method of Berjot et al [6] using reference spectra for α-helical, β-sheet (parallel and antiparallel) and undefined (reverse turn and non-repeating) structures taken from proteins with known structures. In order to determine the secondary structure composition of the amide I band using these Reference Intensity Profiles a linear baseline was fitted to averaged spectra across a narrow window from 1800-1500 cm^{-1}. Following this, RIP were constructed individually for α-helix, β-sheet and unordered structures using the parameters given by Berjot et al [6] (see Figure 2.12) and these parameters were then used to seed the curve fitting process in order to determine secondary structure

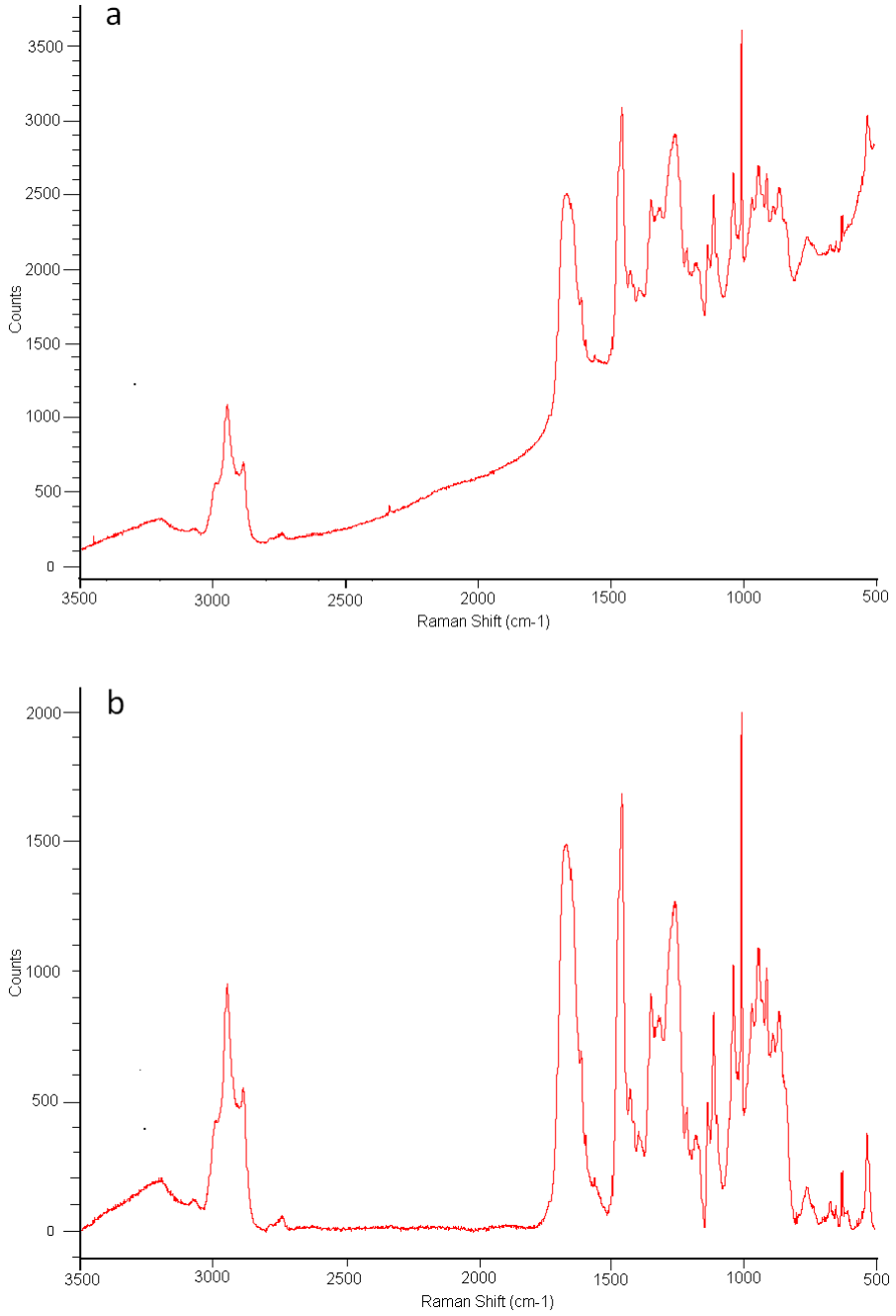

Figure 2.10: Averaged spectrum for fully hydrated nuchal elastin fibres, a) before fluorescence background subtraction, and b) after the application of a cubic spline baseline fitted to the whole spectrum where no peaks were expected. The points used for fitting the baseline were 4000, 3600, 2810, 2400, 2200, 2000, 1800, 1146, 810, 585 and 500 cm^{-1}

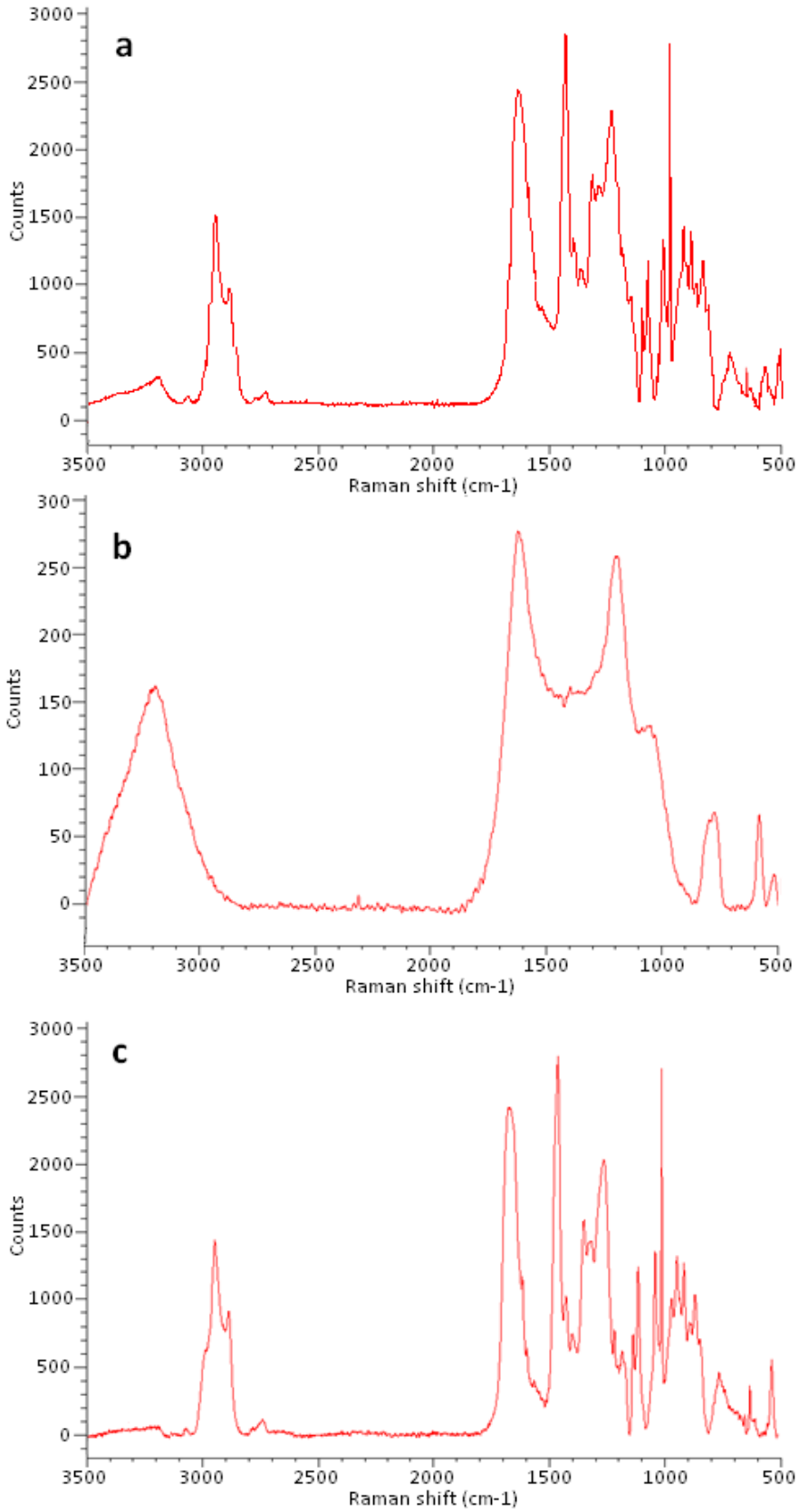

Figure 2.11: Raman spectra to show the effect of bulk water and quartz subtraction for fully hydrated aortic elastin; a) raw elastin spectrum, b) water and quartz spectrum, and c) result of subtracting water / quartz from original elastin spectrum.

composition of the amide I band.

We found that this method of analysis did not fit the data under all conditions and it has been criticized by others because it is likely to underestimate overlapping spectral components and, by restricting the analysis to the region between 1630 cm-1 and 1700 cm-1, it is difficult to account for the effects of neighbouring aromatic peaks [291]. We found that the fit could be improved by adding two additional peaks centred at 1609 and 1587 cm^{-1} which do indeed correspond to two side chain attributions. Moreover, no contribution is included in this method for either β-turns or β-spirals despite the fact that these structures are believed to form an important part of elastin's molecular structure. Using the RIP method we found that, for dry fibrous elastin, there would be 75% β-structures, 8% unordered structures, and 17% α-helices. This is in agreement with data of Debelle et al [204] who estimated 63% $\pm$ 17 β-sheets; 13% $\pm$ 13 β-turns; 6% $\pm$ 6 unordered structures; and 18% $\pm$ 5 α-helices. However, these values disagree with more recent work by the same author [292] who predicted 45% β-structures, 45% unordered structures, and 10% α-helices. Neither do our results agree with that of Berjot et al [6] who gave 21% β-structures, 44% unordered structures, and 35% α-helices. For hydrated specimens we found it necessary to include a contribution from bound water using two 50% Gaussian, 50% Lorentzian peaks centred at 1630 cm^{-1} and 1645 cm^{-1}, band widths not fixed. We then found 85% β-structures, 3 % unordered structures, and 12.0 % α-helices. There are several possible reasons for the differences observed between our results and those of Debelle and Berjot including: the use of pure peptides representing each of the secondary structures, and their use of a complex baseline fitting procedure whereby the protein spectrum is reconstructed from the individual amino acid spectra in order to determine points of minimum intensity. We were unable to resolve these discrepancies and therefore undertook an alternative amide I analysis protocol which was performed on the same datasets as used for the RIP method described above.

The second method used to curve fit the amide I band was based on the procedure described by Maiti et al [2] for native unfolded proteins. This fitting routine involved fitting a two point baseline to the averaged data from 1590-1720 cm^{-1}, following sub-

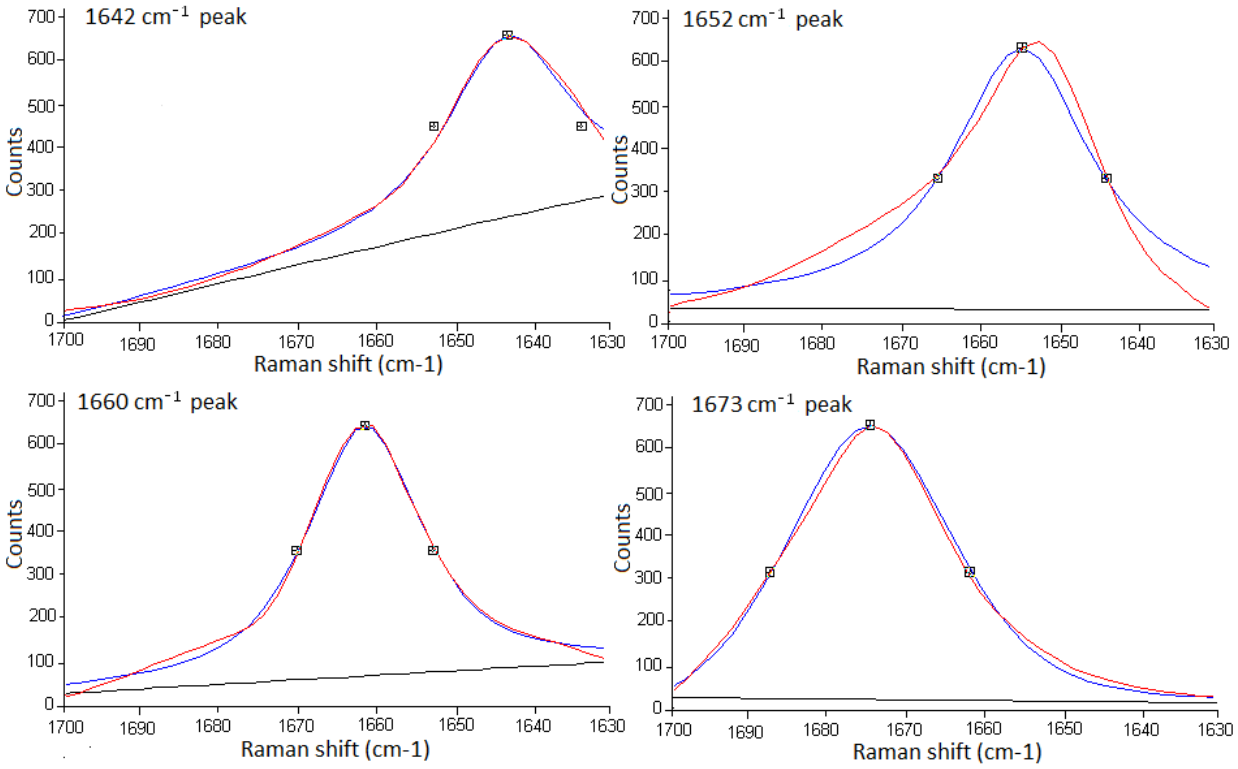

Figure 2.12: Amide I band reference intensity profiles for α-helices (1642 and 1652 cm^{-1}), β-sheet (1673 cm^{-1}) and undefined structures (1660 cm^{-1}) reproduced in WiRE^{TM} software following the frequency and intensity values as specified by Berjot et al [6]. Original data (red line), the fitted spectrum (blue line) and baseline (black line) are shown.

traction of water where applicable. We then fitted three component peaks centred between, i) 1650-1656 cm^{-1}(representing α-helix), ii) 1664-1670 cm^{-1}(β-sheet), and iii) 1674-1685 cm^{-1}(attributed to extended β-strand and PPII). These three amide component peaks were of mixed Gaussian/Lorentzian profile and band width half height (BWHH) was restricted to 25 $cm^{-1}\pm$ 5. It was also found necessary to add a single water peak between 1630-1635 cm^{-1}(in hydrated tissue) and two peaks representing side-chain aromatics at 1605 cm^{-1} and 1619 cm^{-1} in order to improve the overall fit. As in the RIP method described previously, this three component method of analysis does not produce a satisfactory fit to the amide I band for either elastin or the family of lamprey matrix proteins, particularly at the higher wavenumbers. In an attempt to achieve a better fit to our spectra we then undertook an additional, more complicated curve fitting routine based on the procedure of Williams [12] and later refined by Sane et al [3].

In this method the amide I band was analysed between 1800 $cm^{-1}$and 1500 cm^{-1} after fitting a two point baseline across this window and the bulk water and quartz spectrum subtracted. Grams software was then used to perform a second derivative analysis for each of the averaged spectra. For elastin fibres this revealed eight amide I components at ~ 1712, 1685, 1678, 1670, 1664, 1654, 1642 and 1630 cm^{-1} and others associated with side chain vibrations at 1620, 1607, 1588 and 1557 cm^{-1}. The second derivative result for fully hydrated nuchal elastin fibres is shown in figure 2.13. The peak arising at 1630 cm^{-1} was associated with bound water although a second peak at 1640 cm^{-1} has also been assigned to water by Sane et al [3]. The information from the second derivative analysis compared favourably with the peak positions of Sane et al [3] (see table 2.1) and was then used to construct a curve fitting routine. Peaks were fitted with 50% Gaussian and 50% Lorentzian functions, although using pure Gaussian did not significantly alter the quality of the fit. The peak centres were allowed to float by $\pm$ 5 $cm^{-1}$and the width was unconstrained. A minimal number of additional peaks, which were attributed to side chain vibrations in the 1630-1550 cm^{-1}region were added to improve the fit. The individual bands determined by this procedure were close to those obtained by Sane et al [3] and this guided the attribution which were as follows: α-helices were represented by a single

Peak Centre (cm^{-1})	Sane *et al* attribution [a]	Peak Centre (cm^{-1})	Our Experimental data
1714	unordered	**1712**	unordered
1693	β-turn	**1702**	unordered / β-turn
–		**1688**	β-turn
1685	β-turn	**1685**	β-turn
1678	unordered	**1677**	unordered
1671	unordered + sheet	–	
1664	unordered	**1664**	unordered
1657	β-turn	–	
1655	α-helix	**1654**	α-helix
1650	unordered + sheet	–	
1645	water	**1643**	water or unordered
1641	unordered	**1640**	unordered
1630	water	**1631**	water
1615	side chains	**1620**	side chains
1604	side chains	**1608**	side chains
1597	side chains	**1596**	side chains
–		**1588**	side chains
–		**1574**	side chains
–		**1568**	side chains
1585	side chains	–	

[a] Sane et al (1999) Anal Biochem J, **269** , 255-272

Table 2.1: Amide I peak centres and attributions according to Sane et al [3] compared to second derivative analysis of our experimental data

band centred at 1654 cm^{-1}, β-turns by three peaks located between 1685 and 1702 cm^{-1}. Peaks at 1642-1640 $cm^{-1}$and 1663 cm^{-1} as well as minor peaks at 1677 and 1712 cm^{-1} were taken to represent unordered structures. However, the attribution of peaks to unordered helices, parallel and anti-parallel β-sheets is ambiguous [3] and because of this in our results these structures were pooled together although we realize that this is cited as a criticism of the approach by some authors. Bound water was represented by a single peak at 1630 cm^{-1} whilst the aromatic residues, phenylanaline and tyrosine, were fitted with four peaks between 1578 cm^{-1} and 1620 cm^{-1}. The same procedure was performed on data for each of the lamprey matrix proteins which showed strong correlation both with each other and with fibrous elastin. All the peaks detected in elastin amide I were also found in the amide I region of the family of lamprins. The only difference was a slight shift in peak position by $\pm$ 3 wavenumbers.

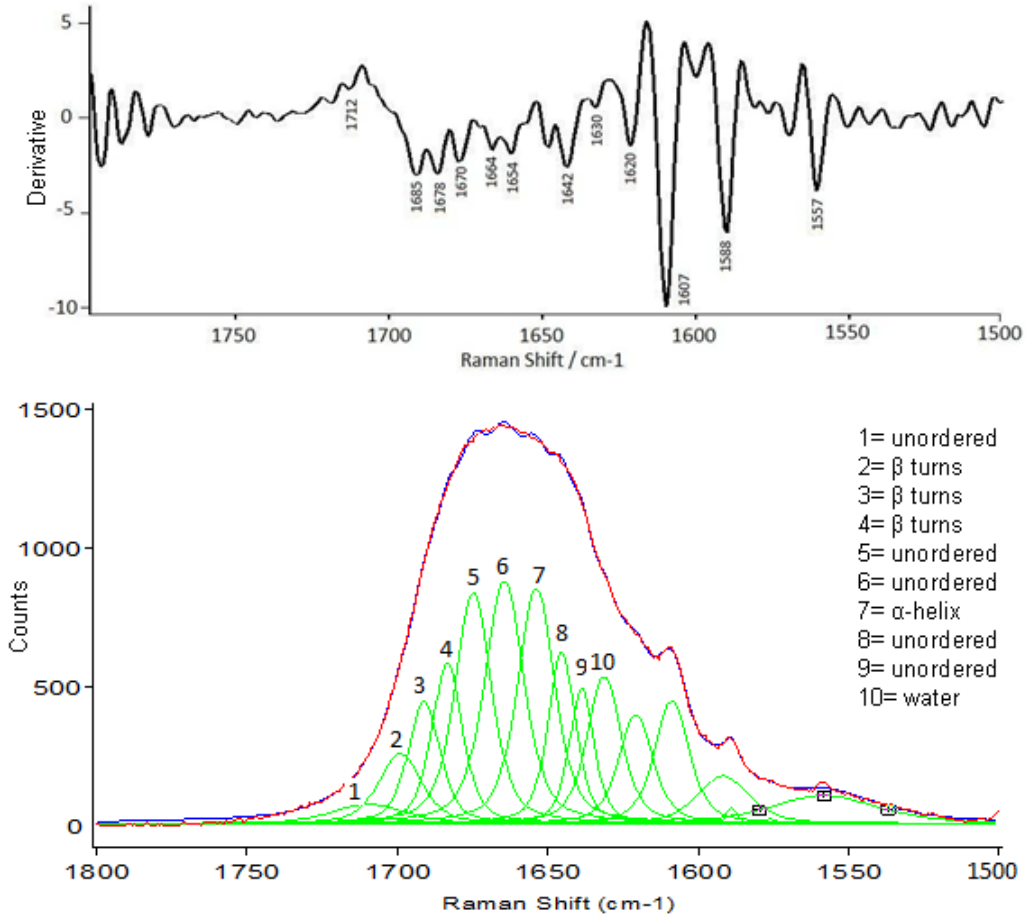

Figure 2.13: Second derivative analysis of the amide I band for hydrated nuchal elastin. Experimental data (red line), the fitted spectrum (blue line) and amide I band components (green line) are shown. The main amide components are located at 1712, 1685, 1678, 1670, 1664, 1554 and 1642 cm^{-1}. Water is assigned to a single peak centred at 1630 cm^{-1}, although the peak at 1642 cm^{-1} may be either unordered structures or water as indicated by Sane et al [3]. The remaining peaks are attributed to side chain vibrations.

Although we chose to adopt the final fitting routine based on that of Sane et al a degree of caution is required when interpreting the results largely because of disagreement throughout the literature relating to secondary structure attribution which largely arises through significant overlapping of secondary structure markers [285]. To illustrate this point table 2.2 gives some indication of this variation using published data for a number of proteins.

The amide III band is also considered to be sensitive to conformation, although many of the modes are non-localized which reduces their sensitivity to local conformation [286] and the analysis is complicated by interference from CH deformation modes. We employed the procedure described by Williams [12].

A linear baseline was fitted across a window from 1570 – 1070 cm^{-1}. Although the amide III contributions are restricted between 1310-1225 cm^{-1} it was necessary to fit additional peaks at both higher and lower wavelengths in order to produce a good fit to this complex region. For elastin the second derivative analysis of this region revealed peaks at 1316 -1320 (PPII), 1274 (α-helix), 1256 -1252 (random structures) and 1225 cm^{-1}(β-sheet). Side chain contributions were fitted over the range from 1209 -1177 cm^{-1}. The second derivative analysis for hydrated nuchal elastin is illustrated in figure 2.14. The amide III and side chain peaks corresponded well to those determined by both Williams [12] and Peticolas [16] and in the light of this work the peak attributions we used were: α-helices and β-sheets represented by single peaks at 1274 cm^{-1} and 1225 cm^{-1} respectively, and unordered structure associated with three peaks in the range 1256 -1247 cm^{-1}. A broad peak located at around 1320 cm^{-1} which is frequently found in random coil structures has been assigned to PPII [140]. Supplementary components were required either side of the PPII peak in order to produce a satisfactory fit to the complete band and were attributed to CH_2, CH_3 deformations and amide III components. Analysis of the PPII band is discussed further in section 2.2.6.3. As in the amide I analysis, no parameters were fixed except the underlying profile which was 50% Gaussian and 50% Lorentzian. Due to the large number of individual spectra used no smoothing was necessary, and calculations were based on the peak area and full width at half-height.

Wavemumber (cm-1)	Sane [a]	Williams [b]	Berjot [c]	Bochicchio [d]	Debelle [e]	Debelle [f]	Maiti [g]	Peticolas [h]	Pelton [i]	Vedantham [j]	Dong [k]	Barth [l]
1612									β-sheet			
1622										β-sheet		
1624											β-sheet	β-sheet
1627											β-sheet	"
1630									β-sheet			"
											β-sheet & extended chain	"
1632												
1633										β-sheet		"
1634						water			β-sheet			"
1635	water					"			β-sheet			"
1636						"			β-sheet			"
										disordered helix +		
1638									β-sheet	random	β-sheet	"
1640				α-helix								
1641	unordered	α-ordered		α-helix					undefined			
1642				α-helix							β-sheet	
1643			α-helix[1]					α-helix	undefined			unordered
1645	water					α-helix		"	undefined			"
	unordered											"
	helix +											
1649	sheet				α-helix	"		"	undefined			α-helix / unordered
										disordered helix +		
1650						"		"	α-helix	random	unordered	"
1652						"		"	"	"		"
1654			α-helix[2]				α-helix	"	"	"		"
1655	α-helix							undefined	"	"		"
1656	β-turn	α-disordered				undefined		"	"	α-helix	α-helix	"
1657						"		"	α-helix			"
1659					undefined	"		"				

a Sane.S. *et al* (1999) Anal. Biochem, **269**
b Williams.R.W. (1986), Methods in Enzymol, **130**
c Berjot.M. *et al* (1987) J.Raman Spectroscopy **18**
d Bochicchio.B. *et al* (2004) Biopolymers **73**
e Debelle.L. *et al* (1998) Eu.J.Biochem **270**
f Debelle.L. *et al* (1995) Eu.J.Biochem **258**
g Maiti.N. *et al* (2004) J.Am.Chem. Soc **126**
h Peticolas.W.L. (1995) Methods in Enzymol **226**
i Pelton.J.T. and McLean. L.R. (2000) Anal. Biochem **277**
j Verdantham.G. *et al* (2000) Anal. Biochem **285**
k Dong.A. *et al* (1990) Biochemistry **29**
l Barth.A. and Zscherp.C. (2002) Q. Rev. Biophys **35**

Wavemumber (cm-1)	Sane [a]	Williams [b]	Berjot [c]	Bochicchio [d]	Debelle [e]	Debelle [f]	Maiti [g]	Peticolas [h]	Pelton [i]	Vedantham [j]	Dong [k]	Barth [l]
1660		undefined		unordered	undefined	"		"				
1661			unordered			"		"				
1663	unordered		"									β-turn
1665			"			undefined	β-sheet	β-sheet				"
1666			"					"		β-turn	β-turn	"
1667						undefined	β-sheet					"
1671	unordered helix + sheet	β-sheet (parallel)			undefined	"		"	β-sheet			"
1672									"	β-turn	β-turn	"
1673			β-sheet	β-strand			extended β-strand + PPII	"	"			"
1675		β-sheet (anti-parallel) or β-turn		β-strand		β-strand	"	"	"			β-sheet / β-turn
1678	unordered	disordered				"	"	"	"			"
1679						"	"	"	"			"
1680							"	"	"	β-turn	β-turn	"
1684	β-turn	α-ordered			β-strand		"		"			"
1686						β-strand			"			β-sheet
1688									"	β-sheet / β-turn	β-turn	"
1691						"						"
1692	β-turn				β-strand							"
1695												
1702												
1714	unordered											

a Sane.S. *et al* (1999) Anal. Biochem, **269**
b Williams.R.W. (1986), Methods in Enzymol, **130**
c Berjot.M. *et al* (1987) J.Raman Spectroscopy **18**
d Bochicchio.B.*et al* (2004) Biopolymers *73*
e Debelle.L. *et al* (1998) Eu.J.Biochem **270**
f Debelle.L. *et al* (1995) Eu.J.Biochem **258**
g Maiti.N.*et al* (2004) J.Am.Chem. Soc **126**
h Peticolas.W.L. (1995) Methods in Enzymol **226**
i Pelton.J.T. and McLean. L.R.(2000) Anal. Biochem **277**
j Verdantham.G. *et al* (2000) Anal. Biochem **285**
k Dong.A. *et al* (1990) Biochemistry **29**
l Barth.A. and Zscherp.C. (2002) Q. Rev. Biophys **35**

Table 2.2: This table shows the variation in secondary structure attribution of the amide I band for various biological tissues based on IR and Raman spectroscopy. There appears to be very little agreement in both terminology and in secondary structure attribution between the authors making estimation of protein secondary structure very difficult. Data were based on :a [3], b [12], c [6], d [13], e [14], f [15], g [2], h [16], i [17], j [18], k [19], l [20]

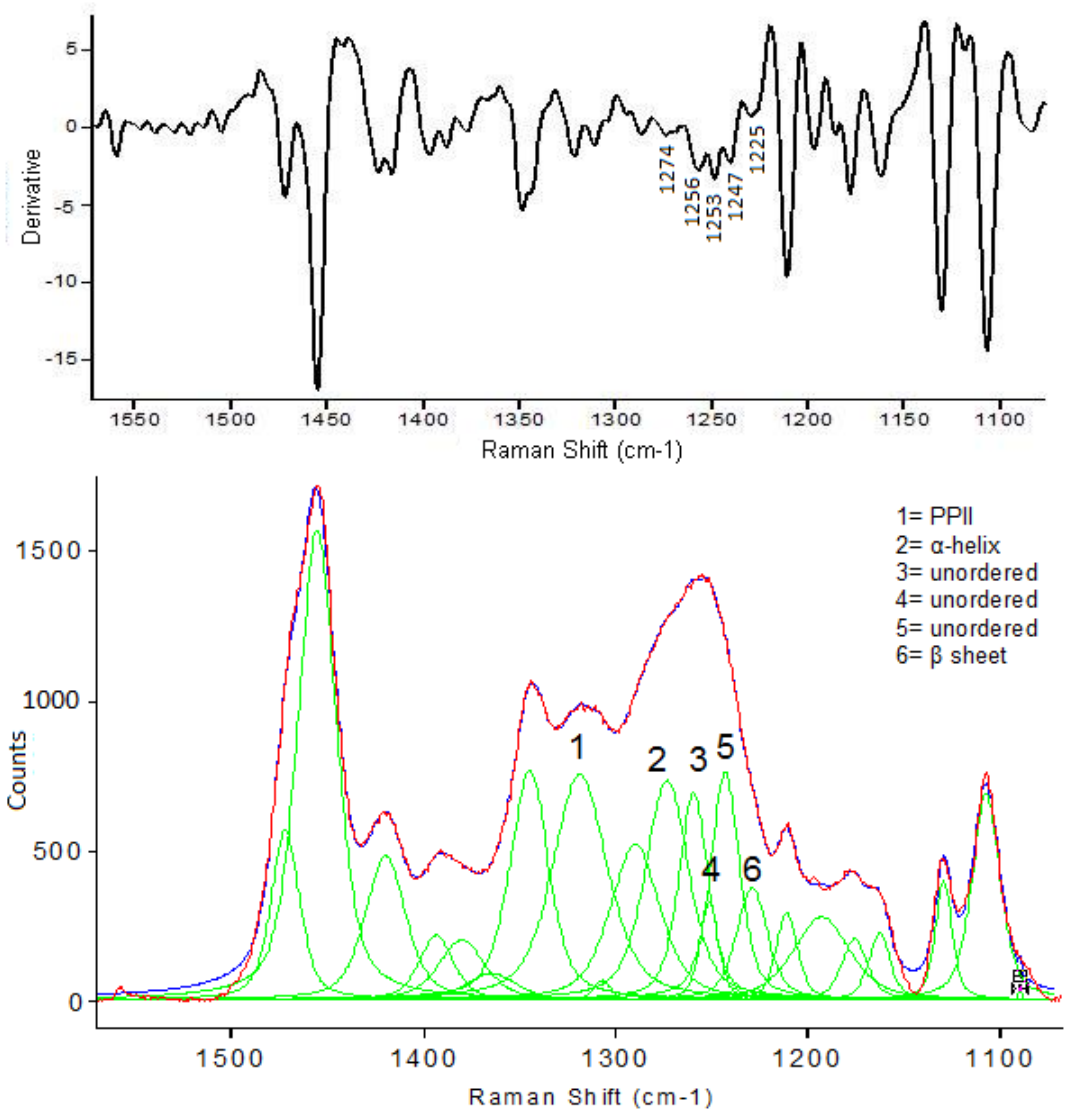

Figure 2.14: Second derivative analysis of the amide III band for hydrated nuchal elastin, based on the fitting parameters of Williams [12]. Components of the amide I band are shown by the green line, experimental data the red line and result of decomposition the blue line, which overlays the red line. The amide components are located at 1274, 1256, 1253, 1247 and 1225 cm^{-1}. In addition the peak centred at 1314 $cm^{-1}$is assigned to polyproline II.

Although the description above gives details of the final procedures used for amide I and amide III analysis which were implemented in WiRE 2.0 software, the initial analysis using almost identical peak parameters such as peak centres and width, were performed using Grams A/1 software. However, this package proved to be unsuitable for analyzing this complex amide band giving inconsistent results which largely resulted from the program's sensitivity to the baseline fit and seeding conditions including initial peak heights etc. WiRE 2.0 software was considerably more robust allowing identical curve fitting procedures to be applied to all samples under all conditions therefore allowing meaningful comparisons to be made with

Peak Centre (cm^{-1})	Attribution according to Williams [a]	Peak Centre (cm^{-1})	Our Experimental data
–		1469	?
1458-1460	CH_2 / CH_3 deformation	–	
1450	CH_2 / CH_3 deformation	1453	CH_2 / CH_3 deformation
1430	CH_2 / CH_3 deformation	–	
1418	N-H stretch	1418	N-H stretch
1388	Tyr	1393	Tyr?
–		1383	Tyr?
–		1360	?
1342	CH_2 / CH_3 deformation	1346	CH_2 / CH_3 deformation (or PPII)
1319	CH_2 / CH_3 deformation (or PPII)	1320	CH_2 / CH_3 deformation (or PPII)
–		1309	?
–		1287	Proline
1272	α-helix	1274	α-helix
–		1253-1256	Random?
1249	Random	1247	Random
1237	β-sheet	1242	β-sheet
1225	β-sheet	1225	β-sheet
1210	Tyr, Phe	1209	Tyr, Phe
1198	?	1196	?
1175	Tyr, Phr, CH stretch	1177	Tyr, Phr, CH stretch
1160	?	1161	?
1128	C-C stretch	1129	C-C stretch
1106	?	1106	?
		1084	?

[a] Williams R.W. (1986) Methods Enzymol, **130** , 311-331

Table 2.3: Amide III band peak attributions according to Williams [12] compared with our second derivative analysis of the same spectral region.

regard to secondary structure compositions.

A peak at 938 cm^{-1} is an additional indicator of α-helical structure. However, it is surrounded by other peaks and not amenable to quantitative analysis, so we measured only whether changes in its height relative to the phenylalanine peak at 1005 cm-1 were consistent with the above analysis.

2.2.6.2 Analysis of Peak Centred at 938 cm^{-1}

According to previous investigations by Debelle et al [15] a peak centred at around 934 cm^{-1} is a characteristic marker for ordered helices. In our data a prominent

peak was located towards slightly higher wavenumbers, at around 938 $cm^{-1}$and was assumed to represent the same molecular vibrations. If this peak is characteristic of ordered helices as suggested, then it seemed reasonable to suggest that the relative height above background or area of this peak relative to other peaks would provide a measure of the proportion of α-helix in each of the proteins.

In order to investigate this, it was decided to calculate the ratio of the 938 cm^{-1} peak to the well defined, sharp peak at 1005 cm^{-1} assigned to phenylalanine. An increase in the 938:1005 cm^{-1} peak ratio was expected to a correspond to an increase in contribution from α-helices within the amide I and amide III bands. Similarly, a lower 938:1005 cm^{-1} peak ratio was expected to be reflected in a decrease in α-helix contribution.

Averaged spectra were used following subtraction of water/quartz in hydrated samples. A cubic spline baseline was fitted across the whole spectrum, followed by a second cubic spline baseline across a narrow window from 1070 - 800 cm^{-1} at points where no peaks were expected (1070, 1015, 994, 955, 916 and 890 cm^{-1}). No smoothing of data was performed. All spectra analysed were normalized to the 1005 cm^{-1} phenylalanine peak of dehydrated elastin in the stretched state. The 938 cm^{-1} peak forms part of a complex band spanning from 1070 to 800 cm^{-1} wavenumbers making it difficult to isolate the peaks of interest from the neighbouring peaks. In the light of this it was found necessary to fit a number of additional peaks representing tyrosine, phenylalanine, C-C, and C-C-N deformations at 1034, 1023, 978, 963, 922, cm^{-1}. These peak centres were used to construct a curve fitting routine with no parameters fixed including, peak centre, height, and peak profile. Relative height / area values for the 938 cm^{-1} peak were recorded and expressed as a ratio to the corresponding values for the 1005 cm^{-1} peak.

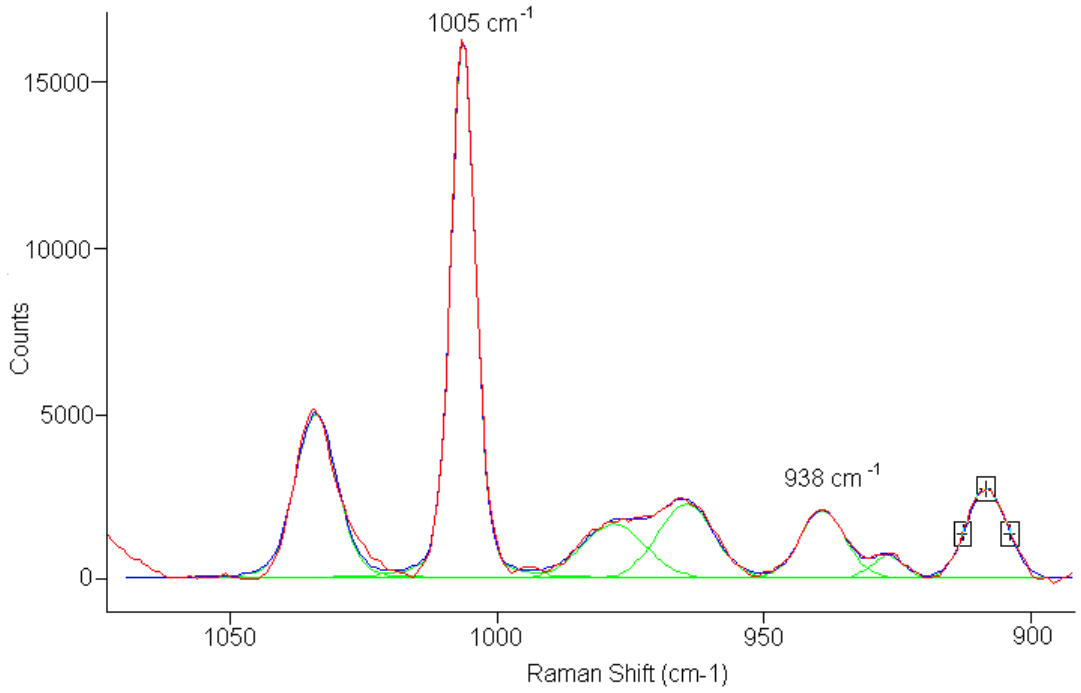

Figure 2.15: Curve fitting of 1070-800 cm^{-1}region of hydrated nuchal elastin fibres in order to determine the ratio of the 938 and 1005 cm^{-1}peaks based on either peak heights or peak areas. Due to the complexity of this region it was deemed necessary to fit a number of additional peaks representing the neighbouring side-chain aromatics, C-C and C-C-N deformations. The original spectrum (red line), result from curve fitting (blue line) and component bands (green lines) are shown.

2.2.6.3 PPII Analysis

In the Raman spectrum of fully hydrated nuchal elastic fibres shown later on as Figure 3.7, a distinct peak can be identified at approximately 1314 cm^{-1} closely adjacent to the amide III band described in section 2.2.6.1. There remains some uncertainty as to the correct attribution for this peak with some literature referring to CH_2CH_3 deformation [12, 22, 23] whilst others support extended polyproline II helices (PPII) [140]. PPII has been proposed to play an important role in both amyloid pre-fibril formation [139] and as the molecular basis of elastin elasticity [141], with some PPII being converted to α-helix or β-structures under conditions of increased temperature or reduction in water. Given the important implications of PPII in elastin elasticity, we sought to identify the presence of a peak representing this structure in our Raman data to determine whether the percentage contribution differed under conditions of dehydration and heating to 60°C. We then extended this analysis to establish whether PPII could be identified in the Raman spectra of the four individual lamprey matrices and if so what effect changing the local

environment had.

Averaged datasets were used, with no further processing apart from the application of a cubic spline baseline fitted across the spectrum from 500-4000 cm^{-1} to minimize any background fluorescence. A second baseline was then applied to a narrow window between 1570-1070 cm $^{-1}$. In our data no peak was located at exactly 1314 cm^{-1} however, a distinctive peak was found within $\pm$ 3 $cm^{-1}$and was taken to represent PPII structures. The 1314 cm^{-1} peak is situated between neighbouring amide III components on one side and CH_2CH_3 deformations on the higher wavenumber side. Substantial overlapping of these adjacent peaks required their inclusion in the fitting regime of this complex region allowing the area of the 1314 cm^{-1} peak to be expressed as a percentage of the total amide and PPII areas.

2.2.6.4 Tyrosine Fermi-Doublet Analysis

The appearance of two tyrosine peaks centred at 850 cm^{-1} and 830 cm^{-1} in proteins is regarded as a useful marker for the side-chain environment. These peaks frequently occur as a doublet originating from Fermi-resonance interactions between ring breathing vibrations and an overtone of an out-of-phase ring bending (C-C-O) mode. The intensity ratio of these two peaks is thought to provide a measure of the state of the phenolic OH and therefore indicate the strength of hydrogen bonding, with tyrosine side chains being either 'buried' (strongly hydrogen-bonded tyrosine) or 'exposed' (weak hydrogen bonding) [293].

We determined the ratio of the 850/830 cm^{-1} peak areas from averaged spectra following a two point background correction across the spectral range from 800-900 cm^{-1}. This region was then fitted with three peaks centred at 870, 850 and 830 cm^{-1} with no constraints on peak centres, width, height or underlying profile.

2.2.6.5 Analysis of the Water Interaction Region

In addition to the amide I and amide III contribution a broad band at 3650-3000 cm^{-1} representing water interactions was also fitted in an attempt to explore possible energetic costs associated with the rearrangement of the hydrogen-bond network

of bulk water caused by the polymer. This method has previously been described in some detail by Leikin et al [7] to investigate the interactions between OH and NH vibrations in Type I collagen fibres. According to the authors, three peaks could be fitted to hydrated collagen in this region with peak centres at 3600 cm^{-1} representing nonhydrogen-bonded OH, and 3450 and 3250 cm−1 representing different OH vibrations respectively. In collagen the N-H peak, representing vibration of backbone amides, is small compared to the O-H modes but was found to persist, even after extensive incubation with deuterium oxide. This peak also appeared to be largely insensitive to water content with only an increase in width at low water contents. For fibrous elastin we found corresponding O-H peaks at 3605, 3391 and 3221 cm^{-1} , each of which could be fitted with a Gaussian profile, following a linear background subtraction across a window between 3700 -2700 cm^{-1} and subtraction of water spectrum in hydrated samples. No N-H vibration associated with vibration of backbone amides could be detected. To produce a satisfactory fit, the neighbouring C-H band was also fitted, using six peaks centred at 3065, 2975, 2935, 2890, 2770 and 2735 cm^{-1}, being allowed to float by $\pm$ 10 cm^{-1} and having mixed Gaussian-Lorentzian profiles. An example of curve fitting of the water interaction region for fully hydrated elastin fibres is shown in Figure 2.16. Again using a similar technique to that used by Leikin, interactions of the protein (elastin fibres and the 'lamprins') with water was quantified both by; i) the ratio of two major OH peaks at 3221 $cm^{-1}$and 3391 cm^{-1}in the water band and ii) the ratio of the total area of free OH to that of the neighbouring CH contribution was calculated.

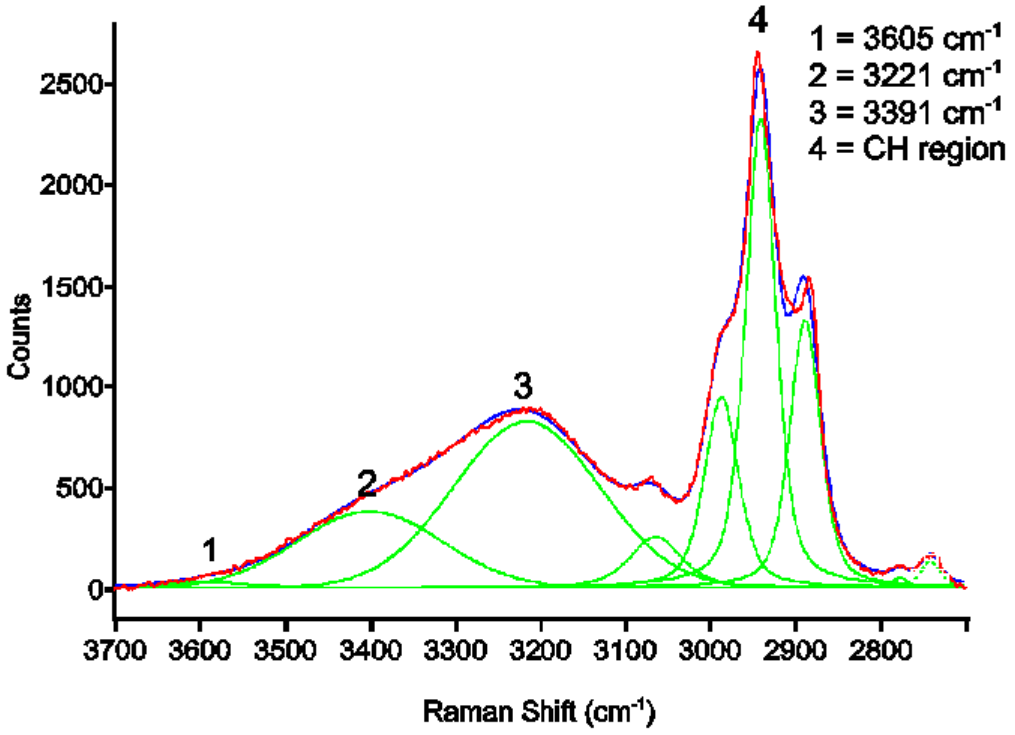

Figure 2.16: Curve fitting of the water interaction region between 3600 and 3100 cm^{-1} and the neighbouring CH band as described by Leikin *et al* [7]. The experimental spectrum is shown by the red line, the fitted spectrum (blue line) and component bands obtained by decomposition (green lines).

2.2.6.6 Polarization Measurements

The intensity and polarization of the Raman scattered beam depends on the orientation of the bond relative to the polarization of the exciting radiation. Analysis of the polarization sensitivity of the spectrum can therefore provide information about bond orientation in fibrous polymers and we used this approach first to investigate molecular organization in elastin fibres and then to enquire whether this organization was influenced by mechanical strain. It was not possible to undertake a similar analysis for the lamprey proteins because of the complex matrix architecture which was revealed by the microscopy described in Section 4.5.

As illustrated in Figure 2.9, the combination of polarization filters and half wave plates in the excitation and scattering paths allowed spectra to be acquired, at the same point in the sample, for the four combinations of polarization of the incident and scattered beams, defined with respect to the fibre axis. The measurements were corrected for the polarization sensitivity of the instrument by measuring the four intensities in an isotropic film of α-elastin dried on an aluminized cover slip. The

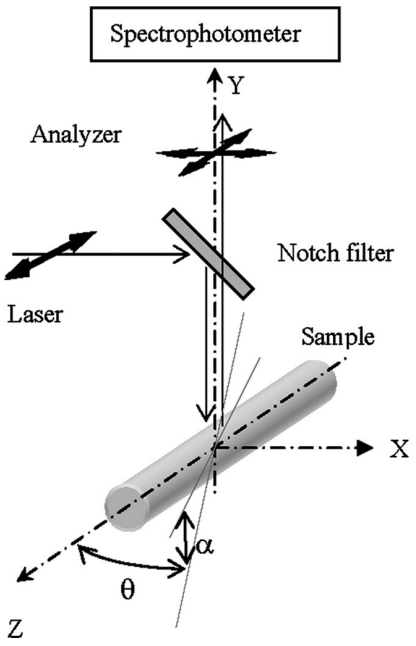

Figure 2.17: Schematic diagram to show the coordinate system used for measuring the polarized Raman spectra of elastin fibres. This image is reproduced from Preghenella et al [294].

coordinate system used for measuring the polarized Raman spectra of elastin fibres is shown schematically in Figure 2.17.

The relationships between intensity ratios and bond angles for a cylindrically symmetric fibre was originally derived by Rousseau et al [295] for the analysis of silk protein fibres. The work by these authors provides a detailed description of the theoretical background of polarized Raman spectroscopy, whilst the basic concepts are outlined below.

The bond orientation for sytems with fibre-type symmetry is described by an orientation distribution function $N(\theta)$, which is represented by a series of Legendre polynomials:

$$N(\theta) = \sum_{l}^{even} \left(l + \frac{1}{2}\right) (P_l)\, P_l\,(cos\theta) \tag{2.1}$$

where $P_l\,(cos\theta)$ are the Legendre polynomials and $\langle P_l \rangle$ represent average values of the Legendre polynomials over the orientation distribution. The angle θ is the angle between the z-axis of the Raman tensor and the fibre axis. For a cylindrically symmetric fibre, the Raman tensor (α) can be represented as follows:

$$\alpha = \begin{pmatrix} \alpha_1 & & \\ & \alpha_1 & \\ & & \alpha_3 \end{pmatrix} = \alpha_3 \times \begin{pmatrix} a & & \\ & a & \\ & & 1 \end{pmatrix} \tag{2.2}$$

where $a = \alpha_1/\alpha_3$.

Using polarized Raman spectroscopy, only the second (P_2) and fourth (P_4) order parameters are considered and the depolarization ratios R_1 ($\parallel$) and R_2 ($\perp$) of the scattered Raman intensities for different orientations of the sample in relation to the incident radiation are measured.

The Raman scattering intensity is given in general by the equation:

$$I = \int_V \int_\Omega \left| E_i^+ \langle \alpha \rangle \ E_s \right|^2 dV \, d\Omega \tag{2.3}$$

where E_s is the scattered field intensity, E_i^+ is the transpose of the incident field and α is the Raman tensor averaged over the sample, V represents the scatter volume and Ω the solid angle of light collected. In our geometry the incident and scattered radiation propegates in the y direction and we acquire four polarised spectra (I_{zz}, I_{zx}, I_{xz} and I_{xx}). Under these conditions the intensity ratios are [296]:

$$R_1 = \tfrac{I_{ZX}}{I_{ZZ}} = \frac{A\left\langle (\alpha_{zx})^2 \right\rangle + B\left\langle (\alpha_{zy})^2 \right\rangle}{A\left\langle (\alpha_{zz})^2 \right\rangle + B\left\langle (\alpha_{zy})^2 \right\rangle} \tag{2.4}$$

$$R_1 = \frac{I_{xz}}{I_{xx}} = \frac{A\left\langle (\alpha_{xz})^2 \right\rangle + B\left\langle (\alpha_{xy})^2 \right\rangle}{A\left\langle (\alpha_{xx})^2 \right\rangle + B\left\langle (\alpha_{xy})^2 \right\rangle} \tag{2.5}$$

where the geometrical constants A and B are determined by integrating the squares of the elements E_s, over Ω in Equation 2.3, but for the objective used in our experiments (NA 0.55) $B \ll A$ so we get:

$$R_1 = \frac{I_{zx}}{I_{zz}} = \frac{\langle \alpha_{zx}^2 \rangle}{\langle \alpha_{zz}^2 \rangle} \tag{2.6}$$

$$R_2 = \frac{I_{xz}}{I_{xx}} = \frac{\langle \alpha_{xz}^2 \rangle}{\langle \alpha_{xx}^2 \rangle} \tag{2.7}$$

Using the assumption of cylindrical symmetry the components of the scattering tensor (α_3 and α_3) become:

$$\left\langle (\alpha_{xx})^2 \right\rangle = \frac{1}{15} - \frac{2}{21} dP_2 + \frac{3}{35} bP_4 \tag{2.8}$$

$$\left\langle (\alpha_{xz})^2 \right\rangle = \left\langle (\alpha_{zx})^2 \right\rangle = \left\langle (\alpha_{zy})^2 \right\rangle = b\left(\frac{1}{15} + \frac{1}{21} P_2 - \frac{4}{35} P_4\right) \tag{2.9}$$

$$\left\langle (\alpha_{zz})^2 \right\rangle = \frac{1}{15} c + \frac{4}{21} dP_2 + \frac{8}{35} bP_4 \tag{2.10}$$

$$\left\langle (\alpha_{xy})^2 \right\rangle = b\left(\frac{1}{15} - \frac{2}{21} P_2 + \frac{1}{35} P_4\right) \tag{2.11}$$

Where,

$$b = {\alpha_3}^2 (1-a)^2 \tag{2.12}$$

$$c = {\alpha_3}^2 \left(3 + 4a + 8a^2\right) \tag{2.13}$$

$$d = {\alpha_3}^2 \left(3 + a - 4a^2\right) \tag{2.14}$$

Applying equations 2.4 and 2.5 to an isotropic sample, for which $P_2 = P_4 = 0$ we can determine a from the depolarization ratio R_{iso}, and hence determine P_2 and P_4 for a fibrous sample.

$$R_{iso} = R_1 = R_2 \tag{2.15}$$

These expressions were then fitted using a routine written in MATLAB (by Dr James Bell) and the bond angle calculated as:

$$\theta_0 = cos^{-1}\left(\frac{2P_2 + 1}{3}\right)^{\frac{1}{2}} \tag{2.16}$$

This analysis was performed on each significant peak and on each component of the water and amide I and III bands.

2.3 Mechanical Testing

2.3.1 Introduction to Mechanical Testing

Mechanical testing is a useful tool in studying the behaviour and mechanical properties of biological tissues although this is no simple task as data interpretation can be quite complex, mainly because these tissues are composite structures composed of a mixture of elastin, collagen and glycosaminoglycans to name but a few. It is difficult to define mechanical properties of multiphasic materials, where a large proportion of the cross-sectional area is water, in relation to classical engineering terminology. Therefore, in this thesis we adopt commonly used nomenclature for biological materials as defined in Table 2.4.

Attribute:	Material property	Units
Normal stress	Force per unit area of tissue over which the force is acting (σ=F/A)	Pa
Normal strain	Ratio of change in length to original length (ε=ΔL/Lo)	no units
Extensibility	Strain at failure (ε_{max})	no units
Hysteresis	Measure of strain energy lost. Calculated as difference in area of force-deflection curves over a complete loading-unloading cycle	Pa
Strength	Stress at rupture (σ_{max})	Pa
Stiffness	Measure of how easily a material is deformed. Calculated as slope of linear region of stress-strain curve ($E=\sigma/\varepsilon$), also referred to as the Young's modulus	Pa

Table 2.4: Description of nomenclature, material propeties and units of quantification commonly used for multiphasic biological tissues.

Biological materials are generally characterized by the relationships between applied stresses and strains. Engineering stress within the material is defined as applied force normalized by the original cross-sectional area of the material and engineering strain is the change in sample length relative to its original length. In this project the tensile strain, as opposed to compressive strain, was investigated. This arises through the application of stretching forces in opposite directions to both ends of the sample. A schematic diagram representing a typical stress-strain curve for a rubber-like material is shown in figure 2.18. When a material is extended to its breaking point then the relative strength and extensibility of the material can be determined. When a material is extended to a point below its breaking strain and allowed to return to its relaxed state, the difference in work done on stretching and relaxing the sample can be calculated. This is referred to as the mechanical

hysteresis loop and provides a measure of the energy lost per unit volume to the system, often expressed as a ratio of energies. The property of stiffness refers to how easily a material can be deformed and is measured in terms of the materials elastic modulus, which is calculated from the slope of the stress-strain curve. All materials have a unique relationship between stress and strain and a considerable amount of information regarding the material elastic behaviour can be gained from careful analysis of these curves. Several models have been developed in an attempt to explain the relationships between stress and strain in non-biological materials but these materials generally show time-dependent and/or strain-dependent behaviour which increases the complexity and compromises the uniqueness of the models.

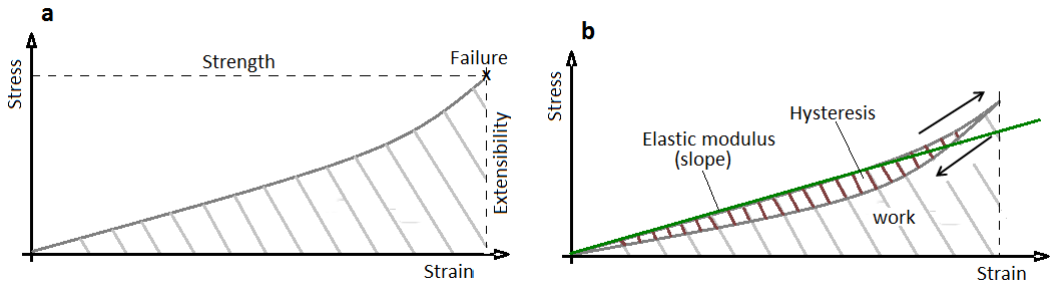

Figure 2.18: Schematic diagram of a typical stress-strain curve for a rubber-like material. In a) the material is extended past its point of failure to provide a measure of the samples strength and extensibility. In b) the material is allowed to undergo a complete load-unload cycle without exceeding its failure point. From this type of plot the Elastic modulus of the material can be determined from the slope of the stress-strain curve as well as calculation of the hysteresis loss.

Materials that display time-dependent behaviour upon loading and are said to be viscoelastic. A standard method used to characterize viscoelastic behaviour is to observe the stress-relaxation response of the material. This is typically done by applying a near instantaneous strain of a fixed amount and recording the stress as a function of time whilst mainaining constant strain. Alternatively, for creep behaviour, the strain required to maintain a sample at a fixed stress is recorded. It has been known for some time that when tissues like tendon are extended to a fixed length and the resulting stress recorded as a function of time, the stress decreases exponentially [55]. This type of behaviour is shown in Figure 2.19 and can be related to the viscoelastic properties intrinsic to the material. A material can be described as viscoelastic if it displays both an elastic (time independent) component and a viscous (time dependent) component on deformation, where energy is stored and dissipated

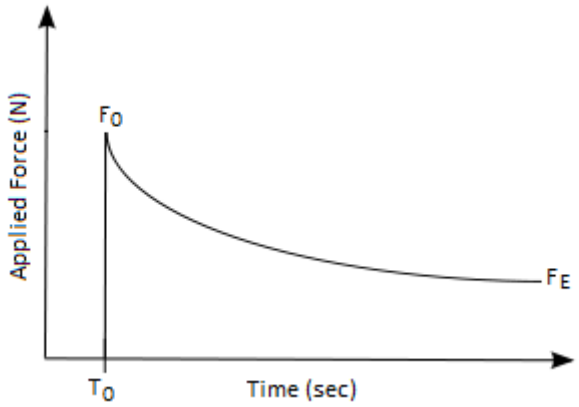

Figure 2.19: Typical stress-relaxation curve of a tissue such as tendon showing exponential decay with time. The force that remains at F_E is time independent and corresponds to the elastic component of the force. The force which is recovered on removal of applied load refers to the elastic fraction, F_E/F_0 and the viscous component, $F_0 - F_E$ is the remaining force that is converted into heat.

respectively. It has been suggested for materials such as rubber that the elastic component involves conformational changes whereas the viscous component involves the sliding of elements past each other [27]. In rubber, numerous cross-links hold the polymer chains in a complex network arrangement which serves to prevent the chains from moving relative to each other. Once an equilibrium point is reached any further mechanical response is said to be independent of time [196], but the rate at which the equilibrium point is reached is dependent largely on molecular interactions. It has long been established that elastin shows time-dependent (viscoelastic) properties similar to those observed in rubber [297, 298, 299] and we conducted a similar investigation in order to establish the viscoelastic behaviour associated with the four individual lamprey matrix proteins.

Viscoelasticity can be modeled as linear combinations of springs and dashpots, either in series or parallel. Springs represent elastic behaviour with a spring constant μ (obeying Hooke's law where stress is proportional to strain but independent of strain rate), and dashpots represent viscous behaviour with a coefficient of velocity η (obeying Newton's law where stress is proportional to strain rate but independent of force). Loading of a viscoelastic material can be expressed as a combination of the elastic and viscous components:

The elastic element being:

$$F = \mu u \tag{2.17}$$

and the viscous element:

$$F = \eta \dot{u} \tag{2.18}$$

where F is the force, u is displacement in the spring and $\dot{u}$ the velocity. Purely elastic materials will eventually return to their original length on removal of force, whereas viscoelastic elements will not.

The three most frequently used models to account for viscoelasticity are the Maxwell model, the Kelvin-Voigt model and the standard linear model (also referred to as the Kelvin model) each of which is illustrated schematically in Figure 2.20. Of these three models, the Maxwell model is the least complicated with a spring and dashpot lying in series. In this model, stresses in both elements will be the same since the stress is transmitted through both the spring and the dashpot. The result of this is the production of a displacement F/μ , in the spring and a velocity F/η , in the dashpot. The total velocity of deformation $\dot{u}$ can therefore be expressed by:

$$\dot{u} = \frac{\dot{F}}{\mu} + \frac{F}{\eta} \tag{2.19}$$

The problem with the Maxwell model is that it predicts that the stress decays to a zero value which is highly unlikely in stress-bearing materials such as those of the extracellular matrix.

The Kelvin-Voigt model is an adaptation of the Maxwell model consisting of the same basic elements. The main difference arises from the arrangement of elements, where the spring and dashpot lie parallel to each other as opposed to being arranged in series. As a consequence of this parallel arrangement, displacement in the spring and dashpot are equal and the total force in this model is therefore the sum of the force in the elastic and viscous components, which can be written as:

$$F = \mu u + \eta \dot{u} \tag{2.20}$$

The standard linear model takes a step further by combining the Maxwell and Kelvin-Voigt models. As can be seen in Figure 2.20, a Maxwell element (η_1 and μ_1) lies parallel to a second spring (μ_0). There have been a number of attempts at con-

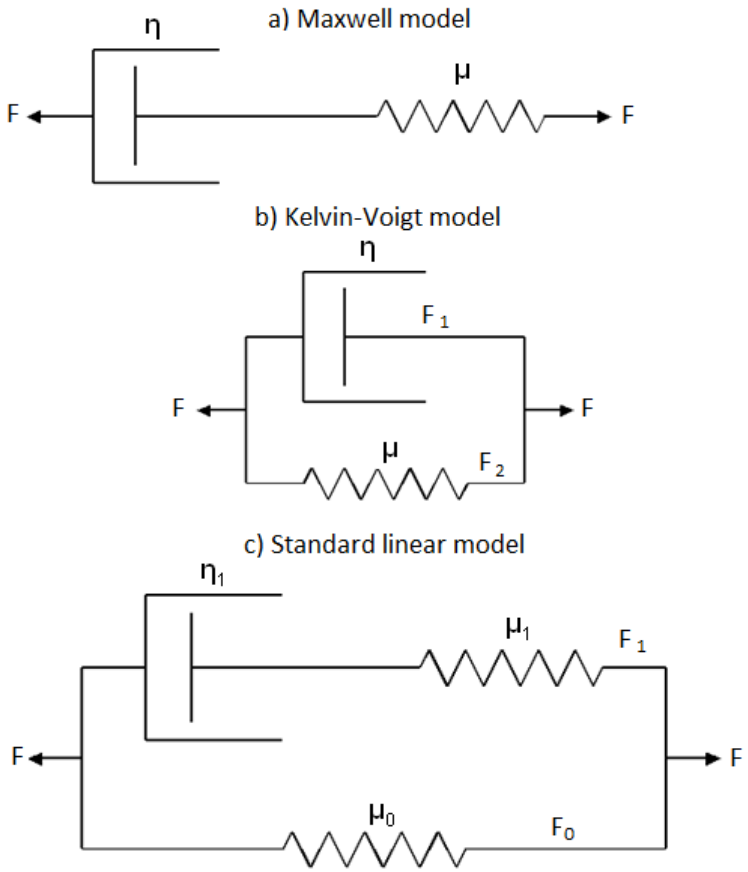

Figure 2.20: Schematic diagrams of the three major viscoelasticity models each of which has an elastic, time-independent component represented by springs and a viscous, time dependent component represented by a dashpot. This figure is adapted from [55]

structing even more complicated viscoelasticity models. However, with this comes more complicated mathematics which is not of enormous benefit in interpreting the viscoelastic behaviour of biological tissues at a molecular level [300].

Figure 2.21 shows the predicted deformation for each of the stress-relaxation models following an instantaneous strain. The Maxwell model predicts an immediate peak force by sudden deformation of the spring which is followed by an exponential decay to zero force as the viscous resistance of the dashpot balances the spring. In the Kelvin-Voigt model the parallel arrangement of spring and dashpot does not permit instantaneous deformation. A similar response to that of the Maxwell model is predicted in the standard linear model, the difference being that force does not return to zero because of the second spring. Viscoelastic responses of biological material are generally complex in nature and none of the models described gives a completely satisfactory explanation. However, of the models available, the standard linear model may be regarded as the best representation with additional exponential

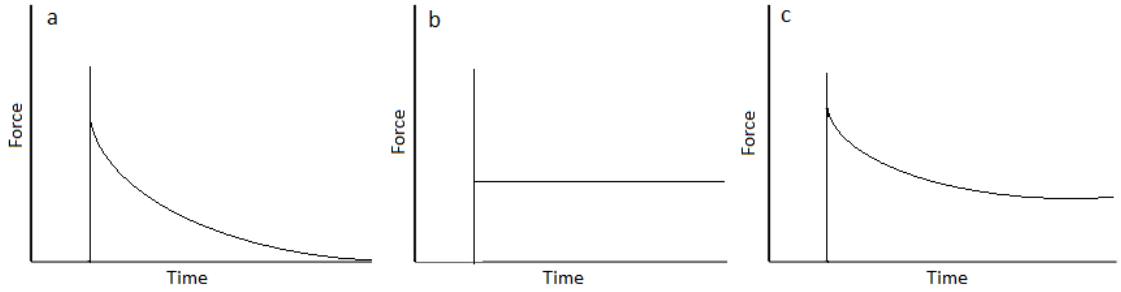

Figure 2.21: Predicted stress-relaxation functions of a) the Maxwell model, b) the Kelvin-Voigt model and c) the standard linear model.

terms added if required and because of this the standard linear model was applied to stress-relaxation data obtained in this study.

The following sections describe the purpose-built mechanical testing apparatus followed by the main types of tensile experiment undertaken in order to address the mechanical properties of elastic fibres and lamprey cartilage material.

2.3.2 Mechanical Testing Apparatus

Mechanical testing was performed using a custom-built testing apparatus (Figures 2.22 and 2.23). The specimens, were cut into uniform strips of approximately 10-15mm in length and 1-5 mm diameter, in order to ensure even distribution of stress across the sample. The strip of tissue was attached to two metal pins using a small quantity of high viscosity Superglue (World Precision Instruments, Ltd) or clamped between custom engineered nylon supports. When using clamping devices it was normally necessary to sandwich the sample between two small pieces of sandpaper or latex to minimize sample breakage. One pin/clamp was attached to a micrometer driven by a pulse generator controlled stepper motor (Radio Spares, 1.8 Deg/pulse) whilst the other end was attached to a rigidly mounted lever force transducer (WPI, FORT100, range $\leq$100 grams). On application of strain, the force was output as a voltage and logged to a computer using a Picologger (Pico Technology Ltd, Pico ADC-200). The voltage output was then converted to force (N) using a calibration curve and finally expressed in megapascals (MPa) by dividing force by cross-sectional area of the protein. Displacement imposed on the sample was controlled via a stepper motor which drives the micrometer at a given strain rate. Data points

were recorded every 1-5 seconds depending on the experiment. The sample lay horizontally, completely immersed in a solution bath resting on a Peltier stage (Dura Tec high power heat pump, 71watt heat capacity) which thermostatically controlled the solution temperature in the range 20-60°C. The temperature of the bathing medium could be recorded via the Picologger, again as a voltage measurement, and converted to degrees Celcius using a calibration curve for the particular thermistor.

Prior to each measurement, the initial length of the sample was measured at the point where the sample was just straight, with no measurable applied force and allowed to equilibrate for a period of 15-20 minutes in bathing medium. Before measurements were made the samples were pre-strained by 20-50%, depending on the highest strain to be applied in the test, at a rate of $2\mu m\ s^{-1}$ in order to minimize variations in tissue. This was repeated at least once more and preferably twice more before allowing the tissue to rest in the bathing medium and commencing the experiments. A recent study by Cheng et al [301] illustrates the importance of pre-conditioning biological tissues prior to mechanical testing, confirming an older report by Fung [55].

2.3.3 Experimental Protocols

In all cases, prior to conducting mechanical tests, the length of the hydrated sample was measured using digital calipers whilst the wet and dry weights were determined at the end of experimentation. Strain was calculated with reference to the sample length at zero force and room temperature and stress could be related either to geometric area or to area of the solid component as described elsewhere [302]. Prior to the start of experimentation, both the force transducer and extension transducer were calibrated. For the force measurements this was done by securing the force transducer in an horizontal position and hanging known weights (0-100g) onto the end. The corresponding voltage output was then recorded and a calibration curve plotted to calculate force. A similar calibration was performed for the extension transducer whereby the micrometer head was moved by known distances, the corresponding voltage read out was recorded and a calibration curve plotted to obtain distance in millimeters. A final calibration was also carried out for the individual

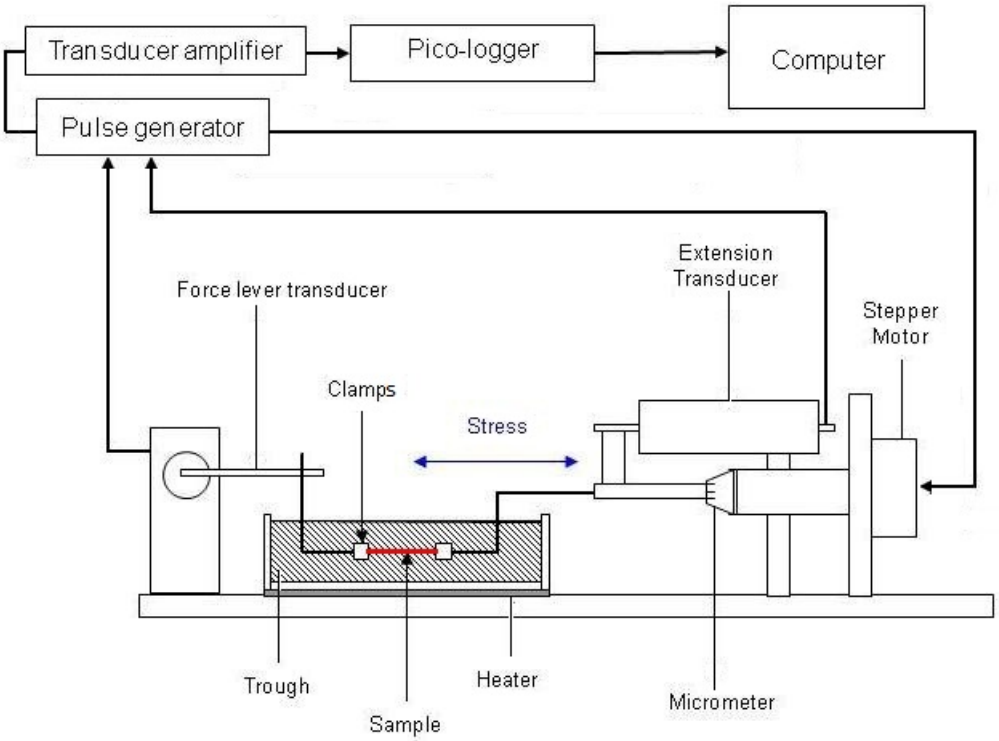

Figure 2.22: Schematic diagram of the purpose built uniaxial testing apparatus used for stress-strain, transient and thermomechanical testing of all samples. The apparatus was equipped with a bathing trough to permit complete immersion of the sample at all times and a Peltier heating stage to control the temperature of the bathing solution. The sample was extended via a stepper motor and micrometer. The voltage outputs from the force transducer and extension transducer were then logged to a computer.

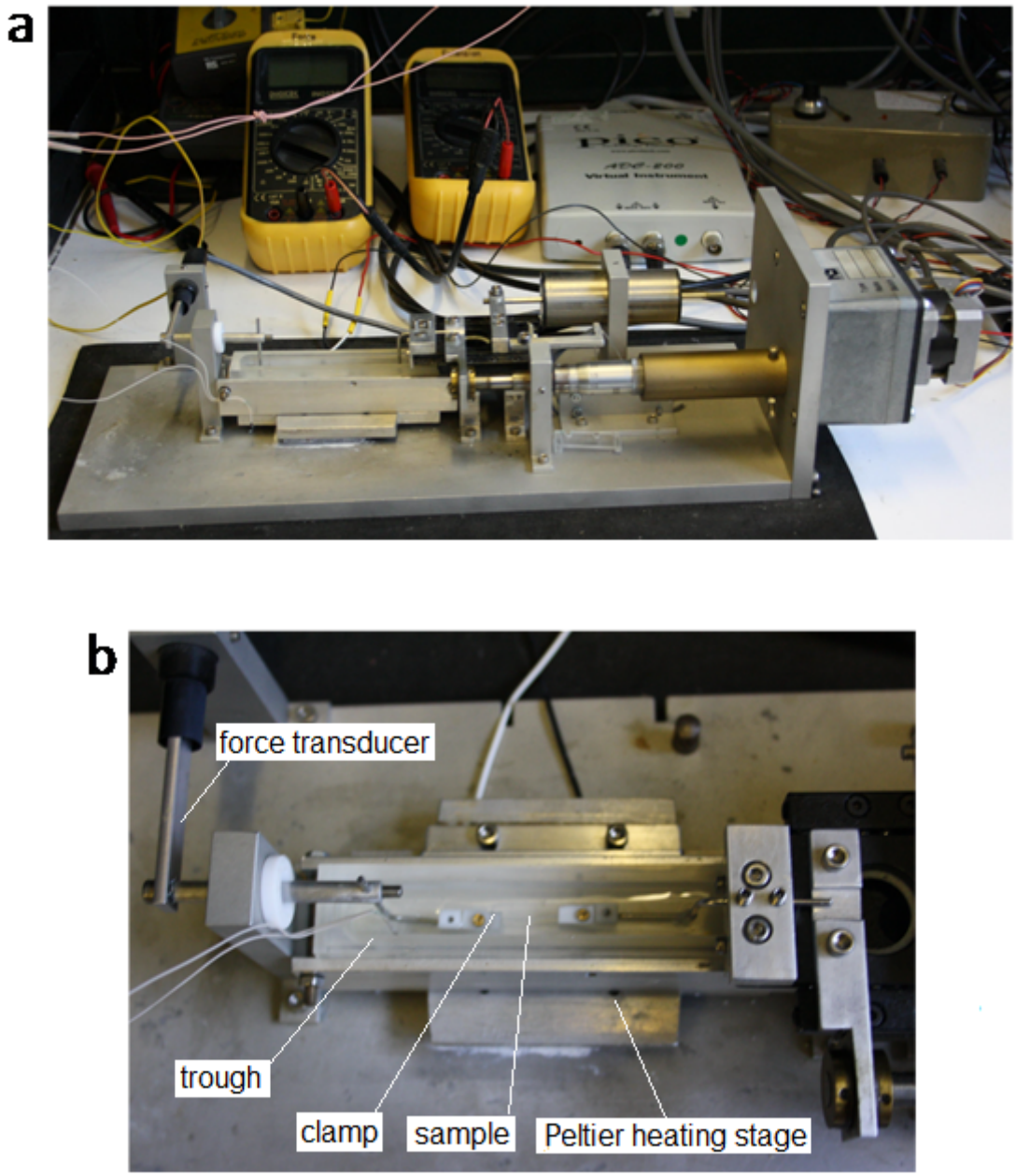

Figure 2.23: Images of the purpose built mechanical testing apparatus in situ a) general view b) close-up of trough set-up in which the bathing medium and sample are contained.

thermistors used to record bathing medium temperature in a limited number of experiments. For this, the voltage output was recorded against known temperatures read off a thermometer and the calibration curve plotted.

2.3.3.1 Uniaxial Stress-Strain Curves

In the first set of experiments samples were mounted as described in section 2.3.2 and then subjected to either cyclic strains of 20% or 50% of the original length or to a point where the sample failed at a constant displacement rate of $2\mu\text{ms}^{-1}$. Stress was then plotted against strain. For each sample the initial and final elastic moduli were derived from the slope of the stress-strain curve by fitting a tangent at zero and 20% or 50% strain. In some samples stress-strain response was recorded whilst the sample was held at a constant temperature of 60°C in order to address the thermomechanical effect. Some additional force-extension measurements were made for ligamentum elastin, the piston cartilage and branchial cartilage in 2,2,2-trifluoroethanol (TFE) (Sigma-Aldrich). In these experiments an initial series of measurements were obtained in deionised water which was then exchanged for TFE whilst the specimen was held at constant 20% strain. The force was then allowed to re-equilibrate before the sample length was adjusted to give zero force and mechanical testing repeated. In some cases, the TFE was exchanged back for deionised water and the force-extension curve repeated under the same conditions as previously. A similar set of measurements was made for each of the lamprey matrix proteins and ligamentum elastin following the exchange of deionised water for deuterium oxide (D_2O).

In order to determine the elastic modulus (the ratio of stress against strain) of the material stress (σ) was plotted against strain (ε) over a given extension range by normalizing these values to the area of the sample being tested.

Extension of the sample was calculated using the following equation:

$$\triangle L = L - L_0 \tag{2.21}$$

where L is the sample length, L0 is the sample length at zero strain and zero

force. Longitudinal strain (ε) was calculated with reference to the sample length at zero force at room temperature using the equation:

$$\varepsilon = (\triangle L)/L_0 \tag{2.22}$$

and stress was related to geometric area using the equation:

$$\sigma = F/A \tag{2.23}$$

where F is applied force and A is cross-sectional area over which the force was applied, or in relation to the solid components as described elsewhere [302]. This is important when relating changes observed to the intrinsic properties of the protein itself and is standard practice within the field. For this method we needed to determine the density of the sample (a constant value for the tissue under investigation), the dry mass and the length. Dry mass of each sample was determined by equilibrating in deionised water for a period of at least 30 minutes after which samples were gently blotted on absorbent tissue and weighed. Following this the samples were dried in an oven at 60°C for 48 hours before being weighed to determine the dry weight.

In order to calculate density we need to know the volume occupied by the tissue and not the volume of tissue plus water. This was achieved using a specific gravity bottle to determine; i) the mass of a specific gravity bottle and total water, ii) the mass of the specific gravity bottle plus total water and mass of the hydrated tissue, minus the displaced water, iii) the mass in (ii) minus the dry mass of the tissue. (We need to subtract the dry tissue mass as opposed to hydrated mass because it is the cross-sectional area of the protein itself that we are interested in and not the contribution played by water). Finally (iii) above was subtracted from the mass of the specific gravity bottle plus total water to give us volume. We now have values for dry tissue mass and volume from which we can calculate density using the expression:

$$\rho = m/V \tag{2.24}$$

where ρ is density, m is mass and V is volume. We also need to use the expression for area:

$$A = V/L \tag{2.25}$$

which leads to the equation:

$$A = m/L\rho \tag{2.26}$$

Following the procedure described above we obtained density values of 1250 kg m^{-3} for dry elastin (which was in agreement with that previously reported by Gotte et al [85] at 1230 kg m^{-3}), 1135 kg m^{-3} for lamprey piston cartilage, 1136 kg m^{-3} for annular cartilage, 1186 kg m^{-3} for branchial and 1113 kg m^{-3} for pericardial sac.

It was also necessary to determine the area of the hysteresis loop. Each stress-strain curve was separated into two separate curves, one for the extension phase and the second for the relaxation phase. If the extension and relaxation curves are the same then the material can be described as Hookean. However, if these two curves differ, then the material has undergone some deformation from which it may or may not recover over time. Using Graph software, a third or fourth order polynomial was fitted to each of the curves separately to give a good fit. The total area beneath the extension curve was first determined and from this the area of the relaxation phase was then subtracted, to give a total value for the area of the hysteresis loop. The hysteresis area is important because it provides a measure of the efficiency of energy storage (resilience) and is highly dependent on the rate of extension. If deformation is too quick then the network may not have sufficient time to respond, resulting in energy being required to overcome the forces that are established, this is released as heat, therefore reducing the resilience of the system.

2.3.3.2 Transient Measurements

In a further set of measurements the unconfined stress-relaxation response (or change in stress as a function of time) was measured following a near instantaneous step increase in strain of 20% of the sample's original length. This specific extension

value was selected in an attempt to minimize premature failure of the samples with branchial and pericardial cartilages being prone to breakage when subjected to high strains. Samples were then held at constant strain and the voltage decay, as a measure of resistance to deformation, was recorded every 5 seconds via a picologger until an equilibrium force was reached. Voltage measurements were then converted to MPa and plotted against time.

To model the stress relaxation behaviour of each of the proteins, relaxation curves were fitted to either a single exponential or biexponential function, using Kaleidagraph 3.5. The biexponential function applied to data was:

$$F(t) = A_1 e^{-t/\tau_1} + A_2 e^{-t/\tau_2} + A_3 \tag{2.27}$$

Where F is force at time t, τ_1 and τ_2 are relaxation time constants and A_1, A_2 and A_3 denote amplitude of components. The mechanical model used to interpret the stress-relaxation response was based on the standard linear model, which is represented by a combination of springs (elastic component) and dashpots (viscous component) (Figure 2.20).

2.3.3.3 Thermoelastic Behaviour

Rubber-like materials are characterized by their unusual thermoelastic behaviour. When held at constant strain the elastic restoring force increases with a rise in temperature. Likewise, when held at constant force, increasing temperature results in rubber-like materials shrinking. Raising the temperature has the effect of increasing molecular motion, which in turn increases the contribution of entropy to the system compared to free energy. Thermoelastic measurements on elastin fibres have established that the elastic behaviour of this protein is consistent with entropic elasticity, having an internal energy component of around 26% involved in its recoil force [52, 201]. In order to quantify the relative contributions made by entropy and energy in the elastic restoring force of elastin and the family of lamprey matrix proteins we performed a series of thermomechanical (force-temperature) tests.

For these measurements samples were initially strained by 20% in deionised water

at room temperature, held at constant strain and then allowed to relax for a period in excess of 1 hour until a state of equilibrium was reached. The change in force as the bath temperature was increased stepwise over the range 20-60 $^\circ$C was then recorded. The change in temperature was imposed sufficiently slowly (10 $^\circ$C per 10 minutes) to ensure that the force equilibrated at each temperature. The change in force was then plotted against Log stress/temperature (K).

The measurements of changes in stress at constant strain as a function of temperature were analysed on the basis of the thermodynamics of rubber-like materials [303], according to which the ratio of the energetic components, f_e, to the total tension force, f, is given by the relation:

$$\frac{f_e}{f} = -T\left(\frac{d\ln\left(\frac{f}{T}\right)}{dT}\right) - \frac{\beta_{eq}T}{\alpha^3\left(V_i/V\right) - 1} \tag{2.28}$$

where the derivative is taken at constant pressure, length and fluid equilibrium, T is the absolute temperature, V_i and V are the sample volumes before and after elongation, β_{eq} is the thermal expansion coefficient and α is the fractional increase in length. As in a similar analysis of elastin [304], the latter term is neglected.

2.4 Microscopy

Understanding of normal tissue structure generally comes from microscopic observations. Various microscopy techniques were employed in this study to relate the mechanical properties observed to the morphology of the tissues in question. The subsections that follow explain the methods used and their relevance in this study.

2.4.1 Light Microscopy

Histology refers to the study of thin slices of tissue under the light microscope. Selective histological stains are frequently employed to enhance visualization and identification of specific microscopic structures. Using conventional histology, the microscopic structure of elastic fibres both from the ligamentum nuchae and large blood vessels has been extensively investigated over several decades [72, 74, 305, 306].

In the current study histological protocols were used to investigate the extracellular matrix architecture of CNBr-extracted and undigested lamprey annular, piston, branchial and pericardial cartilages.

Samples were prepared as previously described in section 2.1.1. Preparation then involved either; i) freezing samples at -20 $^{\circ}$ C and cutting 10-20 μm thick cryo-sections or ii) fixing protein samples in 10% formol saline, followed by dehydration in an ascending series of ethanols, clearing in xylene and finally embedding in paraffin wax prior to cutting into 10-20 μm thick sections. Both transverse and longitudinal sections were cut for the majority of samples. All sections were then mounted onto microscope slides and stained with either; i) Weigert's resorcin-fuchsin or ii) orcein, two of the most commonly used methods for the detection of elastin. Details of these staining techniques are given in Carleton's Histological Technique [307] and Bancroft J.D.[308]. Sections were finally viewed under a Nikon (Eclipse E200) light microscope fitted with a Nikon (Coolpix 4500) camera.

2.4.2 Rhodamine Injections

In order to further characterize the connectivity of the matrix structure of each of the lamprey proteins, micro-injections of 15-20 μl of a fluorescent dye (rhodamine B base) at a concentration of 0.001% were made into the piston and annular cartilages. The branchial and pericardial cartilages were too thin to be injected in this manner, so small pieces (5mm x 5mm for pericardial and 1mm x 10mm for branchial) of tissue were completely immersed in the rhodamine solution which was left to diffuse into the tissue for a period of 2 hours. All samples were briefly washed in deionised water and finally cryo-sectioned so that the spread of the injectate could be followed microscopically. Illumination was achieved using a high-pressure mercury light source and a 515-560 nm excitation filter (Leica N2.1). Open systems are indicated by an even distribution throughout the section, whereas closed systems would be expected to show localized dye distribution.

For branchial and pericardial tissues the effective diffusion coefficient of the Rhodamine dye over time was estimated by the scaling law:

$$D \sim \frac{\lambda^2}{T} \tag{2.29}$$

where D is the diffusion coefficient λ is distance of dye penetration and T is time.

2.4.3 Autofluorescence

Fluorescence can either be induced by labeling with fluorophores or, in some materials can occur naturally. It is this naturally occurring fluourescence, or autofluorescence, that is of particular interest in the current study and is optimized by the use of ultraviolet (UV) excitation. Autofluorescence is often regarded as problematic within the area of fluorescence microscopy resulting in reduction of the signal to noise ratio. However, biological autofluorescence can sometimes be used to highlight structures under investigation by excitation of endogenous fluorophores. There are numerous sources of biological autofluorescence found in both animals and plants alike [309]. Elastin is well-known to emit characteristic blue/green autofluorescence with UV excitation, although the underlying photochemical properties have proved difficult to investigate due to elastin's insolubility in water. This has resulted in an on-going debate regarding the origin of elastin autofluorescence. Studies on elastin hydrolysates have indicated that the aromatic amino acids, tyrosine and phenylalanine, may be the source of elastin autofluorescence [279, 310]. However, this is by no means conclusive since the role of major cross-links, desmosine and isodesmosine, is still debated. Early work of Thornhill [311] ruled out the involvement of desmosine/isodesmosine cross-links, but this was later contradicted by the work of Deyl et al [312]. The limited literature available indicates that branchial cartilage from sea lamprey (petromyzon marinus) also displays autofluorescence, whereas the lamprin based annular and piston cartilages do not. As part of this study we undertook a brief investigation of autofluorescence in the CNBr digested lamprey cartilages to either confirm or refute this opinion.

Frozen sections 5-10μm thick were cut using a cryo-microtome and placed onto

microscope slides with a drop of deionised water. Samples were irradiated in the epi-direction using a high pressure HBO 100W mercury lamp attached to a Leica DMLFS microscope fitted with a Leica I3 filter cube, allowing excitation in the range 450-490 nm. The objective lenses used for observation were a 10x, 0.25 NA and a 50x, 0.55 NA lens . All parameters including contrast, brightness and colour balance were kept constant for all samples and no image processing was performed so that images could be directly compared.

2.4.4 Multiphoton Imaging

Wide field fluorescence microscopy is restricted to providing two-dimensional information. However, for many biological samples, it is desirable to resolve features in the z-direction in the tissue. This can be achieved with laser scanning confocal microscopy (LSCM) the basic mechanism of which involves scanning a finely focused laser beam through a sample. The emitted fluorescence then passes through a pinhole, which rejects out-of-focus light, before being directed to a photomultiplier tube. Three-dimensional images can then be constructed from a series of consecutive two-dimensional scans taken at different depths [313]. As a result, LSCM has become the preferred method to visualize biological samples. The main limitations associated with this technique are the need for exogenous fluorophores, poor depth penetration, sample damage and photobleaching.

These limitations can be largely overcome using a relatively new technique known as multiphoton microscopy (MPM). Like LSCM, multiphoton microscopy involves scanning a tightly focused laser beam through a sample, but confines the signal to the focus spot where the photon flux is highest [314]. Multiphoton microscopy encompasses several different techniques including two-photon fluorescence (TPF), second-harmonic generation (SHG) and coherent anti-Stokes Raman (CARS), with each modality used to illuminate different molecules within a tissue. The major advantages associated with multi-photon microscopy are; sub-micron resolution with 3D sectioning, good depth penetration (up to 1mm), minimal photobleaching and label-free imaging capabilities. Two photon fluorescence (TPF) was of great importance in this study and therefore is described in more detail than the other multiphoton techniques.

Two-photon fluorescence is the simplest and probably the most widely used multi-photon modality for imaging biological tissues being used to excite fluorescence, both induced and indigenous. As its name suggests, TPF occurs when two photons of low energy simultaneously interact with the same molecule resulting in the excitation of the molecule to a higher energy state. If the excited molecule is fluorescent, this leads to the emission of one photon of fluorescence as the energy decays and returns to the ground state. Each of the two photons used to excite the molecule in TPF have half the energy of the one photon used in single-photon fluorescence and double the wavelength [315]. This is illustrated in figure 2.24. For fluorophores that are excited by ultraviolet (UV) light TPF has the advantage of exciting molecules using two photons of lower energy infrared wavelengths that is non-destructive and avoids excessive photo-toxicity to the sample. Because TPF is a weak effect a large number of photons must be delivered to the sample simultaneously in order to increase the probability of non-linear excitation occurring. To achieve this, instead of a constant flow of photons which would damage the sample, a series of high speed, femto-second pulses are generated resulting in high intensity laser light whilst keeping the average power on the sample low [314]. The probability of a two-photon event occurring is dependent on intensity squared and because intensity is dependent on area the likelihood of this happening outside the focal volume decreases rapidly and no fluorescence is emitted. The consequence of this is that TPF-excitation only occurs at the focal volume, there is no out-of-focus fluorescence and therefore the need for a pinhole, as occurs in confocal laser scanning microscopy, is removed. Insertion of a pinhole can result in loss in the number of photons collected because even photons that were in the focal volume on excitation can become scattered on the exit path out of the sample. Consequently, due to use of IR wavelengths and excitation being limited to the focal volume, TPF offers a major advantage in terms of depth penetration.

Second-harmonic generation (SHG) is a second-order non-linear process. Like TPF, SHG requires a high intensity pulsed laser source, but instead of exciting a fluorophore SHG relies on light being passed through a polarizable material that lacks a centre of symmetry [316]. In SHG the photons are not absorbed when they

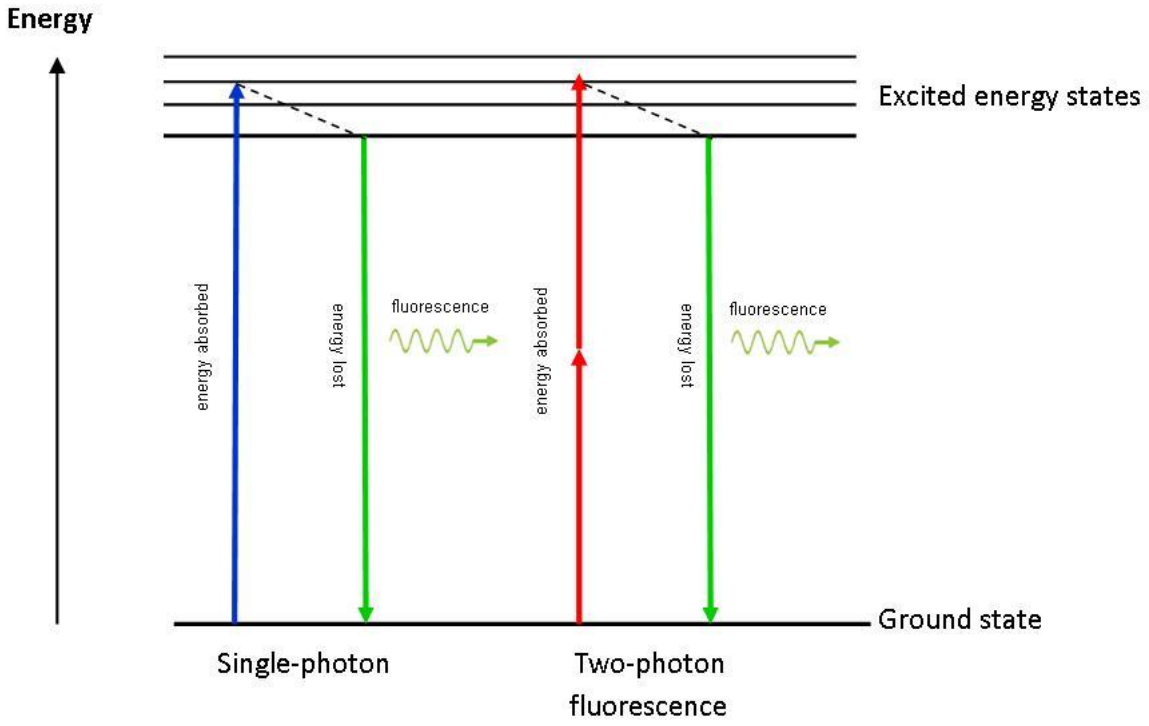

Figure 2.24: Energy level diagram for single- and two-photon fluorescence.

interact with a molecule and neither is the molecule excited to a higher energy level. Instead, the incoming photons are simultaneously scattered and then combine to emit a single photon with double the energy (half the wavelength) of that entering the sample [315]. SHG has proved to be a very useful technique for imaging large, highly ordered structures such as collagen fibres without the need for labeling and avoids photobleaching because no excitation of molecules is involved. The energy level diagram for SHG is illustrated in Figure 2.25

Coherent anti-Stokes Raman scattering (CARS) is a complex non-linear imaging modality which obtains contrast from Raman-active vibrational properties of the sample. The energy level diagram for this process is shown diagrammatically in Figure 2.26. It differs from the other non-linear processes already described because, instead of using single wavelength laser light, CARS imaging requires two synchronized laser beams of different wavelengths [317]. The use of two beams causes the very weak spontaneous Raman signal to be greatly enhanced and, because of this increased sensitivity, CARS is able to visualize molecules, and in particular lipids, within cells and other structures label-free. CARS has the same advantages for tissue imaging as the other two non-linear modalities described earlier.

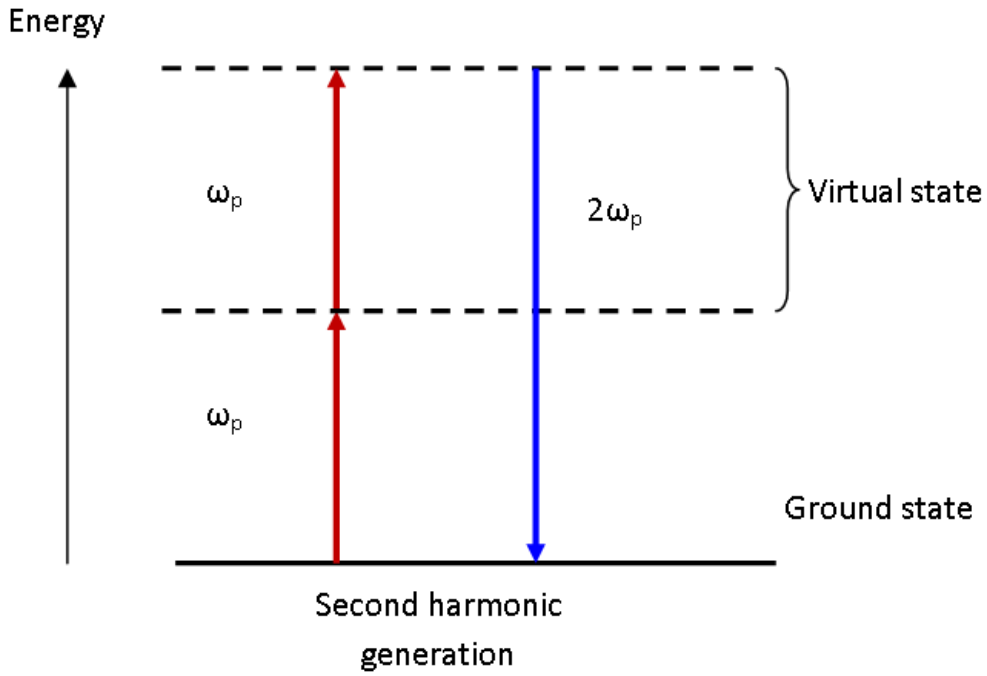

Figure 2.25: Energy level diagram for second-harmonic generation. Photons are neither absorbed nor excited by this process. Instead photons are simultaneously scattered with no loss of energy so that as two photons combine they are emitted as a single photon with half the frequency.

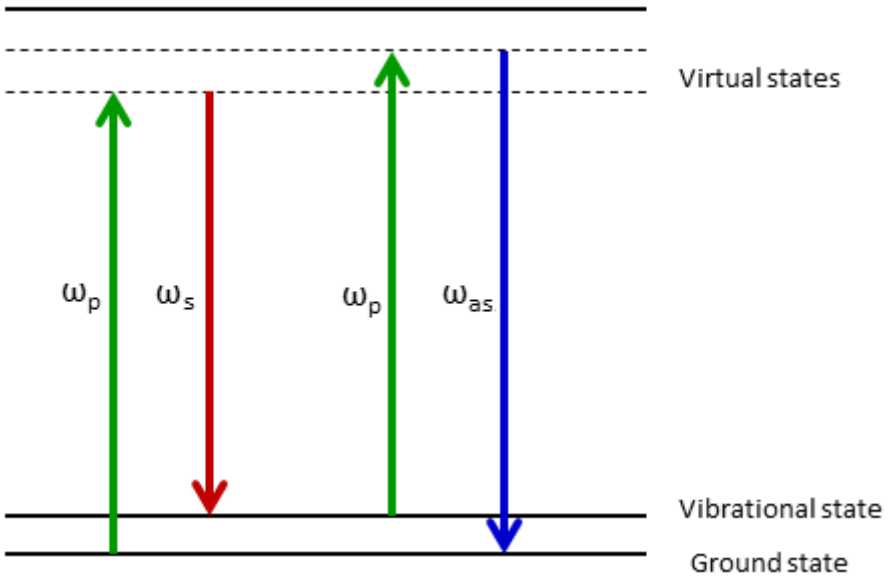

Figure 2.26: Energy level diagram for coherent anti-Stokes Raman.

Each of the modalities described above produces light at a different wavelength allowing the signal to be separated. This allowed us to utilize multi-photon microscopy to investigate the architecture of the extracellular matrix in the small family of lamprey matrix proteins, whilst avoiding the need for staining or fixing.

2.4.4.1 Sample Set-up

The architectures of intact and CNBr digested lamprey cartilage matrices were investigated both in 20μm thick transverse and longitudinal cryo-sections and also from 3D stacks acquired from small tissue blocks (1mm x 2mm x 2mm). The sections were placed with a small amount of deionised water and sandwiched between two 22 x 40 mm cover slips to prevent dehydration. The same procedure was performed on bovine ligamentum elastin as a comparison given its known ability to autofluoresce.

2.4.4.2 Multiphoton Microscope and Imaging

Images were obtained using a modified microscope based on a commercial inverted microscope and confocal laser scanner (IX71 and FV300, Olympus UK). Focusing of the laser onto the sample was achieved using a 60x, 1.2 NA water immersion objective (UPlanS Apo, Olympus UK). SHG was generated in the forward-direction, TPF in the epi-direction and the CARS signal in both the forward and epi-direction. Details of the lasers used and other optical components can be found in [318].

Two-photon fluorescence and second harmonic generation were excited using a mode-locked femtosecond Ti:sapphire oscillator (Mira 900 D; Coherent, USA) which resulted in the generation of 100-fs pulses at 76 MHz repetition rate and 800 nm wavelength. The average power at the sample was in the region of 5 to 30 mW. For CARS microscopy, the synchronized dual laser beams of differing wavelengths were provided by an optical parametric oscillator (OPO) (Levante Emerald, APE , Berlin, Germany) pumped with a frequency doubled Nd:Vanadium picosecond oscillator (High-Q Laser Production GmbH). For CARS microscopy the OPO was tuned to excite the 2845 cm^{-1} CH_2 Raman bond mode; for this the signal beam was tuned to 924 nm and the idler beam to 1254 nm. The maximum combined output power from the signal and idler beams was 2W. However, the power at the sample was restricted to 30-80 mW in order to avoid tissue damage.

Images were constructed by raster scanning the laser focal spot from which two-dimensional intensity plots in the $x - y$ direction could be constructed. Three-dimensional stacks were constructed from a series of two-dimensional scans separated by a distance of 1μm in the z direction. Images were subsequently processed using Image J software (Rasband, 1997-2009) and each of the modalities visualized

separately in digested tissues or overlaid to investigate interaction of extracellular matrix components in the undigested tissues.

2.4.5 Scanning Electron Microscopy

Scanning electron microscopy (SEM) is a standard tool used to study the surface of a specimen. The surface of the sample is scanned with a narrow beam of electrons resulting in the liberation of secondary electrons which add to the signal. These secondary electrons are then collected to form an image. Sample preparation was minimal as the tissues had been digested in CNBr and therefore all cellular content removed prior to observation, which avoided the need for fixation. Samples were dehydrated through an ascending series of ethanols from 70-100% and then dried at 37 $^{\circ}$C whilst fixed to a metal stub using carbon tape. Drying by this method may cause artefacts including shrinkage, twisting, collapse or tearing of the sample and so interpretation of the images should be treated with caution. After dehydration the samples were sputter coated with 20 nm gold to minimize specimen charging using a Polaron SC515 SEM coating system. Samples were then viewed and images captured using a Hitachi S-3200N scanning electron microscope.

2.5 X-ray Diffraction

X-ray diffraction provides a wealth of detailed structural information for biological materials including molecular structure, the arrangement of molecules forming fibrils and their orientation [319]. In biological tissues this information is generally achieved by the use of X-rays with small wavelengths (K_α). How useful X-ray diffraction is for studying any particular biological tissue depends primarily on the degree of ordering within the tissue. In general, materials that diffract strongly are highly ordered whereas a lack of order results in diffuse scattering. Despite the fact that X-ray diffraction has largely been applied to the study of crystals, which are highly ordered, this technique can also be used to obtain X-ray scattering patterns for less ordered materials. For biological samples X-rays with small wavelengths are used which become elastically scattered through many angles.

W.H.Bragg and his son W.L.Bragg in 1912 were the founders of Bragg's law which is commonly used today to explain X-ray patterns of crystal structures. Bragg's law

determines the atomic arrangement of atoms within a crystal and explains why the planes of a crystal act as X-ray reflecting surfaces at certain angles of incidence. It is described by the equation:

$$n\lambda = 2dsin\theta \tag{2.30}$$

where, n is an integer, λ is the wavelength of incident X-ray beam, θ is the angle of the incident X-ray beam and the scattering planes, and d is the distance separating the parallel atomic layers, or planes, of the crystal. Since it's origin, when Bragg's law was used to explain the interference pattern of scattered X-rays of crystals, this equation has also been used to study the molecular structure of many other materials.

Any X-rays that have undergone Bragg reflections can be detected and displayed as a diffraction pattern. Interference between scattered X-rays at different levels is dependent on the degree of order of the elements in the sample. Therefore, biological materials which tend to be less well ordered structures produce diffuse diffraction patterns compared to crystals which are highly ordered and produce discrete reflections which can be clearly identified. If a material has no preferred orientation, then the background scatter or diffuse scatter may contain some limited structural information.

Periodicity within a sample results in a series of reflections which are numbered from the centre outwards (orders of diffraction). If a bundle of fibres is held vertically in a collimated X-ray beam, then X-rays that are scattered parallel to the fibres result in meridonal reflections and those scattered perpendicular to the sample result in equatorial patterns. This is shown diagrammatically in Figure 2.27. Wide angle X-ray scattering (WAXS) is a well established technique that has traditionally been used to investigate small scale structures ($\sim 10^{-9}$m). The pattern produced results from X-rays that have been scattered through large angles, is achieved typically by a sample-detector separation of tens of centimetres and is frequently used to gain information on intramolecular structure. The scattered intensity is plotted as a function of the angle of the incident X-ray beam (2θ) and the observed pattern is intimately related to the internal structure of the sample. A crystal structure

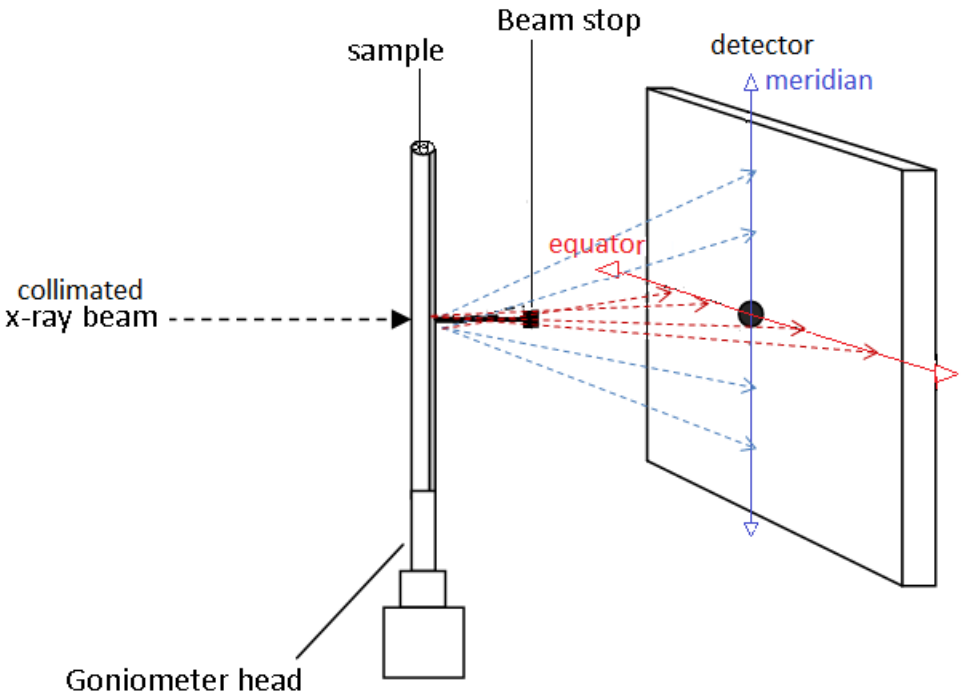

Figure 2.27: A schematic diagram to illustrate the production of meridonal and equatorial patterns from a bundle of fibres held vertical to the incident X-ray beam.

is composed of regularly spaced atoms, through which planes can be defined. The distance between the planes is the d-spacing, whilst the intensity is proportional to the type and distribution of atoms within the planes. Diffuse scattering is common in the diffraction pattern of many biological tissues and should not be ignored since the location and intensity of this scatter can still provide important information. Small angle X-ray scattering (SAXS) is basically the same technique as WAXS except that it is generated by scattering through smaller angles. Practically, this is achieved by using a larger sample-detector distance (typically several metres) and has been developed in an attempt to investigate larger-scale structures. This may require the use of sensitive detectors and intense (synchrotron) radiation sources.

The sample is irradiated by an X-ray source (a monochromatic and collimated beam) and the resulting scattering pattern is measured by a 2-D position sensitive detector.

2.5.1 WAXS Experimental Set-up

Wide angle X-ray scattering was conducted using a MAR345 (Mar research) image plate mounted on a rotating anode generator (Bruker AXS). The latter was operated

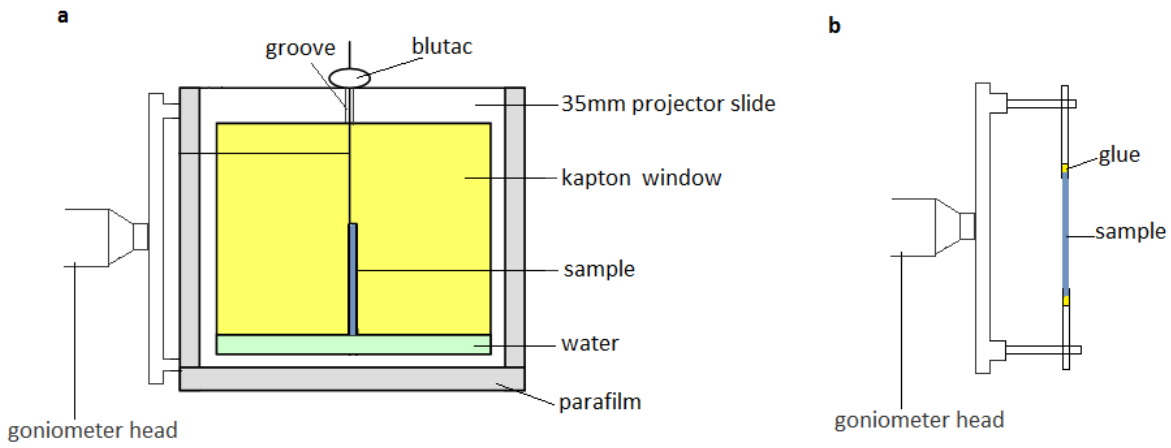

Figure 2.28: Sample setup for X-ray diffraction a) hydrated and b) dehydrated.

at 100 mA and 35 KV (3.5 kW) producing copper Kα radiation which was collimated using XENOCS FOX2D CU25_25P mirrors. The sample to detector distance used for all measurements was 150 mm whilst exposure times were a minimum of 2 hours. Type I collagen from rat tail tendon was used as a calibration.

In the present study, WAXS was performed on fibrous ligamentum elastin and the four lamprey matrix proteins both in the hydrated and dehydrated states. Samples were either mounted fully hydrated or dehydrated in a relaxed or extended (by 50% extension) state by drying at 37°C for a period of 72 hours. Fully hydrated samples were placed with a few drops of deionised water into a simple holder constructed from the outer casing of a 35mm projector slide and two pieces of 8μm thick Kapton film and sealed with Parafilm sealing film to minimize water loss. The sample was kept wet due to a reservoir of water and the sample was held straight using fine thread attached to the sample at the upper end and secured onto the holder. This arrangement is shown in figure 2.28. Data were analysed using FIT2D (Hammersley. A., 1998), a 2-D data analysis program that allowed us to determine d-spacings and intensities.

2.6 Calorimetry

Calorimetry is the science concerned with measuring the thermal properties of a material which can then be related to certain physical properties of that material. Calorimetry is a widely used technique in subject areas such as chemistry, pharmacology, cell biology, biophysics and materials science. Several different types of

calorimetry have evolved in order to extract different information, but, despite this, all calorimeters have several underlying features in common. i) They all have a chamber in which a thermal experiment is performed and is isolated from the surrounding environment and ii) all calorimeters measure heat exchange between the sample and calorimeter. In this study, one of the most popular techniques, differential scanning calorimetry, or DSC, is used to measure changes in both temperature and heat flow associated with phase transitions of elastic proteins as a function of time.

2.6.1 Differential Scanning Calorimetry

DSC, is a powerful analytical technique that measures the amount of heat released or absorbed by a material as it is heated linearly. DSC can be sub-divided into two broad categories, being heat flux DSC and power-compensated DSC. These two types of DSC differ both in their measuring principles and in the design of the calorimeter itself. The calorimeter used in this present study was a heat-flux DSC where the sample being analysed (of known mass) is sealed into one pan and an identical but empty pan is used as a reference. Both the sample and reference pans sit on a heat sensor disk located within the DSC cell and are heated by a single electrical heat source at a constant rate within the surrounding furnace. Heat is transferred to the reference and sample pans via a thermoelectric disc. Both the temperature range and the heating / cooling rates are computer-controlled. This type of set-up is shown in figure 2.29. The temperature difference between the reference pan and the sample pan which arises due to the heat capacity of the sample, is measured by thermocouples as an electrical potential difference and the heat flow, or transfer of thermal energy from one part of a system to another, is determined.

$$Q = \Delta T / R$$

where Q is heat flow, ΔT is the temperature difference between the reference and sample and R is the resistance of the thermoelectric disc. Heat will only flow

if there is a temperature difference present. If there is no difference in the differential temperature between the sample and reference then the electrical potential difference will also be zero and the DSC thermogram will take the form of a straight line. If, however, a phase transition in the sample occurs then equilibrium will be disturbed resulting in the production of a differential signal which is proportional to the difference in heat flow to the sample and reference pans.

DSC is frequently used to detect transitions in the material including the glass transition (T_g), melting temperature (T_m) and crystallization temperature (T_c) as well as heat capacities associated with a given material. Although each of these transitions provides valuable information regarding the thermal properties of materials, it is the glass transition that is of greatest interest in the current study. In polymers T_g is the point at which the material changes from a hard glassy state to a pliant rubbery state. Although the glass-transition temperature provides valuable information on the stiffness, heat capacity and thermal expansion coefficient of polymers, these are not the only materials that undergo glass-transitions. In biological materials, the T_g is also considered to be of great importance, often providing an insight into the material's physical structure and, in the case of proteins, changes in the underlying network [320]. Many biological materials, such as elastin, can be best described as random, with little order in the solid state. As these materials are heated, so their heat capacity increases until a specific point is reached where the material has enough heat to become mobile. This glass transition point appears as a downward step in a heat flux DSC thermogram as shown diagrammatically in Figure 2.30.

The following section describes the experimental parameters used in this current investigation to confirm T_g values for dehydrated elastin as reported previously in the literature [320, 321, 322] and then employ the same protocol to determine the T_g values for each of the proteins isolated from lamprey cartilage.

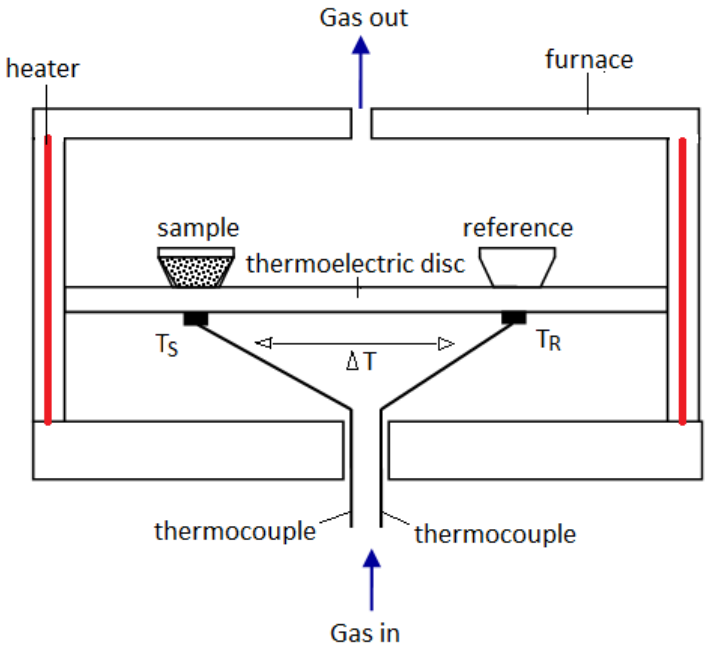

Figure 2.29: Schematic diagram of a typical heat flux calorimeter where heat is supplied by a single source. Heat is generated within the sample pan, leading to an increase in temperature of the sample when compared to the temperature of the empty reference pan, which is measured by thermocouples.

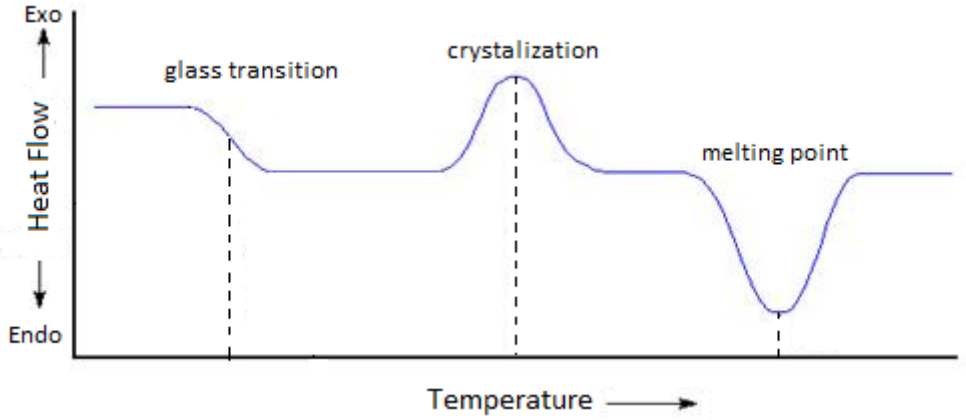

Figure 2.30: Diagrammatic representation of a heat flux DSC plot showing the most frequently encountered transitions including glass transition, crystallization and melting. Of particular interest for amorphous or random biological materials is the glass transition where the sample has absorbed heat resulting in an increase in its heat capacity so that the material becomes mobile.

2.6.1.1 DSC Experimental Set-Up

Samples on which DSC measurements were to be performed were purified by methods described in section 2.1.1. Elastin was prepared from porcine aorta either by the Lansing method (see section 2.1.1.1 for full details) or solubilised with oxalic acid (see section 2.1.1.4) to produce α-elastin. The lamprey matrix proteins were

extracted with CNBr (see section 2.1.1.5). Samples were then fully dehydrated by freeze-drying or by prolonged heating at 60°C and finely ground to produce grains of roughly equal size.

DSC thermograms were recorded using a Mettler Toledo DSC821, which had previously been calibrated using indium and tin standards. Glass transition temperatures were deduced from the DSC thermogram by extrapolating the pre- and post-transition baselines and determining the midpoint between the onset and end point temperatures. Samples of known mass (between 2-5 mg) were placed into standard 40 μl aluminium pans and sealed using a press whilst an identical, but empty pan, was used as the reference. Measurements were made on at least two samples. Following the experimental conditions detailed in similar studies [322, 323] a heating range of 30 to 150°C was selected for the first scan followed by a further two scans over 30 to 250°C. Both the sample and the reference were heated at a constant rate of 20°C per minute whilst cooling was at a slower rate (10°C per minute). Different heating rates can compromise resolution and sensitivity in the thermogram produced. The heating rate of 20°C/min was chosen on the basis of previous investigations which indicated that this rate resulted in well-defined glass transitions [322].

Chapter 3

Molecular Bases of Elastin Mechanics

The aim of the investigations in this chapter was to use Raman spectroscopy to establish the molecular bases of elastin mechanics. There is already an extensive literature on the mechanical and thermomechanical properties of elastin. However, we first report a small series of experiments undertaken to confirm the behaviour of our preparation to define conditions for the spectroscopy. We also report on a series of experiments using differential scanning calorimetry interactions with a similar objective. The final section summarises structural data acquired by X-ray diffraction.

3.1 Mechanics

3.1.1 Stress-Strain Analysis

Quasi-equilibrium stress-strain curves were obtained for nuchal elastin fibres over a range of extensions. Figure 3.1 shows typical stress-strain behaviour for fully hydrated nuchal elastin at room temperature over the strain range of 0% to 50%.

The mean initial and final elastic moduli did not differ significantly across the range of extensions tested resulting in stress-strain behaviour that could best described as linear. The average initial modulus (at 0.01 strain) at room temperature was 0.24 MPa $\pm$ 0.05 (n=8), which is the same order of magnitude as that given in the literature [54, 324]. The slight discrepancy between our results and that of previous studies (0.3-0.6 MPa) stems from the fact that our calculations were based

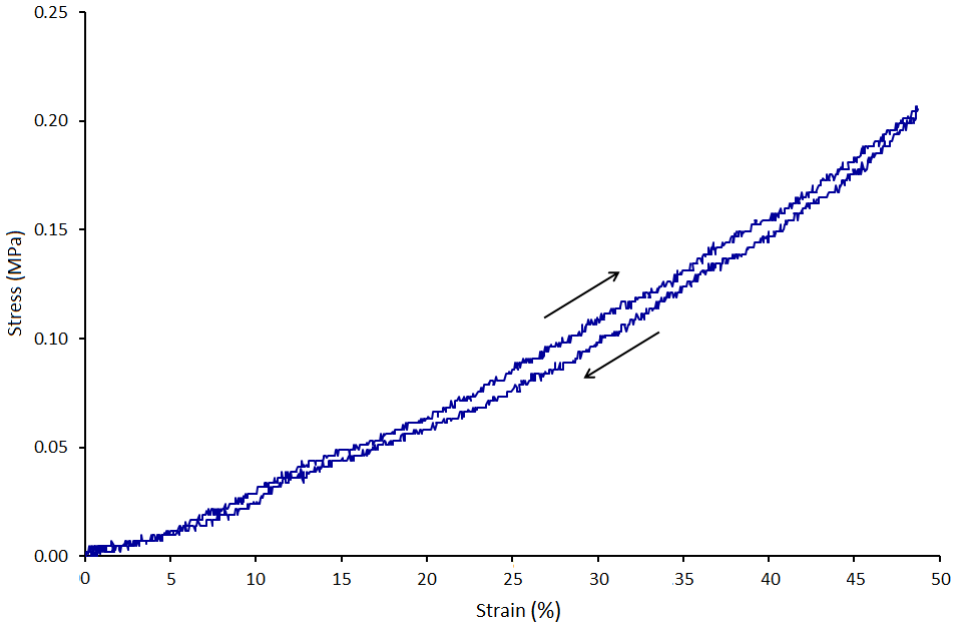

Figure 3.1: Typical stress-strain behaviour for nuchal elastin fibres subjected to uniaxial strain of 50%. All measurements are made in de-ionized water at room temperature at a strain rate of 2 μm s^{-1}.

on density values rather than physical sample dimensions as described in the Methods 2.3.3.1. The modulus at 20% extension was calculated to be 0.36 MPa ± 0.14 (n=8) and that at 50% strain was 0.60 ± 0.17 MPa. At 20% strain hysteresis loss for fibrous elastin was small with a value of 0.0009± 0.0005 MPa (n=13), indicating efficient recovery of energy of deformation and the mean breaking strain was 0.54±0.11 (n=10), although this value was probably an under-estimate of the true breaking strain as sample failure generally occurred at the point of fixing rather than in the bulk tissue.

3.1.2 Stress-Relaxation

Figure 3.2 shows a typical stress-relaxation curve for fibrous elastin over a period of 2000 seconds following a step-application of 20% strain. The transient behaviour of fibrous elastin could best be fitted by the biexponential function:

$$F(t) = A_1 e^{-t/\tau_1} + A_2 e^{-t/\tau_2} + A_3 \tag{3.1}$$

and the parameters for elastin are shown in table 3.1. The data for elastin could actually be fitted by a single exponential function, as expected for the standard

linear (Kelvin) model. However, the purpose of the present measurements was to provide comparisons of the lamprey matrix proteins and these required a biexponential function as described further in section 4.1.2. The mechanical response of elastin was fully recoverable up to approximately 2000 seconds, but beyond this point elastin displayed a prolonged period of creep behaviour (with a further fall in stress in the order of 15% over 40,000 seconds) whose basis was not investigated.

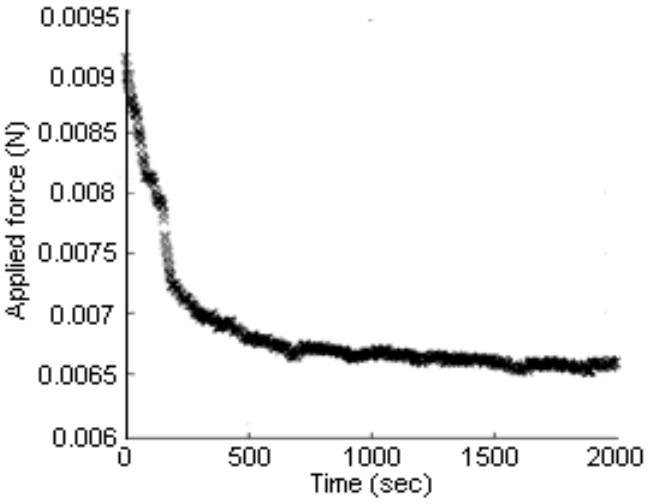

Figure 3.2: Characteristic stress-relaxation curve over a period of 2000 seconds for nuchal elastin fibres following applied strain of 20% in deionised water at room temperature. The curve was fitted to a biexponential function the parameters from which are summarized in a Table 3.1.

	$A_1 \times 10^{-4}$ (Nm^2) (Mean, std dev), (n)	$\tau_1 \times 10^{-3}$ (sec^{-1}) (Mean, std dev), (n)	$A_2 \times 10^{-4}$ (Nm^2) (Mean, std dev), (n)	$\tau_2 \times 10^{-3}$ (sec^{-1}) (Mean, std dev), (n)
Elastin fibres	2.17 ± 2.32 (n=3)	14.19 ± 17.6 (n=3)	11.59 ± 7.25 (n=3)	1.69 ± 1.38 (n=3)

Table 3.1: Parameters for the stress-relaxation curves shown in Figure 3.2 fitted with the biexponential function $F(t) = A_1 e^{-t/\tau_1} + A_2 e^{-t/\tau_2} + A_3$

3.1.3 Thermomechanical Testing

Thermomechanical measurements were made both of the quasi-equilibrium stress-strain behaviour at different temperatures and of the changes in stress as the temperature was changed in a sample held at a constant strain of 20%. The stress-strain behaviour of elastin, summarised by the ratio of moduli at room temperature and at 60°C, showed a number of differences, as can be seen in Table 3.2.

Material	Ratio of Initial Moduli at 0.01 Strain, 60°C/room temp (mean, std dev), (n)	Ratio of Final Moduli at 0.20 Strain, 60°C/room temp (mean, std dev), (n)	Ratio of Hysteresis Loop area/MPa, (mean, std dev), (n)
Elastin Fibres	0.76 ± 0.01 (n=4)	0.76 ± 0.13 (n=4)	0.88 ± 0.34 (n=4)

Table 3.2: Effects of temperature on mechanical properties of ligamentum elastin fibres. Mean values for initial (0.01% strain) and final (0.20% strain) elastic moduli and hysteresis areas are expressed as the ratio of values at 60 ° C and room temperature.

Both the initial and final moduli fell by approximately 25% ±0.13 with increasing temperature, whilst the hysteresis area fell by 12% ±0.34 compared to that at room temperature. These data are in agreement with the work of Dorrington and McCrum [200] indicating that solvent interactions become less important and entropic interactions become increasingly important at higher temperatures. Following heating to 60°C the sample and bathing medium were allowed to return to room temperature, and the stress-strain cycle repeated after a period of 2 hours. From Figure 3.3 it can be seen that the stress-strain behaviour does not retrace the original at room temperature, although both the elastic moduli and hysteresis area do increase (initial modulus of 0.29 ± 0.06 and final modulus of 0.40 ± 0.09). Like the creep in the stress-relaxation measurements this is another indication of relaxation processes occurring on a long time scale.

Using equation 2.28, the results of the measurements of force at constant strain, as a function of temperature are shown in Figure 3.4. A purely entropic mechanism of elasticity would require the slope of the curve to be zero. As reported by others, for elastin there is an increase in retractive force with increased temperature and, at high temperatures, entropic mechanisms dominate [325] as indicated by the plateau at around 45°C. However, at low (physiological) temperatures there is a significant energetic component, greater than that previously reported [52, 201] (approximately 25%), with water contributing to the energetic component of elastin elasticity.

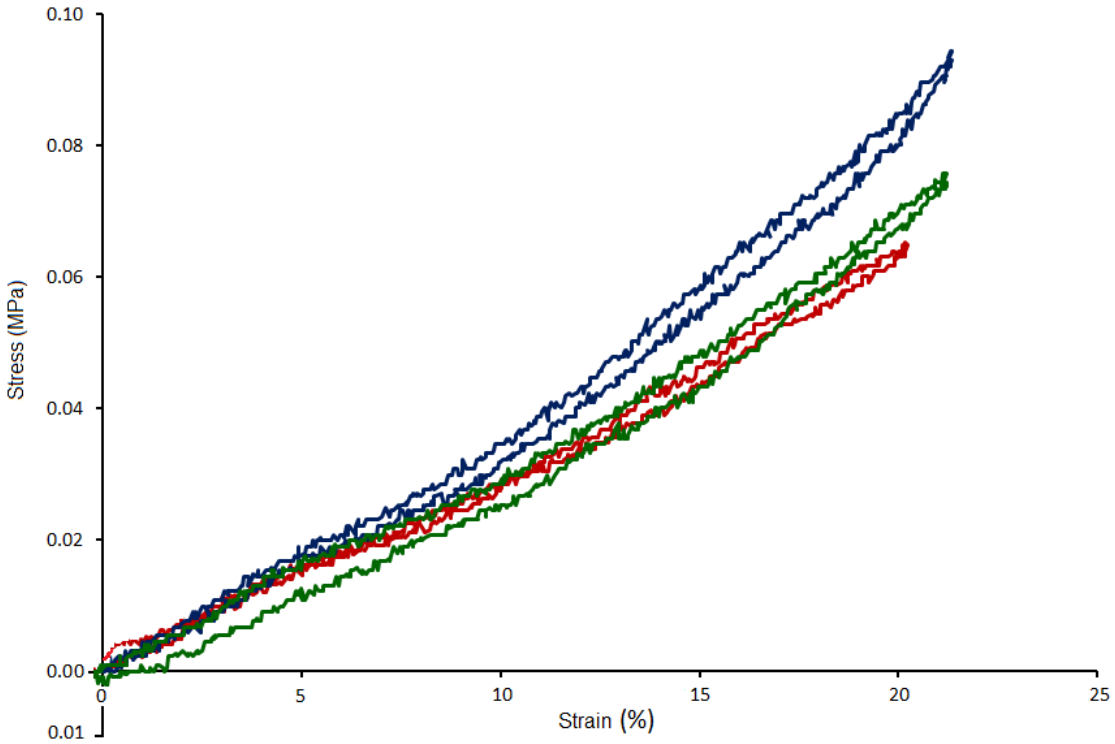

Figure 3.3: Typical stress-strain behaviour for nuchal elastin fibres subjected to uniaxial strains of 20% in deionised water at room temperature (blue), heated to 60°C (red), and after cooling back to room temperature over a period of 2 hours (green).

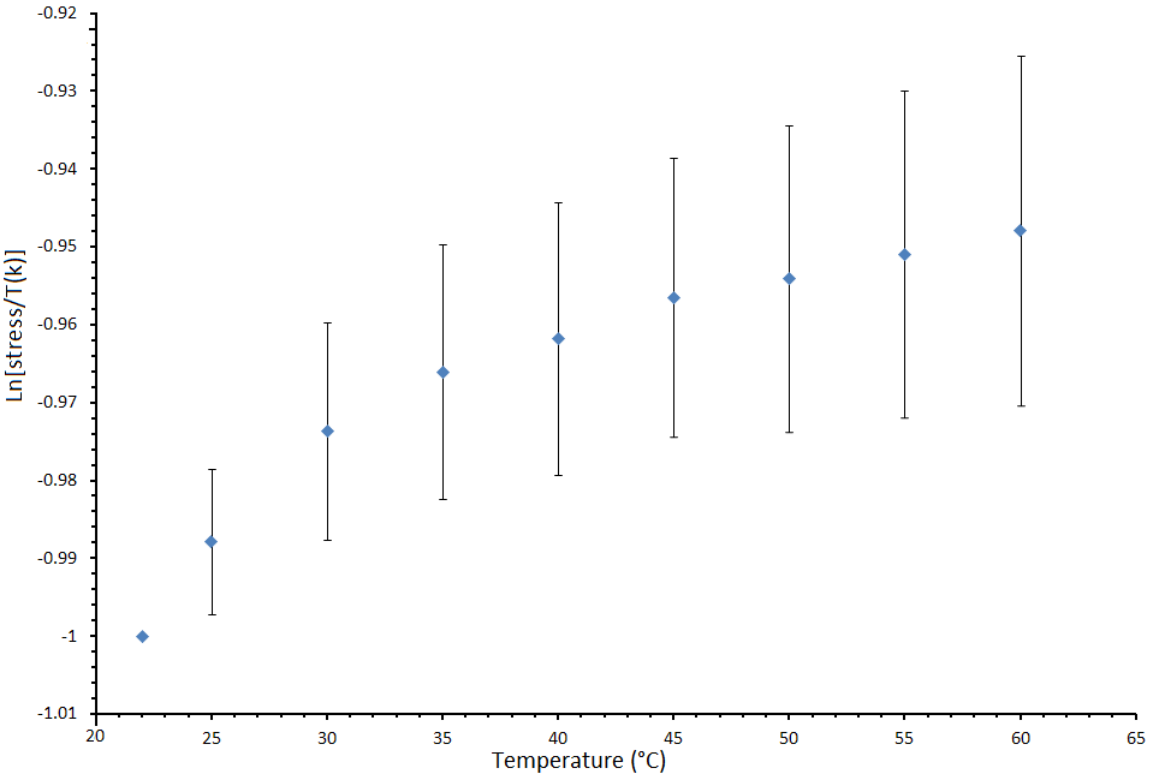

Figure 3.4: Thermoelasticity plots for nuchal elastin fibres (n = 5). Elastin fibres were extended by 20% at room temperature and held at fixed 20% extension. The force was then measured as temperature was increased from room temperature to 60°C, following equation 2.28.

3.1.4 Mechanics in Trifluoroethanol

The importance of solvent interactions was confirmed by exchanging water for the non-aqueous solvent, TFE, which resulted in several noticeable changes in behaviour. The interpretation of experiments on the behaviour of elastin in mixed solvents has been critisised because of uncertainties regarding the partitioning of the different molecules between compartments within the fibrous matrix [200, 201] and for this reason we made measurements in 100% TFE. A typical stress-strain curve for elastin fibres first in water at room temperature and then following exchange of water for TFE, (allowed to equilibrate for a period in excess of 2 hours), is shown in Figure 3.5 and the change in reference lengths (length at zero strain), initial modulus, modulus at 20% strain and hysteresis loop areas are summarized in Table 3.3. For elastin fibres held at constant 20% strain during exchange of water for TFE there was a large increase in the reference length of the sample, which was completely reversible when TFE was replaced by water. The initial and final elastic moduli as well as the hysteresis loop area were also effected, all becoming substantially higher on exchange of water for TFE, indicating that the material had become stiffer and elastic energy was less efficiently recovered upon removal of the applied force. The stress-strain curves in (b) and (c) of Figure 3.5 also show the response after TFE had been exchanged back for water and allowed to re-equilibrate for at least 2 hours. The effect of solvent exchange is reversible, with the elastic moduli and hysteresis area returning to their original values. The relaxation phase of curve (b) shows a negative stress value, but once again over a further period of approximately 30 minutes this behaviour is fully recoverable and is therefore not due to plastic deformation.

Material, (n)	Ratio of reference lengths: TFE/water	Ratio of initial moduli: TFE/water	Ratio of moduli at 20% strain: TFE/water	Hysteresis area: TFE/water
Elastin fibres (n=4)	1.35 ± 0.04	1.95 ± 0.54	2.69 ± 1.09	6.60 ± 3.96

Table 3.3: Effects of solvent on mechanical properties of elastin fibres. Mean values for initial and final (20% strain) elastic moduli, reference length and hysteresis loop areas expressed as the ratio of values in TFE and water.

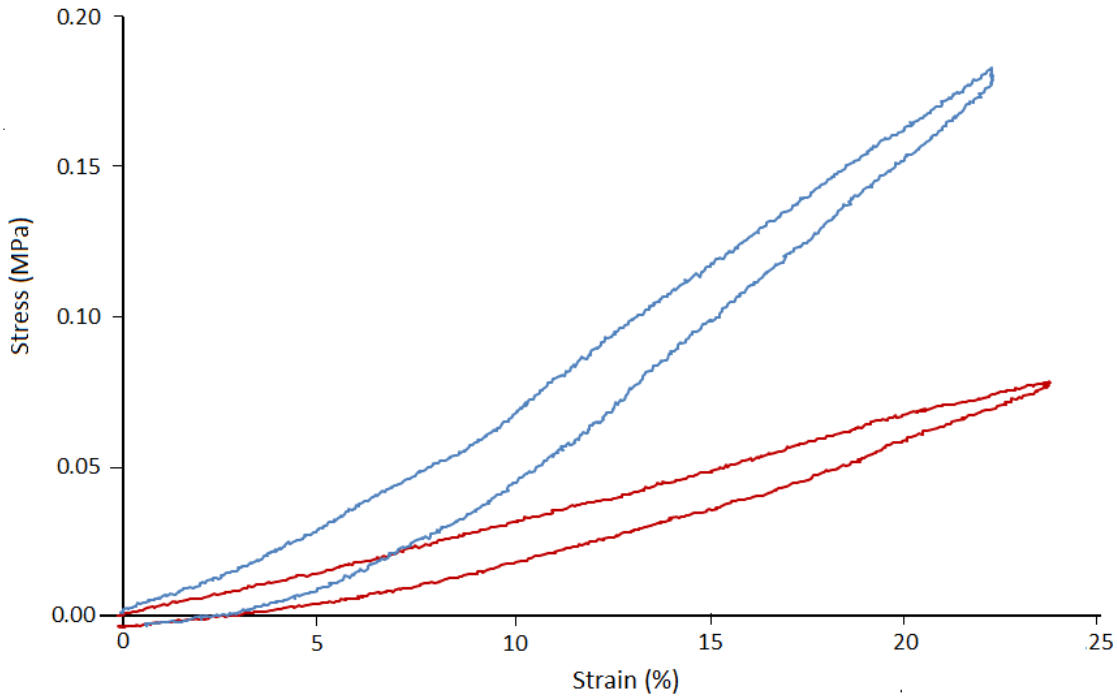

Figure 3.5: Typical stress-strain curves for elastin fibres in water at room temperature (red) and in TFE (blue). The data shown are for individual small bundles of elastin fibres strained by 22-24% of the original length.

3.1.5 Mechanics in Deuterium Oxide

In order to further investigate specific effects of water on elastin mechanics a small number of experiments were undertaken (n = 5), where water was exchanged for deuterium oxide whilst elastin fibres were held at constant 20% extension, and stress-strain cycles repeated over a strain range of 0-20%, following an equilibrium period in excess of 2 hours. Previous studies have shown that hydrogen-deuterium exchange can effect protein flexibility either by forming stronger bonds with deuterium oxide or by forming additional intramolecular bonds [326]. Exchange of water for deuterium oxide resulted in a negligable increase (4.7% $\pm$ 2.1) in stress at constant length. Figure 3.6 shows typical stress-strain curves for elastin fibres in deionised water, deuterium oxide and finally following re-equilibration in water. The values for elastic moduli, hysteresis areas and work involved in stretching the sample by 20% in water and deuterium oxide are shown in Table 3.4. Initial and final elastic moduli, hysteresis area and work involved in straining elastin fibres by 20% extension are all unaffected by exchanging water for deuterium oxide.

a

Sample	Initial modulus (0.01 strain) in H_2O (mean, std dev) (n)	Final modulus (0.20 strain) in H_2O (mean, std dev) (n)	Work to 20% strain (MPa) in H_2O (mean, std dev)(n)	Hysteresis loop area (MPa) in H_2O (mean,std dev)(n)
Nuchal elastin fibres	0.28 ± 0.10 (n=5)	0.29 ± 0.02 (n=5)	0.007 ± 0.002 (n=5)	0.0005 ± 0.0001 (n=5)

b

Sample	Initial modulus (0.01 strain) in D_2O (mean, std dev) (n)	Final modulus (0.20 strain) in D_2O (mean, std dev) (n)	Work to 20% strain (MPa) in D_2O (mean, std dev)(n)	Hysteresis loop area (MPa) in D_2O (mean,std dev)(n)
Nuchal elastin fibres	0.28 ± 0.13 (n=5)	0.28 ± 0.04 (n=5)	0.007 ± 0.002 (n=5)	0.0004 ± 0.0001 (n=5)

Table 3.4: Tables (a) and (b) summarize the elastic moduli, work to 20% extension and hysteresis loss for nuchal elastin fibres in deionised water and following exchange for deuterium oxide respectively.

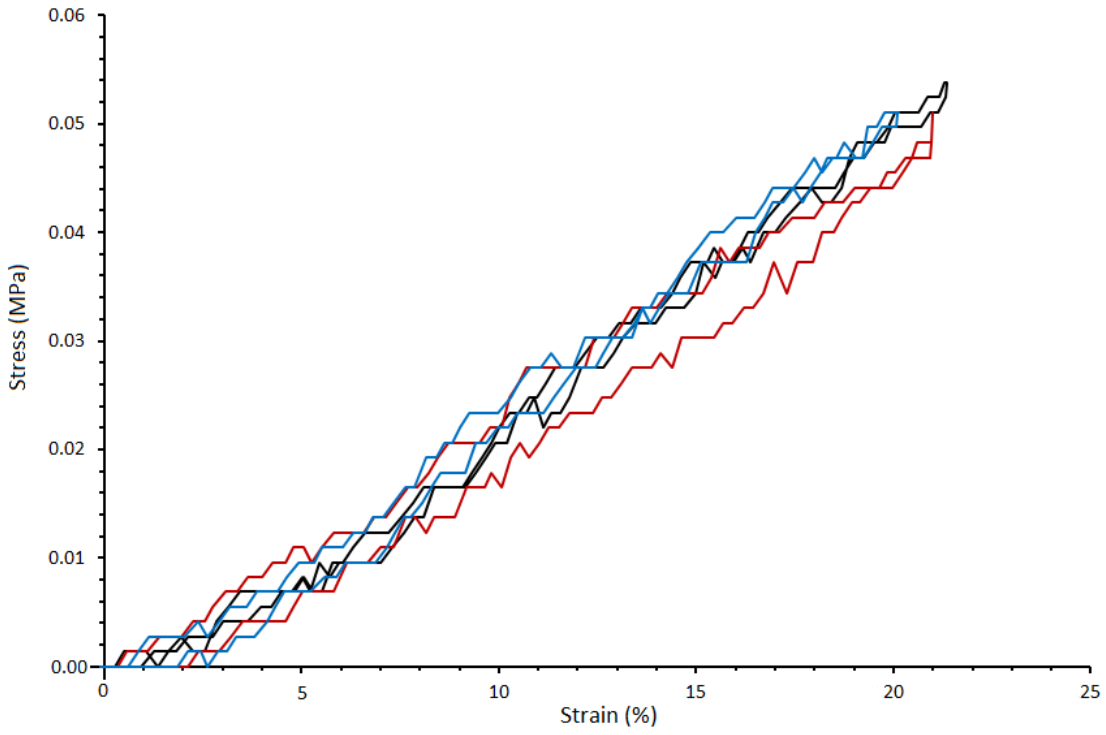

Figure 3.6: Representitive stress-strain curve for fibrous elastin over a strain range of 0-20% in deionised water (blue), following exchange of water for deuterium oxide (red) and after re-equilibration in deionised water (black).

3.2 Raman Spectroscopy

We begin this section by describing the Raman spectrum obtained for fully hydrated alkali-extracted nuchal elastin fibres. Following this a comparison is made with aortic

elastin prepared by procedures that are regarded as being more gentle than the alkali-extraction method, in an attempt to better preserve the fibre structure. In addition, this procedure was modified to either preserve or remove microfibrillar components of the elastic fibre. This enabled us to investigate both the direct contribution of microfibrils to the spectra and their possible effects on elastin structure. To better understand the relationship between the structure of the fibrous protein and that of the monomer, α-elastin, a comparison was made between nuchal elastin fibres and α-elastin.

Having discussed the whole spectrum differences we then consider secondary structure by analysing the amide I and amide III bands of all the elastin preparations.

The next section investigates solvent interactions including the effect of exchanging H_2O for D_2O (deuterium oxide) and TFE (trifluoroethanol) on both the whole spectrum and amide band composition.

Finally, two groups of experiments are reported that explored the responses to mechanical strain. The first investigates the spectral changes associated with application of mechanical strain and the second compares the spectra of the proteins held at constant strain, whilst heated over a temperature range that is associated with significant changes in the energetics of elasticity.

All spectra are averages of at least 50-100 measurements at different points within a sample and on different samples. Intra-sample and inter-sample variations were comparable in magnitude. The standard deviation of peak positions was less than ± 2 $cm^{-1}$and variation in area for the amide band individual components between samples was of the order of $\pm 5\%$.

3.2.1 The Raman Spectrum of Elastin

3.2.1.1 Nuchal Elastin

The average spectrum obtained from elastic fibres held in a relaxed state in deionised water at room temperature, following background and bulk water subtraction, is shown in Figure 3.7. Peak attributions are based on the data in Table 3.5 which summarizes Raman peak attributions previously proposed for elastin and other bi-

ological materials. Several sources of information have been employed in compiling this table primarily because there is significant variation in peak positions for the vibrational modes given in the literature.

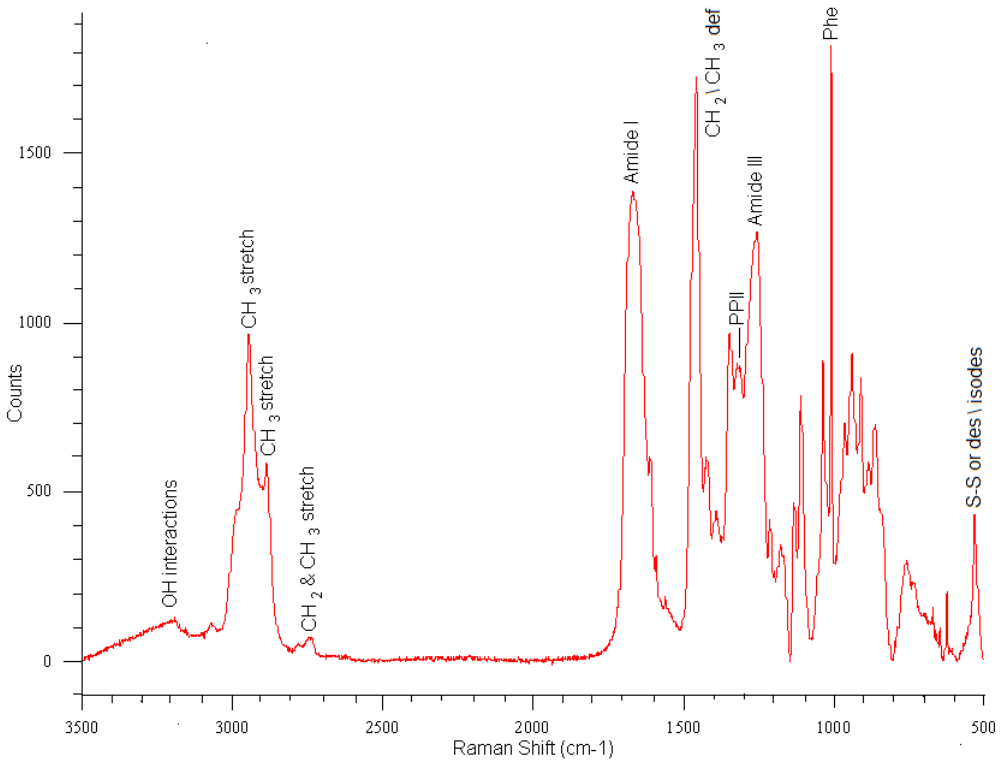

Figure 3.7: Averaged Raman spectra for fully hydrated nuchal elastic fibres. The spectrum is background and water subtracted and is an average of more than 100 acquisitions. The amide I and amide III bands as well as PPII and water interaction regions are highlighted, the details of which are discussed in sections to follow.

Peak Centre / cm-1	Attribution	Reference
3308	Amide A	b
3057	Amide B	b
2971	CH_3 stretch, CH stretch	b
2931	CH_2 stretch	b
2877	CH_2 stretch	b
2848	CH_3 stretch	b
2732	CH	b
1670-1688	Amide I	a,b, c
1663	Amide I	d
1655	Amide I	b, d
1611-1614	Tyrosine	a, b, c
1604-1607	Phenylalanine	b, d
1586	Phenylalanine	b
1580	Tryptophan	d
1553-1555	Tryptophan	b, d
1465	CH_2 def	d
1448-1454	CH_3, CH_2 def	a, c, d
1440	Tyrosine, Tryptophan	d
1428	CH_3, CH_2 def	d
1418	CH def, CH_2 wag, CH_2 twist	c
1418	Tryptophan, N-H stretch	b
1390	Tyrosine, Tryptophan	d
1340-1343	CH def, CH_2 wag, CH_2 twist	a, b, d
1319	CH_2 def or PPII	d
1298	Amide III	d
1266-1280	Amide III	a, b, c, d
1254	Amide II	a, c
1246	Amide III	d
1238	Amide III	b
1211	Tyrosine	a, c
1207	Tyrosine, Phenylalanine	b, d
1178	Tyrosine	a, b, c, d
1165		
1155	C-N stretch	b
1128	C-C stretch	d
1125	C-N stretch	a, b, c
1108	Des/Isodes?	a, c
1096	C-N stretch	b
1088-1080	C-N stretch	a, b, c
1085	C-C stretch	d
1065	C-C stretch	d
1053		
1032-1034	Phenylalanine	a, b, c, d
1001-1006	Phenylalanine	a, b, c, d
966	Des/Isodes?	a, c
952	CH_2	b
939-934	C-C stretch	b, d
908	C-C-N stretch	a, c
900-898	C-C stretch	b,
881	Tryptophan, Tyrosine	b, d
859	Tyrosine	c
855	Tyrosine	d
850	Tyrosine	a, b
842	Tyrosine	c
828-830	Tyrosine, Phenylalanine	a, b, d
757	Tryptophan	b
661	C-S stretch	b
642	Tyrosine	b
618-625	Phenylalanine	a, b, c
545	S-S	b
532	S-S	b
529	Des/Isodes?	a, c
519	S-S	b
512	S-S	b

a. Frushour & Koenig (elastin powder)
b. Carter (wool)
c. Carter (elastin)
d. Haston (fibrillin microfibrils)

Table 3.5: Summary of the tentative Raman peak attributions for elastin and other biological tissues as detailed in studies by Frushour and Koenig [21], Edwards and Carter [22] and Haston [23]

The spectra were similar to those reported previously for dried elastin [15, 21]. The amide I band, arising from C=O stretching at 1715-1640 cm^{-1} and the amide III band representing N-H in plane deformations at 1310-1230 cm^{-1}were both well resolved. The broad band extending between 3600-3100 cm^{-1}, evident only in the hydrated tissue arose from free and structural water. All of these features are discussed in greater detail in the sections that follow. Peaks at 1005, 1033, and 830-861 cm^{-1}were attributed to the aromatic side chains, phenylalanine (Phe) and tyrosine (Tyr). Various peaks could be assigned to CH bonds including those centred at 1455, 1344 cm^{-1} and 2730-2970 cm^{-1}. Peaks at 962-938 cm^{-1}arise from C-C bonds and that at 1106 $cm^{-1}$from C-N vibrations. A sharp peak at 527 cm^{-1} has been assigned to disulphide bonds and a peak at 529 $cm^{-1}$to the crosslink, desmosine [21]. However, a Raman spectrum obtained for pure desmosine, shown in Figure 3.8, was complex and did not contain any peak centred at 529 cm^{-1} or any other feature that could unambiguously be resolved in the elastin spectrum.

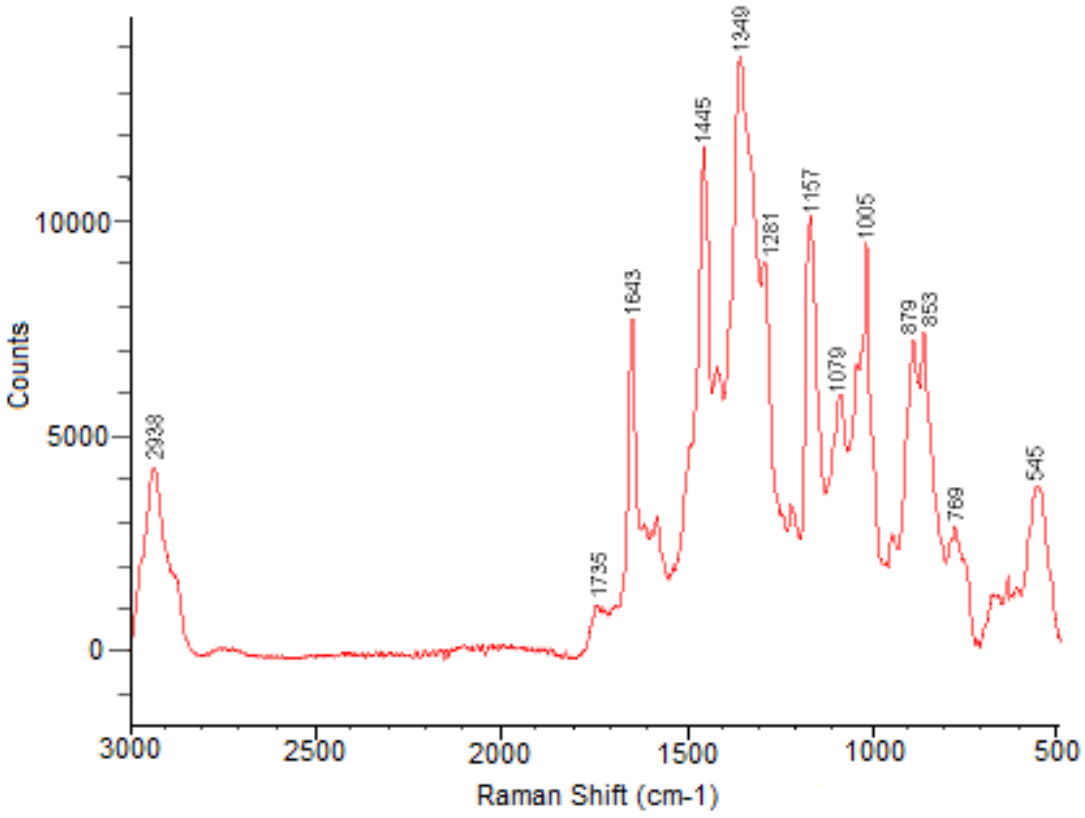

Figure 3.8: Averaged Raman spectrum (n=30) of the elastin cross-link, desmosine (kindly supplied by Prof B. Starcher). It is clear that desmosine has complex spectral features, but contrary to expectations, no distinguishable peak could be detected at 529 cm^{-1}, which has previously been regarded as indicative of desmosine.

3.2.1.2 Aortic Elastin

Figure 3.9 shows the averaged Raman spectrum for fully hydrated aortic elastin prepared by the Lansing procedure which is compared to fully hydrated nuchal elastin fibres prepared by the same method. Both of these spectra have been background corrected, bulk water subtracted and normalized to the CH peak centred at 1445 cm^{-1}. There are no significant differences in peak positions, peak ratios or the presence/absence of peaks. The only minor difference is the slight increase in the relative intensities of the peaks located between 952-830 cm^{-1}, representing the amino acid tyrosine and C-C stretch vibrational modes. However, the lower wavelength ends of the spectra were very sensitive to background correction and therefore caution is required when making comparisons in this region. Overall, elastin spectral features appear to be remarkably consistent between nuchal and aortic samples prepared by the same method consistent with reported similarities in amino acid composition and appearance of fibres in scanning electron micrographs (see Figure 3.31).

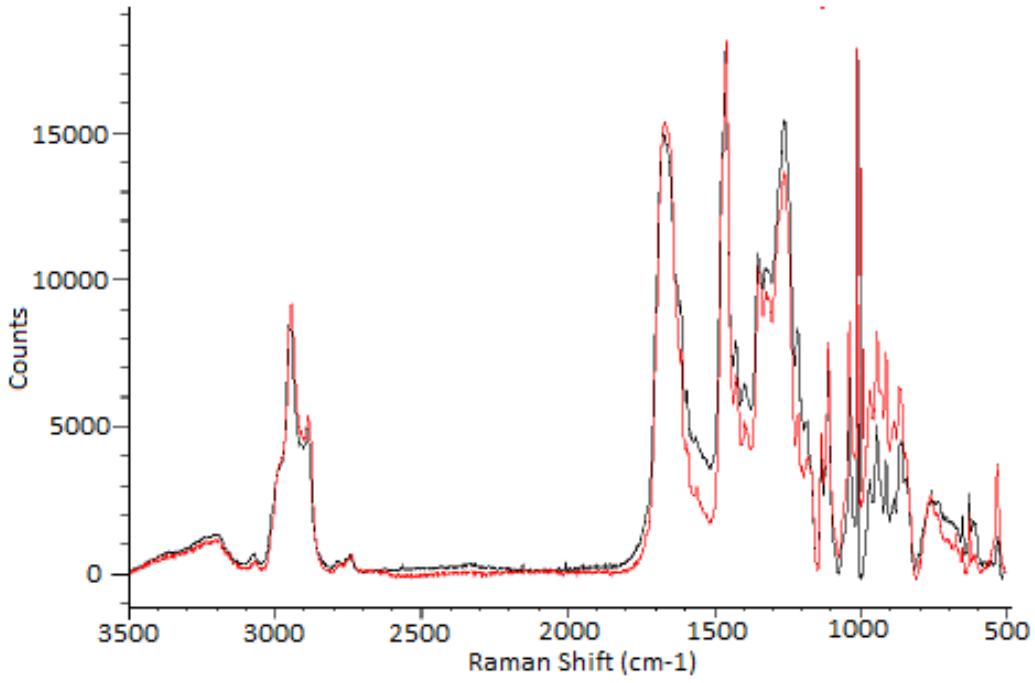

Figure 3.9: Whole spectra of NaOH digested aortic elastin (black) and NaOH digested nuchal elastin (red). Both spectra have had water subtracted and have been fitted with a cubic spline baseline. Spectra are averages of at least 100 individual acquisitions. In order to make comparisons, both spectra were normalized to the CH peak centred at 1445 cm^{-1}. The spectral features appear to be very consistent between nuchal and aortic samples, the only visible differences being that of peak intensities at lower wavelengths.

3.2.1.3 Effect of Preparation Method

In order to investigate the effect of the method of preparation on the structure of elastin, averaged Raman spectra were acquired for cyanogen bromide-extracted aortic elastin (to better preserve structure), and collagenase purified aortic elastin with or without subsequent extraction with DTE (to detect spectral differences associated with microfibrils), in addition to alkali-extracted elastin as previously described in section 3.9. Raman spectra for the various preparations are shown in Figure 3.10. No significant differences in either peak positions ($\pm$ 2 cm^{-1}) or the relative peak intensities could be resolved between the various preparations. The effects of small differences in amino acid compositions and cross-linking modifications were therefore considered to be too small to be detected by Raman spectroscopy. The contribution of microfibrillar glycoproteins was also too small for spectral detection.

Purification of elastin using hot alkali has previously been reported to be very harsh, resulting in a product that lacks amino acid sequences important in the intact tissue and causing damage to the peptide bond [327]. However, we found no difference in the Raman spectrum when compared to the more gentle purification methods (CNBr or GuHCl with or without DTE). The absence of spectral differences in these preparations provided the justification to use hot alkali-extracted elastin for the majority of the spectral acquisitions as it was both easier ans less costly to isolate.

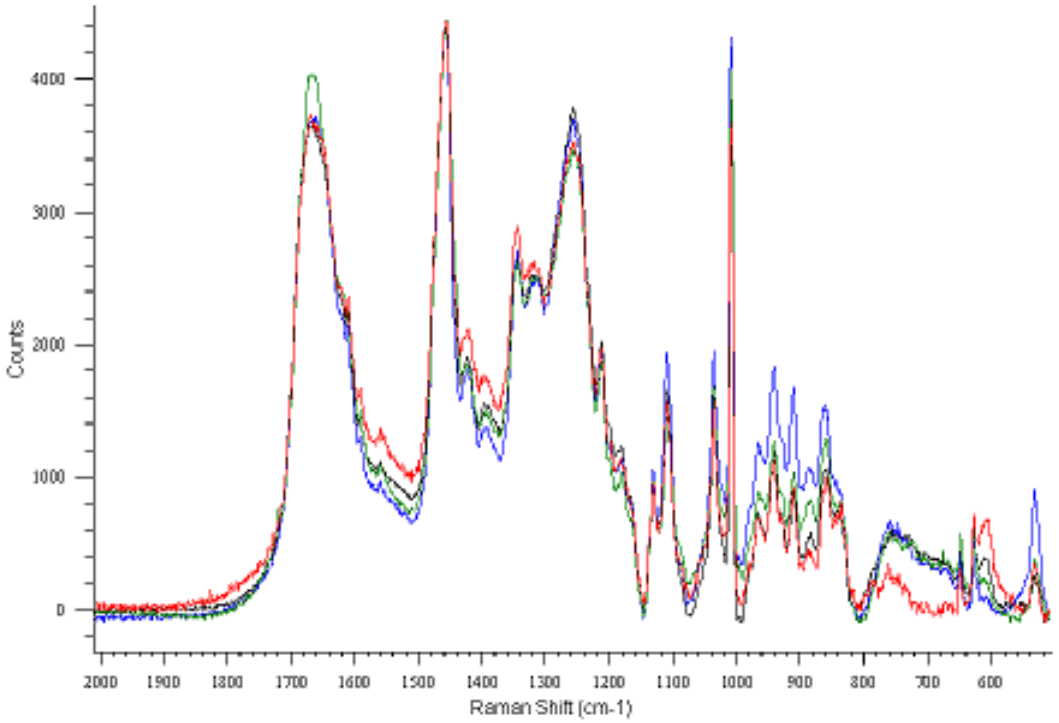

Figure 3.10: Raman spectra of aortic elastin prepared by the protocols described in section 2.1.1. Spectra are averages of at least 100 individual acquisitions which have been baselined following subtraction of water and normalized to the CH peak centred at 1445 cm^{-1}. The method of preparation had minimal impact on Raman spectral features with only differences in peak intensities visible. Comparison of the GuHCl (red) to GuHCl + DTE (blue) preparations did not reveal any individual peak that could be assigned to microfibrillar content. The hot alkali preparation is shown in black and that prepared by cyanogen bromide is shown in green.

3.2.1.4 Soluble Elastin (α-elastin)

The averaged and background corrected spectra of α-elastin are shown in Figure 3.11. Both the dry powdered form and in water (at a concentration of 100 mg/ml, pH 7.0) were found to be very similar to fibrous elastin with no differences that could be attributed to the presence of intermolecular cross-links in either preparation. The CH vibrational mode at 1340 cm^{-1} and that of CH or PPII at 1314-1319 cm^{-1} formed two distinct peaks in solution, but in the dry powdered form these two peaks appeared to merge forming a single peak at 1337 cm^{-1}, preventing the two individual peaks from being clearly resolved. In addition, the ratio of the amide III band to the neighbouring CH peak(s) was greater when α-elastin was in solution compared to powdered form. No other differences were apparent either between the two α-elastin preparations or when compared to hydrated nuchal elastin.

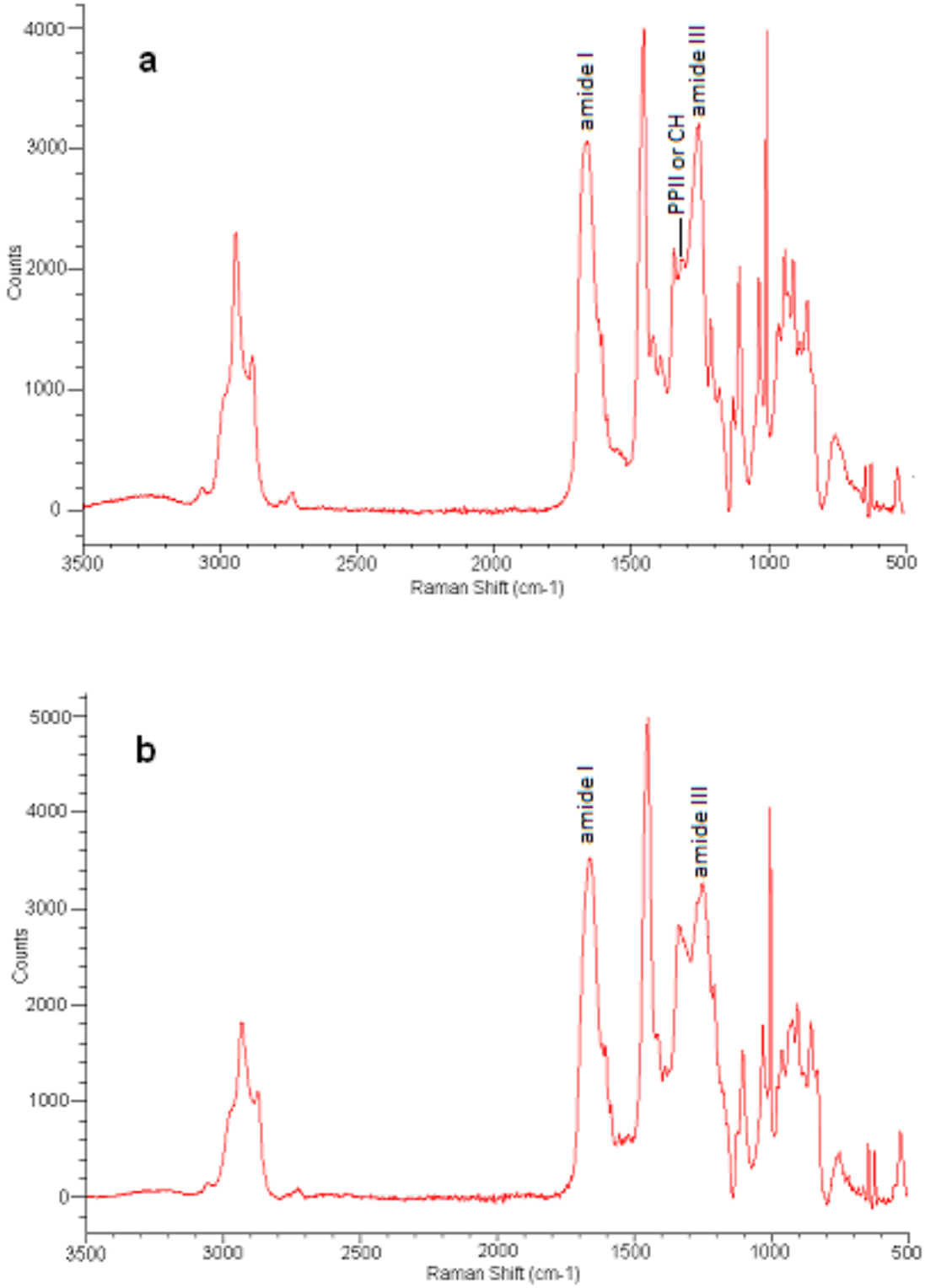

Figure 3.11: Averaged Raman spectra of α-elastin (n=20) following background correction, a) in solution at a concentration of 100 mg/ml (water subtracted) and, b) dry powdered form.

3.2.2 Secondary Structure Composition

In this section we compare three approaches to secondary structure determination.

3.2.2.1 Amide I : Reference Intensity Profile method (RIP)

The Reference Intensity Profile (RIP) method of peak analysis has previously been used by Berjot et al [6] and Debelle et al [15] to probe the amide I band secondary structure composition of proteins. In dried elastin, Berjot et al found 21% β-structures, 35% unordered structures and 44% α-helices whilst a similar study by Debelle predicted 45% β-structures, 45% unordered and only 10% α-helix. When this method was applied to the present data for dry elastin samples it gave 75% β-structures, 8% unordered and 17% α-helix which clearly differs from the results of both Berjot and Debelle. However, using only four peaks to represent the secondary structures did not produce a good fit to our data, particularly at lower wavelengths (Figure 3.12) and we found it necessary to add two peaks centred at 1590 and 1610 cm^{-1} , representing side chain aromatics, to improve the fit at lower wavenumbers. For hydrated samples it was also necessary to include an additional contribution from bound water using two 50% Gaussian, 50% Lorentzian peaks centred around 1630 and 1645 cm^{-1}, which then gave 85% β-structures, 3% unordered and 12% α-helix. This fit is shown in Figure 3.13(b). The secondary structure compositions are summarized in Tables 3.6 and 3.7 using no water peaks and two water peaks respectively.

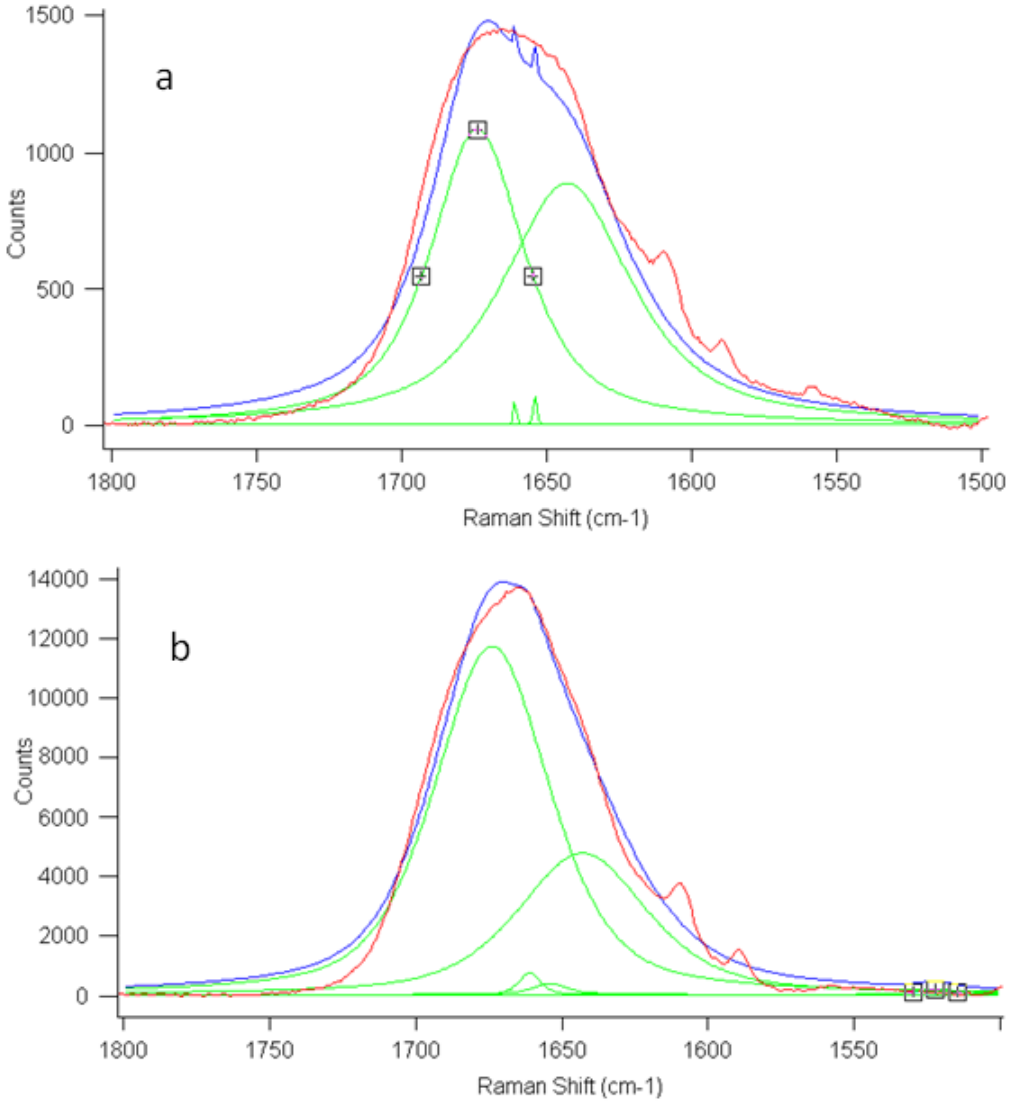

Figure 3.12: RIP analysis [6] of the amide I band for, a) fully hydrated nuchal elastin fibres and b) dehydrated elastin fibres. Spectra are averages of at least 100 individual acquisitions after baselining and subtraction of bulk water for the hydrated fibres. The band decomposition produced (blue) is poor in both cases. Also shown are the original experimental spectra (red) and component bands (green).

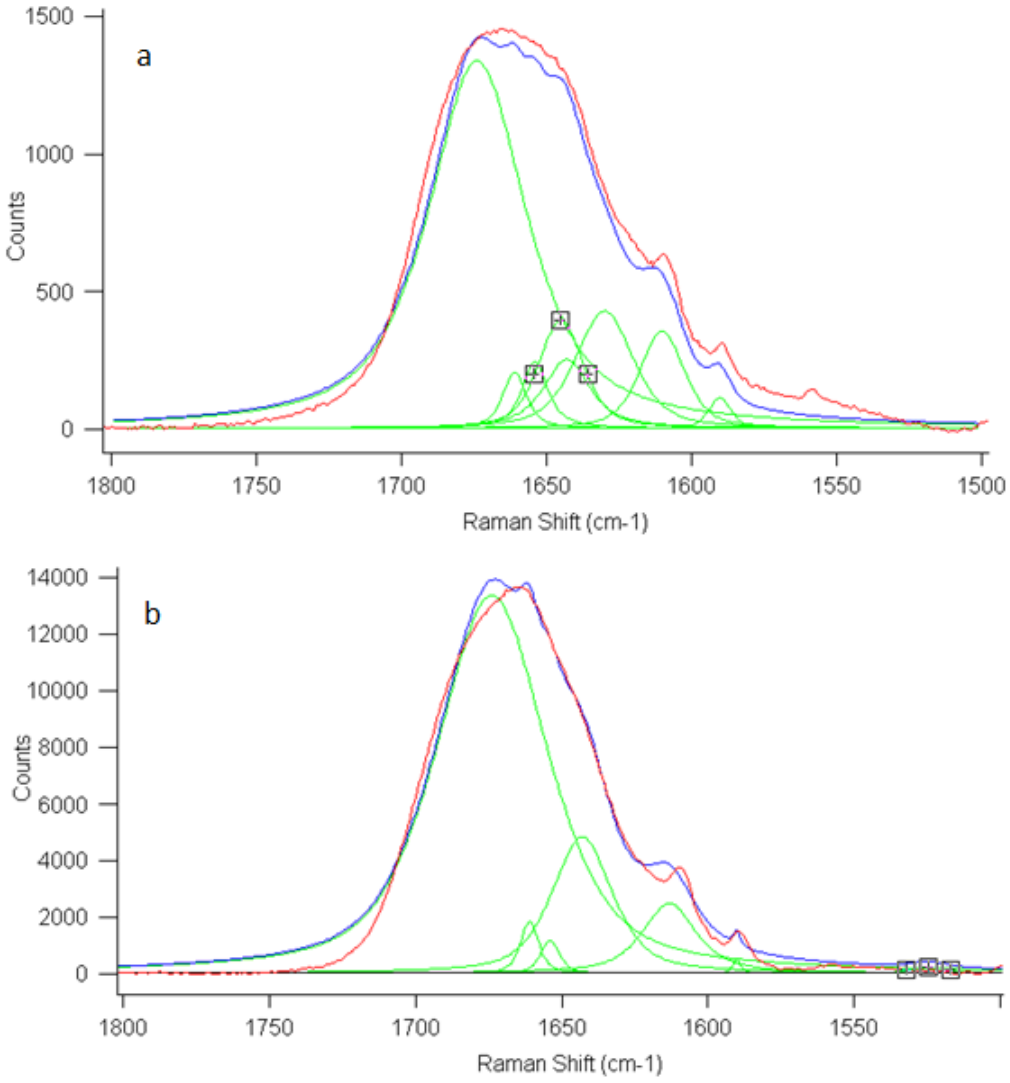

Figure 3.13: RIP analysis of the amide I band with the addition of two peaks centred at 1610 and 1590 cm^{-1} representing side-chain aromatics, a) Averaged spectrum for hydrated nuchal elastin fibres which, in addition to the two aromatic peaks, also required the inclusion of two water peaks centred at 1645 and 1630 cm^{-1}, b) dehydrated nuchal elastin fitted with six peaks. The inclusion of additional peaks to account for side-chain aromatics and two water peaks in the case of hydrated elastin did improve the overall fit of the amide I band, but still remained sensitive to slight differences in baselining and smoothing. The original spectrum (red line), result of decomposition (blue line) and component bands (green lines) are shown.

Material, (n)		α-helix[1] (%)	α-helix[2] (%)	β-sheet (%)	Unordered (%)
Dehydrated elastin fibres	(n=100)	16.7	0.4	75.2	7.9
Hydrated elastin fibres	(n=100)	36.1	0.9	62.0	0.7
Fibres heated to 60˚C	(n=100)	24.0	0.6	75.0	0.5
α-elastin powder	(n=20)	23.2	3.7	69.9	3.2
α-elastin solution	(n=20)	25.2	8.3	39.6	26.9

Table 3.6: Summary of RIP amide I analysis for elastin preparations (no water peaks) based on averaged spectra.

Material, (n)		α-helix[1] (%)	α-helix[2] (%)	β-sheet (%)	Unordered (%)
Dehydrated elastin fibres	(n=100)	3.5	0.1	75.1	21.3
Hydrated elastin fibres	(n=100)	7.8	4.2	84.8	3.2
Fibres heated to 60˚C	(n=100)	3.8	0.2	94.4	1.7
α-elastin powder	(n=20)	0.02	3.6	92.8	3.6
α-elastin solution	(n=20)	0.0	6.0	85.3	8.7

Table 3.7: Summary of RIP amide I analysis for elastin preparations (inclusion of two water peaks at 1630 and 1645 cm^{-1}).

From the Tables it can be seen that regardless as to whether water peaks were permitted or not, all the elastin preparations were dominated by β-structures, varying from 40-94% of the amide I band. Hydrated elastin fibres were shown to have the greatest percentage of α-helices whilst dehydrated fibres have the least. Unordered structures showed the largest variation ranging from 0.5% to 27%.

When the RIP method of analysis is applied to our data, with or without the addition of water peaks, the predictions of secondary structure differ significantly from that of previous investigations. All our data suggest a higher fraction of β-structures, and a greatly reduced unordered contribution. The percentage contribution from α-helix was found to be particularly sensitive to the inclusion or absence of water peaks in the fitting regime used. The reason for this is likely to be due to the close proximity, and therefore a high degree of overlapping, of the α-helices (1642-1652 cm^{-1}) and the water peaks centred at 1630 cm^{-1} and 1645 cm^{-1}. The values obtained were also found to be very sensitive to the widths permitted for the water peaks, which is consistent with the concerns expressed by other researchers about the difficulty in accounting for the effects of neighbouring aromatics [286].

3.2.2.2 Amide I: Method According to Maiti et al [2]

An alternative approach as employed by Maiti et al [2] for the analysis of natively unfolded proteins was also applied to our averaged elastin spectra. The simplicity of this approach is comparable to that of the RIP method, with only three component amide peaks attributed to α- helix, $\beta-$sheet and extended β - strand and PPII. This method failed to produce a satisfactory fit, being particularly noticeable at the

longshift end of the amide I band. Figure 3.14 shows the resulting band decomposition for fully hydrated aortic elastin after the addition of a water peak centred at 1630-1635 cm^{-1} and two peaks representing side chain aromatics at 1605 and 1619 cm^{-1}. Each of the secondary structure components was calculated as a percentage of the total amide area (excluding water and side chain contribution). As a result the extended β-strand and PPII was established as the dominant structure (48%), followed by α-helix (30%) with β-sheet contribution being smallest at 22%. Water was also found to contribute significantly (9%) to the amide I band as did the side chains constituting approximately 19% of the amide band. An almost identical result was obtained by curve fitting the averaged nuchal elastin spectrum, although the contribution from water was significantly greater at 19% whilst the side chain contribution fell by a comparable amount to 9%.

An additional concern regarding this method of curve fitting is that the peaks specified correspond only approximately to those identified by the second derivative analysis, limiting our confidence in this approach. The secondary structure compositions predicted as a result of the RIP method (see section 3.2.2.1) and the Maiti method showed considerable variation. The Maiti method predicted almost triple the α-helix contribution and approximately one quarter β-sheet contribution. Both of these curve fitting procedures were found to have several limitations associated with sensitivity to background subtraction and height of the initial seeding conditions. These complications and the difficulty in achieving consistent results proved to be central in our decision to abandon the simplified amide I band curve fitting routines and led us to favour the more complex method of Sane et al [3].

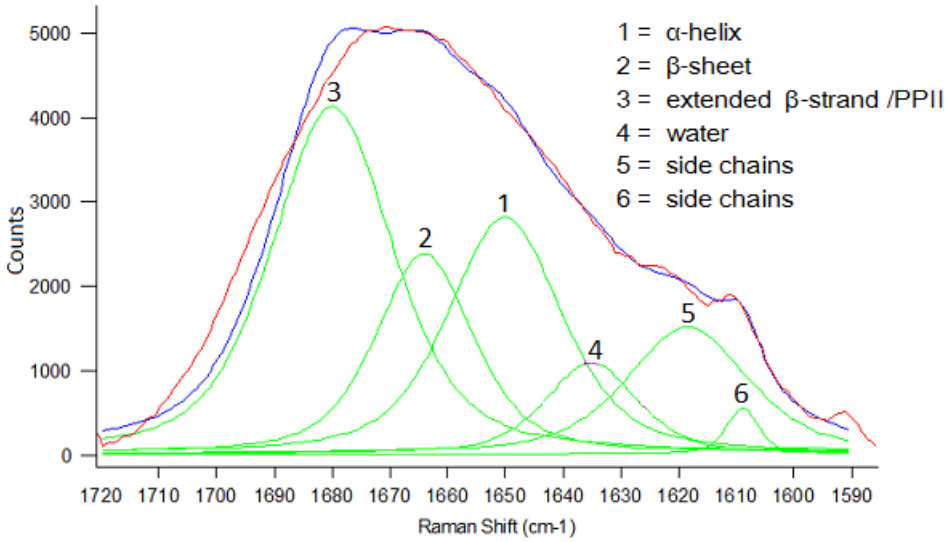

Figure 3.14: Decomposition of the amide I band for the averaged aortic elastin spectrum (n=100) based on the method described by Maiti *et al* [2], with the addition of a single water peak centred at 1630-1635 cm^{-1}. Peak numbers 1, 2 and 3 represent the amide components whilst two peaks at 1605 and 1618 cm^{-1} account for side chain aromatic contribution in order to improve the overall fit. The experimental (red line) and fitted spectra (blue line) are shown. Components corresponding to secondary structure and side-chain contributions are represented by green lines.

3.2.2.3 Amide I : Method According to Sane et al [3]

Despite reservations by some researchers regarding the number of peaks used to curve fit the amide I band we decided to use the approach of Sane et al [3], which we found to be more robust, allowing us to compare the same protein under different conditions and make comparisons with lamprey matrix proteins. An example of the fitting of the amide I band for fully hydrated nuchal elastin is shown in Figure 3.15 and the peak areas, expressed as a fraction of the total area of the amide I band components, excluding water, are summarized in Table 3.8. The major fraction was shown to be unordered structures (57%), followed by β-turns (24%), whilst α-helices contributed the lowest fraction (18%). Water also has an important part to play comprising approximately 11%.

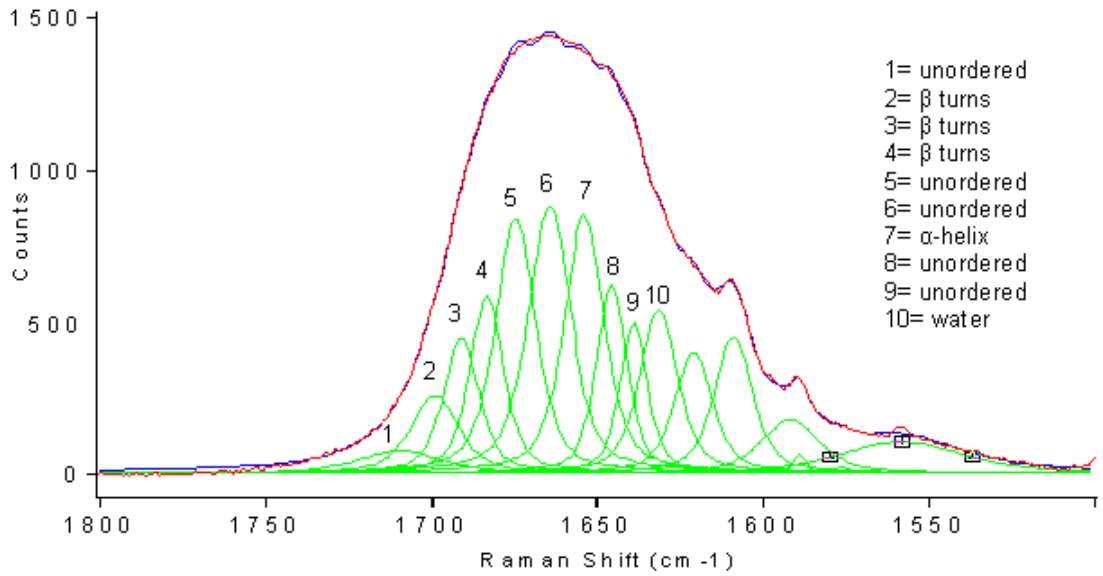

Figure 3.15: Curve fitting of the amide I band, following the method of Sane et al [3], for fully hydrated nuchal elastin in the relaxed state after background subtraction between 1800-1500 cm^{-1}. The original spectrum used (red line) is an average of ≥100 acquisitions. The spectrum resulting from curve fitting (blue line) and component bands (green line) are also shown. Peak areas and structural attributions are shown in table 3.8.

	β-turns (%)	Unordered (%)	α-helix (%)	Water (%)
Hydrated fibres: Relaxed	24.4	57.4	18.2	10.7
Hydrated fibres: Heated to 60°C	31.8	51.4	16.9	7.40
Dehydrated fibres: Relaxed	36.3	46.1	17.6	6.0
α-elastin powder	29.4	53.0	17.6	10.5
α-elastin solution	23.4	58.3	18.3	13.2
Aortic elastin (NaOH digested)	28.9	54.9	16.2	9.1
Aortic elastin (CNBr digested)	28.7	55.2	16.1	8.6
Aortic elastin (GuHCl digested)	28.3	54.3	17.4	9.0
Aortic elastin (GuHCl + DTE digested)	27.7	56.3	16.0	8.4

Table 3.8: Raman amide I band secondary structure curve fitting (following the method of Sane et al [3]) for nuchal elastin fibres in relaxed and strained states, under conditions of hydration, dehydration and heating. The total contribution for each secondary structure was normalized to 100% whilst the fractions of water and side-chains in the total peak were expressed as a percentage of this total.

Analysis of the amide I band for fully hydrated elastin fibres in the relaxed state as described above was performed on the final averaged spectrum, which consisted of more than 200 individual spectra. However, individual spectra were found to

be very reproducible with no visible differences in any part of the spectral range. In order to justify using the final averaged spectra for analysis of the secondary structure composition of the amide I band we determined the standard deviation for one dataset. This consisted of 10 individual averages, with each averaged spectrum being composed of 20-30 separate spectra taken from different fibre bundles. The results for the standard deviation around the mean are given in Table 3.9 as well as the values for each secondary structure from curve fitting of the final averaged spectrum for fully hydrated elastin fibres. It can be seen that the mean values compare favourably with the results taken from final average spectrum and that the standard deviations are relatively low. The largest standard deviation value obtained was for the aromatic residues with a value of 26.55 ± 6.66. Given the overall reproducibility of the curve fitting results, from this point onwards only final averaged spectra for the various proteins and conditions will be discussed.

Secondary structure	Final average (%)	Individual averages: mean (%), and standard deviation
α-helix	18.23	16.97 ± 1.60
Unordered structures	57.35	57.67 ± 2.01
β-turns	24.43	25.36 ± 2.71
Water	10.70	11.83 ± 2.72
Aromatics	26.55	28.90 ± 6.66

Table 3.9: Results for curve fitting of the amide I band for fully hydrated nuchal elastin fibres in the relaxed state from the final average spectrum and mean and standard deviation values for 10 individual averages acquired from separate fibres. It can be seen that the mean values compare favourably with the results taken from final average spectrum and that the standard deviations are relatively small. The total contribution for each secondary structure was normalized to 100% whilst the fractions of water and side-chains in the total peak were expressed as a percentage of this total.

In the dehydrated state, unordered structures again dominated the amide I band, although this fell from 57.4% of the total amide I band contribution in hydrated fibres to 46.2% when dehydrated. i.e. the unordered contribution decreased by 19.7%. Drying also had no effect on the α-helix contribution but a large difference was seen in the β-structure fraction increasing by 49%. Extensive drying ($\geq$72 hours at 60°C) failed to remove all the water, which only fell from 10.7% to 6%, supporting the opinion that some of the water component is tightly bound. The slight decrease

in water contribution is potentially responsible for a large part of the change in shape of the amide I band on dehydration seen in Figure 3.16

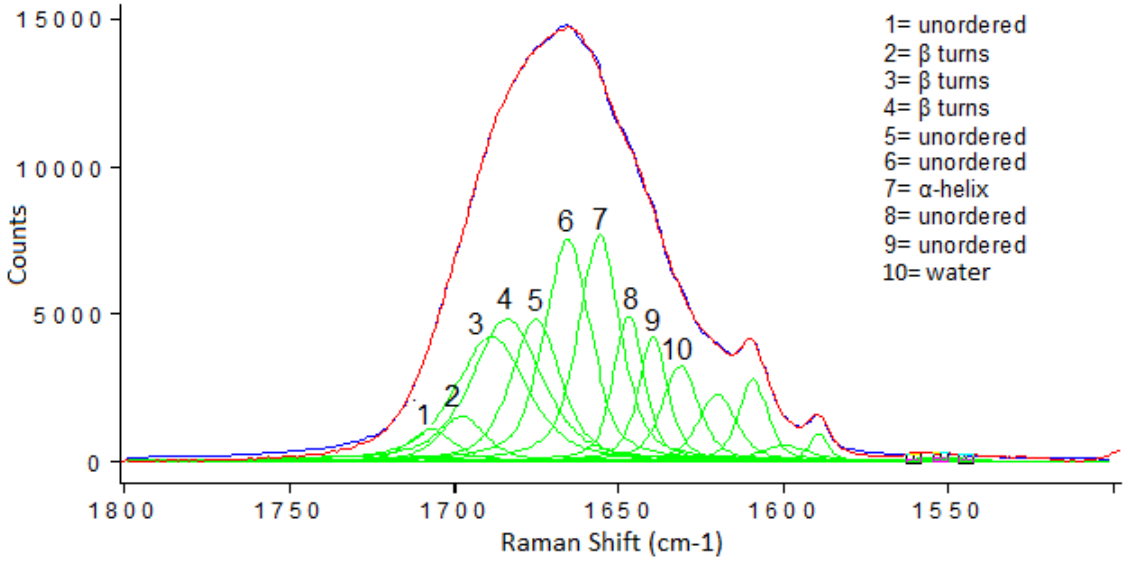

Figure 3.16: Curve fitting of the amide I band for dehydrated nuchal elastin following the approach of Sane *et al* [3]. Curve fitting is based on averaged data, comprising more than 100 individual spectra, followed by background subtraction between 1800-1500 cm^{-1}. The original spectral envelope (red line), the fitted spectrum (blue line) and component bands corresponding to secondary structure elements and side-chains (green lines) are shown.

Decomposition of the amide I band for aortic elastin was found to be almost identical to that for hydrated nuchal elastin fibres. The only noticeable difference in secondary structure composition was a 18% increase in β-turns and a 11% decrease in α-helix, whilst unordered structures showed no significant change. Aortic elastin was also used to investigate the effect of method of preparation. Decomposition of the amide I band established that secondary structure was not sensitive to the method of preparation, although it did confirm that the water content of aortic elastin is lower than that of nuchal elastin.

Figure 3.17 shows the curve fit of the amide I band for α-elastin both as a dry powder and in water (100 mg/ml, pH 7.0). A slight difference in line shape is evident between these two forms which is most likely to be accounted for by variation in water content although small variations in secondary structure compositions could have limited effect. The secondary structure composition of α-elastin in solution showed striking similarity to hydrated nuchal elastin fibres indicating that molecular conformation is not affected significantly by fibre formation. Compared to α-elastin in solution, dry α-elastin had a larger contribution from β-turns (increased by 26%)

and reduction in unordered structures (decreased by 10%). The ordered helices remained unchanged and a substantial amount of bound water remained even after prolonged drying.

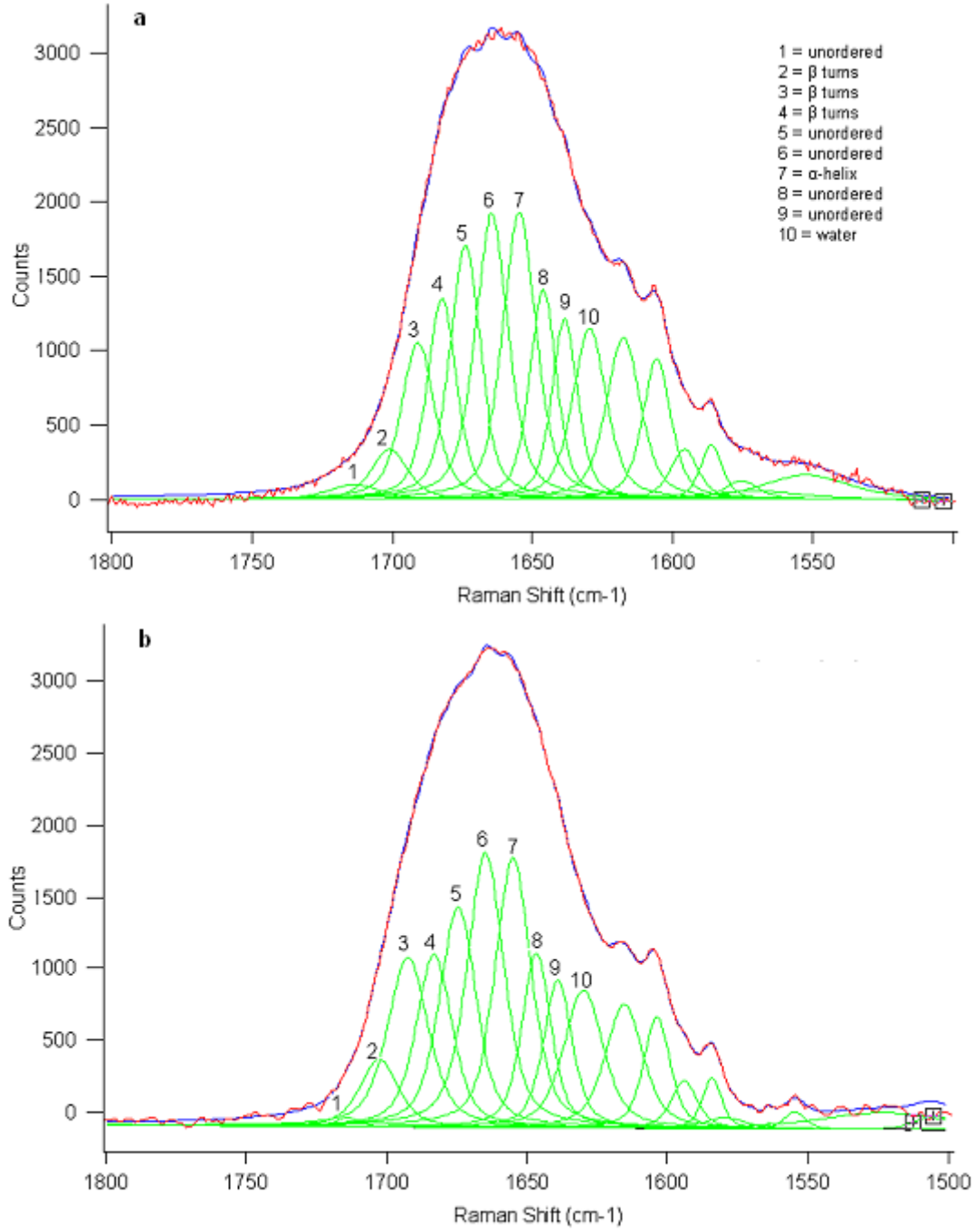

Figure 3.17: Results of amide I band curve fitting for alpha elastin, a) in solution and b) dry, powdered form based on averaged data (n=20). Peak areas and structural attributions are summarized in Table 3.8. Component bands resulting from curve fitting (green lines), their sums (blue line) and the original experimental data (red line) are shown.

3.2.2.4 Amide III Band Analysis

The amide III band has been less extensively analysed compared to the amide I band,

despite being regarded as sensitive to changes in secondary structure composition. We found that the main problems associated with curve fitting this region were interference from the neighbouring PPII / CH peaks and side-chain modes.

The fitting of the amide III band for hydrated nuchal elastin following the procedure of Williams [12] is shown in Figure 3.18 and peak areas summarized in Table 3.10. Structural predictions were significantly different from the results of the amide I analysis, giving a higher contribution from α-helix (33.3%), 50% lower proportion of β-structures (13.4%), whilst that of unordered structures was relatively unchanged (53.3%).

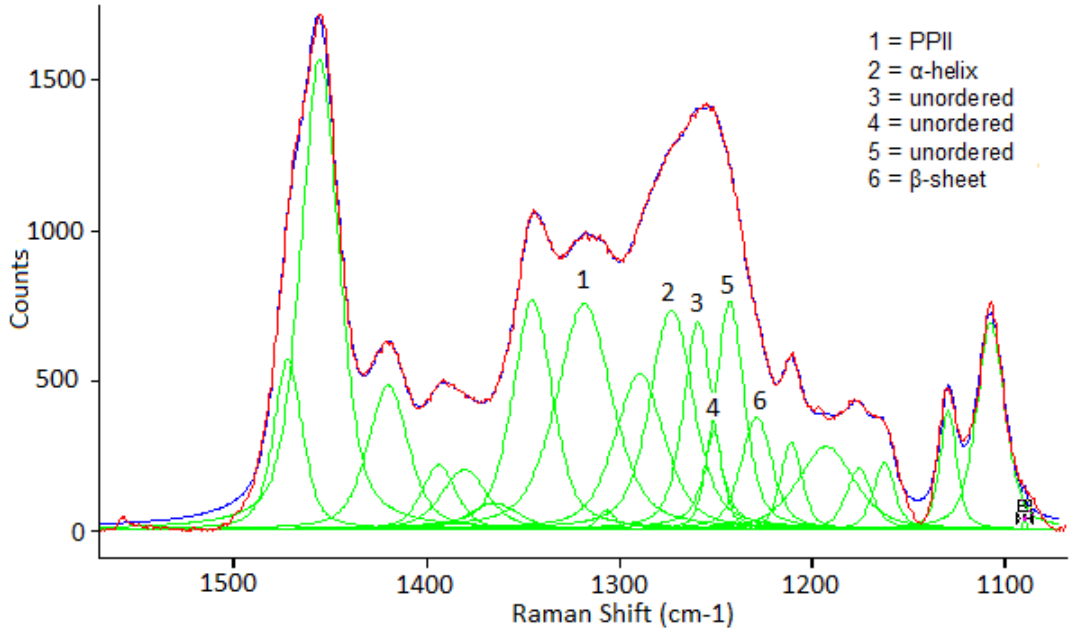

Figure 3.18: Curve fitting of the amide III band for fully hydrated nuchal elastin fibres after background subtraction. Peak areas and attributions are summarized in Table 3.10. The original spectrum (red line), the result from curve fitting (blue line) and component bands (green line) are shown.

	β-sheet (%)	Unordered (%)	α-helix (%)
Hydrated fibres: relaxed	13.4	53.3	33.3
Dehydrated fibres: relaxed	15.1	52.3	32.6
Fibres heated to 60°C	20.3	51.8	28.0
α-elastin powder	26.8	46.7	26.5
α-elastin solution	18.9	52.1	29.0
Aortic elastin (NaOH digested)	16.5	54.7	28.9
Aortic elastin (CNBr digested)	17.6	48.8	33.6
Aortic elastin (GuHCl digested)	16.2	52.7	31.2
Aortic elastin (GuHCl + DTE digested)	14.7	53.8	31.5

Table 3.10: Raman amide III band secondary structure curve fitting for aortic elastin by different preparation methods, and nuchal elastin fibres in relaxed and strained states, under conditions of hydration, dehydration and heating to 60°C. The total contribution for each secondary structure type was expressed as percentage of the total amide III band area.

The amide III region was found to be less sensitive to dehydration and although the curve fitting of this complex band (see Figure 3.19) looks very different to that of elastin fibres in the hydrated state (Figure 3.18), these differences are not reflected in the corresponding peak areas for each of the amide III components (32.6% α-helix, 15.1% β-sheet and 52.3% unordered).

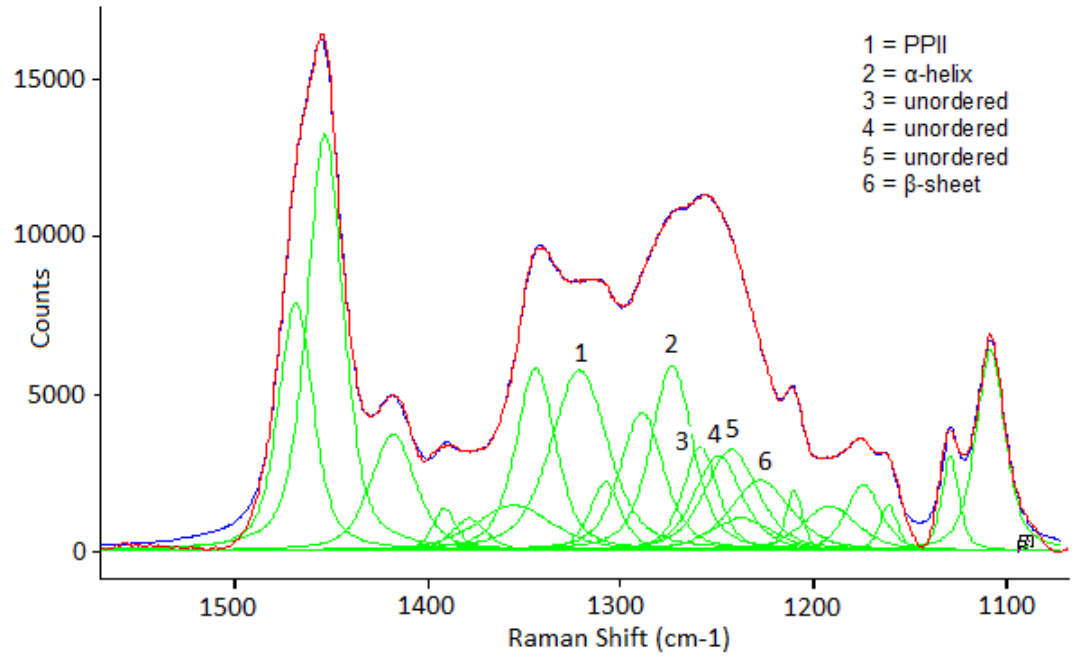

Figure 3.19: Curve fitting of the amide III band for dehydrated nuchal elastin fibres after background subtraction. Peak areas and structural attributions are summarized in Table 3.10. Component bands resulting from curve fitting (green lines), the fitted spectrm (blue line) and the experimental data (red line) are shown.

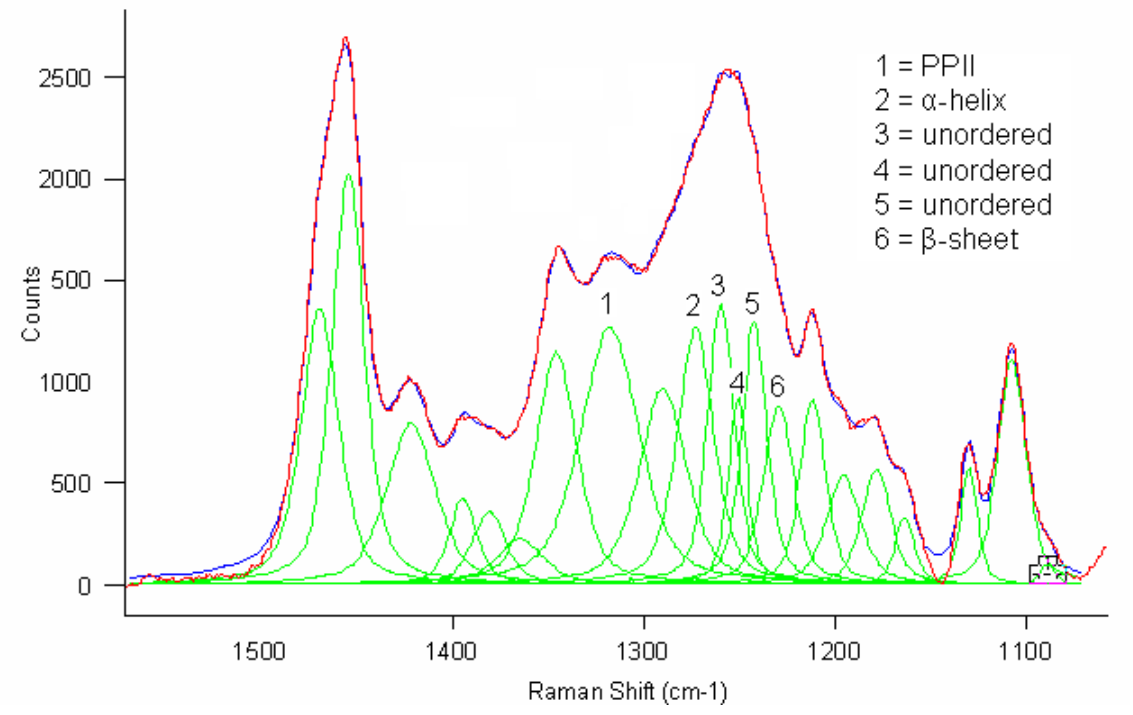

Figure 3.20: Curve fitting of the amide III band after background subtraction for fully hydrated aortic elastin. Component bands resulting from curve fitting (green lines), the fitted spectrm (blue line) and the experimental data (red line) are shown

As can be seen in Figure 3.20 and the summary of results in Table 3.10, decomposition of the aortic elastin amide III band shows significant similarities to that of nuchal elastin. In all aorta preparations the amide III band is well resolved with a

slight change in line shape when compred to nuchal elastin. Another observation to be made is the noticeable increase in amplitude of the amide band to that of the neighbouring CH_2 peaks. It is difficult to correlate these differences to changes in the corresponding secondary structure compositions which again indicate only minor variations between preparations compared to fibrous elastin. The largest difference was accounted for by a 10-30% increase in β-sheet depending on the method of preparation. The other two components, the α-helices and unordered structures, either remain unchanged or showed a slight decrease (8% and 13% respectively) when compared to hydrated nuchal elastin fibres.

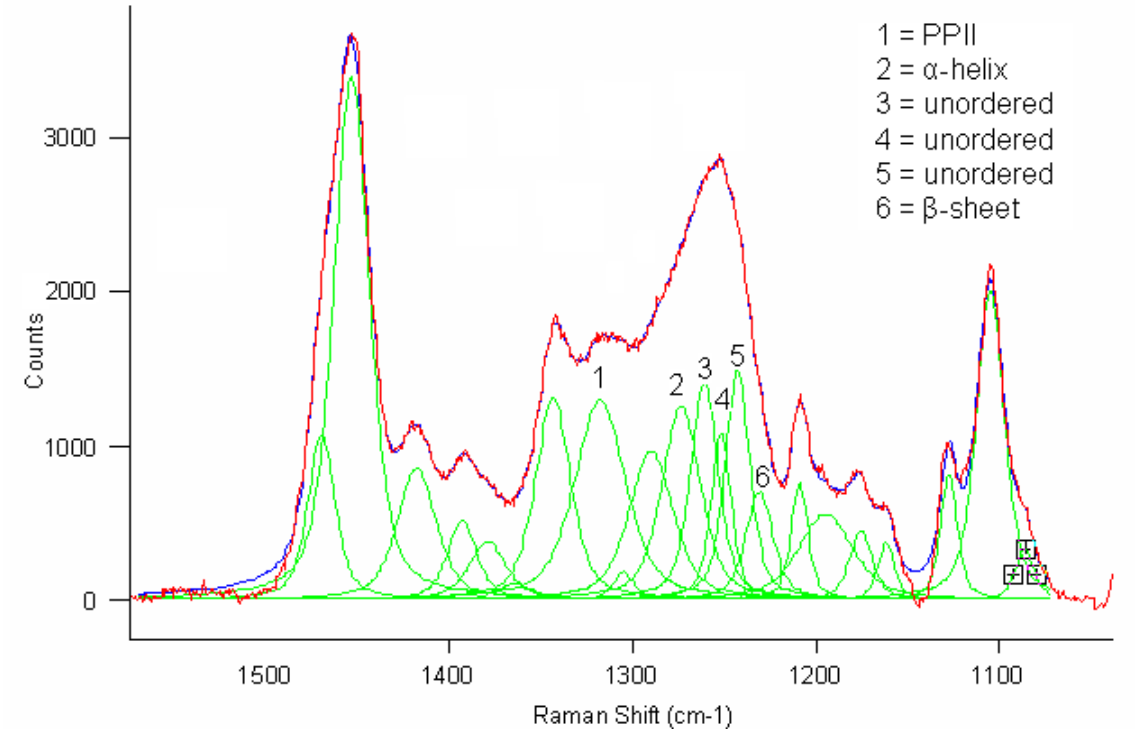

Figure 3.21: Curve fitting of the amide III band for α-elastin in solution at a concentration of 100 mg/ml. The averaged spectrum (red line) has been used for fitting (n=20) and peak areas are summarized in Table 3.10. Also shown are the fitted spectrum (blue line) and the individual component bands (green line).

Decomposition of the amide III band for α-elastin showed strong similarities to that of aortic elastin, as illustrated in Figure 3.21. Once again, the β-structures exhibited the greatest difference, being doubled in dry α-elastin, compared to hydrated nuchal elastin. Our data also indicated a small decrease in α-helix content whilst the contribution made by unordered structures (in the powdered form) decreased by 12%.

3.2.2.5 938 cm^{-1} Peak Analysis

Despite not forming part of either the amide I or amide III bands, another peak centred at around 934-938 cm^{-1} is regarded as being characteristic of ordered α-helix and therefore may confirm conclusions arrived at by decomposition of the amide bands. We determined the ratio of the 1005 cm^{-1} peak for phenylalanine to that of the 938 cm^{-1} (C-C stretch), both by area and by height above background, and compared this to the α-helix contribution in the amide I and amide III bands for each of the elastin preparations. The results are summarized in Table 3.11. There is no correlation between the intensity or area of the 938 cm^{-1} peak and the α-helix content in either the amide I or amide III bands as expected. This may in part be due to the sensitivity of this region to background subtraction which consequently affects curve fitting of overlapping peaks.

	RATIO: 938 cm^{-1} : 1005 cm^{-1} based on peak height	RATIO: 938 cm^{-1} : 1005 cm^{-1} based on peak areas	α-helix: % in amide I band	α-helix: % in amide III band
Hydrated elastin fibres: relaxed	6.02	2.96	14.9	47.1
Hydrated elastin fibres: stretched	5.65	4.76	13.5	46.9
Dehydrated elastin fibres: relaxed	10.63	5.59	10.7	50.1
Dehydrated elastin fibres: stretched	10.35	6.34	10.3	48.8
Elastin fibres heated to 60°C: relaxed	8.14	5.07	12.9	44.8
Elastin fibres heated to 60°C: stretched	7.95	2.65	11.7	43.7
α-elastin: dry powder	11.25	5.36	19.5	44.3
α-elastin in solution	6.69	3.73	2.8	28.3

Table 3.11: Summary of the 1005:938 cm^{-1} peak ratios for nuchal elastin fibres, compared to the percentage contribution made by α-helices in both the amide I and amide III bands under conditions of hydration, dehydration, heating and $\geq$50% extension. Values are also given for α-elastin as a powder and in solution.

3.2.2.6 PPII Analysis

The peak centred at 1314 cm^{-1} has tentatively been assigned to PPII structures.

This structure is proposed to have important implications in elastin's elastic behaviour. Raman spectra of elastin fibres (hydrated and heated to 60°C) revealed a distinct peak centred at around 1314 ± 3 cm^{-1} . Visual comparisons of the spectra revealed a less well resolved peak under conditions of dehydration and on exchange of water for deuterium oxide. Quantitative analysis of this peak proved particularly difficult with interference from neighbouring amide III components at lower wavelengths and overlapping CH vibrations at higher wavelength. Table 3.12 summarizes the contribution made by the 1314 cm^{-1} peak expressed as a percentage of the total amide III band plus the neighbouring CH peak at 1342 cm^{-1}. From these results we were unable to confirm any significant change in PPII. However, analysis of the neighbouring amide III band did indicate increased β-sheet contribution, which would support conversion of PPII to β-structures with increased temperature or dehydration as previously reported [140]. The α-elastin preparations, both powdered and in solution, showed a very similar PPII content both to each other and to that of nuchal and aortic elastin.

Sample:	Area of 1314 cm^{-1} peak expressed as percentage of amide III band + neighbouring CH peak (%)
Hydrated nuchal elastin: relaxed	30.0
Hydrated nuchal elastin: stretched by ≥ 50%	25.7
Dehydrated nuchal elastin: relaxed	29.4
Dehydrated nuchal elastin: stretched by ≥ 50%	26.7
Nuchal elastin heated to 60°C: relaxed	28.2
Nuchal elastin heated to 60°C: stretched by ≥ 50%	30.2
Hydrated aortic elastin: relaxed	31.1
α-elastin: dry powder	28.5
α-elastin in solution (100 mg/ml)	26.1

Table 3.12: Polyproline II has previously been attributed to a peak at 1314 cm^{-1}. This Table summarizes the area of this peak expressed as a percentage of the amide III band and neighbouring CH peak for nuchal elastin, aortic elastin and alpha elastin. Also included are the effects of dehydration and heating to 60°C. Analysis was performed on averaged spectra consisting of at least 100 individual datasets (for α-elastin, n=20).

3.2.3 Solvent Interactions

3.2.3.1 Interactions with Solvent Water

We have already shown that water forms an important component of the elastic fibre and that a tightly bound component remains following extensive drying. Using Raman spectroscopy we investigated further the interactions of elastin fibres with water by quantifying both by the ratio of the total area of the broad water band to that of the neighbouring CH peaks and by the ratio of the two major peaks present within the water band. These measurements were performed for nuchal elastin at room temperature and at 60°C both relaxed and at $\geq$50% extension of the original length and also for α-elastin in water. The curve fitting of this region has been shown previously in Figure 2.16 and the results for all conditions are summarized in Table 3.13. The most noticeable difference is a substantial decrease in the magnitude of the total water to that of the neighbouring CH peak in fibres heated to 60°C. Heating also had the effect of halving the ratio of the two component OH peaks. Strain appeared to have no effect on the ratio of the two major OH peaks, but did result in a small increase in the area of total water compared to that of the CH peak. Similar changes, but of lower magnitude, were also observed for α-elastin with the ratio of OH to CH falling from 0.68 in hydrated fibres to 0.55 for α.-elastin The ratio of the two dominant OH peaks similarly decreased from 2.7 in elastin fibres to 1.9 in a soluble form.

Sample	Ratio 3221/3391 cm^{-1} peaks	Ratio of total OH to CH
Hydrated elastin fibres/Relaxed	2.7	0.68
Hydrated elastin fibres/Stretched	2.8	0.75
Hydrated elastin fibres heated to 60°C/ Relaxed	1.3	0.41
Hydrared elastin fibres heated to 60°C/Stretched	1.4	0.51
α-elastin in solution	1.9	0.55
Water	10.2	N/A

Table 3.13: Analysis of hydroxyl modes for relaxed and strained nuchal elastin fibres, fully hydrated in water at room temperature and heated to 60°C and for α-elastin in solution at a concentration of 100 mg/ml. Data for bulk water is also included as a comparison. The right-hand column gives the ratio of the total area of free OH to that of CH whilst the left-hand column shows the ratio of the peak areas for the two major OH components, providing a measure of disruption to structural water caused by the protein.

3.2.3.2 Deuterium Oxide Exchange

Nuchal elastin fibres were strained by 20% extension and de-ionized water exchanged for deuterium oxide (D_2O). Raman spectra were acquired and compared to elastin fibres hydrated in water. Exchanging water for D_2O had the effect of altering a number of spectral features as can be seen in Figure 3.22. D_2O modes appeared at 2475 and 2400 cm^{-1} but, importantly in a biophysical context, exchange with water was incomplete even after prolonged incubation. The ratio of the water peak (3600-3100 cm^{-1}) to the neighbouring CH peak fell from 0.68 to 0.21. However, this was not consistent with analysis of the amide I band, which revealed an increase of 25% in the peak attributed to hydration water (this will be considered further in the discussion in section 3.5). The amide I band showed a change in line shape, becoming narrower with a downshift of the peak centre by 8 cm^{-1} (Figure3.23). Curve fitting of the amide I band attributed this to an increase in unordered structures (from 57% to 63%) and a fall in β-turns (from 24% to 15%), whilst the α-helix content remained unchanged (18%). Analysis of the amide III band (Figure 3.24) failed to reveal any significant shift, as previously reported [12], whereby dissolving proteins, such as insulin and concanavalin in D_2O, resulted in a downward shift by as much as 300 cm^{-1}, provided that H-D exchange was complete. Our results do show that the amplitude of the amide III band is reduced relative to neighbouring bands and that the constituent peaks were less well resolved. Changes in secondary structure composition were accounted for by a decrease in unordered structures (from 53% to 43%) and an increase in the contribution made by α-helices (33% in H_2O, 41% in D_2O) and β-sheet (13% in H_2O, 16% in D_2O). Although the PPII peak was less well resolved on exchange of water for D_2O, curve fitting of this complex region showed no significant change in the area of this peak.

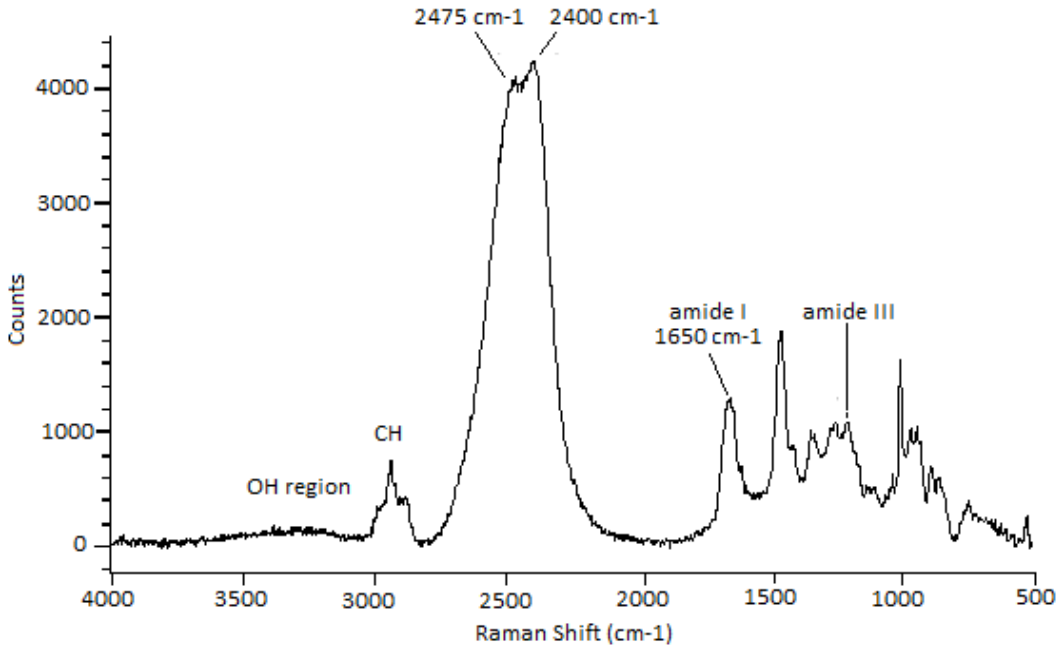

Figure 3.22: Averaged Raman spectrum for fully hydrated nuchal elastin fibres in deuterium oxide (n=75). There is a strong double peak centred at 2475 and 2400 cm^{-1}. The OH band between 3600 and 3100 cm^{-1} remains even after prolonged incubation in deuterium oxide. The amide I band shifts from 1665 to 1658 cm^{-1} and also shows a change in line shape because of the long-wave components being suppressed.

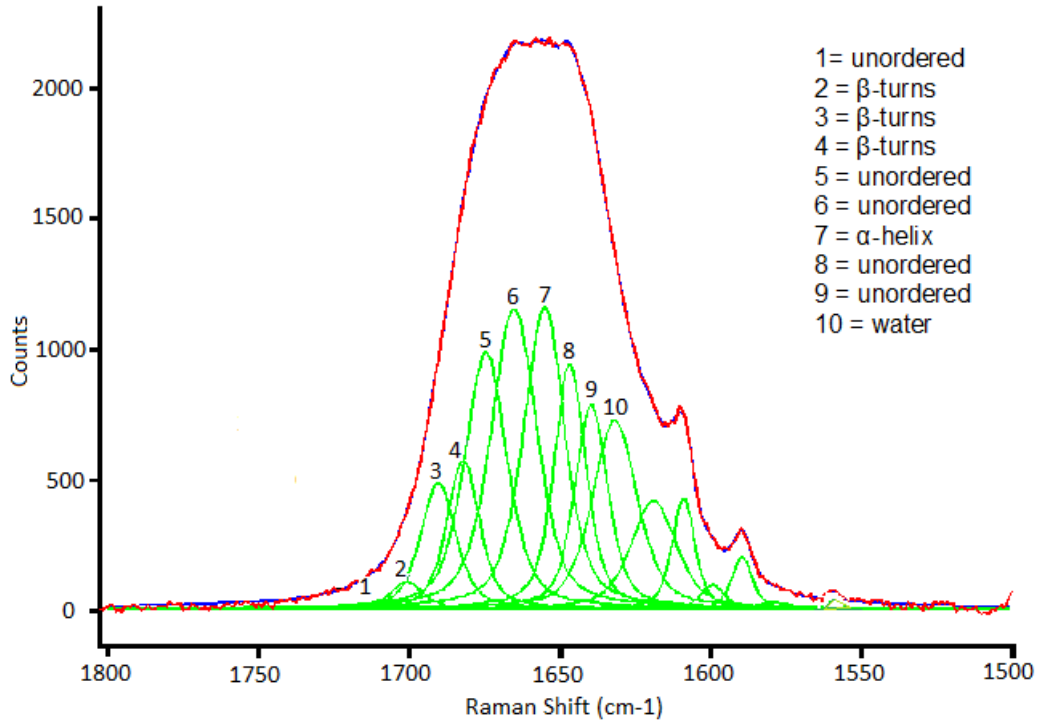

Figure 3.23: Curve fitting of the amide I band for nuchal elastin fibres following the exchange of water for deuterium oxide. Prior to performing the curve fitting routine the averaged spectrum (n=75) was background corrected following subtraction of deuterium oxide (red line). The fitted spectrum is represented by the blue line and individual amide I band components by green lines.

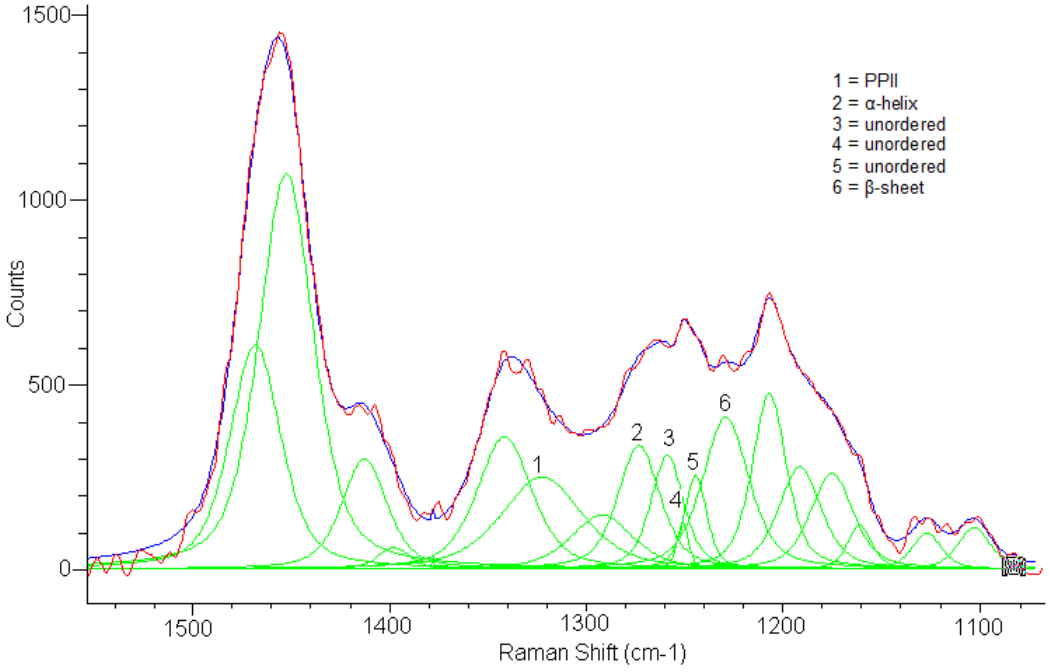

Figure 3.24: Curve fitting of the amide III band and neighbouring peaks after background correction for nuchal elastin fibres following the exchange of water for deuterium oxide. The original spectrum (red line), the fitted spectrum (blue line) and component bands (green line) are shown.

3.2.3.3 TFE Exchange

Trifluoroethanol (TFE) has been reported to induce α-helix formation in proteins in solution [135, 328], which is likely to result in loss of long-range elasticity. This reduction in elasticity was confirmed for native elastin by mechanical changes previously discussed in section 3.1.4. We therefore decided to undertake a study in an attempt to resolve the effect of solvent interactions on the molecular composition of fibrous elastin by replacing water as the bathing medium with TFE whilst the sample held at constant 20% strain. Raman spectra were then collected with elastin fibres in the relaxed state.

When water was exchanged for TFE we found that the Raman spectrum of the solvent heavily overlapped those of the protein. We therefore had to confine our analysis to a comparison of elastin dried following equilibration with water and TFE. Figure 3.25 shows the overlaid spectra for fibrous elastin dehydrated from water and TFE. Few spectral differences can be seen, although there was a shift to lower wavenumbers in a number of CH bands (2946 to 2925 cm^{-1}, 1456 to 1450 cm^{-1} and 1341 to 1336 cm^{-1}) whilst curve fitting of the amide I band revealed a small (5%) increase in α-helix content, as observed in other proteins [182, 183, 184].

This is unlikely to account for the slight change in line shape. Analysis of the amide III band showed a similar increase in α-helix (7%), a substantial increase in β-sheet (56%) and a decrease of 6% in random structures.

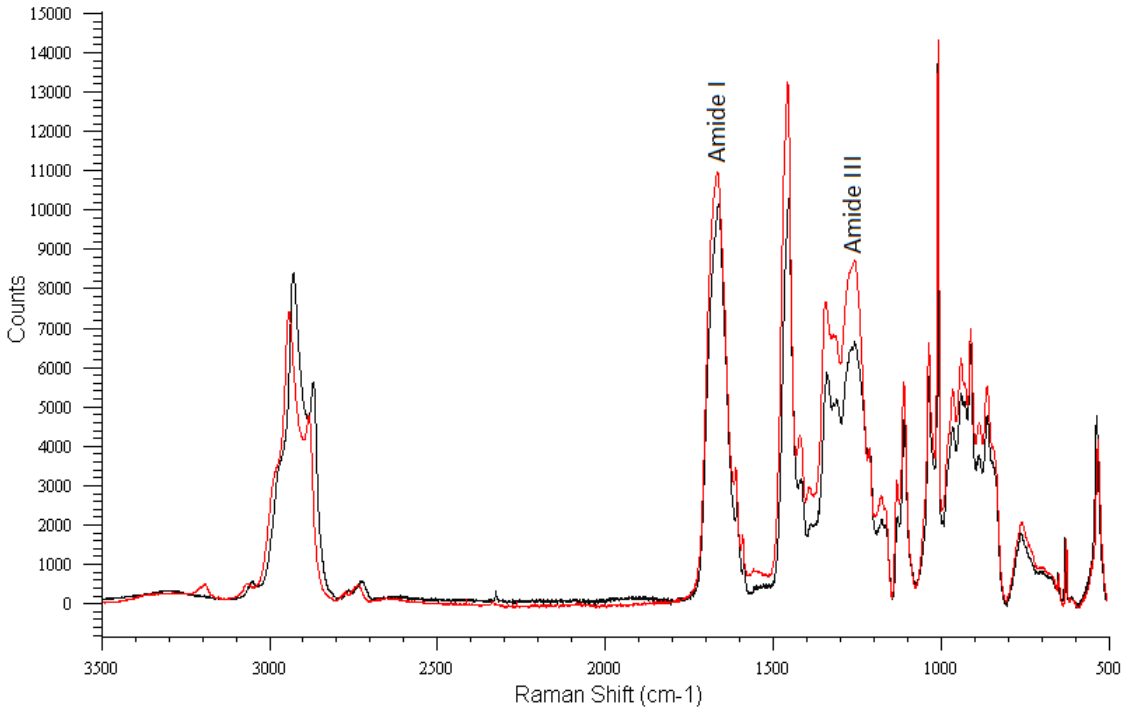

Figure 3.25: Raman spectra for nuchal elastin dried from water (red) and TFE (black). Both spectra are averages of at least 50 individual spectra following cubic spline background correction across the whole spectral range and normalization to the 1006 cm^{-1} phenylalanine peak.

3.2.4 Thermal Effects

Nuchal elastin fibres were held at 20% extension as the bath temperature was increased from room temperature to 60°C resulting in stress of up to 100%. Spectra were compared at these two temperatures. Mechanical changes are discussed in section 3.1.3.

Analysis of the amide I band revealed a minor upwards shift in the peak position from 1664 cm^{-1} at room temperature (20°C) to 1669 cm^{-1} at 60°C. Curve fitting established that this shift was the result of a 30% increase in the proportion of β-turns and a decrease of 10% in the unordered component and a 7% decrease in α-helix. Analysis of the amide III region revealed a much larger increase in the proportion of β-structures (52%) at elevated temperatures and a moderate fall in α-helix content (16%) whilst unordered structures remained unchanged. β-structures are believed to play an important role in elastin elasticity, so an increase in these

structures may have the effect of promoting long-range elasticity, as suggested from our thermomechanical data. There was also a substantial decrease in the magnitude of the water interaction band relative to the neighbouring CH peak, and the ratio of the two component OH peaks was halved (see Table 3.13).

3.2.5 Effect of Mechanical Stretch

Investigations into the effects of mechanical strain on elastin fibres was a primary aim of this study. With the equipment available, it was impossible to apply strain to a single elastin fibre. We were therefore restricted to applying mechanical strain to a small bundle of ligamentum fibres, within which some individual fibres are likely to experience lower strains than others. This might have resulted in an underestimation of the effect of strain in our data. At strains in excess of 60% applied to the fibre bundle, individual fibres frequently broke during spectral measurements.

Comparisons were made both of spectra from an individual fibre bundle, relaxed and at 60% strain, and of averaged data for relaxed and strained fibres. In neither case could any significant differences be resolved either in peak position ($\pm 2\ \mathrm{cm}^{-1}$) or in intensities of any major side-chain peaks. Amide I and amide III band fitting also failed to reveal significant differences in the positions and areas of the constituent peaks corresponding to secondary structures. In this way our results differ from those observed in other proteins [329, 330, 331, 332]. However, there were slight effects both on interactions with water and on the polarization of the spectrum.

The interactions of the elastin fibres with water were quantified both by the ratio of the total area of the water band to that of the neighbouring CH band and by the ratio of the two major peaks present in the water band (see Figure 2.16). There was a slight increase in the former in stretched fibres, but no change in the latter, as summarized in Table 3.13.

The most striking effect of strain was on polarization. Raman spectra of hydrated nuchal elastin fibres in the unstretched state revealed that all the major peaks were polarization sensitive.

Leikin et al [7] showed that for collagen the two major water interaction peaks (3391 and 3221 cm^{-1}) had different polarization characteristics. This is also true

for elastin which indicates that the 3991 cm^{-1} peak has a polarization ratio of 1.85 compared with 0.96 for the 3221 cm^{-1} peak. The various structures contributing to the amide I band also have different orientations, but only in the order of 3°. The principle polarization ratios and angles of orientation to the fibre axis are shown in Table 3.14.

Rousseau's results for spider silk [295], showed bond angles to the fibre axis close to 90°. In contrast, for elastin fibres in the relaxed state, most bonds show an angle of 40-50°. On application of $\geq 50\%$ strain all bonds, with the exception of β-sheet within the amide III band, orientated to become less perpendicular to the fibre axis.

Changes associated with the application of mechanical strain occurred mainly in the aromatic side-chains, tyrosine and phenylalanine, in the water interactions region and to a lesser extent in components of the amide I band. The peptides were least sensitive to strain and this lack of ordering could be explained in part by their conformational flexibility. This was not the case for the side-chains, phenylalanine and tyrosine, which have bulky ring structures. Stretching elastin fibres resulted in the altered alignment of these residues to the peptides in the relaxed state. This change in alignment was greatest for tyrosine which is located primarily at the boundary between cross-linking and hydrophobic domains. Application of strain also had a marked effect on water. Our data show a reduction in the depolarization ratio ($\rho \perp / \rho \parallel$) of both the dominant peaks comprising the water region, which is consistent with the thought that stretching elastin can alter interactions of the hydrophobic domains with water, leading to changes in water structure.

	Relaxed fibres: ρ⊥	Relaxed fibres: ρ∥	Relaxed fibres: ρ⊥ / ρ∥	Relaxed Bond angles (Degrees)	Stretched fibres: ρ⊥	Stretched fibres: ρ∥	Stretched fibres: ρ⊥ / ρ∥	Stretched Bond angles (Degrees)
Amide I band								
Unordered	0.62	0.24	**2.62**	**46°**	0.56	0.30	**1.89**	**49°**
β-turns	0.68	0.22	**3.11**	**44°**	0.58	0.21	**2.73**	**45°**
α-helix	0.76	0.21	**3.56**	**45°**	0.64	0.31	**2.07**	**48°**
water	0.89	0.25	**3.53**	**41°**	0.62	0.39	**1.58**	**51°**
Amide III band								
Unordered	0.85	0.46	**1.85**	**48°**	0.55	0.47	**1.17**	**54°**
β-sheet	0.73	0.46	**1.59**	**50°**	1.13	0.41	**2.74**	**45°**
α-helix	0.88	0.43	**2.06**	**48°**	0.93	0.64	**1.45**	**51°**
PPII	1.05	0.46	**2.27**	**48°**	0.76	0.59	**1.29**	**53°**
Phenylalanine & Tyrosine								
1006cm^{-1} phenylalanine	0.42	0.09	**4.70**	**39°**	0.38	0.11	**3.45**	**42°**
860cm^{-1} tyrosine	0.59	0.09	**6.67**	**35°**	0.39	0.21	**1.85**	**49°**
Water Interactions								
3391cm^{-1}	0.83	0.45	**1.85**		0.61	0.46	**1.33**	
3221cm	0.61	0.64	**0.96**		0.51	0.71	**0.71**	

Table 3.14: Polarization measurements on averaged spectra for relaxed and stretched nuchal elastin fibres (n=15). The polarization intensities ($\rho \parallel$ and $\rho \perp$) and depolarization ratios ($\rho \perp / \rho \parallel$) are shown. In the case of the amide I band and aromatic side chain residues, the bond angles calculated from the depolarization ratios are also shown.

3.3 Differential Scanning Calorimetry

Figure 3.26 shows the first thermogram scans between 30 and 150°C for dehydrated ligamentum nuchal elastin, prepared by extraction in hot alkali, and for α-elastin. These scans are characterized by a single, broad endothermic peak with a maximum at around 100°C which disappears on successive scans and is associated with evaporation and vaporization of bound water and agree closely with those reported in the literature [333].

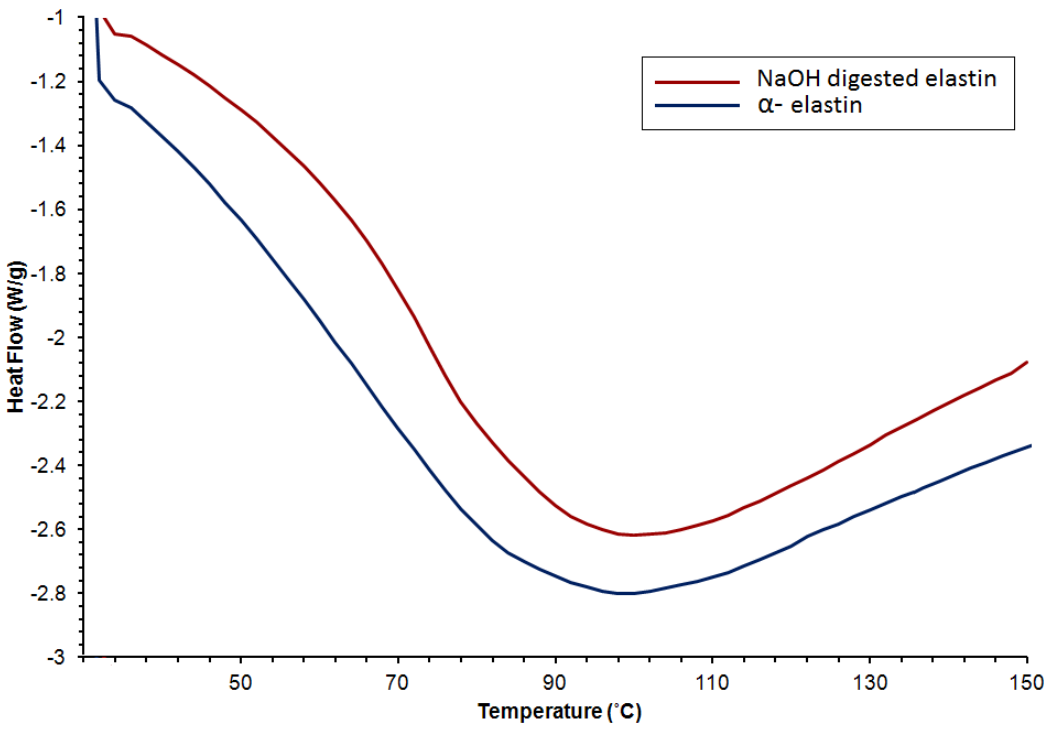

Figure 3.26: Typical DSC thermograms (1st scans) for NaOH digested ligamentum elastin and α-elastin, heated between 30-150°C at a rate of 20°C/min.

No first order transitions were observed for purified nuchal elastin or α-elastin, indicating a lack of long-range order, and this agrees with the earlier observations of Samouillan [322]. The authors propose that lack of long-range order provides support for Tamburro's model of elastin elasticity [56]. Second and third scans recorded between 30 and 250°C were almost identical. Figure 3.27 shows typical second thermograms for dehydrated NaOH digested ligamentum elastin and α-elastin. From these thermograms a T_g of 180°C was determined for NaOH digested elastin and 191°C for α-elastin. Our results for α-elastin are in agreement with those of Samouillan for κ-elastin (190°C). However, our T_g value for purified nuchal elastin was much lower (Samouillan determined a value of 203°C [322]). This result is difficult to explain because nuchal elastin, with its associated 3D-architecture, would be expected to have a higher T_g temperature caused by stiffening of the network, whereas soluble elastin, with its loss of 3D-structure and increased volume should have a lower T_g. One possible factor is that the DSC curve for nuchal elastin had no distinct deviations of the DSC curve that could be extrapolated to give reliable onset and end temperatures, making calculation of T_g very subjective.

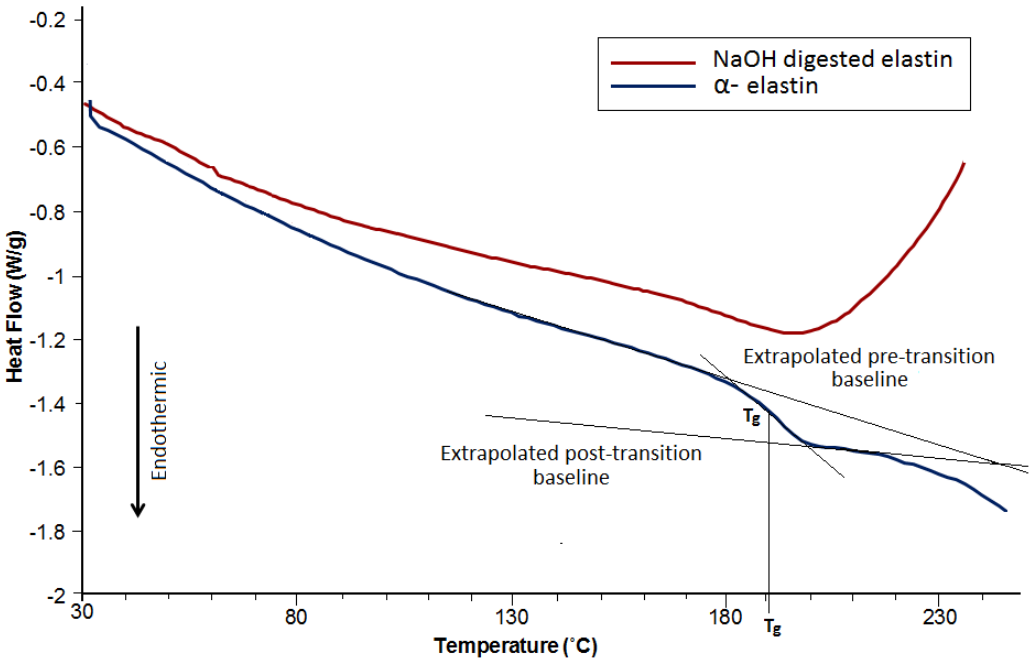

Figure 3.27: DSC thermograms (2nd scans) for dehydrated ligamentum elastin prepared by the Lansing method (red) and α-elastin (blue), heated from 30-250°C at a rate of 20°C/ min. The lines superimposed on the scan for α-elastin illustrate the method by which the glass transition temperature is determined, i.e. the midpoint between onset of the transition and the endpoint. For α-elastin we determined a glass transition point of 191°C.

3.4 Structural Investigations

3.4.1 X-ray Diffraction

WAXS diffraction studies were undertaken to determine d-spacings of the lamprey matrix proteins, which will be discussed in section 4.5.1. Here we present the diffraction patterns for nuchal elastin fibres, prepared by digestion with hot alkali, as a comparison to the lamprey matrix proteins obtained using the same system. Samples were mounted as described in section 2.5.1 either dehydrated or fully hydrated in water and the instrument was calibrated with type I collagen from rat tail tendon. Figure 3.28 shows typical WAXS diffraction images for unstrained elastin fibres and the corresponding intensity plots. In elastin fibres only limited structure was detected as indicated by just two diffuse rings corresponding to d-spacings of 0.47 and 0.92 nm, which showed no change under the application of strains of the order of 50% extension. These values are in good agreement with previous investigations [87] where d-spacings of 0.45 nm and 0.93 nm were recorded, corresponding to the lateral spacing of β-sheets and hydrophobic interactions between sheets. The

hydrated protein (Figure 3.28b), showed a spacing at 0.46 nm. Lines at 0.53 and 0.85 nm are due to Kapton and that at 0.35 nm corresponds to water. Application of 50% strain to small bundles of fibres in the dehydrated state again revealed no change in d-spacing, again in agreement with earlier studies [87].

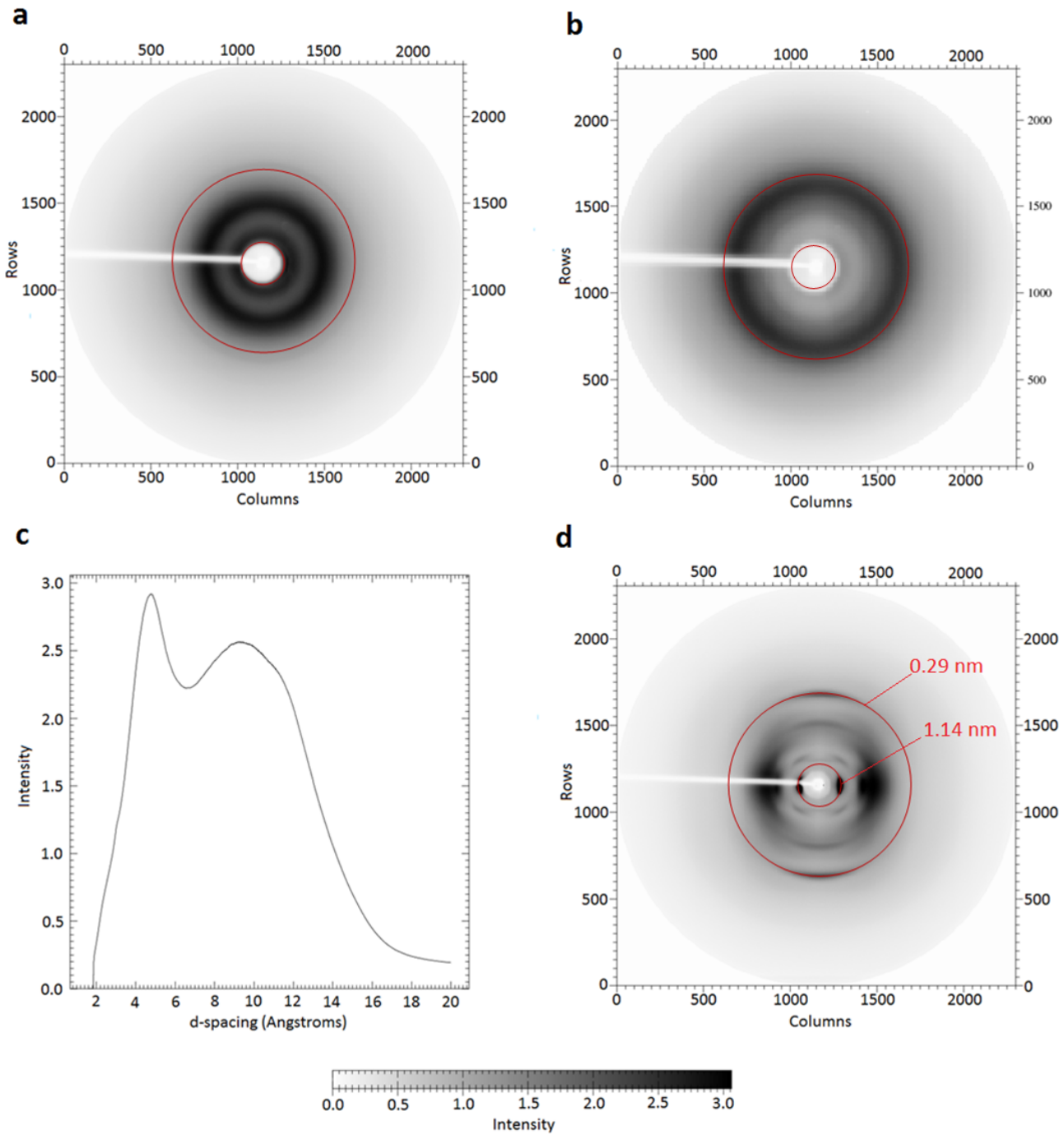

Figure 3.28: Typical WAXS diffraction images of unstrained nuchal elastin fibres, (a) dehydrated and (b) fully hydrated in water. The insert (c) shows the WAXS d-spacing peaks for dehydrated elastin fibres and (d) is a typical WAXS diffraction image of type I collagen isolated from rat tail which is used as a calibration. Characteristic d-spacings at 0.29 nm and 1.14 nm are highlighted by red circles, which are also used as a scale in (a) and (b).

3.4.2 Multiphoton Microscopy

We found the relatively new technique of multiphoton microscopy was an excellent tool for investigating the architecture of extracellular matrix, allowing us to visualize the network of elastin fibres and their interaction with surrounding collagen fibres. In the tissues studied, elastin fibres were identified by their intrinsic two-photon fluorescence (TPF) signal and collagen fibres visualized by second harmonic generation (SHG). Any lipids present, such as those of the plasma membrane, were detected by coherent anti-Stokes Raman scattering (CARS).

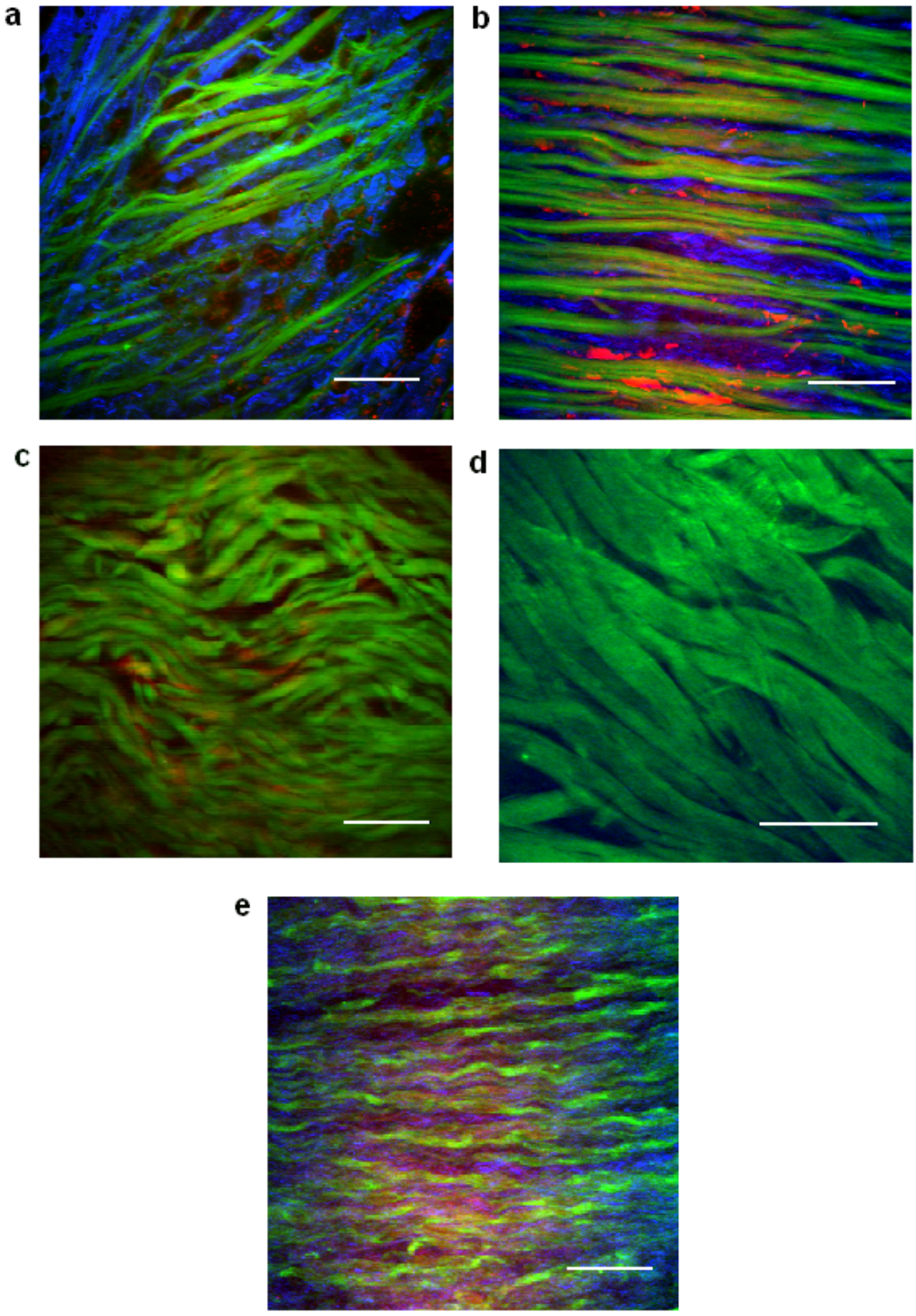

Figure 3.29: Representitive multiphoton microscopy images of bovine ligamentum elastin (long axis of the fibre). In all images two-photon fluorescence is shown in green, second harmonic generation in blue and coherent anti-Stokes Raman in red. The scale bar in each case represents 50 μm. (a) and (b) are typical images of mature, undigested elastic fibres and (c) and (d) nuchal elastin fibres following purification with hot alkali. Image (e) is of undigested foetal ligamentum fibres.

Figure 3.29 shows a series of representative multiphoton images of mature nuchal elastin fibres both undigested (a) and (b), and following purification using hot alkali (c) and (d). The images clearly demonstrate an extensive network of fine collagen

fibres (blue) winding around elastin fibres (green) interspersed with a small number of lipid droplets or cells (red). Elastin fibres are aligned predominantly in the direction of applied strain whilst the fine collagen fibres appear to be corrugated and intertwined with elastin. Image (e) shows a similar image taken from foetal ligamentum nuchae and although elastin and collagen fibres form a similar network arrangement to that in mature fibres, the elastin fibres appear corrugated.

3.4.3 Scanning Electron Microscopy

Scanning electron micrographs of ligamentum elastin and aortic elastin are shown in Figures 3.30 and 3.31 respectively.

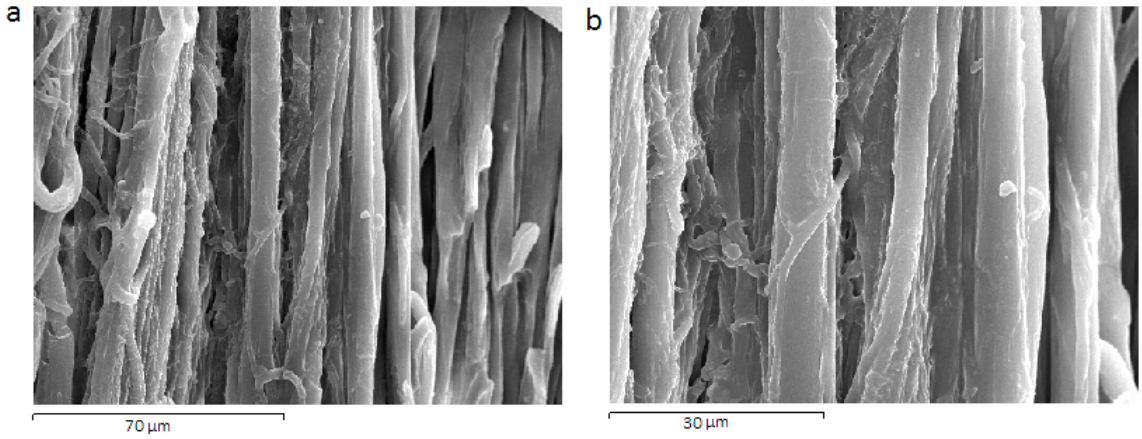

Figure 3.30: SEM images of NaOH digested nuchal elastin fibres done at two magnifications. (a) at x 500 and (b) at x1000.

It is clear that elastin fibres are arranged differently in these two tissues. In ligamentum elastin individual fibres vary in diameter but all appear largely unbranched and aligned parallel to each other. There is some evidence of small fibres that appear to split and diverge from the main fibres, or twist in a rope-like manner but it is uncertain whether this is real or a result of processing.

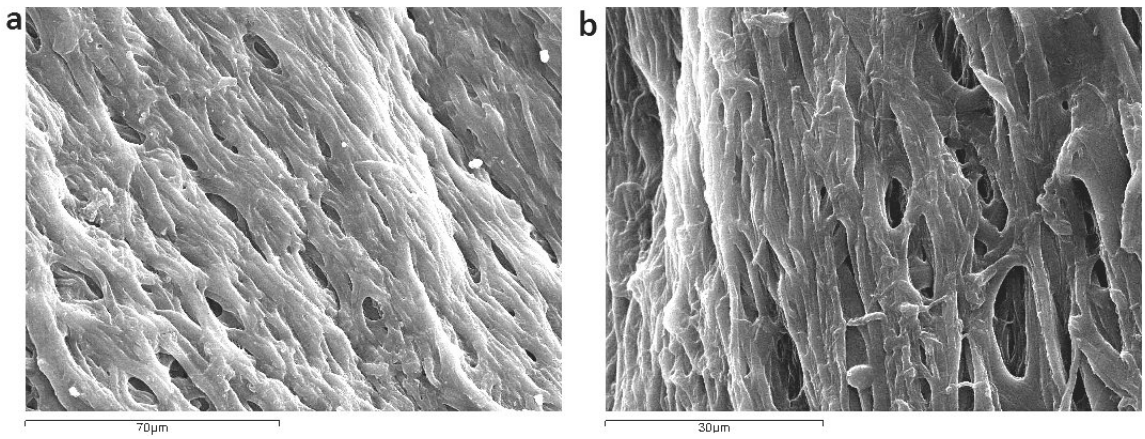

Figure 3.31: SEM micrographs of NaOH digested porcine aortic elastin at two magnifications (a) at x500 and (b) at x1000.

The appearance of aortic elastin is very different when compared to ligamentum elastin with individual fibres being more difficult to resolve. There is a large variation in fibre diameter ranging from 6-7 μm down to less than 1 μm. Fibres are not arranged parallel to each other but instead form a complex, interwoven network composed of numerous highly branched fibres. This is likely to be important in tissues such as major blood vessels which have to withstand multi-directional forces.

3.5 Discussion and Future Work

In this present study some of the work relating to elastin mechanics was confirmatory. Our results confirmed that elastin fibres display long-range elasticity with minimal force and recover on removal of stress with minimal energy loss as previously reported [54] and in agreement with the random-chain elasticity model. In section 1.5.7 we discussed in some detail the major models proposed in an attempt to explain elastin's remarkable elastic properties. The random chain model is based on classical theory of rubber-like elasticity which implies that elastin is isotropic and lacking structure. Alternative models, such as the liquid drop and oiled coil models, differ in that elastin is considered to be composed of both a water phase and protein phase and where these models permit regions of local order. In these two models, the hydrophobic residues buried in the core of the protein become exposed to solvents on extension, which, consequently lead to a decrease in entropy in the system. The fibrillar model proposed by Urry et al suggests that elasticity arises from a regular

β-spiral arrangement. Upon stretching there is a reduction in the librational entropy which provides the driving force for elastic recoil. A similar model, again highlighting the importance of flexible β-turns, has been proposed by Tamburo et al.

Although these models are incompatible in some respects, there is general agreement that a component of the elastic restoring force is entropy driven. Elastin is an extremely hydrophobic protein whose amino acid sequence is known to encode for predominantly unordered structures, consistent with entropy elasticity. However, some recent studies have shown that there are regions of the elastin molecule that contain local order. Our Raman spectra showed 55-58% unordered structures, 24-28% β-structures and 16-18% α-helix (Table 3.8). Under strain there was no significant change in peptide backbone configuration, only reorientation of the few bulky side chains (Table 3.14). These results demonstrate firstly, that the structure is significantly, but not exclusively, disordered and that the changes in backbone strain energy cannot account for elastic recoil. The α-helices are probably associated with cross-linking and our polarized Raman results and X-ray diffraction (Figure 3.28) data suggest that the network is ordered rather than random, as in simple rubbers.

One of the main limitations of the random chain model is that it does not explain why elastin is not self-lubricating like rubber, i.e. elastin is brittle and inextensible when dry. Water contributes significantly to the conformational entropy of elastin but, despite decades of investigations, its precise molecular role is still poorly understood. It has been suggested that there are three dominant phases these being; the hydrophobic polypeptide chain, tightly bound hydration water and bulk solvent water [56]. Our Raman data have confirmed the existence of tightly bound hydration water that remains even after extensive drying (Table 3.13), whilst our mechanical testing data demonstrate the importance of water as a medium. When water was exchanged for the hydrophobic solvent TFE, we found that the work required to strain elastin fibres more than doubled (Figure 3.5). Water molecules interact directly with the protein and with each other. Each interaction is likely to make both an energetic and an entropic contribution to the work of stretching. It is probable that interactions between TFE molecules are negligible and it is unlikely

that TFE binds to elastin [334]. The increase in unloaded length of 35% presumably reflects the unfolding of the hydrophobic domains (although no significant changes in secondary structure composition were detected) and so strain presumably reflects the extension of the hydrophilic domains. It therefore appears that the high compliance of elastin can be attributed to the hydrophobic domains. Deuterium oxide has been shown to form additional and stronger intramolecular bonds compared to hydrogen although intermolecular interactions are similar to those associated with water. Exchange for deuterium oxide produced an increase in unordered structures at the expense of β-structures but H-D exchange was incomplete. It seems however, that in contrast to TFE, the changes had no effect on elastin mechanics or relaxed length. In conclusion, it appears that the polar nature of water is central to its effect on elastin mechanics due to protein-water interactions or to the effect of the protein in disrupting water structure. Our Raman spectra of bulk water suggest that the latter is likely to be true (Table 3.13).

Rubber-like materials can be characterized by their thermoelastic response, which, when held at constant extension, exhibits an increase in force proportional to the increase in temperature. This results from an increase in molecular motion of the molecules at elevated temperatures, which consequently increases the contribution of entropy elasticity to the system. Our thermomechanical data provide some evidence to support a component of entropy elasticity (Figure 3.4), although only at high temperatures. At low temperatures other processes must also be operating presumably involving interactions with solvent. It is unfortunate that the high volatility of TFE prevented investigations of its effects on thermal elasticity. The Urry and Tamburro models hold different molecular structures responsible for conformational changes under strain. Our Raman data are in favour of the latter.

It is clear that even at the molecular level, elastin elasticity has some features consistent with all the models of elasticity, but none is sufficiently detailed in its discussion of interactions with solvent to be considered a comprehensive description. Our experimental data does not support the random chain model but does offer some evidence in support of the other three models. Clearly further experimental data are required. However, difficulties arise here because measurements are unavoidably

performed on fibril assemblies, within which molecular organisation and distribution of solvents and molecular strains under load are still incompletely understood.

Better quantification of the enthalpic contribution could be achieved by calorimetry experiments. The principle aim of such a study would be to measure enthalpy changes in individual elastin fibres (or small bundles) under the application of mechanical strain, whilst immersed in different solvents. To this end, we have already designed and constructed a system that combines a microcalorimeter (Microscal) with mechanical testing apparatus. This apparatus should also allow us to estimate changes in enthalpy of hydrophobic interactions by measuring the enthalpy of hydration of elastin and comparing it to that of the lamprey matrix proteins.

Although we showed that elastin fibres do indeed display time-dependent behaviour, we still do not understand the basis of such time-dependence. The questions that immediately arise are; is the time-dependence related to molecular conformation and associated with re-arrangement under strain or, does it relate to behaviour of elastin fibres at the fibrillar level, for example, as water molecules are moved between intra and inter-fibrillar spaces? We have demonstrated in this thesis the value of Raman spectroscopy and there is undoubtedly more to be done to establish mechanisms of solute-elastin interactions by combining Raman spectroscopy with experiments on the effects of solutions such as sucrose or glucose on elastin mechanics which were reported some time ago [299, 335].

In a structural context, there still remains an on-going debate concerning the presence or absence of structural order within elastin fibres with two alternative views. The limited X-ray diffraction performed as part of this current study has demonstrated the existence of some structural order, which we now believe to be related to intra and inter-molecular hydrophobic interactions. The X-ray diffraction facilities to which we had access have very limited resolution. We had initially begun a set of experiments on hydrated elastin fibres under a range of applied strains at the Synchrotron Radiation Source (SRS, Daresbury, Station 4.1), but were unable to continue this work following demise of the SRS. However, following the recent availability of a new facility at Diamond (Oxford), we hope to pursue our initial investigations and, in addition, explore the effect of exposure to different solvents.

Using the same approach we may also be able to shed some light on the question as to whether the same level of organization exists in all tissues.

Elastin was previously considered to be confined to only a few tissues, but recently it has become apparent that elastin is more widely distributed. For example, elastin fibres have now been detected in articular cartilage [318, 336, 337] and also within the intervertebral disc (IVD) [338, 339] and work is underway to investigate the functional role of these fine fibres in dense collagenous networks. Complementing this work we would also like to explore the structure of these elastin fibres at the molecular level and compare them to those located in the major blood vessels and ligamentum tissue. We have conducted some preliminary spectral analysis of IVD elastin, but to date have been unable to recover a characteristic elastin Raman spectrum. This is consistent with biochemical analysis which cannot be reconciled with the amino acid composition of elastin. These differences clearly need to be resolved for IVD elastin and then expanded to encompass elastin fibres isolated from other sources.

Raman spectroscopy has previously been employed to investigate the molecular structure of elastin fragmentation products [14, 15], and ligamentum elastin [21] but this study has been the first to probe the effect of mechanical strain and solvent interactions on the structure of insoluble elastin fibres using Raman spectroscopy. A major part of this task involved developing the methodology to be used as well as the most appropriate method of spectral analysis. Analysis of the amide I band was of central importance, although this issue has been fraught with controversy amongst researchers in protein structure. We realize the limitations of the method adopted for amide I band analysis, but we have some confidence in our results which were robust over a wide range of smoothing and averaging and peaks used in the fitting routine were recovered from second derivative analysis. Our Raman spectroscopy data revealed new information on the molecular structure of elastin fibres and of the importance of water interactions. Using the approach of Sane et al [3], our results differed from that of previous predictions [6, 15], although we confirmed the dominance of unordered structures. The differences may be largely due to the different approaches used to determine structure. By comparing the amide band

structure of α-elastin in solution with that of hydrated elastin fibres, we conclude that the molecular conformation is little affected by fibre formation. There were, however, slight differences between ligament and aortic elastin in secondary structure composition. A wider study, probably involving elastin with differences in proline content, which is believed to be a major structural determinant [91], could help to clarify relationships between amino acid composition and fibril properties. An alternative approach which has recently become popular is that of principle component analysis (PCA), a multivariate technique used to analyse inherent structure of datasets. This technique is widely used in spectroscopy where it can detect groups of variables that describe the main source of variation within the data. PCA has the potential to reveal unexpected peaks representing secondary structure vibrational modes and it would be an interesting, but non-trivial task, to apply these methods to our data. Some success has already been achieved to reveal secondary structure modes of proteins using the partial least square (PLS) approach [340, 341].

An important outcome of our study has been the demonstration that water makes an important contribution to the elastin fibre organization and its mechanical behaviour. This study has shown the presence of a tightly bound water component which could not be completely removed even by prolonged drying or deuterium oxide exchange. Analysis of the 3600-3100 cm^{-1} region of the Raman spectrum showed that it could be fitted with just two principle peaks which are associated with different modes of O-H vibrations. In the case of collagen [7], the ratio of these peaks is taken to be a measure of disruption of the hydrogen-bond network of bulk water caused by the polymer. For collagen, a significant decrease in the ratio of the OH peaks was proposed to be associated with energy costs of intermolecular interactions. This may also be a factor to consider in elastin thermomechanics.

Within the amide I band a peak centred at 1630 cm^{-1} has previously been attributed to hydration water [3, 15]. However, rather unexpectedly, exchanging deionised water for deuterium oxide resulted in a 25 % increase in the contribution of this peak to the total amide I band area, casting doubt on the accepted attribution.

One of the main technical problems encountered in the present study was the

relatively poor spatial resolution of the instrument available. During the course of this study substantially improved and more sophisticated Raman systems have become available, with the capability of automated Raman mapping as well as vastly improved spatial resolution. In the near future this will allow us to extend the work by scanning individual fibres to establish the heterogeneity of the structure and responses to strain.

Another frustration resulting from this study is the inability to detect unique spectral features for the identification of glycoproteins and cross-links associated with elastin, which are likely to be important determinants of mechanics and of changes with age and disease. Our measurements of spectra from cross-links showed particularly complex structures and a collaboration with biochemists would be valuable to resolve this issue.

When we began this study we had the initial expectation to be able to resolve spectral differences associated with the application of mechanical strain as previously reported for other proteins. Given that this was a major goal of this project, our lack of evidence for changes in peak position or relative intensities was somewhat disappointing. This may be because we were unable to apply strain to individual fibres, and in applying strain to fibre bundles it is possible that a number of fibres will experience much lower strains. Because of this, some effects may be underestimated, although the higher resolution measurements alluded to above may clarify this issue. In this respect elastin appears to differ from collagen [329], bone [330] and other polymers [342] including those such as wool and silk which resemble elastin in some respects. Wool [331] and silk [332], for example, both showed a reduction in α-helix with application of strain. Similar studies on synthetic elastin hydrogels [273] have reported a downshift in frequency for the amide I band and an increase in frequency for the amide III band, which they claim is associated with a stretch-dependent increase in α-helix. A possible interpretation of our results for fibrous elastin may be that the strain is borne by β-structures, where there is enough dynamic freedom to accommodate strain without changes in secondary structure or simply that, as suggested by Tamburro, the structure is very flexible. Polarization of Raman scattered light provides useful information concerning the ordering and

orientation of molecules affected by strain. For our data, analysis of polarization spectra of elastin fibres revealed that strain does produce some structural changes within the aromatic side chains, in the water interaction region and to some extent within the amide I band. These results confirm the presence of some structural order within elastin fibres as previously revealed by X-ray diffraction, but contrary to the classical expectations of rubber-like polymers.

The current work has clarified some of the biophysical properties of "normal" elastin, but the methodologies we have employed could be used to investigate changes with age and disease and the process of elastic fibre formation.

Elastin is the most inert of matrix proteins, but loss of elasticity in skin is a consequence of ageing and in blood vessels and lung may have important functional consequences. However, the molecular correlates of these changes are almost completely unexplored.

At the other end of the life-history of the elastic fibre the processes involved in the formation and export of fibres are poorly understood. The elastic fibre is a very complex structure and although cell culture systems in which fibre formation occurs are now available, unravelling the biochemical processes has been challenging. Raman spectral imaging and multiphoton microscopy could provide powerful new tools in following these processes in living systems.

Chapter 4

Molecular Bases of Elasticity of Lamprey Matrix Proteins

This chapter summarizes a group of experiments undertaken on the four lamprey cartilages that parallel those on elastin described in the previous chapter.

4.1 Mechanics

4.1.1 Stress-Strain Analysis

Stress-strain curves were obtained for each of the CNBr digested lamprey matrix proteins over a range of strains. Typical stress-strain curves are shown in figure 4.1 and the mean values for initial moduli (tangent at zero strain), final moduli (at 20% strain), hysteresis area, breaking strains and water contents are given in Table 4.1. The values for fibrous elastin are given as a comparison and have already been discussed in section 3.1.1.

This study has shown that the mechanical behaviours of the lamprey matrix proteins fall into two distinct groups. The stress-strain behaviour of branchial and pericardial cartilages were very similar to each other and, over an extension of 20% of their original length were more linear than that of fibrous elastin. The initial moduli of these two lamprey matrix proteins were also significantly lower than that of elastin and in the case of branchial cartilage was almost halved. The final moduli were equal to, or slightly lower than that of fibrous elastin. From these results these two lamprey proteins may be described as being more 'elastic' than elastin, requiring

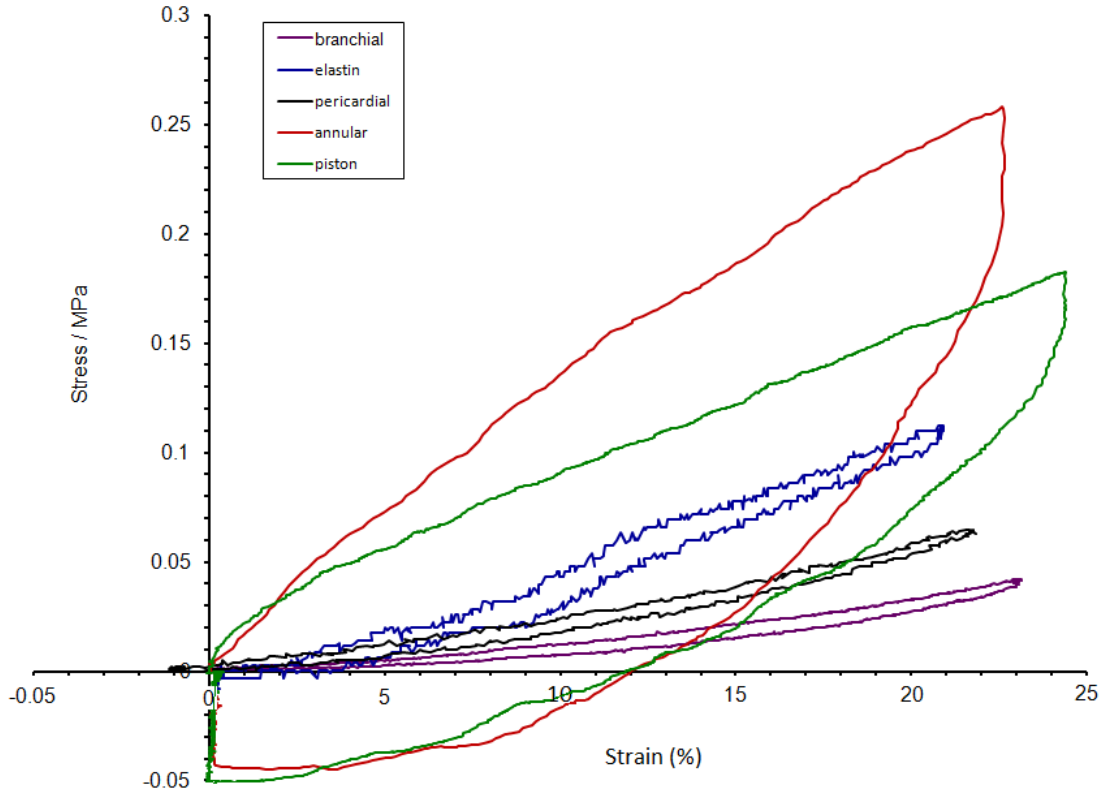

Figure 4.1: Typical stress-strain behaviour for each of the cyanogen bromide digested lamprey matrix proteins and elastin from bovine ligamentum nuchae subjected to uniaxial strain of 20-25% of the original length. All measurements were performed in deionised water at room temperature.

less compliant force to stretch the proteins by the same amount. The piston and annular proteins were again similar to each other but differed qualitatively from all the other proteins having higher initial and final elastic moduli and higher breaking strains. In this respect they are intermediate in properties between mammalian elastin and collagens. The initial moduli showed greatest overall variation with the branchial and pericardial cartilages having the lowest mean values of 0.13 $\pm$0.10 and 0.17 $\pm$0.06 MPa respectively.

Branchial and pericardial proteins both showed small hysteresis losses very similar to that for fibrous elastin and of the order of 0.001 MPa. Values for the piston and annular cartilages were an order of magnitude greater. Despite the very large overshoot on recovery of the piston and annular proteins, these tissues did recover fully their original length over a time-scale of several hours and a repeat stress-strain cycle retraced the original curve, showing that the behaviour was indeed hysteresis as opposed to irreversible sample damage. We are not aware of comparable behaviour in any other biopolymer and whether their behaviour has any biological significance is unclear.

Material	Initial Modulus at 0.01 strain / MPa (mean, std dev),(n)	Final Modulus at 0.20 strain / MPa (mean, std dev),(n)	Hysteresis Loop Area / MPa (mean, std dev),(n)	Breaking Strain / % (mean, std dev),(n)	Water Content / % (mean, std dev), (n)
Elastin Fibres	0.24 ±0.05 (n=8)	0.36 ±0.14 (n=8)	0.0009 ±0.0005 (n=13)	54 ±11 (n=10)	54.49 ±7.89 (n=10)
Branchial Cartilage	0.13 ±0.10 (n=19)	0.32 ±0.28 (n=19)	0.0015 ±0.0012 (n=20)	41 ± 11 (n=26)	80.05 ±8.04 (n=40)
PericardialCartilage	0.17 ±0.06 (n=14)	0.35 ±0.12 (n=14)	0.0010 ±0.0004 (n=10)	49 ± 10 (n=10)	81.24 ±7.26 (n=17)
Annular Cartilage	0.27 ±0.24 (n=7)	0.75 ±0.78 (n=7)	0.0190 ±0.0114 (n=20)	80 ± 18 (n=11)	69.79 ±5.44 (n=21)
Piston Cartilage	0.54 ±0.25 (n=7)	0.35 ±0.28 (n=7)	0.0117 ±0.0111 (n=11)	60 ± 17 (n=9)	68.03 ±4.25 (n=22)

Table 4.1: Mean values for the initial elastic moduli, final elastic moduli, hysteresis areas, breaking strains and water contents for each of the lamprey cartilages and nuchal elastin fibres. Water content was calculated as a percentage value of the wet mass.

All the lamprey matrix proteins (and elastin) had breaking strains in excess of 40% of their original length, and in the case of annular cartilage on average exceeded 80% extension before failure. Like that of elastin, these values are probably underestimates because failure occurred at the point of attachment.

Water contents were calculated as a percentage value of the wet mass of each of the tissues. The branchial and pericardial proteins had the highest water contents (80% ±8, 81% ±7 respectively), whilst the annular and piston cartilages had slightly lower water contents at around 70% ±5 and 68%±4 respectively. Fibrous elastin had the lowest value at 55%. ±8. The exceptionally high water content of each of the lamprey matrix proteins suggests that interactions of water with the hydrophobic domains of these proteins are likely to be important to their mechanical properties.

4.1.2 Stress-Relaxation

Figure 4.2 shows typical stress-relaxation curves for each of the four individual lamprey matrix proteins over a 2000 second period following a near instantaneous step-application of 20% strain. These curves show that each of the lamprey matrix proteins shows time-dependent (viscoelastic) behaviour. Like fibrous elastin, described previously in section 3.1.2, the behaviour of the pericardial sac could best be described by a single exponential function. However, as shown in Table 4.2, the time constant for the pericardial protein was an order of magnitude lower than

that for elastin. The branchial, annular and piston proteins all required a second exponential of comparable amplitude, but significantly different in time constant in order to produce a good fit. In a small number of experiments recoverability was investigated by re-testing after a recovery period of approximately 30-120 minutes. In each case the results were superimposable (data not shown).

Beyond 2000 seconds the annular and piston proteins asymptote and are close to equilibrium, whereas branchial and pericardial proteins show a similar response to elastin displaying a long period of creep failing to reach an equilibrium even after 20,000 seconds.

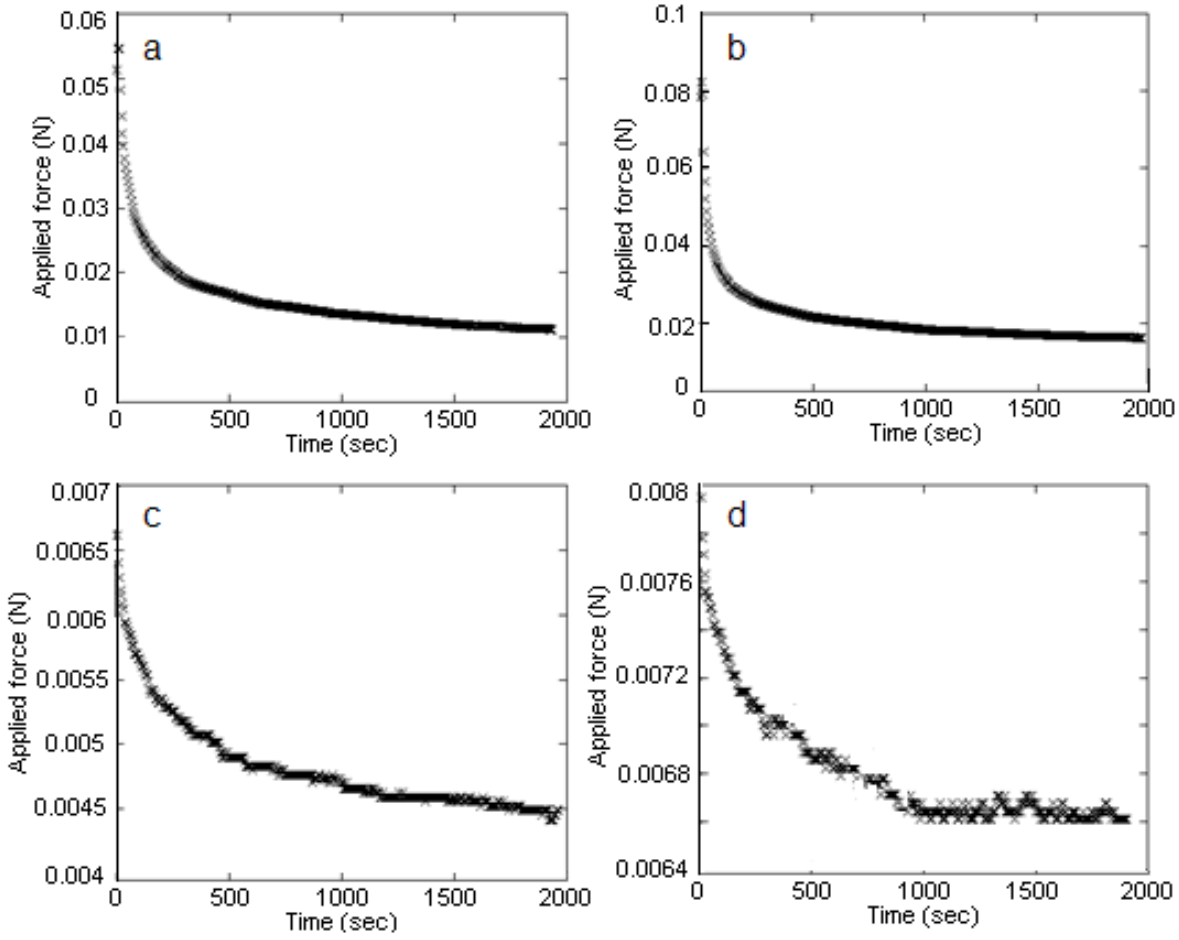

Figure 4.2: Characteristic stress-relaxation curves over a period of 2000 seconds for, (a) annular, (b) piston, (c) branchial and (d) pericardial proteins following the application of near-instantaneous 20% strain. The curves were each fitted with a two exponential function, the parameters of which are summarized in Table 4.2.

Material, (n)	A_1 x 10^{-4} (Nm^2) (Mean, std dev)	τ_1 x 10^{-3} (sec^{-1}) (Mean, std dev)	A_2 x 10^{-4} (Nm^2) (Mean, std dev)	τ_2 x 10^{-3} (sec^{-1}) (Mean, std dev)
Annular cartilage (n=7)	7.05 ± 4.10	15.09 ± 3.30	3.72 ± 1.48	0.61 ± 0.09
Piston cartilage (n=5)	12.07 ± 7.37	16.56 ± 4.17	5.24 ± 1.45	0.53 ±0.07
Branchial cartilage(n=9)	0.32 ± 0.12	10.45 ± 5.18	1.06 ± 0.44	0.87 ± 0.51
Pericardial sac (n=4)	0.14 ± 0.05	3.53 ± 2.43	1.22 ± 0.55	-
Elastin fibres (n=3)	2.17 ± 2.32	14.19 ± 17.6	11.59 ± 7.25	1.69 ± 1.38

Table 4.2: Parameters for the stress-relaxation curves shown in Figure 4.2 fitted with the two exponential function: $F(t) = A_1 e^{-t/\tau 1} + A_2 e^{-t/\tau 2} + A_3$

4.1.3 Thermomechanical Testing

Thermomechanical testing of the lamprey matrix proteins comprised two separate measurements; i) quasi-equilibrium stress-strain behaviour at room temperature and at 60°C, and ii) changes in stress as the temperature of a sample held at 20% strain was increased. The results of the quasi-equilibrium measurements for the annular, piston and branchial proteins are summarized in Table 4.3 and typical stress-strain curves shown in Figure 4.3. No values for pericardial protein have been included due to lack of material, but measurements for fibrous elastin have been added to the table as a comparison.

Material	Ratio of Initial Moduli at 0.01 strain, 60°C/room temp (mean, std dev),(n)	Ratio of Final Moduli at 0.20 strain, 60°C/room temp (mean, std dev),(n)	Ratio of Hysteresis Loop Areas / MPa, 60°C/room temp (mean, std dev),(n)
Elastin Fibres	0.76 ± 0.12 (n=4)	0.76 ± 0.13 (n=4)	0.88 ± 0.34 (n=4)
Branchial Cartilage	0.84 ± 0.27 (n=6)	0.88 ± 0.37 (n=6)	0.65 ± 0.44 (n=6)
Piston Cartilage	0.25 ± 0.13 (n=6)	0.55 ± 0.15 (n=6)	0.12 ± 0.13 (n=5)
Annular Cartilage	0.25 ± 0.02 (n=3)	0.64 ± 0.34 (n=3)	0.12 ± 0.05 (N=3)

Table 4.3: Thermomechanical properties of the lamprey annular, piston and branchial proteins. The mean values for initial and final elastic moduli and hysteresis loop areas are expressed as the ratio of values at room temperature and at 60°C. Values for fibrous elastin are also given for comparison.

Stress-strain behaviour of lamprey cartilages at elevated temperatures showed a similar response to that of fibrous elastin (see section 3.1.3). Branchial cartilage shows a decrease in ratio for both the initial (0.84 ± 0.27) and final (0.88 ± 0.37) elastic moduli with increasing temperature, although the decrease in area of the hysteresis loop was significantly greater (0.65 ± 0.44). The change in mechanical properties with increased temperature was much larger in the annular and piston proteins where the ratio of initial moduli fell to 0.25 ± 0.13 whilst the fall in the

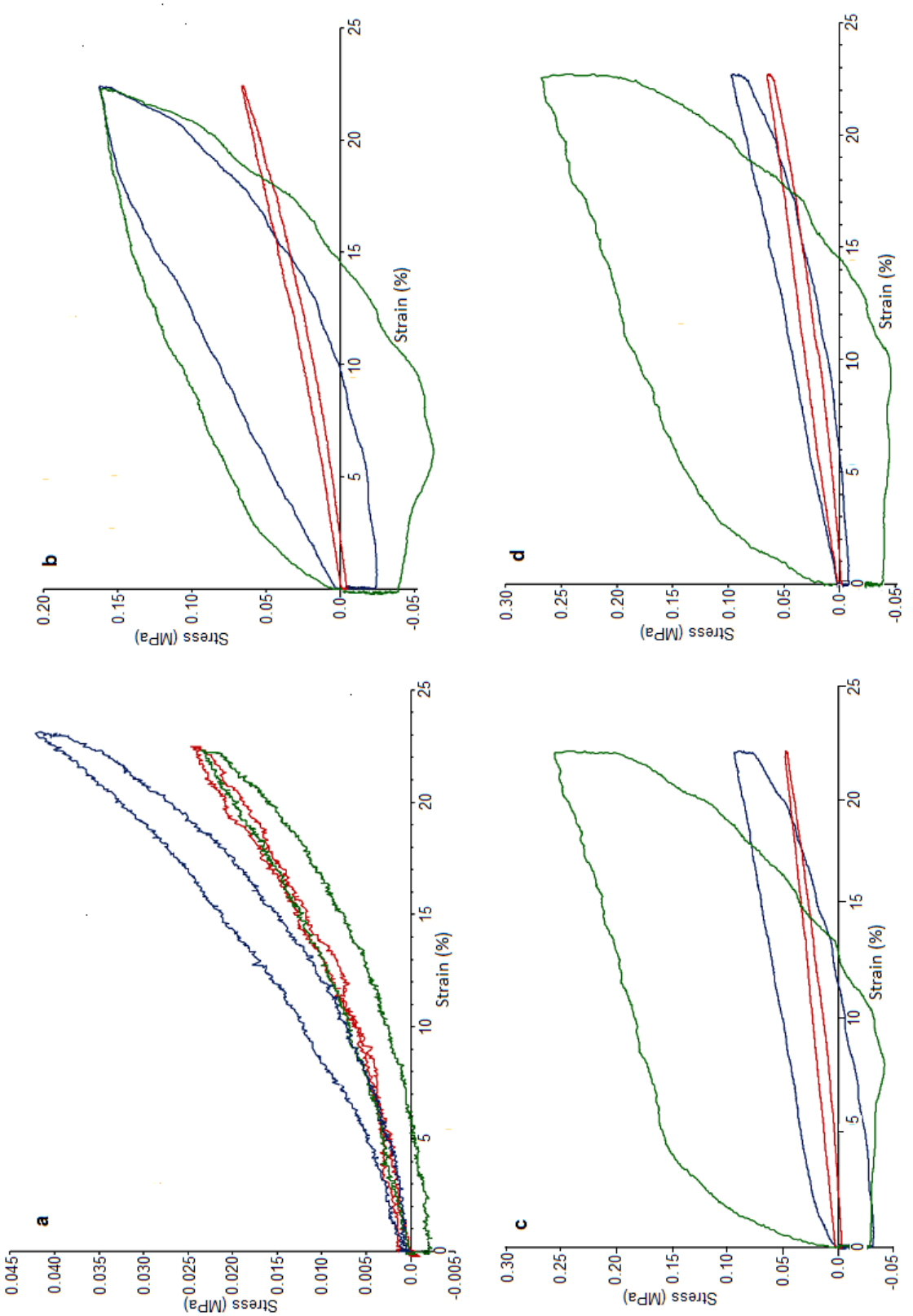

Figure 4.3: Typical stress-strain curves for lamprey a) branchial, b) annular and c) piston proteins at room temperature (blue) heated to 60°C (red) and after cooling back to room temperature (green). The curve shown in d) is for piston cartilage heated to a lower temperature of 30°C.

final modulus was slightly less at 0.64 ± 0.34 in the annulus and 0.55 ± 0.15 in the piston. In addition, there was a substantial decrease in the hysteresis area of both these proteins at 60°C, falling by 88% from that at room temperature. Following measurements at high temperatures the samples were allowed to cool back to room temperature after which the stress-strain cycle was repeated over the same strain range. As summarized in Figure 4.3 it can be seen that none of the lamprey matrix proteins showed complete recovery following heating over a ≥12 hour period. Branchial cartilage showed an increase in hysteresis area on cooling. However, the elastic moduli remained at the lower values. The annular cartilage showed some evidence of recovery following heating although the hysteresis area remained greater than the original measurement at room temperature. The piston cartilage was affected the most by increased temperatures and failed to regain any of its original mechanical properties even after heating to a lower temperature of 30°C (n=1), with an average decrease in initial elastic modulus (0.01 strain) of 30% and 75% decrease in final elastic modulus (0.20 strain). Heating to 30°C also resulted in a 90% decrease in hysteresis loop area.

Following equation 2.28 typical results of the measurements of force at constant strain, as a function of temperature are shown in Figures 4.4, 4.5, 4.6, 4.7. Branchial cartilage behaved in a similar manner to fibrous elastin from room temperature up to 60°C (Figure 3.4), with entropic mechanisms being more important at higher temperatures. The piston, annular and pericardial cartilages all showed similar responses, with an increase in retractive force as the temperature is increased. Again entropic mechanisms dominate at high temperatures. This is particularly noticeable for piston cartilage (Figure 4.7), where entropic mechanisms of elasticity dominate at lower temperatures, indicated by the plateau seen at a little over 40°C. Both the piston and annular proteins were much less stable at temperatures in excess of 30°C with 8 out of 13 samples showing thermally induced denaturation (irreversible loss of mechanical properties), and were excluded from our analysis. In most cases thermally induced denaturation was accompanied by an increase in the sample's reference length that failed to recover completely following heating. The effect of thermally induced denaturation on thermoelasticity plots for annular proteins is

shown in figure 4.8. During sample preparation with cyanogen bromide all tissues are heated briefly to 100°C and therefore the observed thermal instability should be treated with caution. It is possible that the other tissue components during the initial extractions serve to stabilize the structures or that instability only manifests itself under combined thermal and mechanical stress.

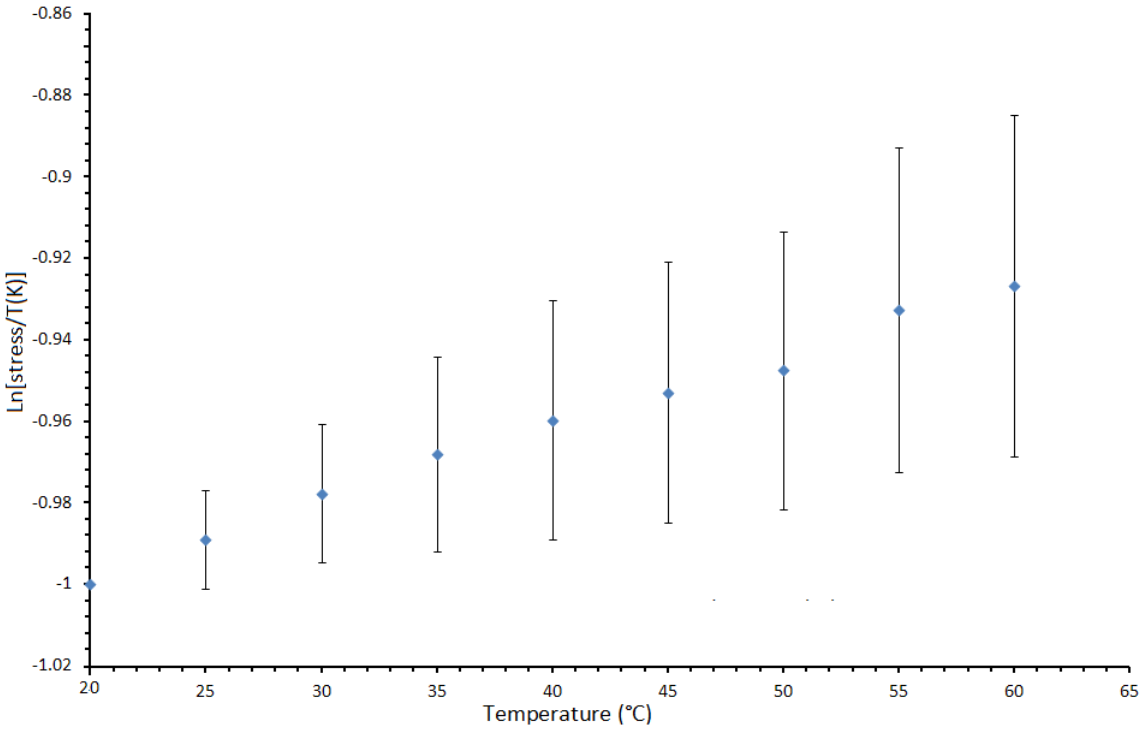

Figure 4.4: Thermoelasticity plots for lamprey branchial cartilage held at constant 20% strain (n =12) over a temperature range of 20 to 60°C. A near zero slope indicate would indicate that entropic processes are dominating. For branchial cartilage this does not occur even at temperatures approaching 60°C.

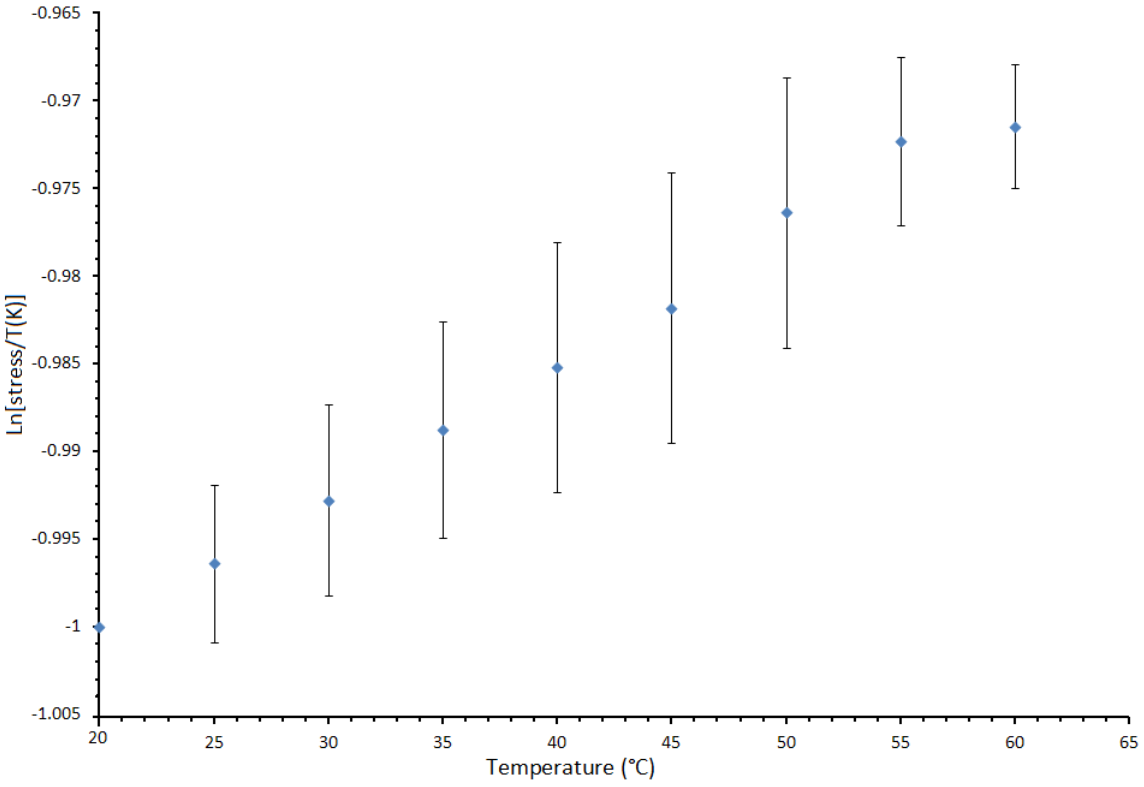

Figure 4.5: Thermoelasticity plots for lamprey pericardial protein held at constant 20% strain (n = 6) over a temperature range of 20 to 60°C. When the data is plotted as Ln [stress/T(K)] vs temperature, a zero slope occurs when f_e/f is equal to zero. For pericardial cartilage a near zero slope is not obtained even at temperatures in the region of 60°C.

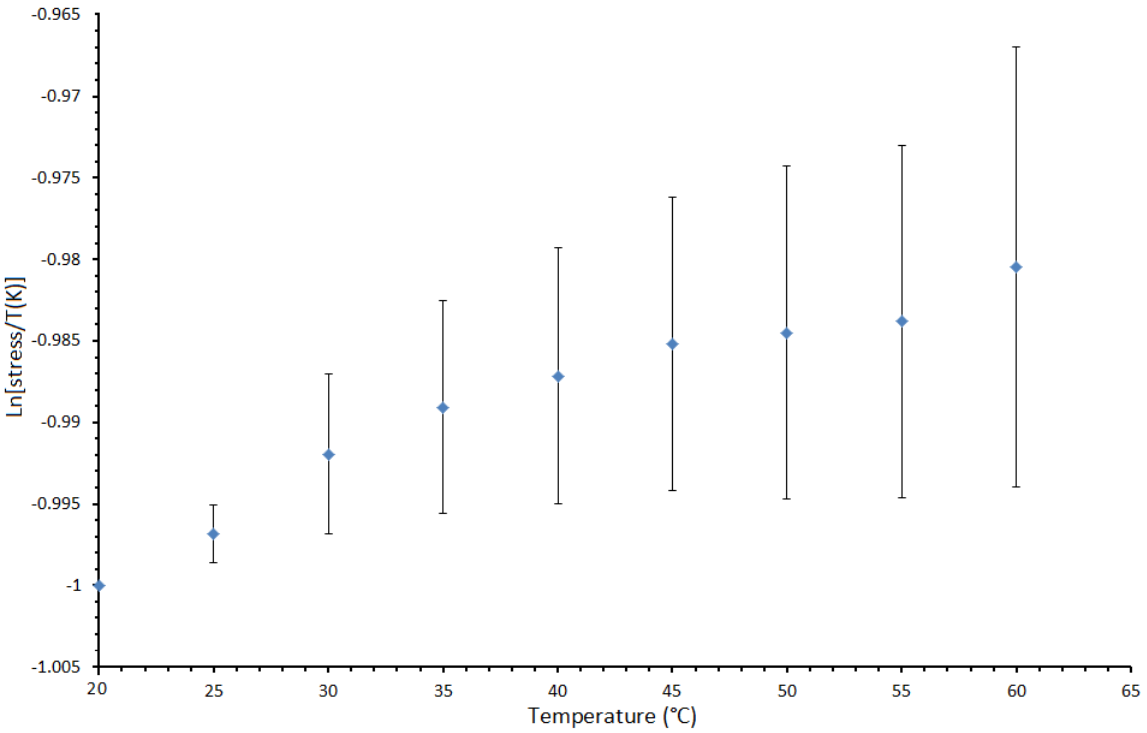

Figure 4.6: Thermoelasticity plots for lamprey annular cartilage whilst held at constant 20% strain over a temperature range of 20 to 60° C (n = 3). When data is plotted as ln[stress/T(K)] vs. temperature, a zero slope occurs when f_e/f is equal to zero. For annular cartilage the slope approaches zero at around $50°C$ indicating that it is an entropic elastomer. Only samples which did not display thermally induced denaturation are shown.

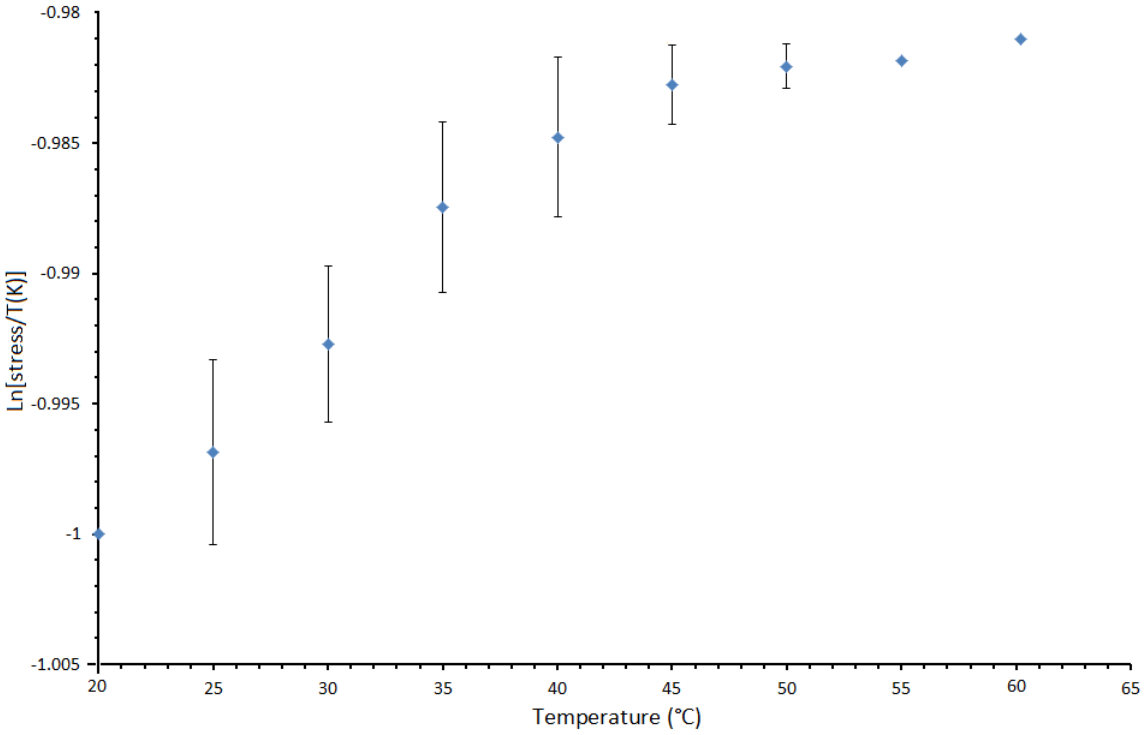

Figure 4.7: Thermoelasticity plots for lamprey piston cartilage. The tissue was extended by approximately 20% in water at room temperature and then held at fixed extension. The force was then measured as temperature was slowly increased from room temperature to 60° C (n = 2). Data was plotted as ln[stress/T(K)] vs. temperature, and according to equation 2.28 a zero slope occurs when f_e/f is equal to zero. For piston cartilage the slope approaches zero at around $55°C$, indicating that at higher temperatures entropic processes dominate. Again only samples which did not display thermally induced denaturation are shown.

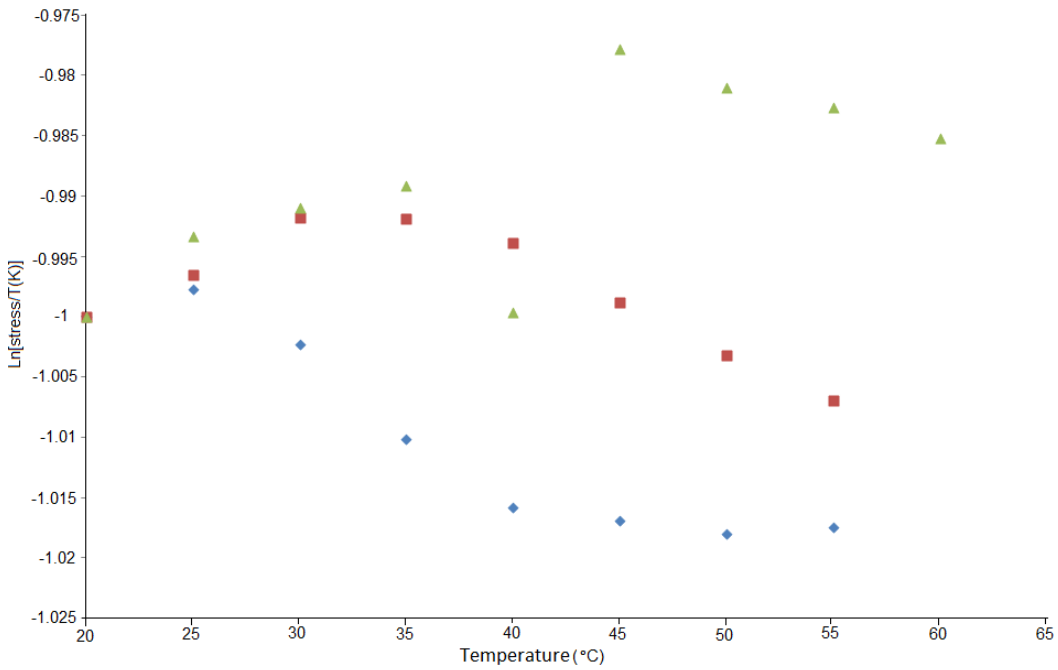

Figure 4.8: Thermoelasticity plots for lamprey annular cartilage held at constant 20% strain having experienced permanent thermally induced denaturation. In most cases denaturation is seen to occur at temperatures exceeding 35°C and is normally accompanied by an increase in sample length that does not recover completely over time.

For all the lamprey matrix proteins tested the entropic component of elasticity becomes dominant only at higher temperatures, although this occurs much earlier for the piston and annular proteins. In this respect they may be regarded as better examples of rubber-like elasticity than elastin.

4.1.4 Mechanics in Trifluoroethanol

In order to determine the importance of solvent interactions, the mechanical properties of branchial and piston proteins were tested in TFE. Typical stress-strain curves are shown in Figure 4.9 and Table 4.4 summarises the initial and final elastic moduli, reference lengths and hysteresis loop areas all expressed as the ratio for values in TFE and water at room temperature.

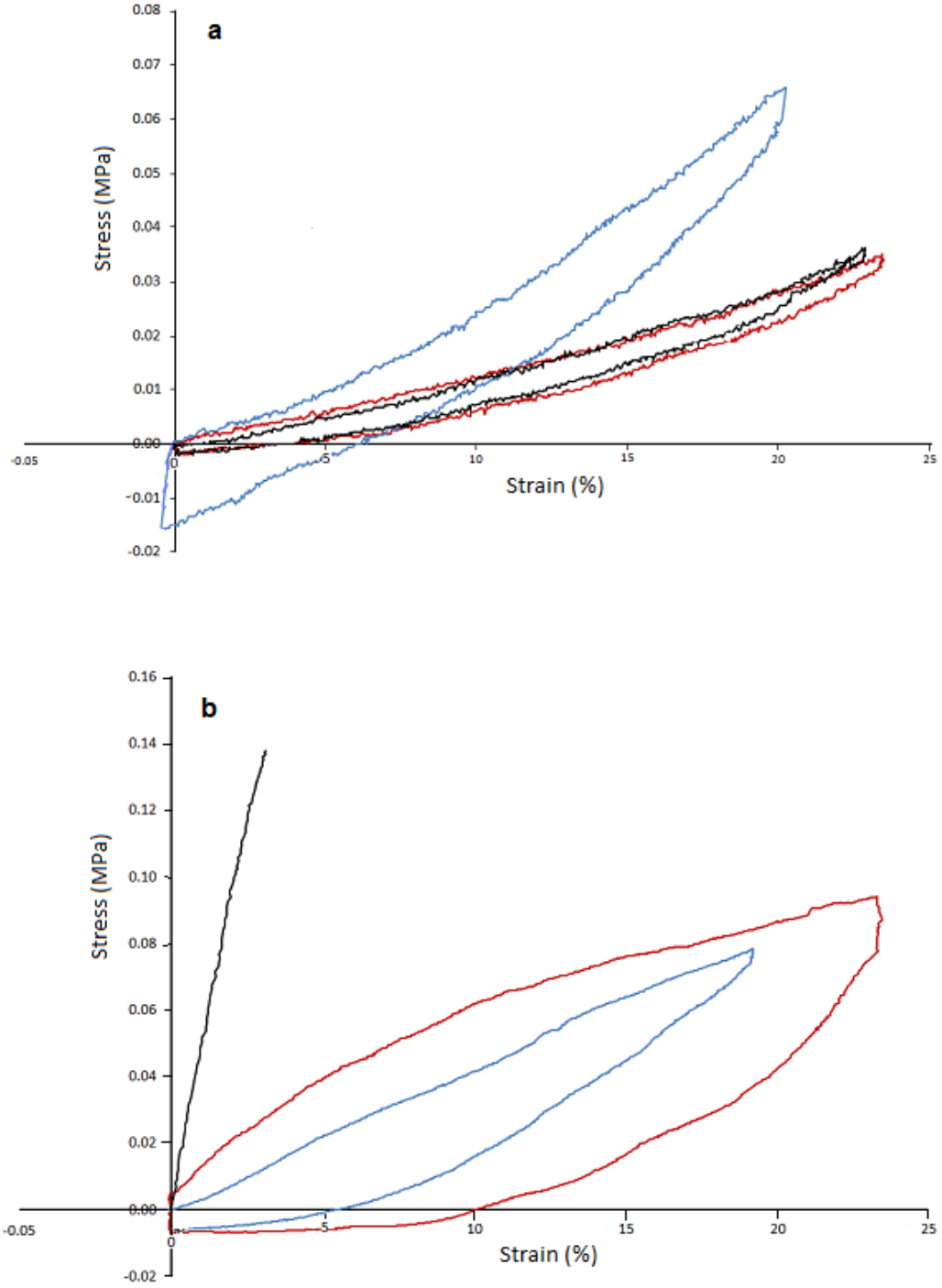

Figure 4.9: Typical stress-strain curves representing the mechanical behaviour of a) lamprey branchial cartilage and b) piston cartilage on exchange of water (red) for TFE (blue). The black curve represents a repeat of the stress-strain cycle in water following re-exchange of TFE for water. For piston cartilage this always resulted in failure of the sample at low strains and therefore the curve is incomplete.

Material, (n)	Ratio of initial moduli (0.01 strain): TFE/water	Ratio of initial moduli (0.20 strain): TFE/water	Ratio of reference lengths: TFE/ water	Ratio of hysteresis loop area: TFE/water
Branchial, (n=5)	2.92 ±1.15	2.39 ±0.51	1.17 ±0.03	6.16 ±2.86
Piston, (n=4)	0.48 ±0.22	1.97 ±0.33	1.31 ±0.11	0.43 ±0.19
Elastin, (n=4)	1.95 ±0.54	2.69 ±1.09	1.35 ±0.04	6.60 ±3.96

Table 4.4: Effects of solvent on mechanical properties. Mean values for initial and final elastic moduli, reference lengths and hysteresis areas of lamprey branchial and piston proteins. Values are also included for fibrous elastin as a comparison. All data are expressed as the ratio of values in TFE and water

The response of branchial cartilage was similar to that of elastin demonstrating the similarities between these two proteins, with the network stiffening, as indicated by a large increase in initial and final elastic moduli as well as a six-fold increase in hysteresis area. The increase in sample reference length at zero strain in TFE may indicate unfolding of the hydrophobic domains which may account for the observed stiffening of the tissue. This change in length was fully reversible for branchial cartilage when TFE was exchanged back for water whilst held at 20% extension, proving that permanent deformation had not occurred. These observations support the view that elastin and the 'soft' lamprey matrix proteins possess similar mechanical properties.

The piston cartilage showed a very different response. Only the elastic modulus at 20% extension increased in TFE whilst the initial modulus was halved and the hysteresis area fell by around 60% of that in water. There was a similar increase in sample length on exchange of water for TFE but, unlike elastin or branchial cartilage, these changes in mechanical properties were not reversible on return to water with the protein network maintaining increased stiffness and the sample visibly deformed, which is likely to indicate unfolding or denaturation of the hydrophobic domains in the presence of TFE.

4.1.5 Mechanics in Deuterium Oxide

A limited number of mechanical tests were performed on each of the digested lamprey matrix proteins, firstly in deionised water and then following exchange of water for deuterium oxide. The solution exchange was made at 20% strain and any change

in force noted. Representitive stress-strain curves to 20% extension are shown in Figure 4.10 and the results are summarized in Tables 4.5 (a) and 4.5 (b).

The stress-strain behaviours of branchial and pericardial proteins, like elastin, show few differences when tested in deionised water or deuterium oxide with only a small change in force on exchange of solvents (5.7% ±2.1). Elastic moduli, work done on straining samples by 20% and hysteresis loop areas showed no significant change even on a paired basis.

In contrast, the annular and piston cartilages displayed a complicated, non-linear stress-strain relationship following deuterium oxide exchange. The initial modulus showed a moderate increase. However, the elastic modulus increased rapidly between 5 and 12% strain and thereafter the incremental modulus decreased. This behaviour can be seen in Figure 4.10 (a) and (b), but only initial and final moduli are given in Table 4.5 (a) and (b). There was also a larger increase in force on exchange of water for deuterium oxide whilst the samples were held at constant strain (10.7% ±3.6), although, unlike the response of these proteins in TFE, there was no corresponding increase in reference length. Work required to strain the tissue by 20% increased four-fold in deuterium oxide compared to water for both the piston and annulus, whilst the recovery phase showed an increase in hysterisis area of similar magnitude. On returning the tissue to deionised water, after overnight incubation, only partial recovery was observed with final elastic modulus, work to 20% extension and hysteresis area values double their original values. Due to technical considerations it was not possible to leave samples to incubate in water for longer prior to testing. Increased protein rigidity in deuterium oxide has previously been reported [326] which the authors attributed to increased compaction of the structure caused by formation of additional intramolecular bonds or preference for stronger deuterium intramolecular bonds over hydrogen bonds. If this is sufficient to prevent complete re-equilibration with water it may account for the partial recovery of mechanical properties as observed in our data.

In order to investigate the time-course of deuterium oxide exchange we performed stress-strain curves on two piston samples within 30 minutes of solvent exchange. Both the initial and final moduli increased by $\geq$60% and the work to strain the

sample by 20% increased by 20-100%. It is suggested in the literature [326] that this rapid response indicates that the effects arise from solvent-polymer interactions rather than intramolecular interactions, which occur on a longer time scale. To verify these results we would need to employ a much larger dataset.

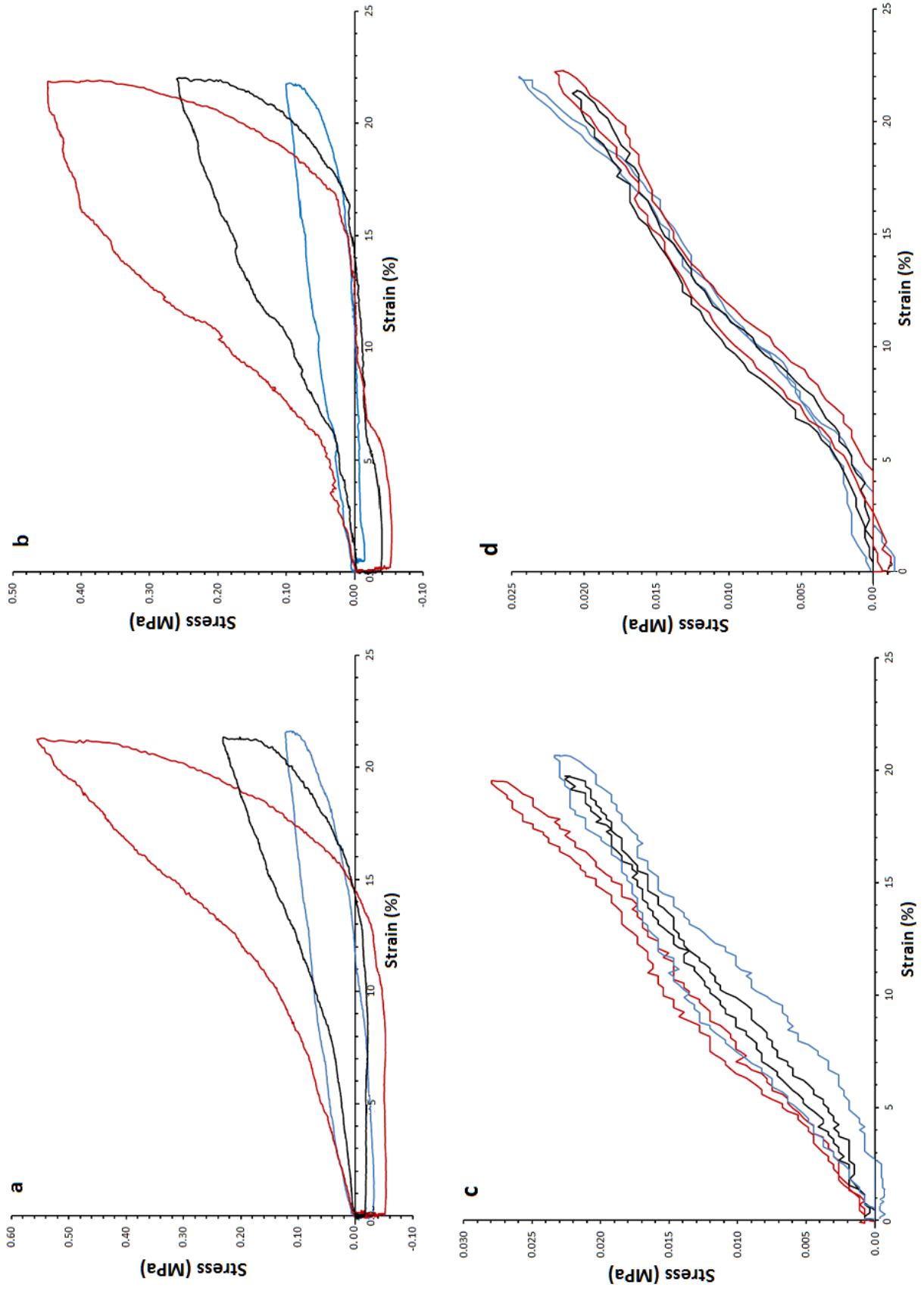

Figure 4.10: Representitive stress-strain curves representing the mechanical behaviour of a) lamprey annular, b) piston, c) branchial and d) pericardial cartilages in water (blue), and following exchange of water for deuterium oxide (red). The black curve represents a repeat of the stress-strain cycle in water following re-exchange of deuterium oxide for water.

a

Sample	Initial modulus (0.01 strain) in H_2O (MPa) (mean, std dev) (n)	Final modulus (0.20 strain) in H_2O (MPa)(mean, std dev) (n)	Work to 20% strain in H_2O (MPa) (mean, std dev)(n)	Hysteresis loop area in H_2O (MPa)(mean,std dev)(n)
Branchial cartilage	0.09 ± 0.02 (n=5)	0.13 ± 0.05 (n=5)	0.003 ± 0.0007 (n=5)	0.0007 ± 0.0003 (n=5)
Pericardial cartilage	0.21 ± 0.09 (n=4)	0.26 ± 0.12 (n=4)	0.0029 ± 0.0009 (n=4)	0.0007 ± 0.0004 (n=4)
Annular cartilage	0.51 ± 0.45 (n=3)	0.42 ± 0.04 (n=3)	0.014 ± 0.003 (n=3)	0.011 ± 0.004 (n=3)
Piston cartilage	0.68 ± 0.50 (n=4)	0.41 ± 0.06 (n=4)	0.014 ± 0.004 (n=4)	0.010 ± 0.005 (n=4)

b

Sample	Initial modulus (0.01 strain) in D_2O (MPa) (mean std dev) (n)	Final modulus (0.20 strain) in D_2O (MPa) (mean, std dev) (n)	Work to 20% strain in D_2O (MPa) (mean, std dev)(n)	Hysteresis loop area in D_2O (MPa)(mean,std dev)(n)
Branchial cartilage	0.10 ± 0.02 (n=5)	0.16 ± 0.07 (n=5)	0.003 ± 0.0004 (n=5)	0.0005 ± 0.00005 (n=5)
Pericardial cartilage	0.23 ± 0.08 (n=4)	0.32 ± 0.15 (n=4)	0.0035 ± 0.0009 (n=4)	0.0009 ± 0.0006 (n=4)
Annular cartilage	1.56 ± 1.03 (n=3)	2.24 ± 1.18 (n=3)	0.065 ± 0.016 (n=3)	0.057 ± 0.016 (n=3)
Piston cartilage	1.08 ± 1.09 (n=4)	1.37 ± 0.88 (n=4)	0.052 ± 0.005 (n=4)	0.044 ± 0.016 (n=4)

Table 4.5: Tables (a) and (b) summarize the initial and final moduli, work to 20% extension and hysteresis loop areas in deionised water and following exchange for deuterium oxide respectively for each of the lamprey matrix proteins.

4.2 Raman Spectroscopy

4.2.1 Lamprey Matrix Proteins Whole Spectra

Figure 4.11 shows the averaged Raman spectra for the four lamprey matrix proteins together with that for CNBr digested aortic elastin as a comparison. There is a high degree of similarity both between the lamprins and with aortic elastin. Each of the averaged datasets possesses spectral characteristics expected in a protein Raman spectrum, although peak positions and intensities differ between the proteins reflecting differences in amino acid content and side-chain environment. In the "fingerprint" region between 1500 and 500 cm^{-1} the phenylalanine peaks (centred at 1609, 1585, 1033, 1005 and 622 cm^{-1}) are lower in all the lamprey matrix proteins than in elastin, as expected from their amino acid compositions [5]. The dominant phenylalanine line at 1005 cm^{-1} was most intense in the piston and annular proteins, although this does not agree with the amino acid composition and if, as in elastin, these modes are highly polarized, it probably reflects the differences in the orien-

tation of these bulky side chains. Because of the complex structure of this tissue (see Figures 4.34 and 4.35), it was not possible to investigate polarization effects in these samples. The lamprey proteins have higher intensity tyrosine peaks (1210, 1176, 851, 830 and 644 cm^{-1}) compared to elastin, which is consistent with the amino acid composition. A vibrational mode centred at 908 cm^{-1} (C-C-N stretch) in elastin was not found in any of the lamprey proteins, whereas that at 924 cm^{-1} due to C-C stretch (probably of proline) was of greater intensity. This latter peak forms a doublet with another peak at 938 cm^{-1} (C-C stretch of α-helix). The peak at 962 cm^{-1} is unassigned in proteins and in our spectra was found to be present only in elastin, the piston and annular proteins, but absent from both the branchial and pericardial proteins. Frushour and Koenig [21] assigned a peak at 966 cm^{-1} in elastin to desmosine/isodesmosine. However, these cross-links have not previously been reported to be present in any of the lamprey matrix proteins and in section 3.2.1.1 we questioned this attribution.

There was no indication of any disulphide bridges (527 cm^{-1}) in any of the four lamprey proteins, which is consistent with the biochemical evidence of the absence of these cross-links. Lysyl pyridinoline has been reported to play a vital role in the cross-linking of branchial cartilage [234]. However, an analysis of the Raman spectrum of pyridinoline (kindly supplied by Dr S. Robins of the Rowlett Institute of Nutrition and Health, Aberdeen) failed to reveal any characteristic features that could be clearly identified in the branchial spectrum. This may be because of the small number of cross-links present in the protein. The spectrum for pyridinoline is shown in Figure 4.12.

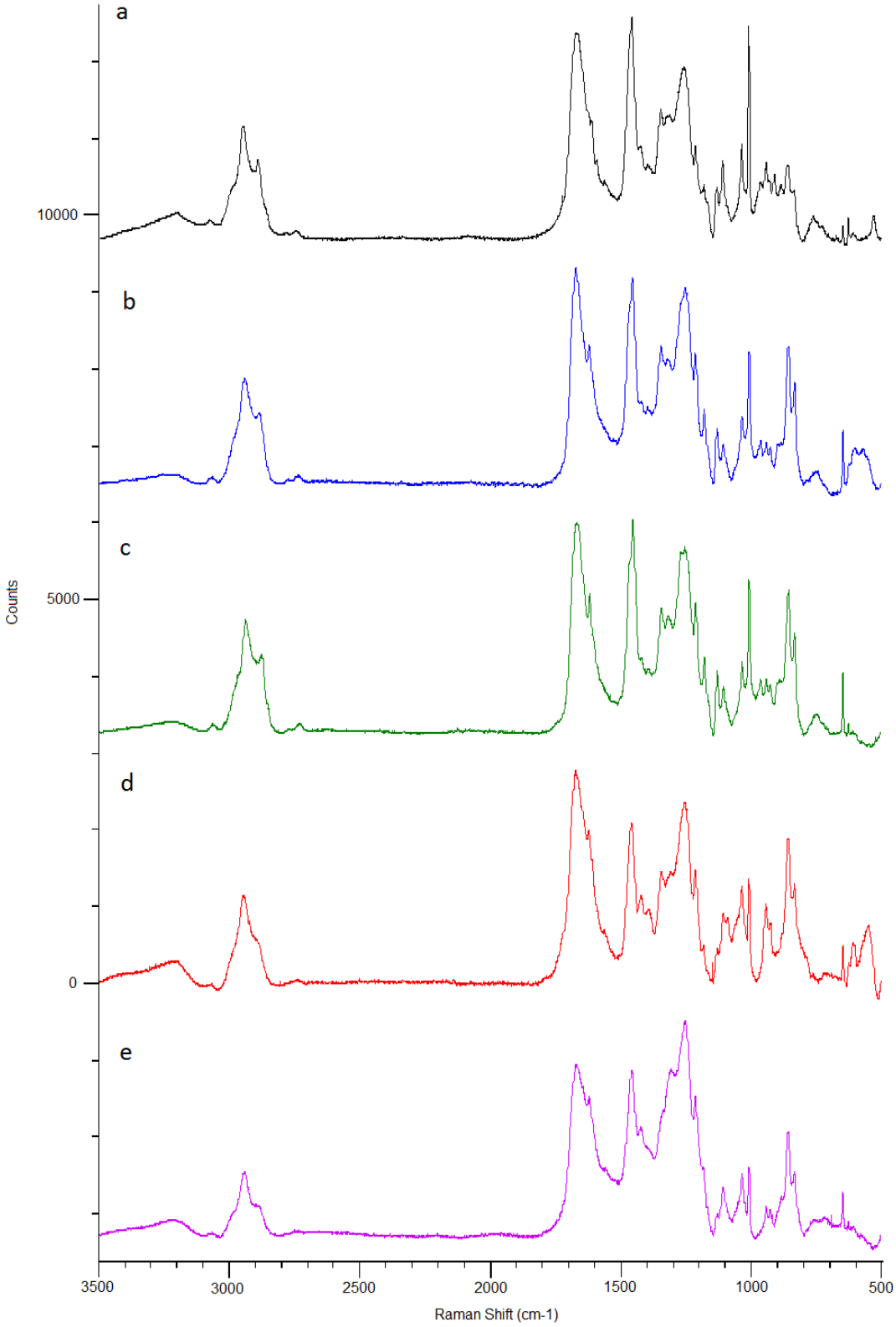

Figure 4.11: Raman spectra for (a) aortic elastin, (b) piston cartilage, (c) annular cartilage, (d) branchial cartilage and (e) pericardial sac. Each spectrum has been background subtracted and is an average of at least 50 individual acquisitions. The spectrum of elastin has been discussed in section 3.2.1 and is included here as a comparison.

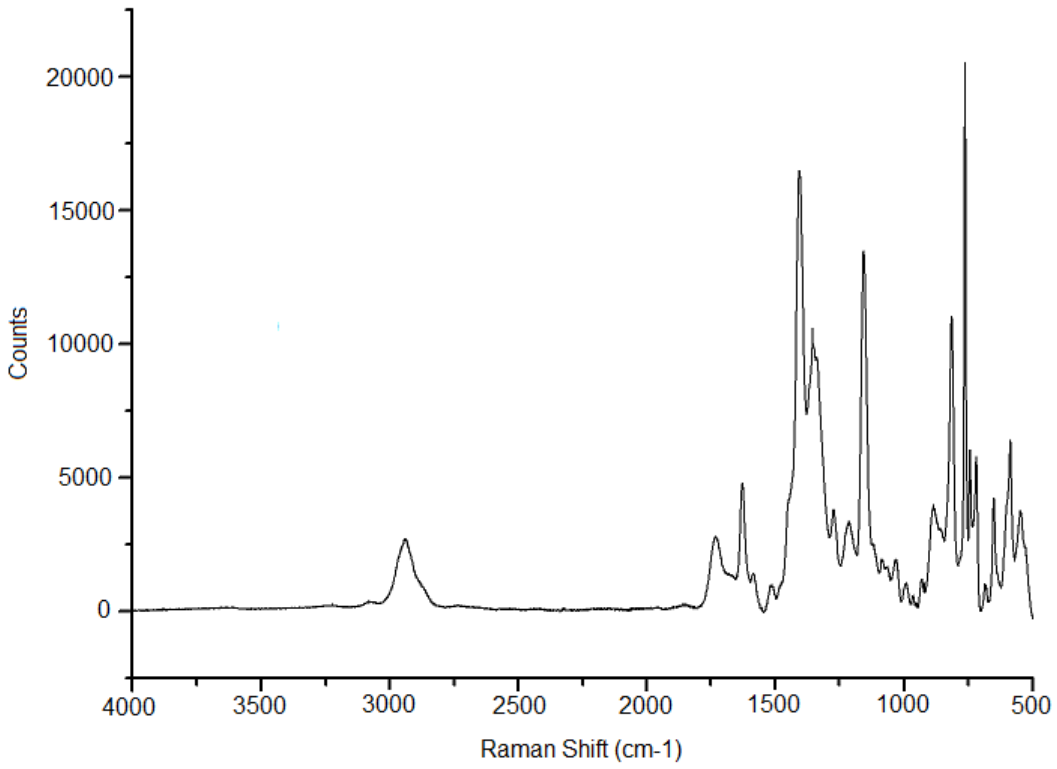

Figure 4.12: Averaged Raman spectrum of dry, powdered pyridinoline (n=36) following baseline subtraction (kindly supplied by Dr S. Robins of the Rowlett Institute of Nutrition and Health, Aberdeen).

4.2.2 Amide Band Analysis

4.2.2.1 Amide I Band

As for fibrous elastin we tried analyzing the amide I band using several different approaches, but found that only the method of Sane et al [3] produced a good fit to all data. Second derivative spectra of the amide I region for each of the lamprey proteins are shown in Figure 4.13 which revealed eight amide components and a single water peak. The results of the curve fitting for each of the lamprey proteins are shown in Figure 4.14 and the peak areas of each secondary structure, expressed as a fraction of the total amide band area, excluding contributions from water and side chains, are given in Table 4.6. Figure 4.14 shows the strong similarity between all the lamprey matrix proteins with the annular and piston being almost identical visually and the branchial and pericardial again being almost indistinguishable. Most of the variation within the amide components appears to be attributable to unordered structures, whilst the non-amide components (water and side-chains) also show slight differences. These similarities are reflected in the calculated secondary

structure composition of the individual lamprey proteins. From Table 4.6 it can be seen that the dominant component in each of the proteins is unordered structures, which constitute more than half the total amide I area, and are consistent with requirements for entropic elasticity. The proportion of β-turns showed some variation between proteins with the lowest contribution (26%) found in the annular and pericardial proteins. The piston and branchial proteins had slightly higher levels of β-turns (29.8 and 31.6% respectively), which was also remarkably similar to that of aortic elastin (29.5%). The proportion of α-helix was similar in all the proteins ranging between 15.5% and 18.8%. The differences in line shape of the amide I band is likely to be due to the variation in water modes. Of the lamprey matrix proteins, the water peak was smallest in annular and piston cartilages (9.9% and 10.5% respectively), which incidentally is very similar to elastin (9.4%), whilst the branchial and pericardial cartilages had an increased water content being 13.6% and 11.5% respectively.

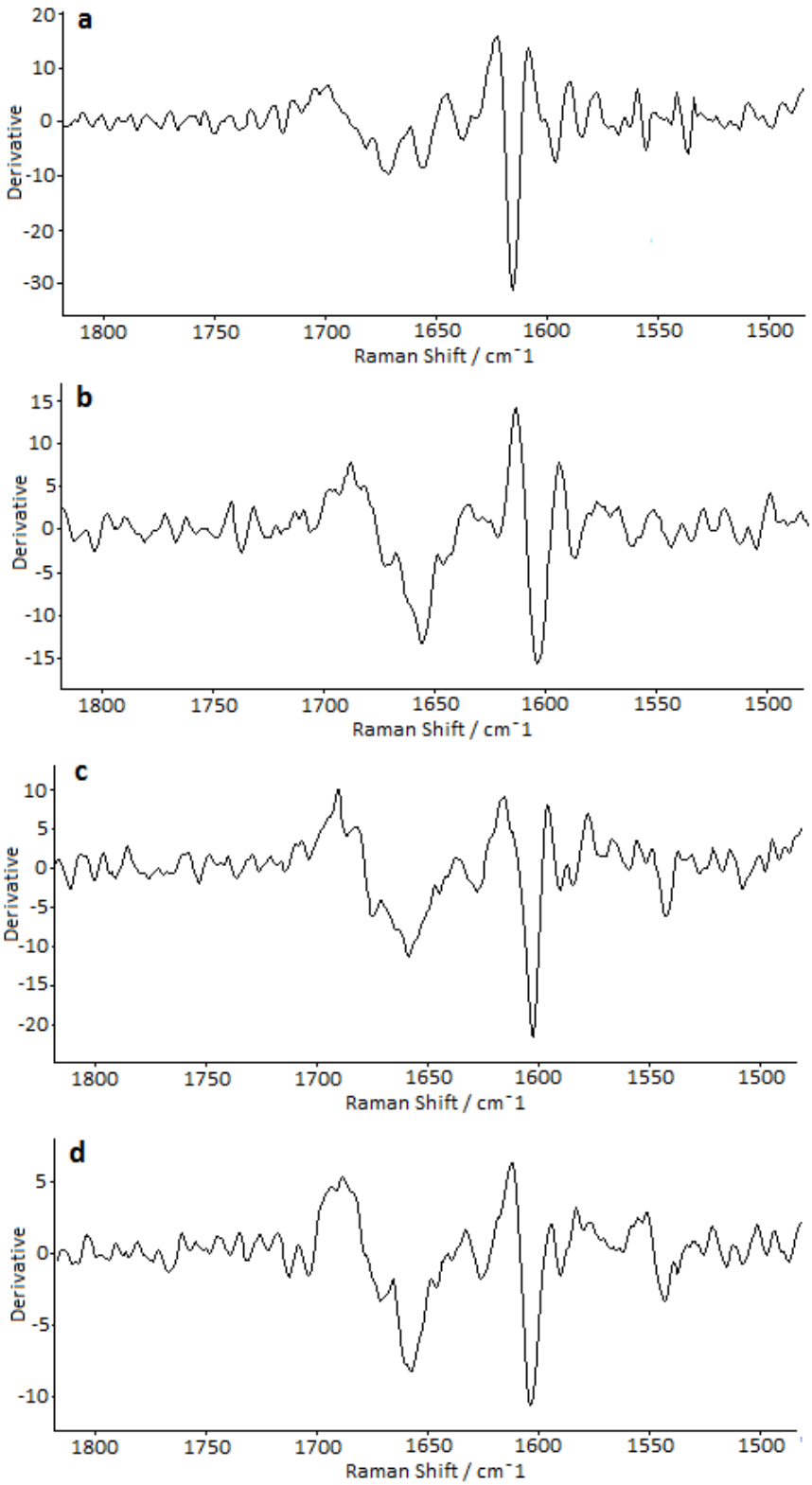

Figure 4.13: Second derivative spectra of the amide I region for (a) lamprey annular cartilage, (b) piston cartilage, (c) branchial cartilage and (d) pericardial sac.

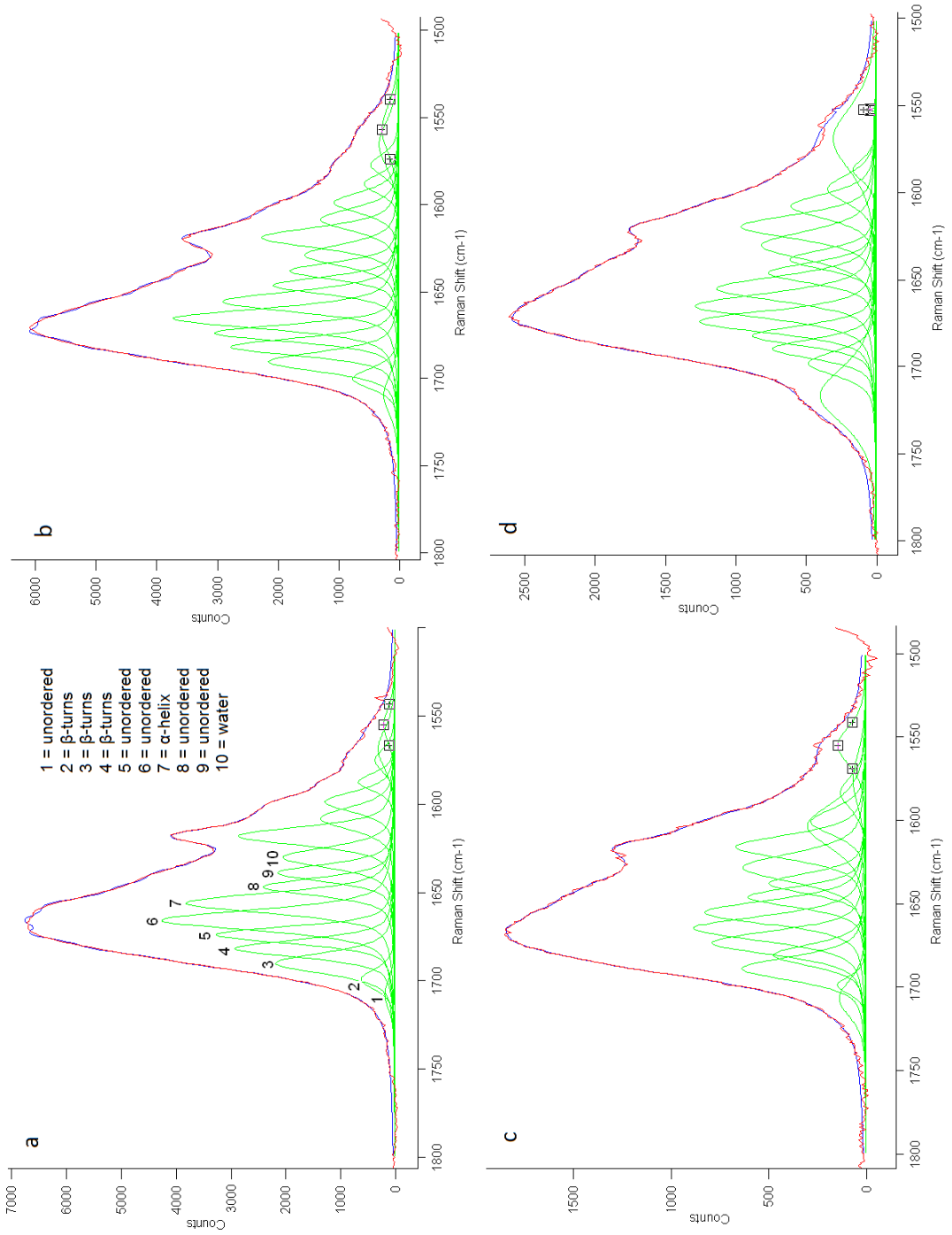

Figure 4.14: Decomposition of the amide I band for fully hydrated (a) annular cartilage, (b) piston, (c) branchial cartilage and (d) pericardial sac. Analysis has been performed on averaged spectra (n=50) following background correction and water subtraction. Peak areas and secondary structure attributions are given in Table 4.6. The original spectral envelope (red line), the fitted spectrm (blue line) and component bands obtained by decomposition of the amide I band (green lines) are shown.

Sample	Beta turns (%)	Unordered (%)	Alpha helix (%)	Water (%)	Other (%)
Annular cartilage	25.8	55.3	18.8	9.9	34.0
Piston cartilage	29.8	53.7	16.6	10.5	38.0
Branchial cartilage	31.6	52.0	16.4	13.6	40.0
Pericardial sac	25.5	59.0	15.5	11.5	37.9
Aortic elastin	29.5	54.4	16.1	9.4	31.1

Table 4.6: Results of curve fitting the amide I band for fully hydrated annular cartilage, piston, branchial cartilage, pericardial cartilage and aortic elastin. Total contribution from amide I band components were normalized to 100%. Total contribution from each secondary structure was then expressed as a percentage of the total amide I band. The fraction of water and side-chains in the peak were also expressed as a percentage of this total. The curve fitting was based on the procedure of Sane *et al* [3].

4.2.2.2 Amide III Band

Secondary structure determination based on analysis of the amide III band is less well developed than for the amide I band. However, our results appear to be consistent with the observations made on the amide I band as discussed in the previous section. The results of the fitting for each of the lamprey proteins are shown in Figure 4.15 and the peak areas of each secondary structure, expressed as a fraction of the total amide III band area are given in Table 4.7. In agreement with the amide I band analysis, the amide III band is also dominated by unordered structures, constituting approximately 50% of the total amide III area. The annular and piston proteins have slightly less unordered structures (45.2% and 47.3% respectively) and in this respect are similar to dry α-elastin with 46.7%. Annular, piston and branchial proteins were found to have similar β-sheet contributions (22-24%), whilst that of pericardial protein is lower at 16.2%. This high β-sheet content in each of the lamprey matrix proteins is in agreement with predictions made by Robson et al [58], where it is suggested that these structures facilitate self-aggregation by forming 'sticky patches'. There is also some variation in α-helix content between the individual proteins, but all were within 26-31% of the total amide band area and lower than that in fibrous or aortic elastin. It was found that the amide III band is more sensitive to background subtraction than the amide I band which resulted in the curve fitting routine being less robust. Despite this, the results obtained are in general agreement with analysis of the amide I region.

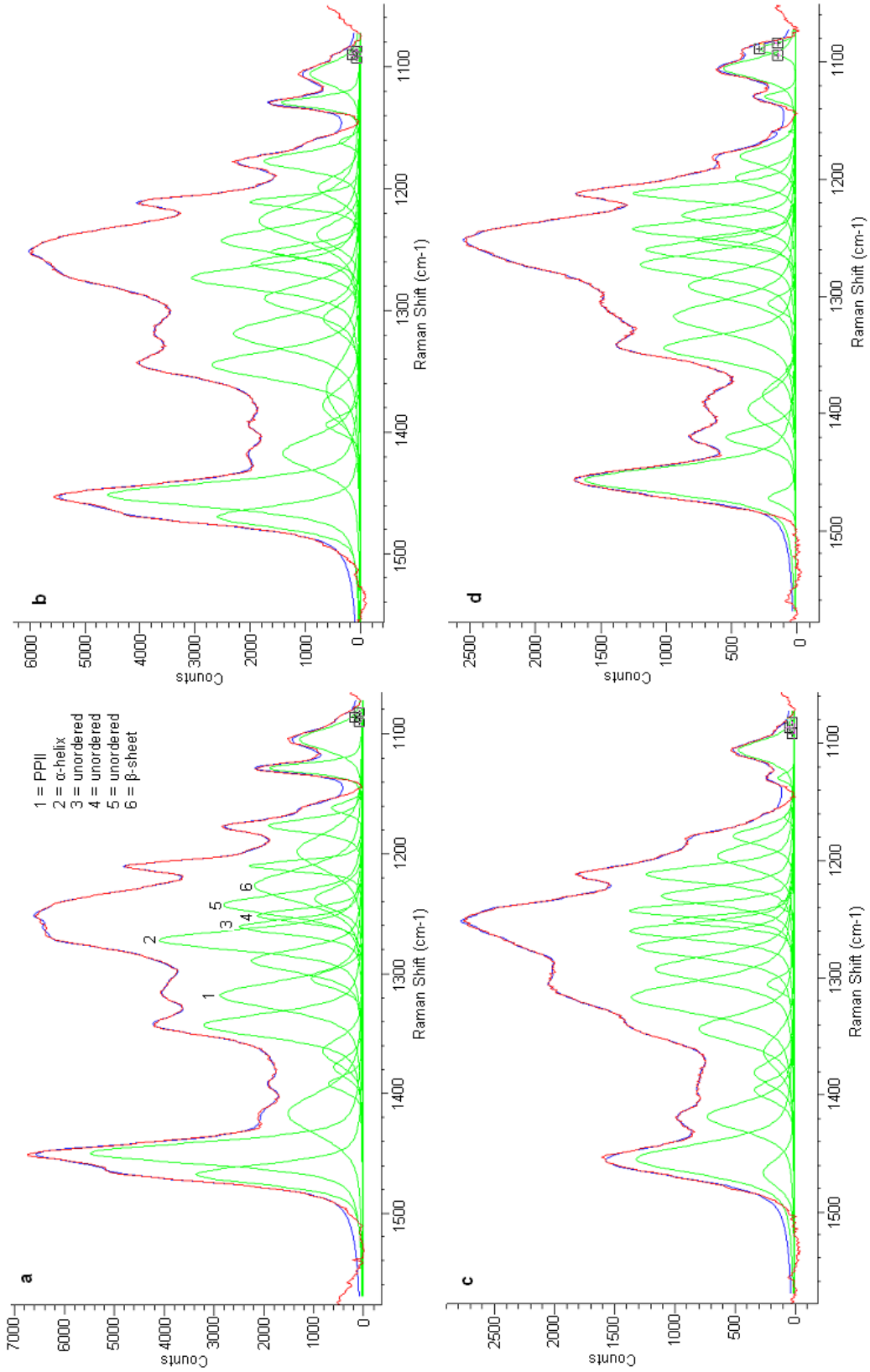

Figure 4.15: Decomposition of the amide III band after background subtraction is shown for (a) annular, (b) piston, (c) branchial and (d) pericardial proteins. Peak areas and structural attributions are summarised in Table 4.7. The experimental spectra (red lines), the fitted spectra (blue lines) and component bands (green lines) are shown.

Material	β-sheet (%)	Unordered (%)	α-helix (%)
Annular cartilage	23.7	45.2	31.1
Piston cartilage	24.2	47.3	28.5
Branchial cartilage	22.3	51.4	26.4
Pericardial cartilage	16.2	54.6	29.3
Aortic elastin	17.6	48.8	33.6

Table 4.7: Raman amide III band secondary structure curve fitting for fully hydrated annular, piston, branchial and pericardial cartilages. Also included are the values for aortic elastin prepared by the same CNBr extraction procedure as a comparison. All values are from final averaged spectra and are expressed as a percentage of the total amide III band area.

4.2.3 PPII Band Analysis

The occurrence of polyproline is regarded as being an important factor in elastin mechanics and is generally detected by the presence of a sharp peak centred at approximately 1314 cm^{-1}. We stated earlier that in the elastin spectrum a well defined peak was observed in this region and likewise lamprey annular and piston proteins also have a sharp peak at around 1320 cm^{-1}. In the branchial and pericardial proteins this PPII peak is less clearly resolved and is observed as a shoulder on the side of the neighbouring amide III band. This can be seen in Figure 4.15. As discussed in section 2.2.6.3 quantitative analysis of this peak is fraught with difficulties due to the overlapping amide III band components and we found no correlation between the relative area of the PPII peak and the α-helix content of either the amide I or amide III bands in any of the proteins.

4.2.4 Fermi Doublet Analysis

A mode at 830 cm^{-1} attributed to tyrosine residues forms a doublet with the neighbouring peak at 850 cm^{-1}, also assigned to tyrosine. This doublet originates from the Fermi-resonance between ring breathing vibrations and an overtone of an out-of-phase ring bending mode. The intensity ratio of these two peaks is thought to provide a measure of the state of phenolic OH and therefore indicates the strength of hydrogen bonding, with tyrosine side-chains being described as either 'buried' or 'exposed' [293]. This doublet was present in all the lamprey proteins and the cal-

culated ratio of the 850:830 cm^{-1} peak areas was highest for the annular cartilage (2.39), followed by the piston (2.07), with the ratio for the branchial and pericardial proteins being lower (1.38 and 1.70 respectively). This would suggest that the two latter proteins experience stronger phenolic hydrogen bonding than the piston and annulus.

4.2.5 Solvent Interactions

4.2.5.1 Interactions with Solvent Water

In order to investigate the interaction of the individual lamprey proteins with water, the spectral region between 3700 and 2700 cm^{-1} was analysed by the method described in section 2.2.6.5. The ratio of the area of the OH peak to that of the neighbouring CH peaks provides a measure of extent of hydration and these ratios are summarised in Table 4.8. The ratio of OH:CH was 40-80% greater in the lamprey matrix proteins compared to that of hydrated elastin (0.68), which was consistent with the high water component present in the amide I band. The ratio of the two principle components of the water band provides a measure of disruption to the hydrogen-bond network of bulk water caused by the protein. This ratio showed some differences between the matrix proteins which exceeded the variation between spectra and the uncertainties in the decomposition described in section 2.2.6. The annular and piston tissues had almost identical ratios that were also very close to that for fibrous elastin (2.7). The branchial and pericardial proteins had lower ratios (1.75 and 1.96 respectively), suggesting a less strong interaction with solvent water.

Material	Ratio 3221/3390 cm^{-1} peaks	Ratio of OH to CH
Branchial cartilage	1.75	1.10
Pericardial cartilage	1.96	1.07
Annular cartilage	2.86	0.96
Piston cartilage	2.68	1.24
Water	10.2	

Table 4.8: Analysis of the hydroxyl modes for hydrated lamprey matrix proteins in the relaxed state. All data analysis are based on averaged spectra and the value for bulk water is included as a comparison. The right hand column gives the ratio of the total area of free OH to that of CH. The left hand column shows the ratio of the peak areas for the two major OH components.

4.2.5.2 Deuterium Oxide Exchange

Figure 4.16 shows the averaged spectrum for piston and branchial cartilages (n = 50) over the spectral range of 1800-500 cm^{-1} following exchange of water for deuterium oxide for a period in excess of 2 hours. The spectra for annular and pericardial cartilages are not shown, although they display the same spectral differences as the piston and branchial cartilages respectively. Exchanging water for deuterium oxide was accompanied by several spectral changes. Most prominent of these changes was a down shift of between 7 and 10 cm^{-1} for the amide I band to lower wavenumbers. The amide III band did not shift in peak position, but did show a change in line shape and became significantly reduced in intensity. An additional difference observed in the spectrum of branchial cartilage was the appearance of a small peak centred at 1780 cm^{-1} in deuterium oxide which we tentatively assigned to C=O [343]. This peak did not arise in any of the other proteins.

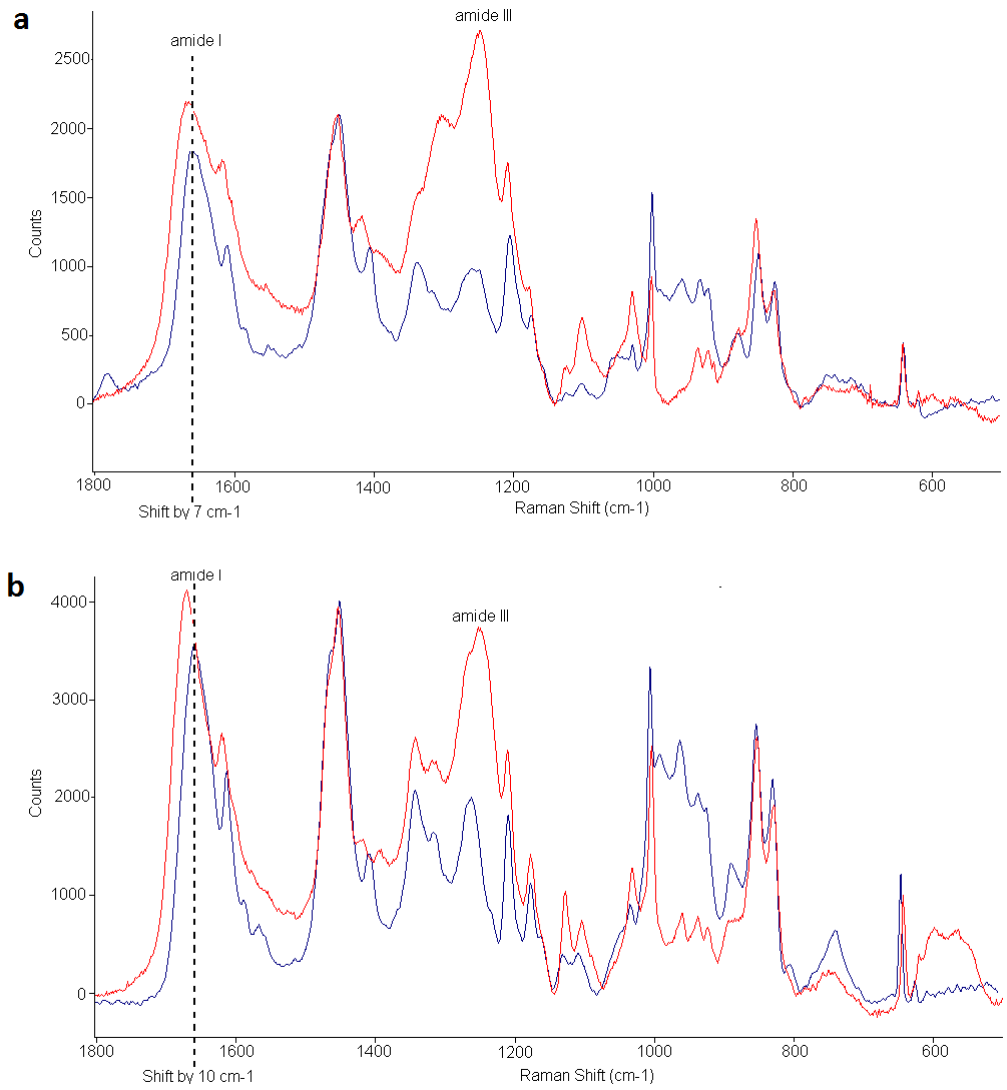

Figure 4.16: Averaged Raman spectra of fully hydrated (a) branchial and (b) piston cartilage in water (red) and following exchange of water with deuterium oxide (blue), over the spectral range 1800-500 cm^{-1}. The dotted line indicates a shift in the amide I band by 7 cm^{-1} in the branchial (and pericardial, not shown) and 10 cm^{-1} in the piston (and annular, not shown) to lower wavenumbers. Other spectral differences include a large reduction in intensity of the amide III band in each of the lamprey matrix proteins and the appearance of a small peak centred at 1785 cm^{-1} in branchial protein spectrum. All spectra have been baseline corrected and are averages of at lease 50 individual acquisitions.

Band decomposition revealed a number of structural differences compared to the same proteins hydrated in deionised water. The results of curve fitting of the amide I band (following the procedure of Sane et al [3]) for each of the lamprey proteins equilibrated in deuterium oxide are shown in Table 4.9 and the results for the amide III band in Table 4.10. Structural predictions of the amide I band in deuterium oxide were significantly different from those in water for each of the proteins. The most striking changes were the large decrease in β-turns (between 58 and 96 %),

the increase in α-helix contribution (between 59 and 66 %) and the increase in unordered structures (between 9 and 29 %). In addition to changes in secondary structure contribution there was also a significant increase (21% to 70%) in the area of the peak centred at 1630 cm^{-1}, which we had previously assigned to water, for each of the lamprey proteins (with the exception of branchial cartilage). Analysis of the amide III band confirmed the changes in secondary structure contribution seen in the amide I band. The contribution made by β-sheet decreased by 93-97%, whilst α- helix contribution increased by between 20-59% and random structures by 11-35% (the pericardial however showed no change in random structures). In a previous study, Cho et al [344] employed circular dichroism and Fourier transform infrared spectroscopy to investigated the contribution made by β-turns and random coil structures in elastin-like polypeptides (ELPs), both in water and deuterium oxide. It was concluded that proteins known to be dominated by β-structures are preferentially stabilized by deuterium oxide with hydrogen bonding playing an important role. In our data the increase in α-helix contribution and decrease in β-structures may explain the reduction in long-range elasticity seen in annular and piston proteins (see section 4.1.5) because a reduction in β-structures is likely to result in reduced flexibility of the polypeptide [206]. However, the corresponding change in secondary structure observed in the branchial and pericardial proteins does not account for their mechanical behaviour which is insensitive to deuterium exchange.

Sample	Beta turns (%)	Unordered (%)	Alpha helix (%)	Water (%)	Other (%)
Annular cartilage	1.1	71.2	27.7	16.4	50.7
Piston cartilage	7.4	64.9	27.7	17.9	50.9
Branchial cartilage	11.0	63.6	25.4	14.6	26.5
Pericardial sac	10.6	64.6	24.9	14.0	31.5

Table 4.9: Amide I band curve fitting for (a) annulus (b) piston, (c) branchial, (d) pericardial cartilages equilibrated in deuterium oxide. Values are expressed as a percentage of the total amide I band area excluding water and side-chain contribution. Comparable data in water are shown in Table 4.6

Sample	Beta Sheet (%)	Random (%)	Alpha helix (%)
Annular cartilage	1.6	61.1	37.3
Piston cartilage	1.4	55.0	43.7
Branchial cartilage	0.94	57.3	41.8
Pericardial sac	0.49	53.0	46.6

Table 4.10: Results for curve fitting of the amide III band for (a) annulus, (b) piston, (c) branchial and (d) pericardial cartilages equilibrated in deuterium oxide. Values are expressed as a percentage of the total amide III band area. Comparable data in water are shown in Table 4.7

Figure 4.17 shows the curve fitting of the water interaction region (3600-3100 cm^{-1}) and the neighbouring CH peak for branchial cartilage following exchange of deionised water for deuterium oxide. Table 4.11 summarizes the results for all the lamprey matrix proteins. As for elastin, exchange of water for deuterium oxide was incomplete, even after prolonged incubation, resulting in a 60-80 % fall in the OH:CH ratio compared to values obtained in water. The ratio of the two principle water peaks also fell substantially. In particular, in the annular and piston cartilages, there was an 18 fold drop due a large decrease in the polarized OH peak centred at 3221 cm^{-1}, indicating that the structural order of water is disrupted by the protein. A smaller fall in ratio of water peaks was observed in the branchial cartilage which again was due mainly to a decrease in the polarized 3221 cm^{-1} peak.

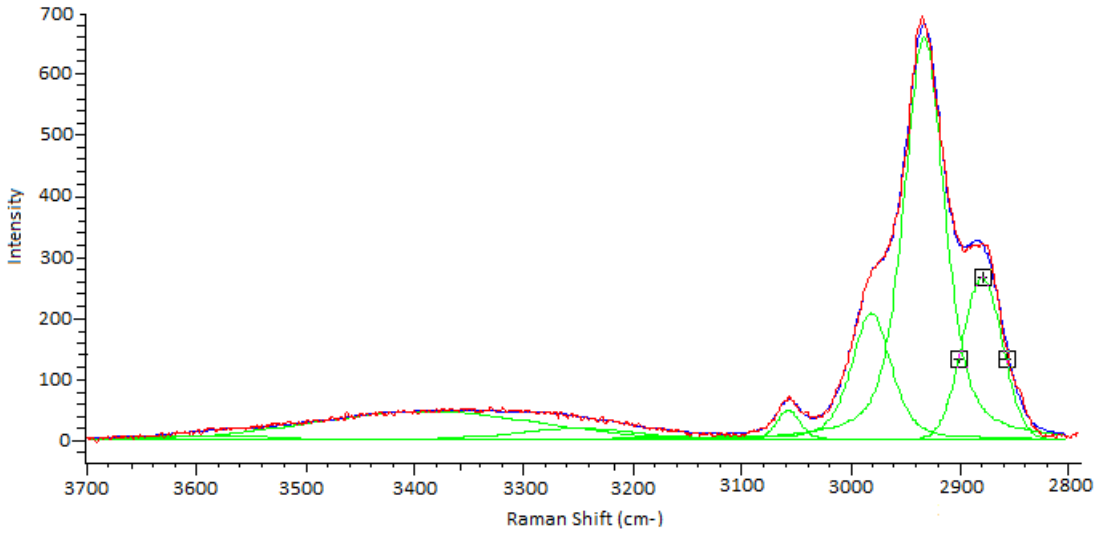

Figure 4.17: Curve fitting of the water interaction region between 3600 and 3100 cm^{-1} and the neighbouring CH band for branchial cartilage equilibrated in deuterium oxide, based on the procedure of Leikin et al [7]. Even after prolonged incubation for a period of 24 hours, exchange of water for deuterium oxide was incomplete. Results of curve fitting for all the lamprey proteins are summarized in Table 4.11. The experimental data (red line), result of curve fitting (blue line) and component bands (green lines) are shown.

Sample	Ratio of 3221/3390 cm^{-1} peaks	Ratio of OH to CH
Branchial cartilage	0.23	0.39
Pericardial cartilage	1.13	0.29
Annular cartilage	0.16	0.28
Piston cartilage	0.14	0.23

Table 4.11: Analysis of the hydroxyl modes for each of the lamprey matrix proteins equilibrated in deuterium oxide. Comparable values in water are shown in Table 4.8

4.2.5.3 TFE Exchange

We exchanged water for 100% TFE whilst the sample was held at constant 20% extension and allowed solvent exchange to occur over a period of $\geq$2 hours before the sample was gradually dehydrated. Figure 4.18 shows the overlaid spectra for branchial cartilage and piston cartilage dehydrated from water and TFE (n = 40). Few spectral differences can be observed, although in both proteins, like elastin, there was a slight shift to lower wavenumbers in a number of the CH bands. In addition, branchial cartilage dried from water and TFE revealed a peak centred at 1780 cm^{-1} which we tentatively assigned to C=O [343]. This peak was not present in the piston cartilage.

Curve fitting of the amide I band (shown in Figure 4.19) did not reveal an increase in α-helix content for either branchial or piston cartilages, as reported for proteins in solution [135, 328, 345]. On the contrary, there was a slight decrease (7% to 11%) in α-helix contribution, which may be due to constraints imposed by intermolecular interactions in the matrix which are not present for individual molecules in solution. Instead there was an increase in β-turn contribution for both proteins (13% increase for the piston and 58% increase for branchial protein). Unordered structure contribution showed little change, but water content appeared to increase, particularly in branchial cartilage. These results are difficult to explain, although it is possible that difficulties experienced in subtracting the underlying TFE spectrum may account for some of the inconsistencies. The results for curve fitting of the amide I band are shown in Table 4.12.

Analysis of the amide III band was consistent with that of the amide I band as can be seen from Table 4.13. For both the branchial and piston proteins there was a

decrease in α-helix contribution, being 13% and 8% respectively and an increase in β-structure contribution (29% and 24% respectively). Unordered structures remained relatively unchanged.

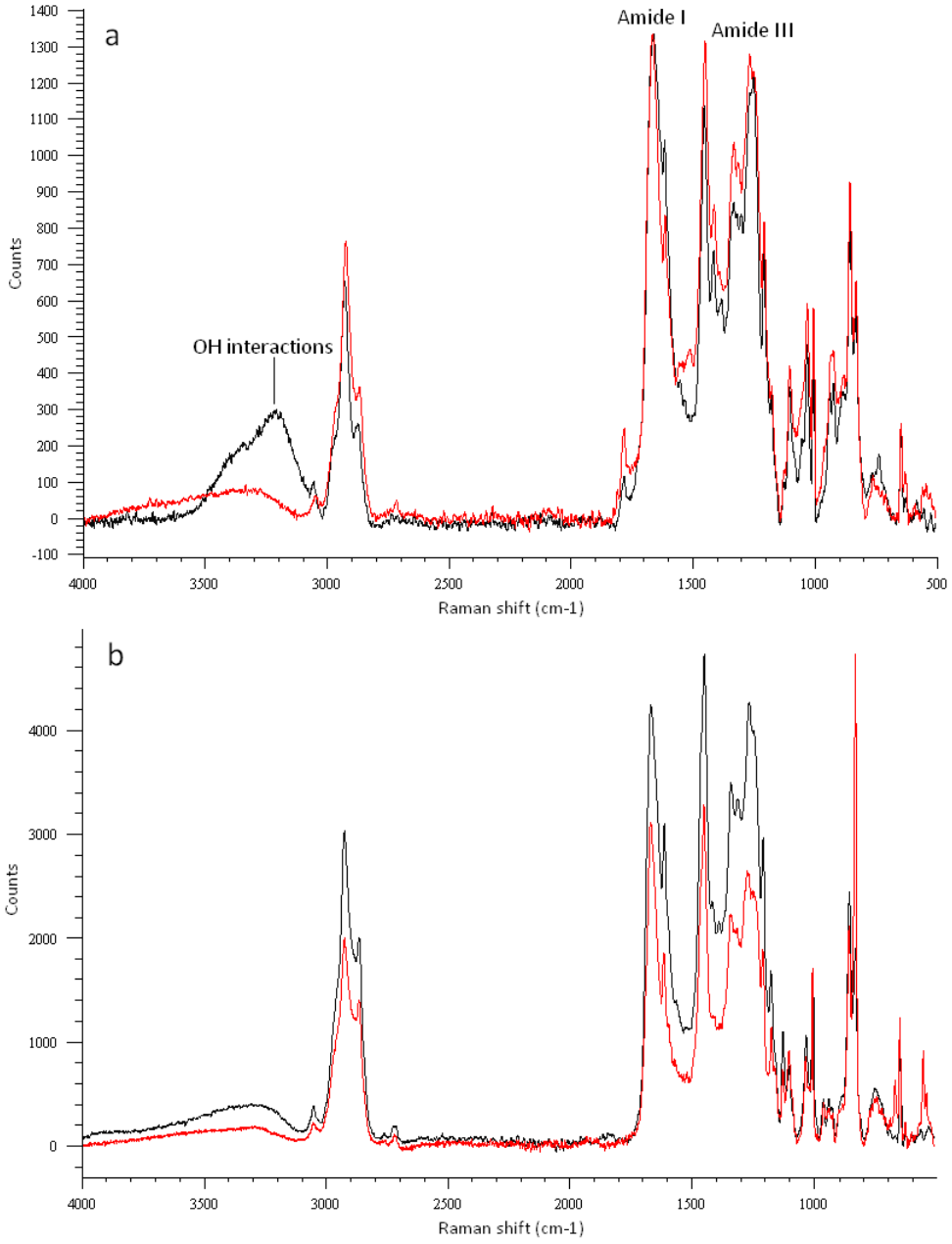

Figure 4.18: Averaged spectra (n = 40) for a) branchial and b) annular proteins dehydrated from deionised water (black) and TFE (red), following baseline correction and TFE subtraction.

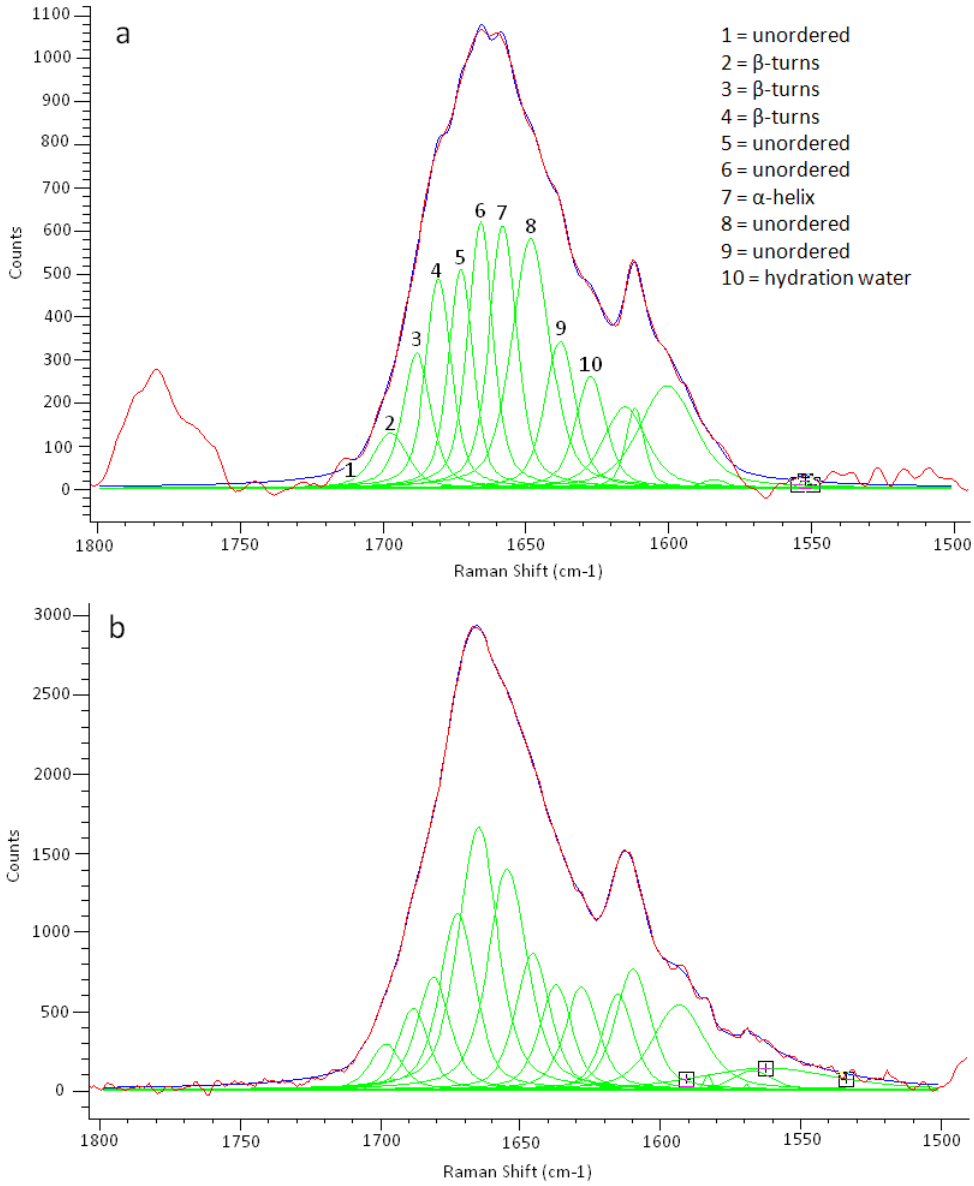

Figure 4.19: Curve fitting of averaged data (n = 40) for the amide I band of a) branchial and b) annular proteins following dehydration from TFE. The component bands resulting from curve fitting (green lines), their sums (blue line) and the original spectra (red lines) are shown.

Sample	β-turns (%)	Unordered (%)	α-helix (%)	Water (%)	Others (%)
Branchial cartilage: Dried from water	16.8	63.9	19.2	9.4	25.9
Branchial cartilage: Dried from TFE	26.6	55.7	17.7	13.4	22.9
Piston cartilage: Dried from water	21.9	57.5	20.7	9.5	34.6
Piston cartilage : Dried from TFE	24.8	56.8	18.5	10.4	28.6

Table 4.12: Results of curve fitting the amide I band for branchial and piston cartilages (n=40) dehydrated from water and TFE. Values are taken from final averaged spectra and are expressed as a percentage of the total amide I band, excluding water and side-chains. Curve fitting was based on the procedure of Sane et al [3]

Sample	β-sheet (%)	Unordered (%)	α-helix (%)
Branchial cartilage: Dried from water	21.4	48.6	30.0
Branchial cartilage: Dried from TFE	27.7	46.2	26.1
Piston cartilage: Dried from water	20.3	46.6	33.1
Piston cartilage : Dried from TFE	25.2	44.3	30.5

Table 4.13: Results of curve fitting the amide III band for branchial and piston cartilages (n=40) dehydrated from water and TFE. Values are taken from final averaged spectra and are expressed as a percentage of the total amide band.Curve fitting was based on the procedure of Williams [12].

Curve fitting of the water interaction region between 3600-3100 cm^{-1} is shown in Figure 4.20, which revealed that exchange of water for TFE was incomplete over a period of 2-24 hours. Table 4.14 summarizes the results of curve fitting for branchial and piston cartilages in the dehydrated state following incubation in water or deuterium oxide. There is a fall in both the ratio of OH to neighbouring CH peaks and the ratio of the two principle water peaks of comparable magnitude to incubation in deuterium oxide.

Sample	Ratio of 3221/3390 cm^{-1} peaks	Ratio of OH to CH
Branchial dehydrated from water	0.28	0.13
Branchial dehydrated from TFE	0.23	0.30
Piston dehydrated from water	0.57	0.16
Piston dehydrated from TFE	0.65	0.18

Table 4.14: Analysis of the hydroxyl modes for branchial and piston cartilages (n=40) dehydrated from water and TFE. The right hand column gives the ratio of the total area of free OH to that of CH. The left hand column shows the ratio of the peak areas for the two major OH components.

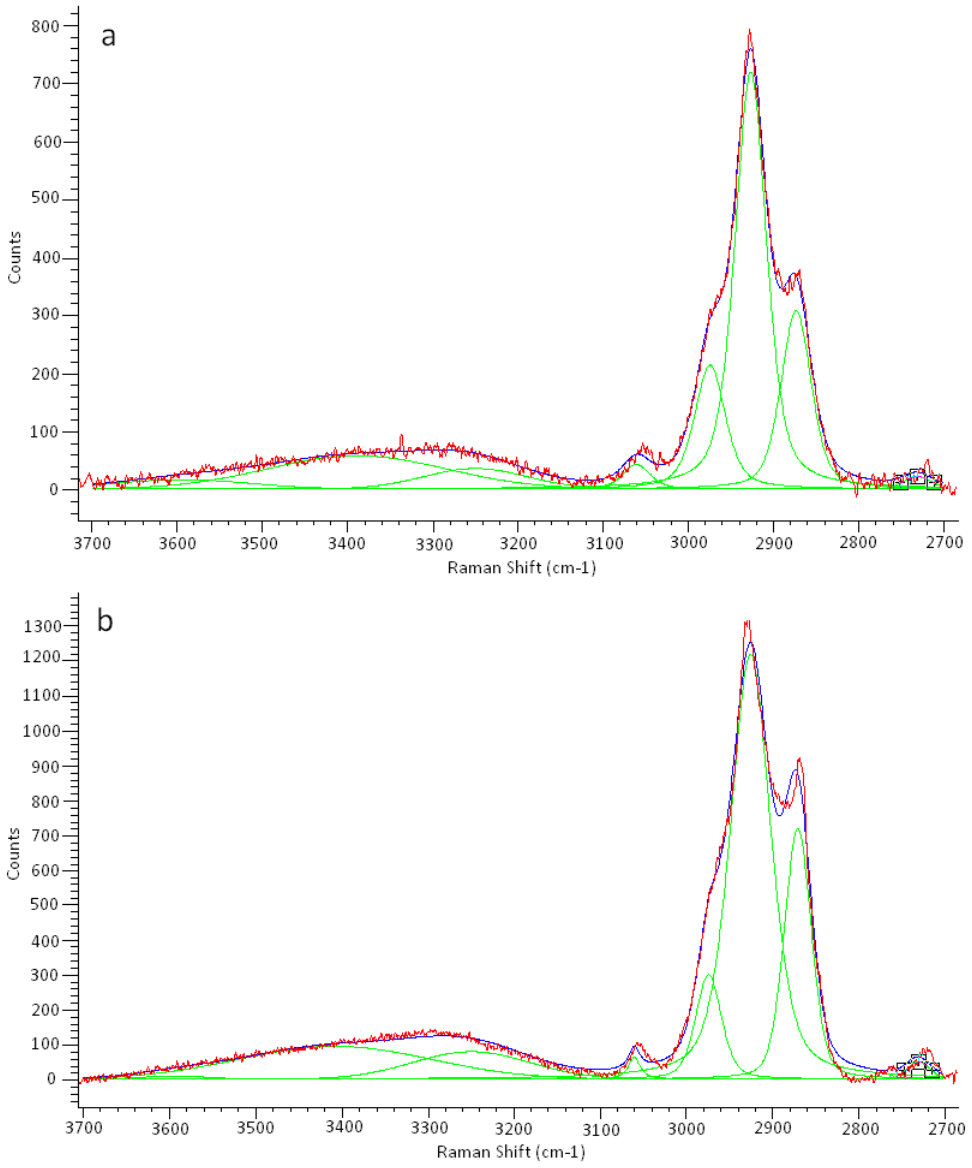

Figure 4.20: Curve fitting of the OH interaction region between 3600-3100 cm^{-1} and the neighbouring CH band for a) branchial protein and b) annular protein, following dehydration from TFE (n=40). Experimental data (red line), results from curve fitting (blue line) and individual component bands (green line) are shown.

4.3 Thermal Effects

Piston and branchial cartilages (n = 100) were held at 20% strain whilst the temperature of the bathing solution increased from room temperature to 60°C. Spectra were aquired and compared at room temperature and at 60°C. The corresponding mechanical changes are discussed in section 4.1.3.

Heating resulted in few spectral changes with no significant differences in peak positions (± 2 cm^{-1}), with the exception of the amide III band of the piston, which showed a shift from 1251 cm^{-1} at room temperature to 1268 cm^{-1} when heated. This we attributed to a decrease in contribution from β-sheet (27%) and a 24% increase in α-helix, whilst no changes were detected in unordered structures. A similar analysis of the amide III band of branchial cartilage revealed smaller differences in secondary structure composition between room temperature and heated to 60°C with only a 15% increase in α-helix and a 9% decrease in unordered structures. Results of the amide III analysis are summarized in Table 4.15. These results differ from those obtained for fibrous elastin which was characterized by an increase in β-sheet, a decrease in α-helix and no change in unordered structures.

	β-sheet (%)	Unordered (%)	α-helix (%)
Piston : Heated	17.7	47.0	35.3
Branchial : Heated	22.9	46.8	30.4

Table 4.15: Results of curve fitting of the amide III band for branchial and piston cartilages following an increase in temperature from room temperature to 60°C. All values are expressed as a percentage of the total amide III area.

Results from analysis of the amide I band (shown in Table 4.16) differed from those of the amide III analysis discussed above. The piston showed a 30% decrease in β-turns contribution, no change α-helix and a 15% increase in unordered structures. The branchial cartilage showed a larger decrease in β-turns (45%), a 24% increase in α-helix and a 20% increase in unordered structures. As for the amide III band, these results differ from those of fibrous elastin (see section 3.2.4) which demonstrated only a minimal increase in α-helix contribution.

For both the branchial and piston cartilages there was a decrease in the magnitude of the water interaction band relative to that of the neighbouring CH peak, in

Sample:	β-turns (%)	Unordered (%)	α-helix (%)	Water (%)
Piston Cartilage Heated	20.9%	61.5%	17.6%	11.0%
Branchial Cartilage Heated	17.4%	62.4%	20.3%	12.9%

Table 4.16: Results of curve fitting of the amide I band for branchial and piston cartilages following an increase in temperature from room temperature to 60°C. All values are expressed as a percentage of the total amide I area, excluding side-chain contribution and water.

Sample	Ratio of 3221 (3250) / 3390 peaks	Ratio of OH/CH
Branchial cartilage: room temperature	1.75	1.10
Branchial cartilage: Heated to 60°C	0.43	0.84
Piston cartilage: room temperature	2.68	1.24
Piston cartilage: Heated to 60°C	1.19	0.30
Water	10.2	

Table 4.17: Analysis of the hydroxyl modes for branchial and pericardial cartilages hydrated in water at room temperature and and heated to 60°C.

particular in the piston with a decrease from 1.24 at room temperature to 0.30 at 60°C. In both tissues there was also a significant decrease in the ratio of the two principle OH peaks (see Table 4.17). For branchial cartilage the largest decrease was seen in the polarized OH peak centred at 3221 cm^{-1}, as seen in elastin, which as for the piston showed a large decrease in the area of the OH peak at 3390 cm^{-1}.

The only other detectable difference in spectra at elevated temperatures was the appearance of a small but distinct peak centred at 1780 cm^{-1} in branchial cartilage, which we have previously attributed to C=O [343].

4.4 Differential Scanning Calorimetry

Differential scanning calorimetry was used to determine first and second order transitions for each of the lamprey matrix proteins in the dehydrated state for comparison with the values obtained from elastin. First order transitions, such as crystallization, provide information on long-range order whereas the second order glass transition (T_g) provides a measure of the protein's molecular dynamics, since conformational fluctuations are suppressed in the glassy state.

The first scans were characterized by a single, broad endothermic peak at approximately 100°C, which disappeared on successive scans. Figure 4.21 shows typical DSC thermograms (second and third scans) recorded between 30 and 250°C, at a

heating rate of 20°C/min, for annular, piston, branchial and pericardial proteins. α-elastin is included as a comparison.

As can be seen, the second and third scans are similar, although T_g appears to be more clearly defined in the third scans for branchial and pericardial proteins in particular. As for elastin, the DSC thermograms show no first order transitions for any of the lamprey matrix proteins, indicating a lack of long-range order. T_g occurred at 202°C, 195°C, 193°C and 192°C for branchial, pericardial, piston and annular proteins respectively. These values were very similar to the T_g reported earlier for α-elastin (T_g= 191°C), but all were significantly higher than that of purified ligamentum elastin (T_g=180°C).

A glass transition temperature exceeding 190°C for each of the lamprey proteins indicates that, in the dehydrated state, these proteins would require operating temperatures above 190°C to permit the required conformational fluctuations in order to function. These results clearly confirm the importance of high levels of hydration for the lamprey matrix proteins to lower the glass transition temperature to within physiological operating temperatures. This has previously been investigated by Samouillan and co-workers for elastin, whereby increasing the hydration level to 30% resulted in a reduction of the glass transition temperature to 30°C [188].

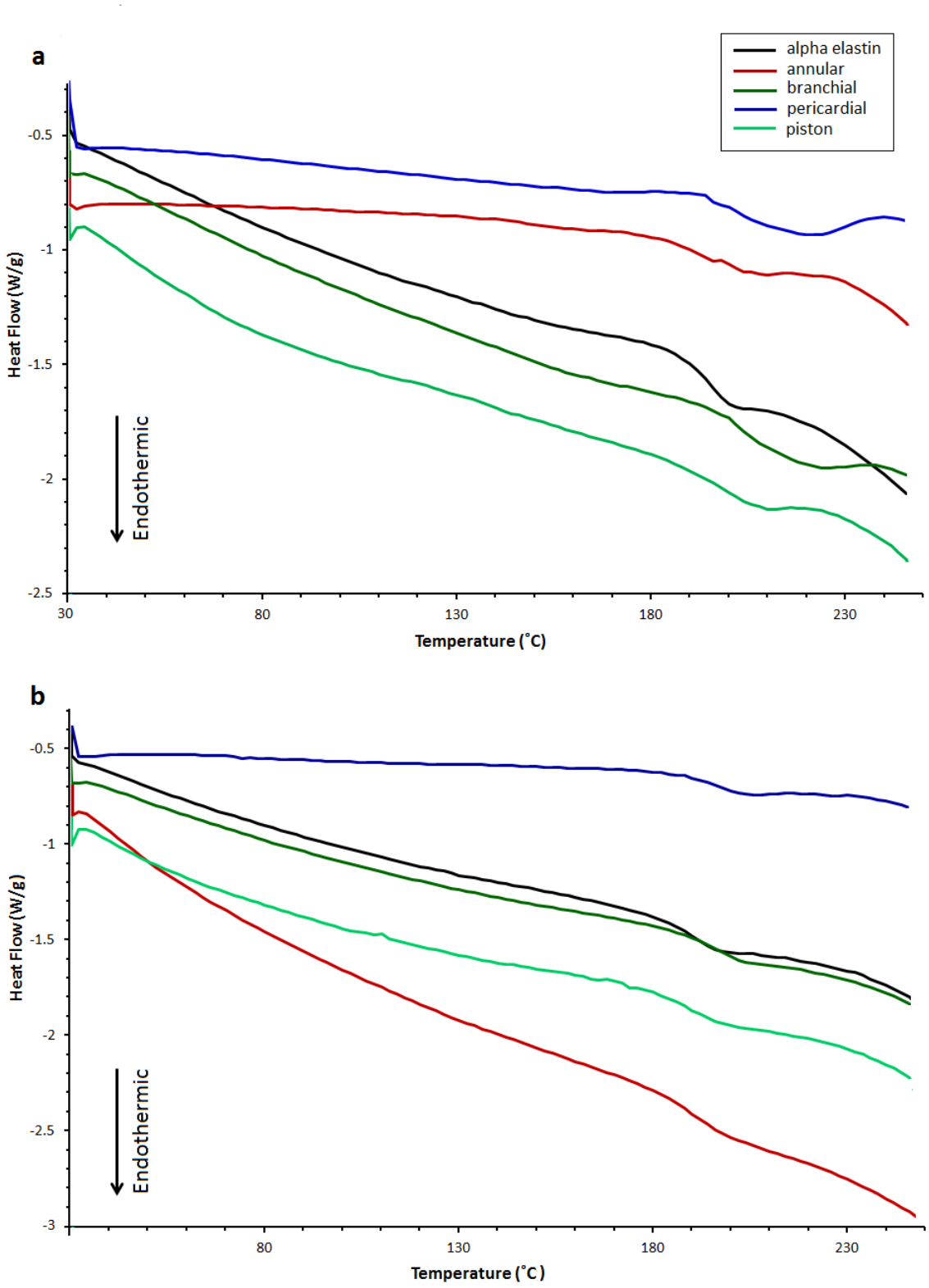

Figure 4.21: DSC plots for α-elastin, branchial, pericardial, annular and piston cartilages heated over a temperature range of 30-250°C, with a heating rate of 20°C/min. (a) are representative 2nd scans and (b) representative 3rd scans for each of the proteins. 1st scans are not shown as these are typically one broad endothermic peak associated with the driving off of freezable water

4.5 Structural Investigations

Mechanical testing has shown that there are noticeable differences between the mechanical properties of the lamprey matrix proteins. However, it is possible that these differences may arise from differences in supramolecular organization rather than from differences in the intrinsic properties of the proteins. We therefore undertook a number of studies to investigate structural variations between the proteins.

4.5.1 X-ray Diffraction

WAXS diffraction studies were undertaken to determine d-spacings of the lamprey matrix proteins. Samples were mounted as described in section 2.5.1 either dehydrated, or fully hydrated in deionised water. Figure 4.22 shows typical WAXS diffraction images for dehydrated lamprey annular and piston proteins and the corresponding intensity plots. For all proteins in the dehydrated state the diffraction rings seen in images are isotropic. Results of d-spacings are summarized in Tables 4.18 and 4.19 for cyanogen bromide digests and intact tissues respectively. As determined for elastin, only limited structure was detected as indicated by just two diffuse rings corresponding to d-spacings of 0.46 nm $\pm$ 0.01 and 0.97 nm $\pm$ 0.02 for the annulus and 0.46 nm $\pm$ 0.01 and 0.94 nm $\pm$ 0.02 for the piston. Application of strains in the order of 50% extension had no effect on d-spacings. Likewise, the branchial protein had d-spacings of 0.46 nm $\pm$ 0.01 and 0.94 nm $\pm$ 0.01, whilst the pericardial sac had spacings of 0.46 nm $\pm$ 0.01 and 1.02 nm $\pm$ 0.04 in the relaxed state. These values are comparable to those obtained for dehydrated elastin fibres (see Section 3.4.1). The hydrated proteins showed a spacings at 0.46 nm only.

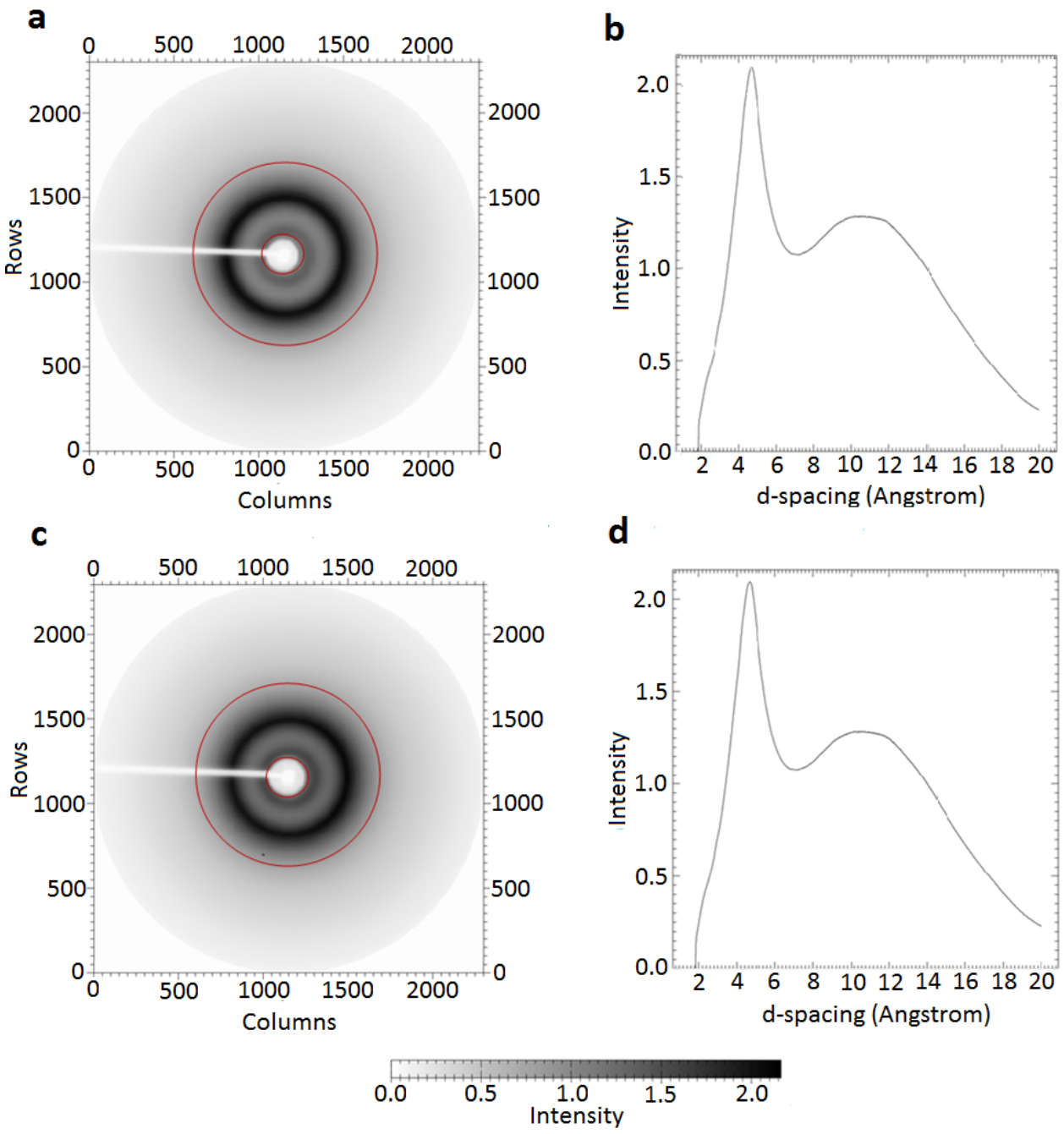

Figure 4.22: Typical WAXS diffraction images and d-spacings for dehydrated (a) annular and (c) piston proteins in the relaxed state. The inner and outer red lines represent d-spacings of 1.14 nm and 0.29 nm respectively. Images (b) and (d) show the WAXS d-spacing peaks for dehydrated annular and piston proteins.

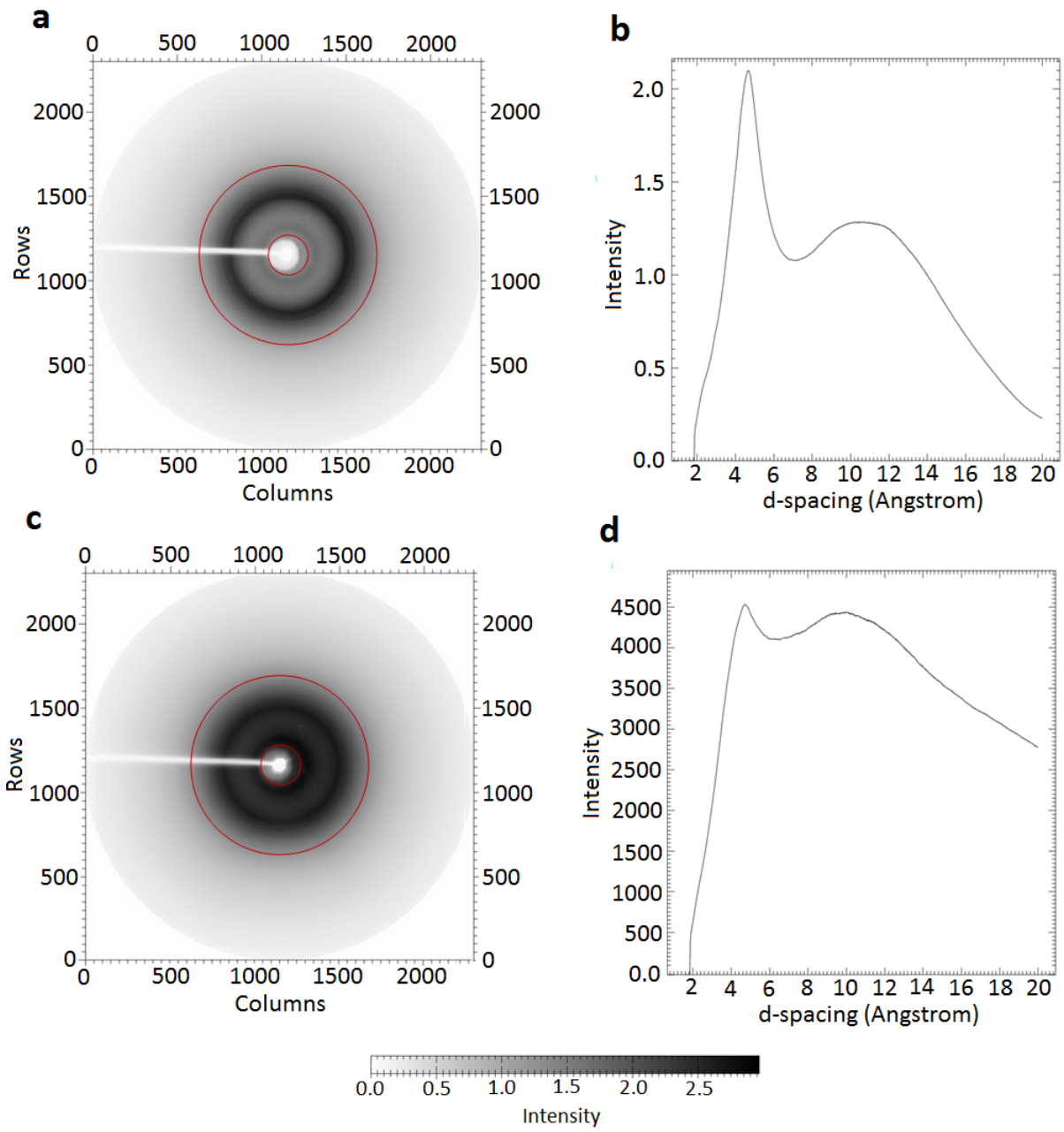

Figure 4.23: Typical WAXS diffraction images and d-spacings for dehydrated (a) branchial and (b) pericardial proteins in the relaxed state. The inner and outer red lines represent d-spacings of 1.14 nm and 0.29 nm respectively. Images (b) and (d) show the WAXS d-spacing peaks for dehydrated branchial and pericardial proteins.

Tissue:		d-spacing (nm), (mean, std dev), (n)	d-spacing (nm), (mean, std dev), (n)
Ligamentum elastin :			
(i)	**Dehydrated / relaxed state**	0.47 ±0.02 (n=4)	0.92 ± 0.02 (n=4)
(i)	**Dehydrated /stretched (≥50%**	0.48 (n=1)	0.94 (n=1)
(ii)	**Hydrated / relaxed state**	0.46 ± 0.01 (n=3)	-
Annular Protein :			
(i)	**Dehydrated / relaxed state**	0.46 ± 0.01 (n=2)	0.97 ± 0.02 (n=2)
(ii)	**Dehydrated / stretched (≥50% strain)**	0.47 ± 0.01 (n=2)	1.00 ± 0.01 (n=2)
(iii)	**Hydrated / relaxed state**	-	-
Piston Protein :			
(i)	**Dehydrated / relaxed state**	0.46 ± 0.01 (n=2)	0.94 ± 0.02 (n=2)
(ii)	**Dehydrated / stretched (≥50% strain)**	0.47 ± 0.01 (n=2)	0.95 ± 0.01 (n=2)
(iii)	**Hydrated / relaxed state**	0.46 ± 0.01 (n=3)	-
Branchial Protein:			
(i)	**Dehydrated / relaxed state**	0.46 ± 0.01 (n=4)	0.94 ± 0.01 (n=4)
(ii)	**Dehydrated / stretched (≥50% strain)**	0.47 (n=1)	0.94 (n=1)
(iii)	**Hydrated / relaxed state**	0.46 ± 0.02 (n=3)	-
Pericardial Protein:			
(i)	**Dehydrated / relaxed state**	0.46 ± 0.01 (n=3)	1.02 ± 0.04(n=3)
(ii)	**Dehydrated / stretched (≥50% strain)**	-	-
(iii)	**Hydrated / relaxed state**	0.46 ± 0.01 (n=2)	-
Kapton		0.53 (n=1)	0.85 (n=1)
Water		0.35 (n=1)	

Table 4.18: d-spacings for purified ligamentum elastin, annular, piston, branchial and pericardial proteins both dehydrated (relaxed and at $\geq$50% extension) and fully hydrated in water. Also given are the d-spacings for kapton and bulk water.

Tissue:		d-spacing (nm), (mean, std dev), (n)	d-spacing (nm), (mean, std dev), (n)
Ligamentum elastin (Undigested) :			
(i)	**Dehydrated / relaxed state**	0.47 ±0.01 (n=2)	0.93 ± 0.01 (n=2)
(i)	**Hydrated / relaxed state**	0.46 ± 0.01 (n=2)	-
Annular Protein (Undigested) :			
(i)	**Dehydrated / relaxed state**	0.47 ± 0.01 (n=4)	1.01 ± 0.05 (n=4)
(ii)	**Hydrated / relaxed state**	0.47 ± 0.01 (n=2)	-
Piston Protein (Undigested) :			
(i)	**Dehydrated / relaxed state**	0.46 ± 0.01 (n=3)	0.99 ± 0.04 (n=3)
(ii)	**Hydrated / relaxed state**	0.46 ± 0.01 (n=3)	-
Pericardial Protein (Undigested) :			
(i)	**Dehydrated / relaxed state**	0.46 (n=1)	1.07 (n=1)
(ii)	**Hydrated / relaxed state**	0.46 (n=1)	-

Table 4.19: d-spacings for undigested ligamentum elastin, annular, piston and pericardial proteins both dehydrated and fully hydrated in water.

4.5.2 Light Microscopy

Intact, undigested lamprey cartilages have in the past been the subject of extensive microscopical investigations [5, 236, 252, 254]. The main observations form these studies included; an avascular cartilage, having a high chondrocyte:ECM ratio, that is surrounded by a dense, richly vascularized perichondrium consisting of collagen fibres and long, thin fibroblasts. The matrix material, composed of randomly arranged, highly branched fibres and matrix granules, is located mainly in thin seams surrounding the chondrocytes.

The purpose of the current histological investigation was to confirm these observations prior to visualizing the same tissues using the novel techniques of multiphoton microscopy, which avoids the need for sample preparation and staining. Figures 4.24, 4.25, and 4.26 show representative images for piston, annular and pericardial cartilages prior to digestion with cyanogen bromide. All images are of 15-20 μm paraffin embedded sections stained with either orcein or Weigert's and Van Gieson stains. Weigert's haematoxylin selectively stains for elastin and has been shown by Wright et al to react similarly with lamprey cartilage [252]. Figures 4.24, 4.25 and 4.26 confirm these earlier observations with matrix material staining positively with Weigert's haematoxylin (red-black) and Van Gieson's staining collagen fibres pink.

No images were obtained for the branchial network because this tissue proved to be remarkably difficult to isolate from the native tissue without digestion.

The piston and annular cartilages could be divided into three distinct regions which can be distinguished by the size and shape of the chondrocytes; the central cartilage forming a 'honeycomb' structure composed of thin seams of matrix material surrounding large, hypertrophied chondrocytes, the subperichondrial cartilage where chondrocytes were slightly smaller and oval in appearance and finally a dense outer perichondrial sheath where cells were considerably smaller and elongated. The thickness of this outer sheath was greatest in the annular cartilage being in the region of 80-120 μm. The lacunae at the centre of the annular and piston cartilages were polygonal in shape and typically 50-60 μm in diameter. In addition, the micrographs show a distinct outer layer (stained pink) situated adjacent to the perichondrial cartilage of the piston and annulus. This layer is the perichondrium, being composed primarily of collagen fibres. Figure 4.26 shows the perichondrium to be particularly thick (approximately 100 μm) on the inner pericardial surface where it surrounds and supports the heart, with collagen fibres being less densely packed compared to the outer pericardial surface (approximately 40 μm thick) which is in contact with the body cavity. Compared to the piston and annulus, the pericardial cartilage is highly cellular having only very thin, irregular seems of matrix material that surround large, irregular chondrocytes. These observations were in good agreement with previous histological observations [11, 236, 245, 252].

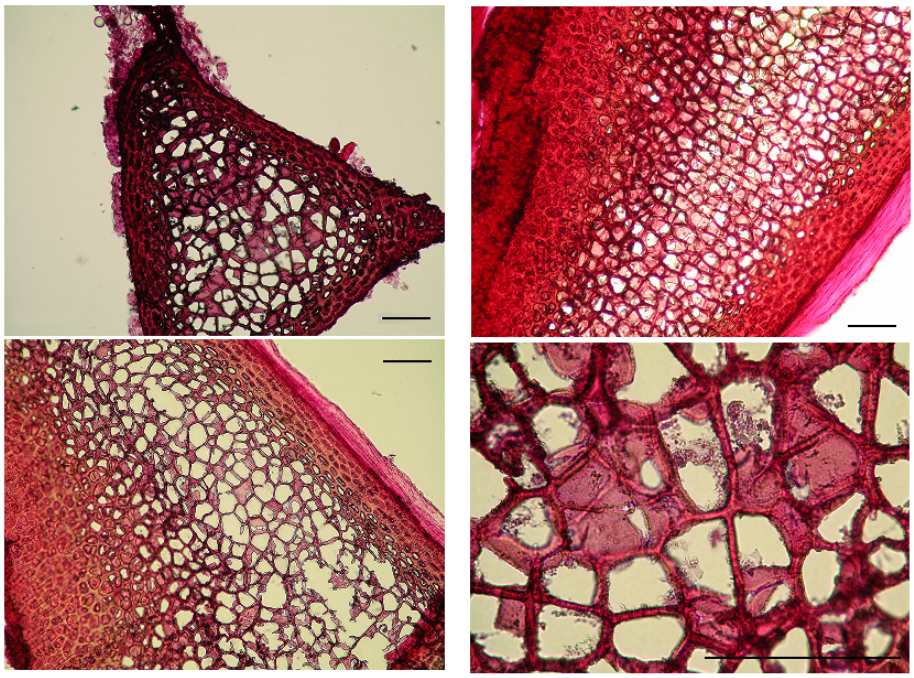

Figure 4.24: Histological sections of the undigested piston cartilage stained with Weigert's (elastin, red-brown) and Van Gieson (for detection of collagen, pink). All sections have been paraffin-embedded and are 15-20μm thick. (a) is cut in transverse section and (b), (c) and (d) cut longitudinally. Scale bar represents 100 μm.

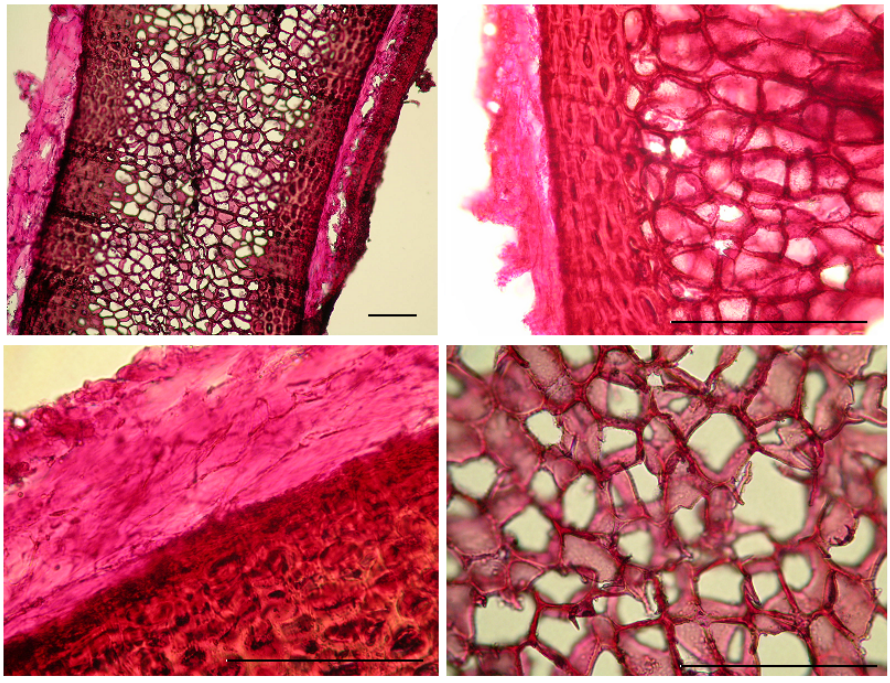

Figure 4.25: Representitive paraffin-embedded histological sections (15-20μm thick) of undigested annular cartilage stained with Weigert's and Van Gieson. In all sections elastin-like material is demonstrated by Weigert's stain and appears red/brown, whilst Van Gieson stains collagen fibres bright pink. Scale bar represents 100 μm.

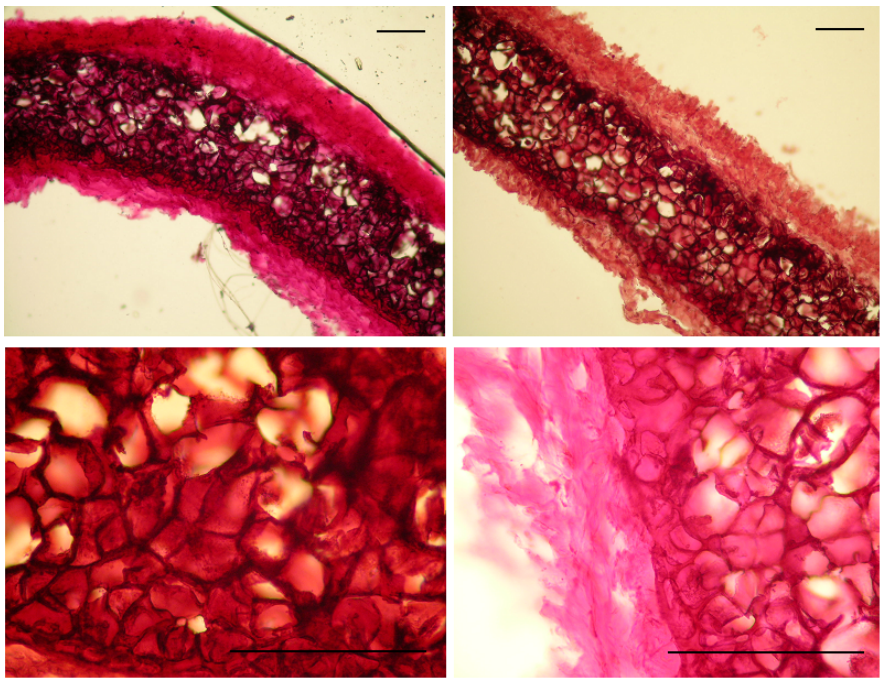

Figure 4.26: Histological sections (15-20μm thick) cut from paraffin-embedded, undigested pericardial sac. (a) and (b) have been stained with Weigert's elastin stain (red/brown) and Van Gieson for detection of collagen (pink), whilst (c) and (d) have been stained with orcein (elastin indicated by brown/black colour). The scale bars represent 100 μm.

4.5.3 Rhodamine Injections/Evans Blue

In this study Evan's blue and rhodamine injections were used with the aim of establishing whether each of the lamprey matrix networks formed open or closed systems. A 1% Evan's blue stain was firstly used and the results of this are illustrated in Figure 4.27 for each of the tissues. The annular and piston networks appear as closed systems, the injectate having failed to spread through the core of the structure but travelling rapidly through the cortex. The branchial and pericardial cartilages were too small to allow injection, but dye added to the bathing solution was allowed to spread through the structure over a period of 2 hours before examination. Figure 4.27 shows diffusion was incomplete over the time period. This observation provided the impetus to perform the same experiment using a less reactive stain. The results are shown in Figure 4.28 These images confirm the existence of a closed network for both the annulus and piston which by forming a water-filled pore structure will restrict the ability of fluid to freely redistribute under strain, but permits diffusion throughout the tissue. These closed systems may also contribute to the slow dynamic responses observed in the annular and piston digests, but whether this is important to the physiological function of these tissues remains uncertain. This was

not the case for branchial and pericardial digests. In these tissues rhodamine was observed to spread throughout the whole tissue over a 2 hour period resulting in an even distribution through to the core, indicating an open systems. Under these conditions fluid would be able to redistribute under strain with little constraint.

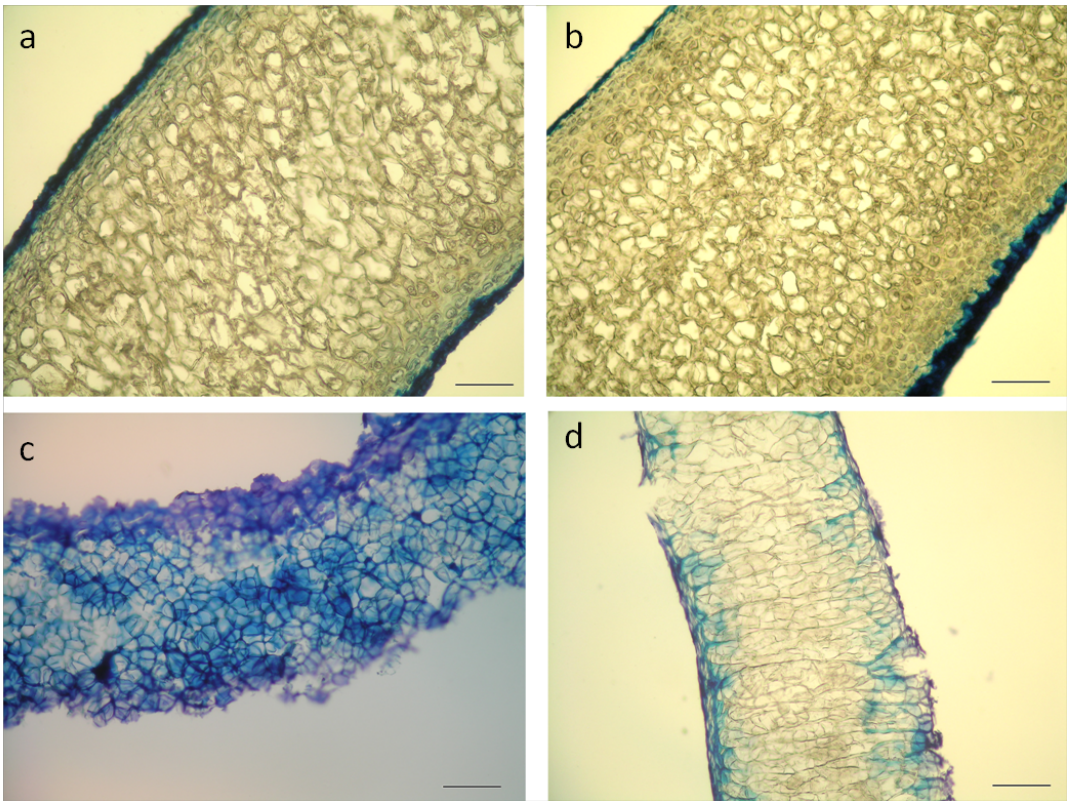

Figure 4.27: Representitive images showing the distribution of 10 µl Evan's Blue stain (1% w/v in phosphate buffered saline) injected into the core of (a) annulus, (b) piston and distribution through (c) branchial cartilage and (d) pericardial sac after bathing in Evan's Blue for a period of 2 hours. All images are of 15-20 μm cryosections cut longitudinally with the exception of the annulus which was cut as a transverse section. The scale bar represents 100μm.

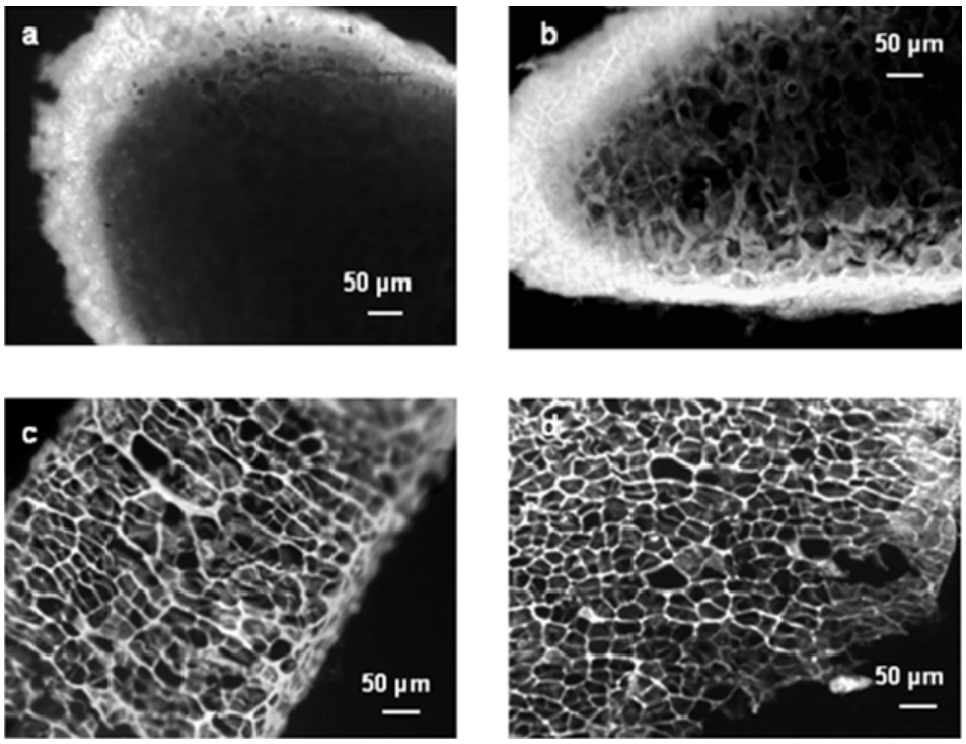

Figure 4.28: Representitive images showing the distribution of 10 µl rhodamine (0.001%) injected into the core of (a) annulus, (b) piston and distribution through (c) branchial cartilage and (d) pericardial sac after bathing in rhodamine solution for a period of 2 hours. The annular and piston cartilages are transverse cryosections (15-20μm) whilst those of the branchial and pericardial cartilages are longitudinal sections.

4.5.4 Autofluorescence

It has long been recognized that elastin exhibits a strong blue/green autofluorescence when irradiated with ultraviolet (UV) light [346]. This property permits detection and visualization of elastin even in composite materials. Other extracellular matrix materials such as collagen also induce autofluorescence. However, the fluorescence is considerably weaker and generally requires the use of high power laser sources for excitation.

Single photon autofluorescence is generated in most proteins by the amino acid residues tryptophan and tyrosine [347]. Tryptophan is absent both in elastin and each of the lamprey matrix proteins, although each of these proteins does have a significant tyrosine content which may account for the autofluorescence we observed in elastin fibres and each of the lamprey matrix proteins investigated. Figures 4.29 and 4.30 are grey scale autofluorescence images of lamprey cartilages transilluminated through a 450-490 nm band pass filter and collected at 510 nm. Figure 4.30 represents autofluorescence from elastin ligamentum fibres taken under the same

conditions as a comparison. The observed autofluorescence from annular, piston and pericardial cartilages, in addition to branchial cartilage, is in disagreement with previous investigations [5], where it was reported that only branchial protein displays UV autofluorescence.

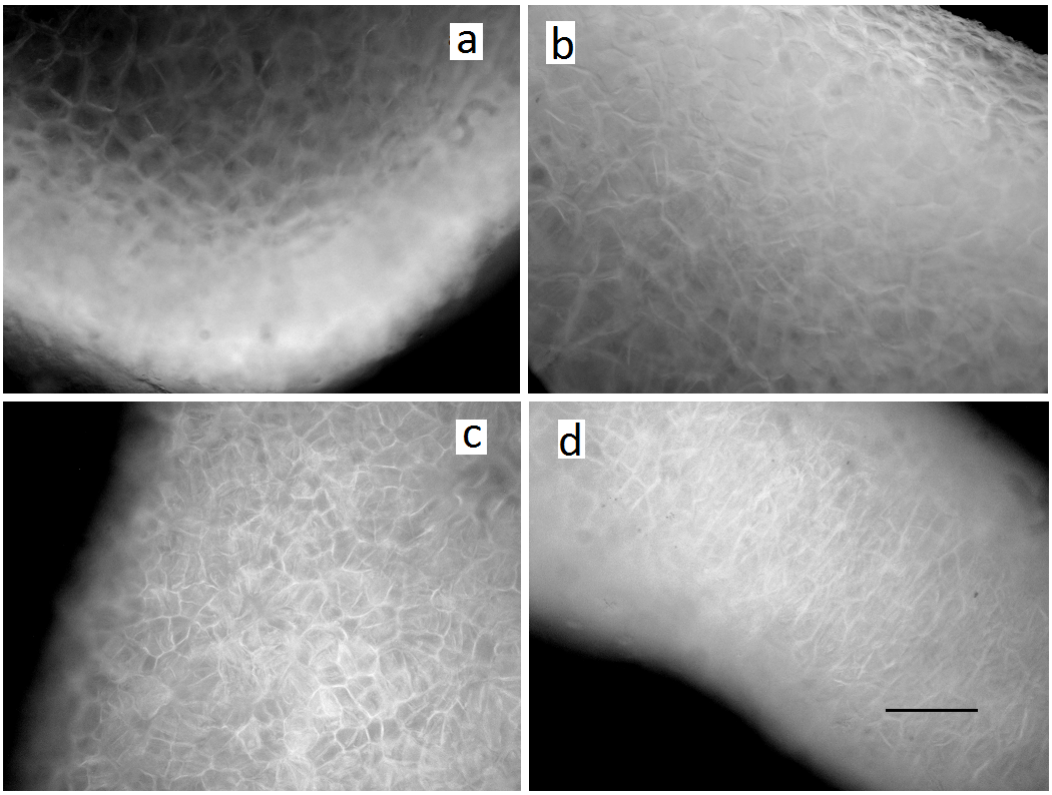

Figure 4.29: Autofluorescence of the residual matrix of a) annular, b) piston, c) branchial and d) pericardial tissue following extraction with cyanogen bromide. Samples were irradiated with light at a wavelength of 515-560 nm. All images were acquired at the same magnification and the scale bar shown in (d) represents 100 μm.

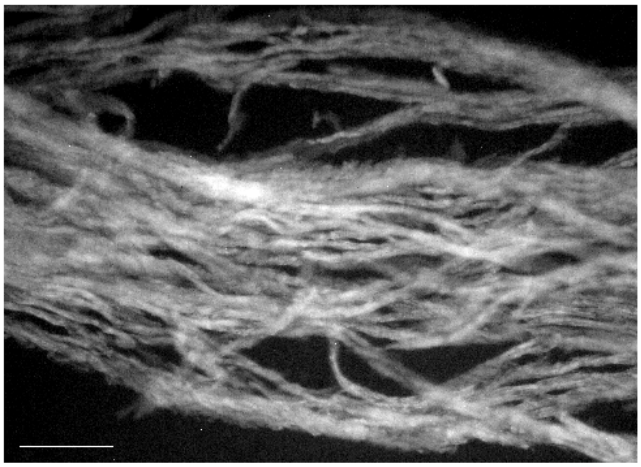

Figure 4.30: Autofluorescence image of ligamentum nuchal elastin fibres irradiated with light at a wavelength of 515-560 nm. Scale bar represents 100μm.

4.5.5 Multiphoton Microscopy

We investigated the morphology of each of the four lamprey matrix proteins both intact and following extraction with cyanogen bromide using the three multiphoton microscopy modalities. Figures 4.31 to 4.33 are representative images of the intact, bulk tissues. In each of the tissues there was a strong intrinsic TPF signal that was very similar to that of elastin, providing a valuable tool for probing matrix architecture. CH bonds could be visualized by CARS, particularly within the central zone of the annular and piston cartilages where hypertrophied chondrocytes are located. The lack of SHG signal from all the cartilages confirmed their non-collagenous nature. Any collagen that was present was confined to the outermost surfaces. These observations are in agreement with previous histological investigations [11].

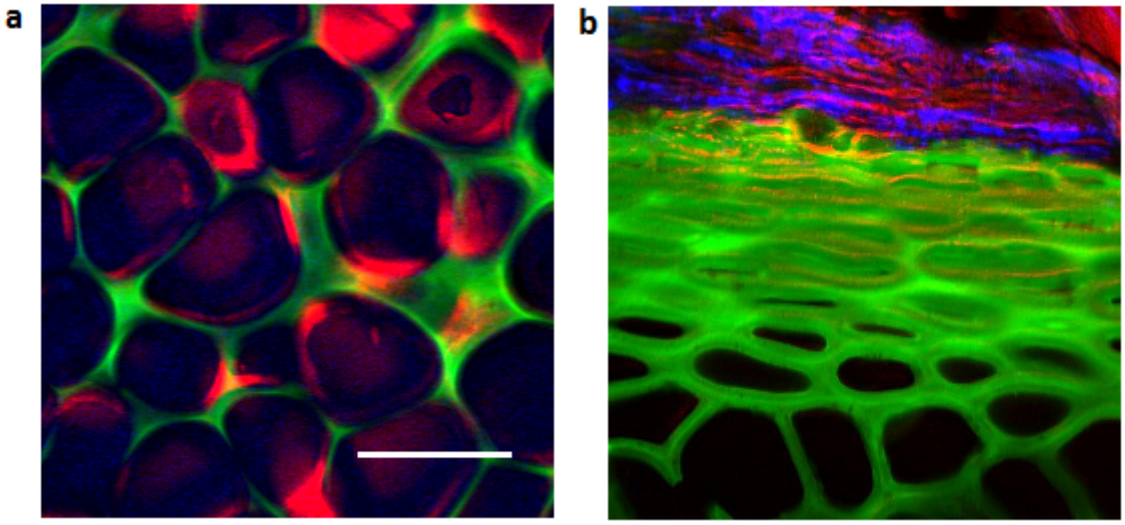

Figure 4.31: Multiphoton images of undigested annular cartilage. Both images are of 20μm thick, transverse sections and the scale bar represents 50 μm. TPF to detect elastin-like tissue is shown in green, SHG for visualization of collagen is blue and CARS for detection of membrane phospholipids is shown in red. Matrix material can be seen to form a dense peripheral zone containing elongated cells and is surrounded by an irregular perichondrium, rich in collagen fibres and lipids. The central zone of the cartilage is a much more open structure filled with cells of varying size.

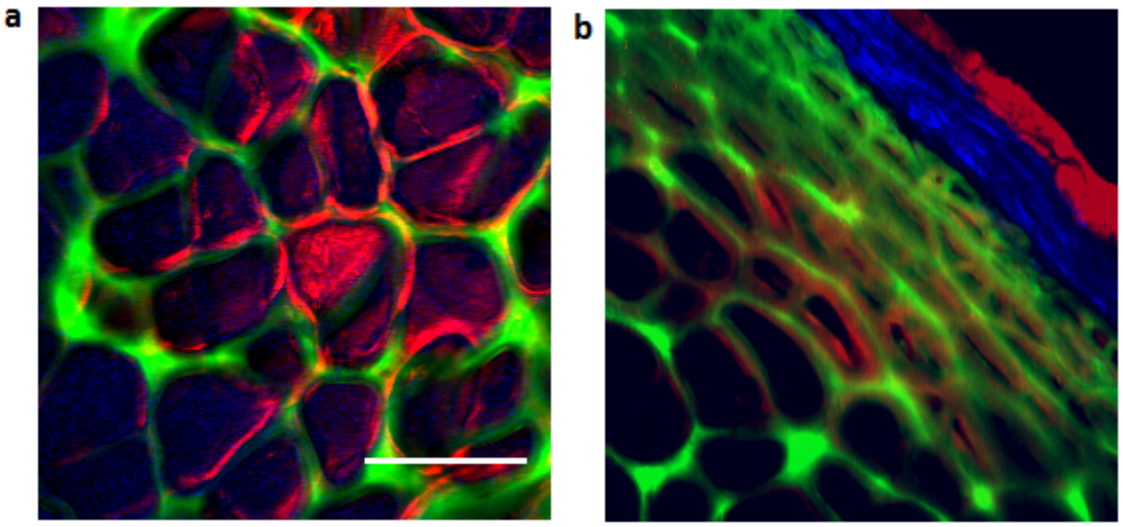

Figure 4.32: Representitive multiphoton images of a 20 μm transverse sections of undigested piston cartilage. TPF is shown in green, SHG in blue and epi CARS in red. The scale bar represents 50 μm. The structure of the piston shows striking similarities to that of the annulus shown in Figure 4.31, with a central core that may be likened to a honeycomb structure, surrounded by a more compact perichondrial zone. A distinct perichondrium composed of 25-80 nm collagen fibres is also apparent at the outermost surface.

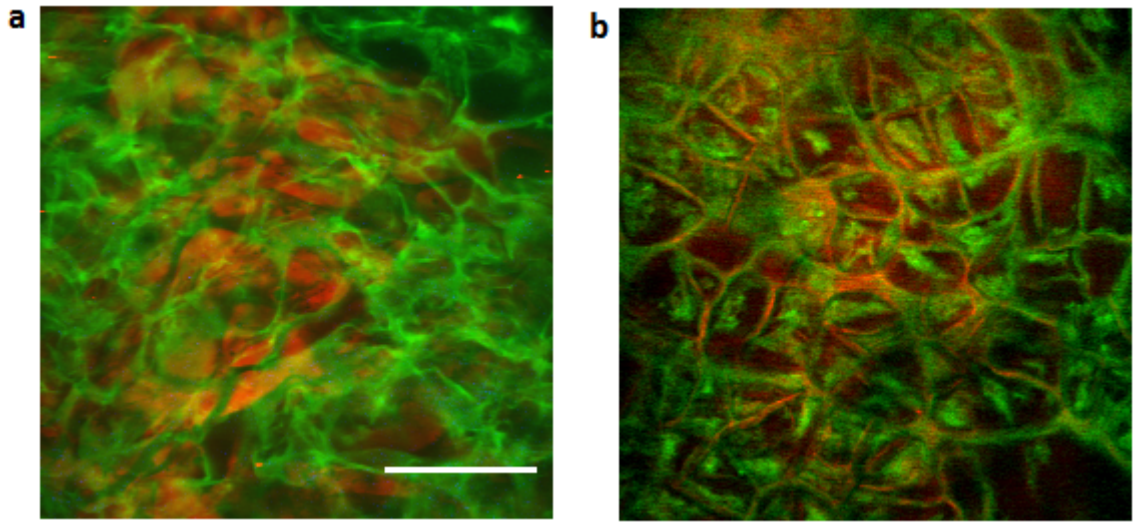

Figure 4.33: Multiphoton images of undigested (a) branchial cartilage and (b) pericardial sac. (Scale bar represents 50 μm). These structures are highly cellular having only thin seams of matrix material (green) surrounding irregular lacunae throughout the tissue which encompass clusters of chondrocytes.

Figures 4.34 to 4.36 show comparative images for matrix material only following digestion with cyanogen bromide which removes collagenous material. The matrix network of the annular and piston structures could be divided into the same three regions as described using conventional histological techniques [236]. The central zone is composed of large lacunae surrounded by seams of matrix material which

become progressively more dense towards the outer perichondrial region and may be likened to the architecture of trabecular bone. The appearance of the branchial and pericardial cartilages differs significantly with no dense matrix material at the outer edges. Instead there is a complex network structure composed of thin seams of matrix protein that surround lacunae of irregular shape and size.

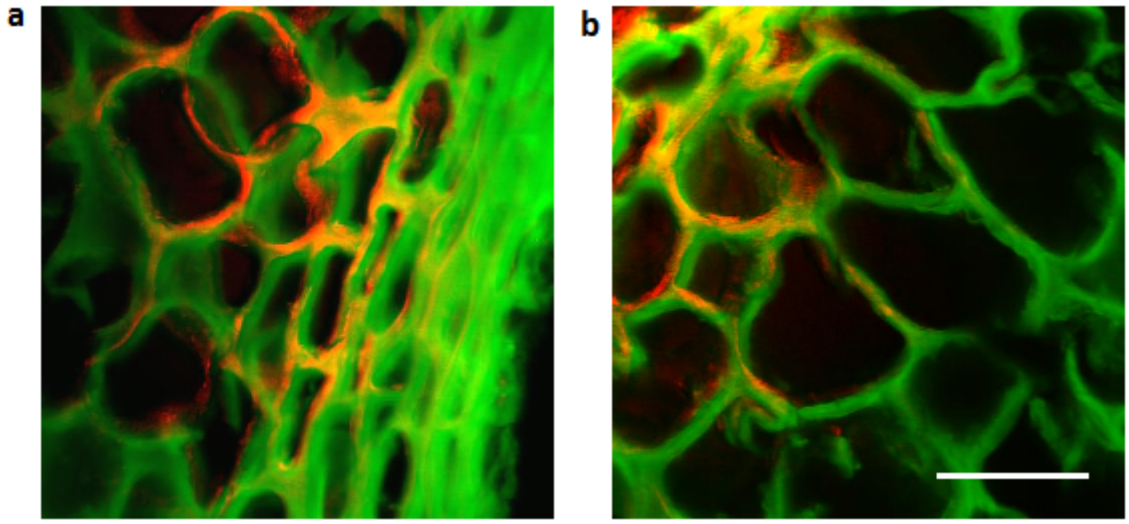

Figure 4.34: Multiphoton images of annular cartilage (20 μm cryo-sections) following extraction with cyanogen bromide to remove collagen fibres. The scale bar represents 50 μm.

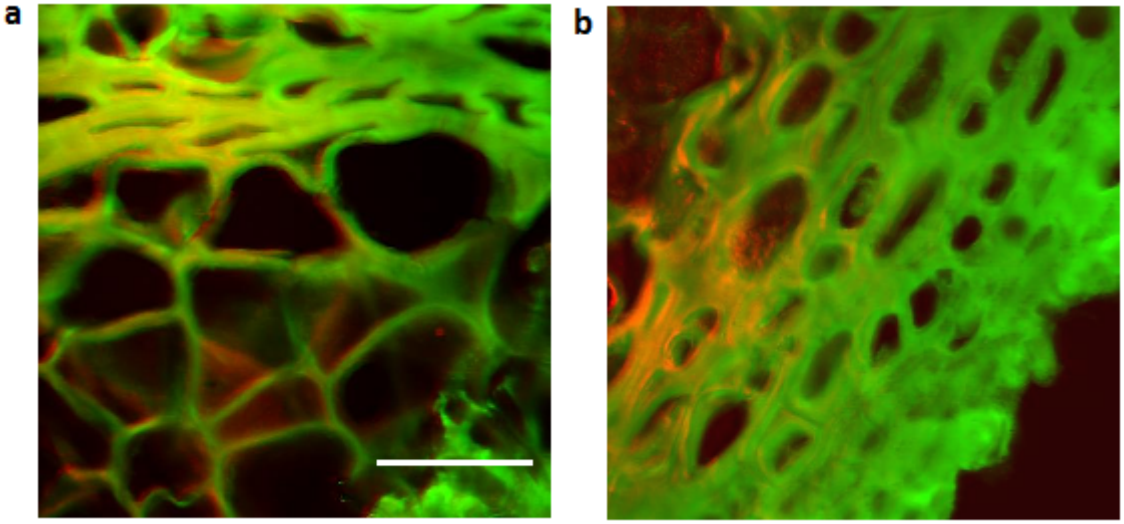

Figure 4.35: Multiphoton images of piston cartilage following extraction with cyanogen bromide. The scale bar represents 50 μm.

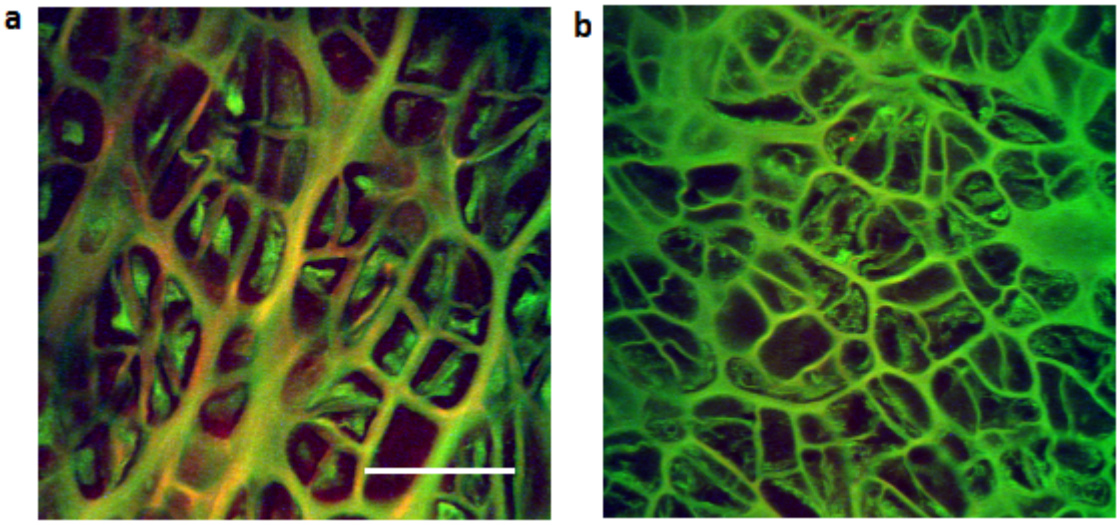

Figure 4.36: Multiphoton images of (a) branchial cartilage and (b) pericardial sac following extraction with cyanogen bromide. The scale bar represents 50 μm.

Two-dimensional TPF images were used to quantify the amount of matrix material relative to voids, which in vivo would have been occupied by chondrocytes. This was done using Image J by converting images to black and white and calculating the number of pixels representing matrix material compared to the number of pixels representing voids, as a percentage of the total area. Only images representing the central core of the cartilages were included in the analysis of matrix material content to avoid any misrepresentation that may be caused by incorporation of the dense outer cortex of annular and piston tissues. Results are summarized in Table 4.20. From this small dataset it can be seen that the two annular and piston cartilages have a higher matrix content (on average 65%) than either the branchial or pericardial cartilages (both 59%).

Sample	Matrix Material (% of total area), (Mean, Std Dev), (n)
Annular cartilage	64.5 ± 9.56 (n=13)
Piston cartilage	64.8 ± 6.71 (n=8)
Branchial cartilage	58.7 ± 6.10 (n=8)
Pericardial cartilage	58.8 ± 8.20 (n=7)

Table 4.20: Calculated amount of matrix material within the central region of each of the cyanogen bromide digested cartilages, expressed as a percentage of the total TPF scan area.

4.5.6 Scanning Electron Microscopy

The scanning electron micrographs in Figures 4.37, 4.38, 4.39 and 4.40 illustrate the complex structural organization of lamprey cartilages and confirm the differences in morphology between the 'hard' piston and annular cartilages and the 'soft', branchial and pericardial cartilages. The SEM images of the outermost surfaces demonstrate the fibrous nature of the matrix material whilst images of the central regions illustrate the variation in size and shape of the lacunae (pores).

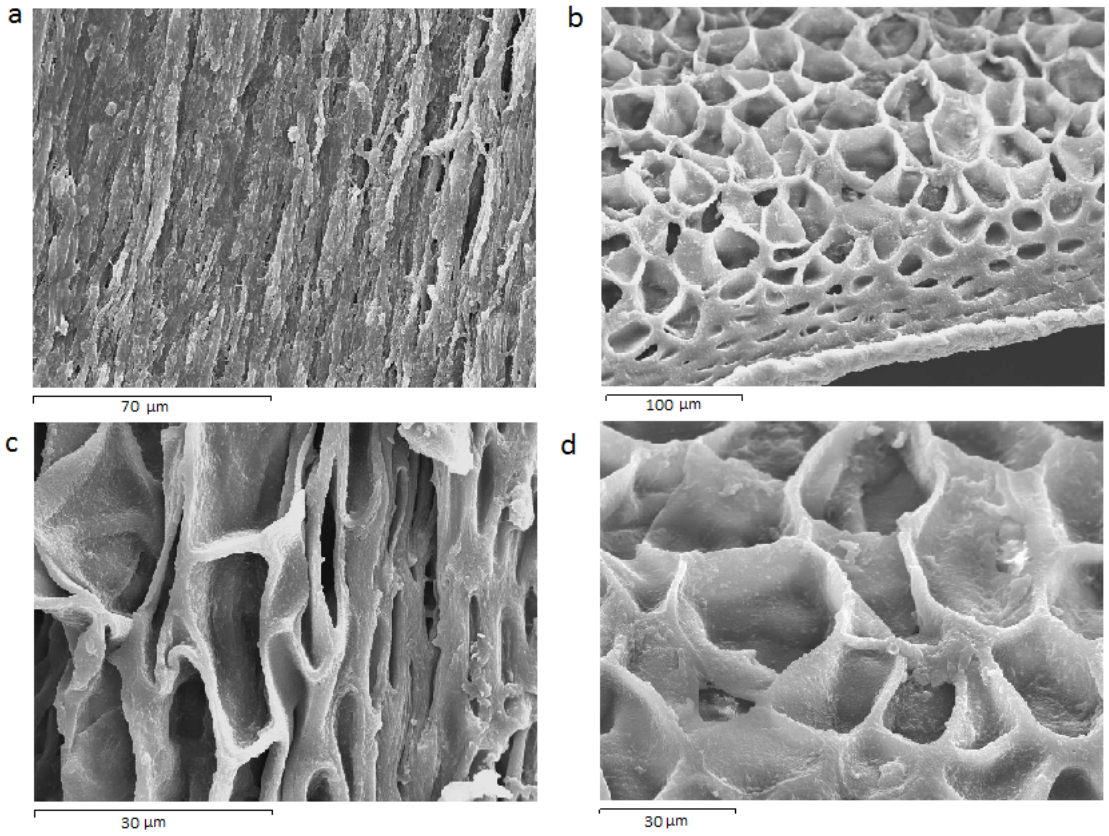

Figure 4.37: Representitive scanning electron micrographs of cyanogen bromide digested annular cartilage. The low magnification image in (a) demonstrates the fibrous arrangement. Transverse sections (b) - (d) show the "honey-comb" arrangement of matrix material in the central region of the cartilage which becomes progressively compact towards the outer surfaces which, in vivo, would be occupied by elongated chondrocytes.

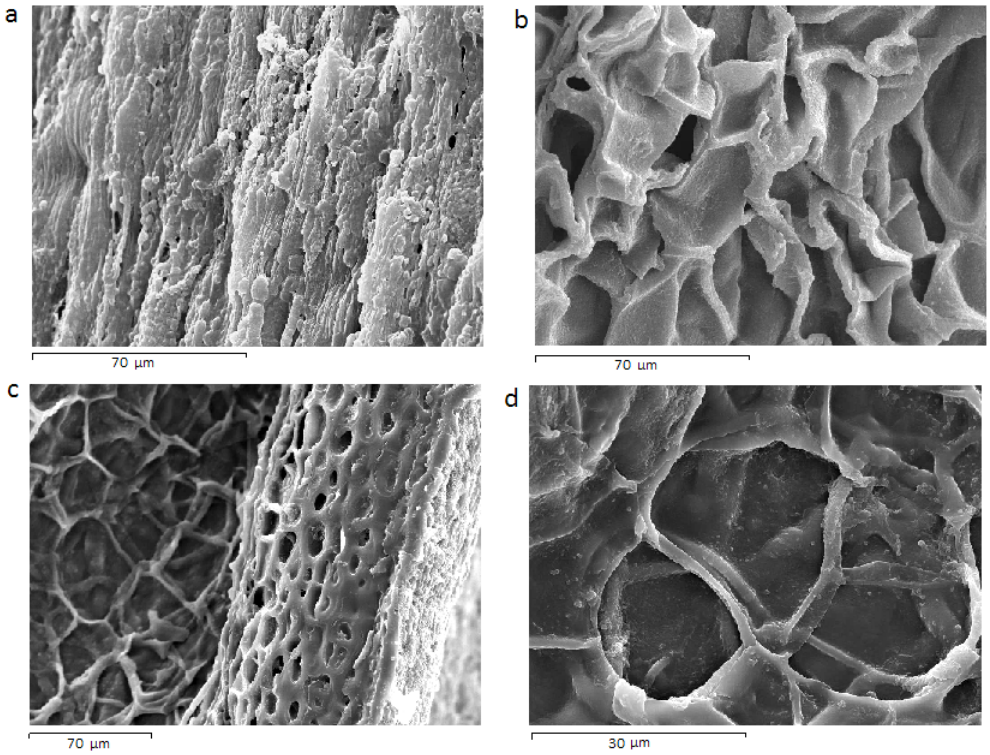

Figure 4.38: Scanning electron micrographs of piston cartilage cut in transverse section. The architecture of the matrix material shows a high degree of similarity to that of the annular cartilage in Figure 4.37 above.

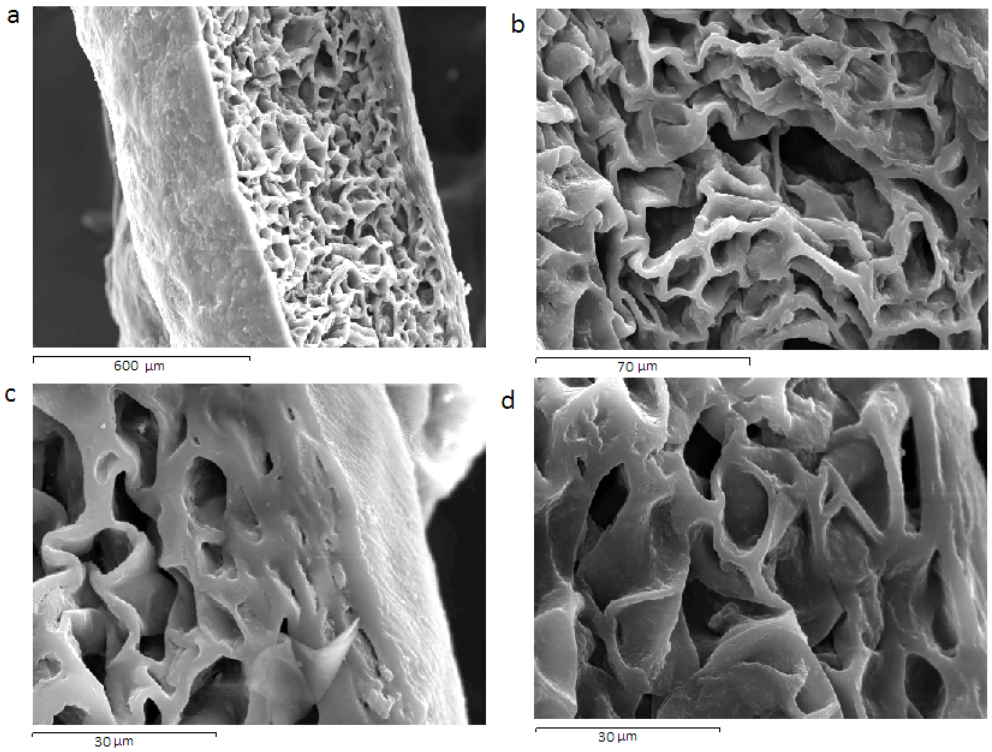

Figure 4.39: Scanning electron micrographs of cyanogen bromide extracted branchial cartilage cut longitudinally. These images show a thin outer shell surrounding an inner core comprising thin seams of matrix material that, prior to digestion, would surround cavities containing chondrocytes. Compared to the annular and piston structures the matrix seams of the branchial cartilage appear less regular in shape.

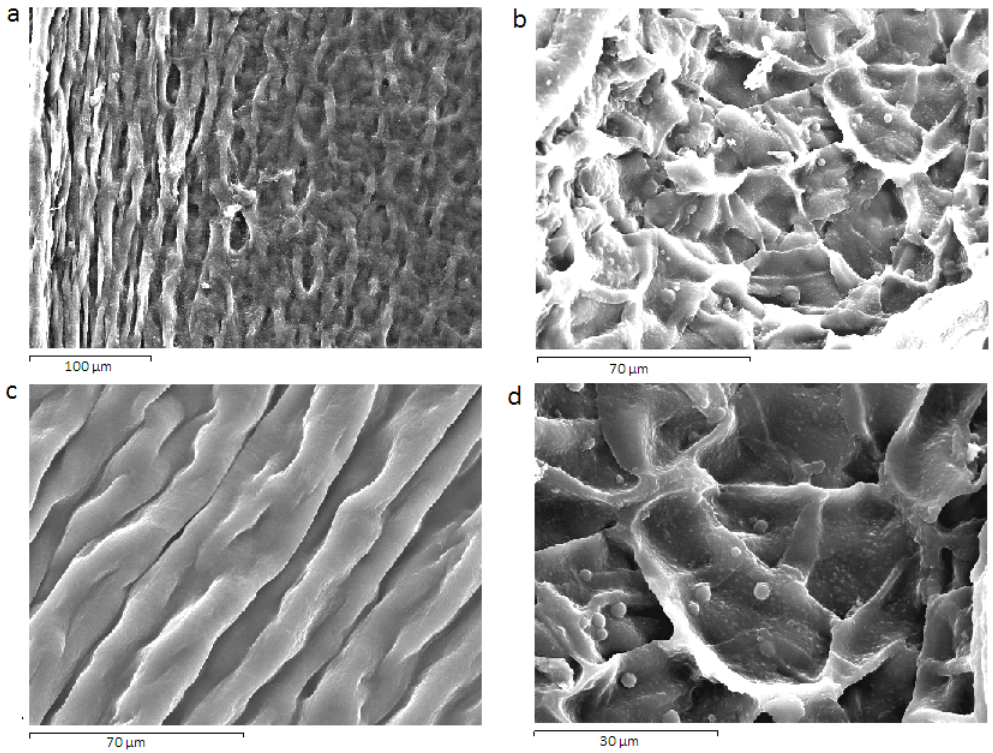

Figure 4.40: Representitive scanning electron micrographs of the pericardial sac. The outer surface as seen in (a) and (c) indicates a fibrous arrangement of matrix material. The arrangement of matrix material within the inner core is similar to that of the other three cartilages. However, the micrographs suggest that seams of matrix that surround cell nests are irregular and less well defined.

4.5.7 Implications for Tissue Mechanics

The architecture observed for the annular and piston cartilages were very similar, comprising of an outer sheath rich in matrix material whilst the central region could be likened to that of a honeycomb structure, with a low ratio of matrix material to lacunae (pores that in vivo would be occupied by chondrocytes). Dye injections indicate that the annular and piston cartilages form closed network structures with water-filled pores. This does not, however, infer that individual cellular compartments are completely sealed as there must be a pathway throughout the tissue to provide necessary nutritional requirements. To this end, we were able to establish that over long time scales (>12 hours), diffusion did occur throughout the tissue. Structural arrangements of this type are likely to result in low hydraulic permeability and restricted fluid redistribution could contribute to long recovery times seen in stress-strain tests. In comparison, the branchial and pericardial cartilages lack a dense outer sheath and have predominantly open networks that are likely to permit free fluid flow throughout the entire tissue, perhaps accounting for their rapid

recovery from deformation.

The open matrix arrangement observed in the branchial and pericardial proteins would offer least resistance to deformation, which would be important in vivo where both these tissues act dynamically, being subjected to repetitive extension and recoil. The annular and piston cartilages, however, act mainly in compression where the the dense outer cortex that surrounds an inner honeycomb structure would provide this structure with both strength and flexibility.

4.6 Discussion and Future Work

This study has demonstrated that the proteins isolated from lamprey cartilages by cyanogen bromide extraction all display long-range elasticity comparable to that of elastin. These tissues also displayed time-dependent (viscoelastic) response to loading. However, the mechanics of these proteins appeared to fall into two distinct types. The 'soft' branchial and pericardial proteins displayed similar mechanical properties to elastin with a linear stress-strain behaviour over a range of strains, though with a lower elastic modulus and smaller hysteresis loss. The 'hard' piston and annular proteins formed a second group, having higher initial and final elastic moduli, higher breaking strains at failure and pronounced hysteresis with a recovery time of hours. In this respect these proteins are intermediate in their mechanical properties between elastin and collagen. It is not clear whether these differences are related to differences at the level of molecular arrangement, as revealed by small differences in their Raman spectra, or alternatively due to macroscopic organization.

Until now, only a single study by Courtland et al [254] has been conducted to investigate the mechanical properties of lamprey cartilage. This study was restricted to young and aged intact annular and pericardial cartilages from which it was concluded that both proteins exhibit a linear stress-strain response over a strain range of approximately 20%, with mean elastic modulus of 0.71 MPa for annular cartilage and a corresponding value of 2.87 MPa for pericardial cartilage, both of which increased with age. Both tissues were found to have a significant water contribution ($\geq$70% wet weight) which gave rise to significant viscoelastic behaviour. Although the current study is in overall agreement with respect to values for water content

and viscoelastic behaviour, our elastic moduli are considerably different, in particular in relation to the pericardial cartilage. This variation is not surprising in the case of pericardial tissue given that in its intact state there is a dense collagenous pericardium.

The 'soft' and 'hard' proteins serve different roles in vivo with the annular and piston cartilages functioning in compression, whereas the branchial and pericardial cartilages function dynamically, being subjected to repeated extension and recoil in a similar manner to elastin. Our results have shown that both the branchial and pericardial proteins are highly extensible and resilient making them particularly well suited to their dynamic roles. The viscoelastic response observed in these tissues may serve to inhibit relaxation during rapid loading/unloading cycles to prevent loss of flexibility [254]. The annular and piston cartilages on the other hand, are stiffer, less resilient and have a large viscoelastic response to deformation. In vivo, the piston is responsible for pushing the tongue into the mouth cavity and for the rasping action of the tongue during feeding, requiring a semi-rigid structure. Similarly, the annulus which supports the mouth parts again requires some rigidity. Increased stiffness is demonstrated by our mechanical testing data whilst it has been suggested that a long viscoelastic response may be associated with reduced fluid flow and low permeability which may provide a method for dissipation of energy over long time scales [254]. The large hysteresis loss associated with these proteins would suggest that they are good energy absorbers, but how this relates to their biological function is less clear. Results from a recent investigation conducted in our lab (Mulligan. R. [unpublished]) have shown that a fifth protein, isolated from the lamprey anterior dorsal plate (nose plate), exhibits very similar mechanical properties in terms of elastic moduli and hysteresis loss to those of the annular and piston proteins. These properties endow the tissue with a combination of strength and elasticity suited to its supportive and protective role in vivo.

Our rhodamine injections have demonstrated for the first time that the branchial and pericardial cartilages form open cell structures, whilst the annulus and piston, at least in the short term, appear to form closed cell structures which may account for some of the variations in their mechanical properties. In vivo, pores of the

honeycomb are filled with chondrocytes whereas in cyanogen bromide digests these are water-filled spaces which will restrict the ability of fluid to freely redistribute under strain in the closed system. These structures may therefore contribute to the slow dynamic responses found in the annular and piston cartilages, but whether this is important to the physiological functions of these tissues is not sure.

Similarities between elastin and the branchial and pericardial proteins extended to their thermomechanical properties with the entropic component of elasticity becoming dominant only at elevated temperatures. A similar response was observed for the annular and piston proteins although they were considerably less thermally stable than the other proteins at temperatures in excess of 30°C. In fact, the annulus and piston may be regarded as better rubber-like elastomers than either elastin or the branchial and piston proteins in the light of the lower temperature for dominance of entropic elasticity. A very similar response was also observed in the nose plate protein although, unlike the annular and piston proteins, complete recovery of mechanical properties was achieved over a long time scale. Further work is now required to establish whether the piston and annular proteins fully recover their original mechanical properties over a similar time scale and if, after further investigation, there turns out to be a real difference in behaviour of the nose plate, then thermomechanical behaviour could be explored further by employing Raman spectroscopy to establish changes in secondary structure associated with increased temperature.

The importance of water interactions with hydrophobic domains on the elastin molecule and their contribution to its mechanical properties have long been recognized. The studies conducted on lamprey matrices parallel those performed on elastin fibres as discussed previously in Chapter 3. To investigate interactions of solvents with lamprey matrix proteins we transferred each of the proteins into deuterium oxide and the non-aqueous solvent, trifluoroethanol (TFE). For elastin and branchial cartilage, transferring to TFE resulted in stiffening of the tissue as well as a substantial increase in hysteresis area, therefore indicating loss of elasticity. The piston showed a very different response with a reduction in both initial modulus and hysteresis loss.

Perhaps the most surprising result was the response of these proteins in deuterium

oxide. Elastin, branchial and pericardial proteins were little affected by deuterium oxide exchange, whereas both the piston and annulus showed both significant stiffening and increase in hysteresis loss that was incompletely recoverable on transferring back to water. The rate of deuterium exchange is dependent on both solvent accessibility and hydrogen bonding such that solvent-exposed amides on the protein surface, hydrogen bonded to water, will exchange rapidly whereas amides buried in the protein core or amides that form intramolecular hydrogen bonds will exchange at a much slower rate [326]. For annular and piston proteins we found that deuterium oxide exerts much of its effect over a short time-course, possibly indicating that solvent-polymer interactions are most greatly affected. Any further effect over a period of $\geq$ 12 hours is likely to be attributable to intramolecular interactions. Our results are in agreement with previously published results for other proteins which indicate loss of flexibility on transferring to deuterium oxide [326] due to an increase in strength of deuterium bonds or an increase in number of intramolecular bonds. The effect of deuterium oxide on polymer-solvent interactions in our elastic proteins needs to be investigated further and one informative experiment would be to employ calorimetric techniques to determine heats of hydration for water and deuterium oxide.

Returning to the question of the mechanism responsible for the differences in mechanics between the proteins, biochemical analysis of the family of lamprey matrix proteins has shown that their amino acid compositions do show some variation which may ultimately be reflected in secondary structure composition, but, equally important, may be the clear variation in architecture as seen using the techniques of light microscopy, electron microscopy and multiphoton microscopy. This is a well-posed problem that requires further investigation. Our multiphoton images of 3-D network structure would be particularly suitable for the development of finite element models, which may shed some light on the relationship between whole tissue structure and their mechanical properties.

Similarity in chemical composition of the 'soft' branchial and pericardial tissues and elastin, as well as the observed similarities in mechanics, suggest that the underlying mechanisms of elasticity are also alike. The annular and piston cartilages

however, show a very different mechanical response, although, over long time scales this may not be true. The biggest difference in stress-strain characteristics of the 'hard' and 'soft' cartilages were in their behavior at low strains and in hysteresis (Figure 4.1). This variation could be explained by differences in supra-molecular organization. However, the different thermomechanical properties and the effect of TFE, suggest differences in the molecular mechanisms of elasticity. Most notably, at high temperatures and on exchange for TFE (Figures 4.3 and 4.9), hysteresis was reduced as was the elastic modulus, suggesting that in these tissues solvent interactions have a large effect. For fibrous elastin we had difficulty in relating the strain applied to the sample to the strains at the molecular level. Given this complication, whether the differences observed in the lamprey matrix proteins on application of strain manifests itself in differences at the molecular level remains to be answered. Until some of these unresolved issues can be clarified, it is difficult to identify a model that reflects the precise mechanisms underlying elasticity in the family of lamprey matrix proteins.

This study is the first to report the secondary structure composition of lamprey matrix proteins as revealed by Raman spectroscopy and analysis of the amide I and amide III bands. It has shown that all the proteins investigated have a similar secondary structure both to each other and to elastin, consisting largely of unordered structures and β-turns / β-sheet, suggesting that they possess the conformational freedom necessary for entropy elasticity. This was emphasized by a previous study by Bochicchio et al [59] who investigated the secondary structure composition of the GGLGY repeat sequence found in lamprin by means of CD, NMR and FT-IR. Our component peaks fitted to the amide I region were in broad agreement, although our attributions showed some differences which are possibly because classical motifs, such as β-sheet and α-helix cannot develop in such short repeat motifs.

For elastin we found that mechanical strain does not lead to any significant change in secondary structure. The most significant effect of application of strain was limited to changes in the orientation of bulky side-chain groups. It is notable that of all the elastic proteins studied in this investigation, the proportion of bulky side-chains was greatest in the less elastic annular and piston proteins which may

impose conformational constraints that inhibit long-range elasticity. However, the complex 3-D structure of the lamprey protein matrices prevented a polarization analysis for these materials.

With respect to the hypothesis that lamprey matrix proteins are evolutionary precursors of elastin, this study suggests that elastin inherits, and exceeds, the mechanical properties of branchial and pericardial cartilages in providing long-range elasticity. The annular and piston cartilages, however, in mechanical terms fall between elastin and collagen, and in some respects display superior mechanical properties. In tissues such as blood vessels and lung, mammals utilize a combination of elastin, to permit high deformations, and collagen, to provide rigidity and strength, in order to meet the desired material properties of the tissue. The question therefore arises as to whether lamprey use a similar combination or whether they use a combination of 'soft' and 'hard' lamprin-based proteins. Brodsky and coworkers have shown that some lamprey tissues do possess collagen (types II, V, XI) [246, 247, 348, 349] and our microscopic observations have confirmed the presence of a limited number of collagen fibres surrounding each of the cartilages, with the pericardial sac being particularly collagen-rich.

An important factor in determining supramolecular organization and fibril-level mechanical properties is cross-linking structure. The large, reversible deformations observed for all the lamprey matrix proteins strongly suggests the requirement for presence of cross-links. However, the only such cross-links that have currently been identified are the lysyl pyridinolines of the branchial cartilage [234], which is one of the more extensible proteins. Further evidence is now required to identify and characterize cross-links of the 'hard' cartilages.

Lamprin has previously been solubilized to reveal two monomers of slightly different molecular weights (10 and 12 kDa) [58]. These are remarkably small for fibrilar matrix proteins, with elastin being in the region of 70 kDa and collagen 300 kDa. These monomers, and in particular the GGLGY repeat sequence, have been shown to self-assemble, but the underlying processes involved are still not fully understood. One suggestion is that these proteins assemble themselves as suggested by the 'lego-like' stacking seen in other proteins. Alternatively, there may be a microfibrillar

skeleton that assists assembly, similar to that proposed for elastin. An important line of future research would involve antibody staining of intact lamprey cartilage to determine whether microfibrillar glycoproteins are present, which would then lend support to the view of microfibrillar-assisted assembly, or alternatively refute this suggestion.

In recent years elastin-based matrices have proved to have many applications in biomedicine and elsewhere serving as elastin replacements where tissue has been damaged through injury or altered/lost through disease. There has also been significant interest in synthesizing peptides based on important elastin amino acid sequences with the intention of replicating its remarkable mechanical properties [118, 269, 270, 350]. Given the range of material properties displayed within the family of lamprey matrix proteins, we suggest that these proteins may form the basis for the development of new, novel biomaterials. These materials may be used in a decellularised form or combined with other elastic proteins to form hybrid biomaterials that can be modified to meet required material properties. Hydrolyzed lamprey matrix proteins could have a number of applications by co-aggregating with other proteins such as collagen or elastin to produce hydrogels, cross-linked films or electrospun fibres with the potential to form 3-D scaffolds with tailored mechanical properties, allowing cell growth and tissue development. Nature itself already uses hybrid materials to meet particular functional requirements. For example, mussel byssal threads which combine flexible elastin-like regions with stiff collagen-like regions. Lamprey matrix proteins would be potentially very attractive as biomaterials if they, like elastin, possess the unusual ability to coacervate on raising the temperature. Biomaterials based on the annular and piston cartilages may also offer the additional benefit of working in compression, providing the opportunity to develop novel compressible elastomers.

Elastic proteins display enormous diversity in location, function and mechanical properties, which ultimately depend on their molecular structure. Elastin and the family of lamprey matrix proteins are no exception. Like many other elastic proteins, they have been shown to display significant structural disorder being dominated by unordered structures with regions of limited order provided by β-turns and β-sheets.

Other elastic proteins, despite sharing little homology in amino acid composition, adopt similar secondary structures within their repeat motifs. For example, the glycine-rich hydrophobic domains of spider silks have been reported to be mainly unordered with some contribution from β-turns and β-spirals [351]. This is true for resilin also, whereas less is known regarding the secondary structure of abductin, although Cao et al predicted the dominance of random coil structures [352]. The molecular structure of these proteins, both in the hydrophobic and cross-linking domains, ultimately determine their mechanical properties. Elastin has an elastic modulus of 0.3-1.0 MPa whilst this study has shown comparative values for lamprey matrix proteins range from 0.1 to 0.75 MPa. Other elastomers that adopt similar secondary structures have very different mechanical properties. For example, the dragline silks produced by spiders are very much stiffer, having an elastic modulus of $1x10^4$ MPa [353], and mussel byssal threads have values of $8.7x10^2$ MPa and 16 MPa at the distal and proximal ends respectively [354]. Other proteins, such as resilin, are much more comparable to the 'soft' lamprey proteins, being highly extensible, with an elastic modulus in the region of 2 MPa [355]. Similarly, there is enormous variation amongst the elastic proteins in terms of their extensibility and resilience. Viscid silks have a maximum extensibility of around 270%, but a low resilience (35%) [353], the byssal thread (distal portion) has an extensibility of 110% and a resilience of only 28% [354], whilst resilin can be extended by 100% its original length with a resilience of 92%. The lamprey matrix proteins investigated in this current study fall into two broad groups, two of which are comparable to elastin and resilin whilst the 'hard' lamprins have properties intermediate between those of elastin and collagen.

Chapter 5

Conclusions

This thesis set out to compare the mechanical properties of lamprey proteins with those of elastin. The relationship between elastin and the family of lamprey matrix proteins is not clear although it has been suggested that lamprin, from the annular and piston cartilages, may be the evolutionary precursor to mammalian elastin [237]. The remarkable mechanical properties of elastin, its other physical properties and molecular composition have been extensively investigated, but much less is known regarding the mechanical properties of lamprin and lamprin-like proteins isolated from lamprey cartilages. One of the principle aims of this thesis was therefore to determine whether, like elastin, long-range elasticity of lamprey matrix proteins arises from entropic and hydrophobic mechanisms. We also investigated secondary structure composition of these proteins, their interactions with water and the effects of mechanical strain using Raman microspectrometry, whilst supramolecular structure was investigated by means of multiphoton microscopy and X-ray diffraction.

Our results for mechanical testing of fibrous elastin are in agreement with those previously reported with mean elastic moduli in the range of 0.2 - 0.4 MPa with entropic mechanisms of elasticity becoming important at high temperatures and a large contribution being made by solvent water. This study has shown that the mechanical properties of branchial and pericardial proteins, which in vivo experience large, cyclic deformations, resemble those of elastin, having similar elastic moduli, breaking strains of approximately 50% and small hysteresis. The annular and piston proteins, which act in compression, exhibited very different behaviour, being much stiffer, having higher breaking strains and pronounced hysteresis with recovery over

several hours, suggesting they sit somewhere between elastin and collagen in terms of their mechanical properties. In respect of their thermomechanical properties, this study has shown that the branchial and pericardial proteins again show striking similarites to elastin, with a decrease in elastic moduli at elevated temperatures where entropic elasticity dominates. The thermomechanical response of the annular and piston proteins was very different. These proteins were much less thermally stable, the reasons for which are unclear. Entropic elasticity was also shown to dominates at lower temperatures, suggesting that the annular and piston proteins may be better rubber-like elastomers than elastin itself.

The importance of solvent interactions was investigated by transferring the proteins to the non-aqueous solvent, TFE, and repeating the mechanical tests. The response of elastin was to become much stiffer, as shown by a doubling of elastic modulus and a large increase in hysteresis area. This comes as no surprise as it is well recognised that the interaction of water with the hydrophobic domains on the elastin molecule make a major contribution to its mechanical properties. The branchial protein showed a very similar response to that of elastin, further highlighting the similarities between these proteins. However, the results for the piston were rather different with a large reduction in the hysteresis loss and incomplete recovery on returning the protein to water, possibly suggesting unfolding of the hydrophobic domains in non-aqueous solvents. In this study we also investigated the effect of deuterium oxide exchange on protein mechanics. The main outcomes from these experiments were that elastin, branchial and pericardial proteins all exhibited a high degree of similarity in their lack of mechanical response to deuterium oxide exchange. The response of the annular and piston proteins was much more complicated with an increase in both the elastic moduli and work required to strain the sample by 20%. On transferring back to water only partial recovery was observed which may be attributed to a preference for the stronger deuterium intramolecular bonds over hydrogen bonds, or alternatively due to an increased number of intramolecular bonds.

There remains considerable debate surrounding the precise mechanisms underlying elastin elasticity with no single structural model providing an unambiguous ex-

planation. Whether elastin adopts random conformation, or whether protein-solvent interactions dominate remains uncertain. The concept of the oiled-coil model is most applicable but, this over simplistic model does not account for the complex protein-solvent interactions that exist. It is likely that the actual mechanisms involved combine elements from each of the models. Given the high degree of similarity between elastin and the 'soft' lamprey proteins, both in chemical composition and mechanics it is likely that elasticity in these proteins is governed by similar molecular mechanisms. The 'hard' lamprey proteins however, display a very different mechanical response, with increased temperature and solvent exchange having a significant impact on their response to strain, therefore suggesting differences in the molecular mechanisms of elasticity involved.

Raman spectroscopy is potentially a very useful tool for determining the unique molecular signature and conformation of elastic proteins under different conditions. Given the complexity and confusions regarding amide band analysis, we first embarked on a comparison of several of the frequently used methods for elastin. Fitting routines involving only a small number of component peaks gave a poor fit to our data and as a result, despite concerns regarding the number of peaks, we decided to use the method of Sane et al [3]. Using this method we were able to detect slight differences between fibrous elastin and each of the lamprey matrix proteins consistent with differences in their amino acid composition, and also between elastin and its fragmentation products. However, Raman spectroscopy was unable to detect a unique signature for either the elastin crosslinks desmosine/isodesmosine, or the pyridinoline crosslinks found in branchial cartilage. For elastin we again were unable to detect any differences associated with the method of preparation. This study has shown that analysis of the amide I, amide III, and water bands is infomative although our predictions of elastin secondary structure differ from those previously reported. Our predictions for the molecular conformation of fibrous elastin are however, in reasonable agreement with previous theoretical predictions. Amide band decomposition revealed only slight differences in secondary structure composition of dehydrated fibrous elastin α-elastin, suggesting that molecular conformation is little affected by fibre formation. Decomposition of the amide I band for each of the

lamprey matrix proteins presented evidence for a very similar secondary structure compositions both with each other and when compared to elastin, being dominated by unordered structures. This agrees with the requirements of a high degree of conformational flexibility for entropy elasticity. The similarities and differences in secondary structure compositions for each of the proteins, under various conditions, are summarized in Tables 5.1 and 5.2. In all the proteins investigated in this study we identified a peak centred at around 1314 cm^{-1} which we tentatively attributed to polyproline II [140] and is regarded as playing an important role in elastin elasticity.

Material	β-turns (%)	Unordered (%)	α-helix (%)
Elastin fibres:			
Hydrated in H_2O (relaxed)	24.4	57.4	18.2
Hydrated in HO (strained by 50%)	24.8	57.0	18.2
Hydrated in D_2O	15.0	63.4	18.1
Dehydrated (from water)	36.6	46.2	17.2
Dehydrated (from TFE)	33.6	48.4	18.1
Heated to 60°C	31.8	51.4	16.9
Aortic elastin:			
Hydrated in H_2O	28.9	54.9	16.2
α-elastin powder	29.4	53.0	17.6
α-elastin in solution	23.4	58.3	18.3
Lamprey cartilages:			
Piston hydrated in HO	29.8	53.7	16.6
Piston hydrated in D_2O	7.4	64.9	27.7
Piston dehydrated (from H_2O)	21.9	57.5	20.7
Piston dehydrated (from TFE)	24.8	56.8	18.5
Piston heated to 60°C	20.9	61.5	17.6
Annular hydrated in H_2O	25.8	55.3	18.8
Annular hydrated in D_2O	1.1	71.2	27.7
Branchial hydrated in H_2O	31.6	52.0	16.4
Branchial hydrated in D_2O	11.0	63.6	25.4
Branchial dehydrated (from H_2O)	16.8	63.9	19.2
Branchial dehydrated (from TFE)	26.6	55.7	17.7
Branchial heated to 60°C	17.4	62.4	20.3
Pericardial hydrated in H_2O	25.5	59.0	15.5
Pericardial hydrated in D_2O	10.6	64.6	24.9

Table 5.1: Summary of results for curve fitting of the amide I band for elastin and each of the lamprey matrix proteins, based on the fitting routine of Sane et al [3]. Values for each of the secondary structures are expressed as a percentage of the total amide I band area.

The effects of solvent interactions on secondary structure were investigated by exchanging water for TFE and deuterium oxide. TFE has previously been reported to induce α-helix formation for a number of proteins in solution which is likely to result in a loss of long-range elasticity. This study has shown that, although this is

Material	β-sheet (%)	Random (%)	α-helix (%)
Elastin fibres:			
Hydrated in H_2O (relaxed)	13.4	53.3	33.3
Hydrated in H_2O (strained by 50%)	13.3	52.6	34.1
Hydrated in D_2O	16.3	42.9	40.8
Dehydrated (from water)	15.1	52.3	32.6
Dehydrated (from TFE)	23.6	49.2	27.3
Heated to 60°C	20.3	51.8	28.0
Aortic elastin:			
Hydrated in H_2O	16.5	54.7	28.9
α-elastin powder	26.8	46.7	26.5
α-elastin in solution	18.9	52.1	29.0
Lamprey cartilages:			
Piston hydrated in HO	24.2	47.3	28.5
Piston hydrated in D_2O	1.40	55.0	43.7
Piston dehydrated from H_2O	20.3	46.6	33.1
Piston dehydrated from TFE	25.2	44.3	30.5
Piston heated to 60°C	17.7	47.0	35.3
Annular hydrated in H_2O	23.7	45.2	31.1
Annular hydrated in D_2O	1.6	61.1	37.3
Branchial hydrated in H_2O	22.3	51.4	26.4
Branchial hydrated in D_2O	0.94	57.3	41.8
Branchial dehydrated from H_2O	21.4	48.6	30.0
Branchial dehydrated from TFE	27.7	46.2	26.1
Branchial heated to 60°C	22.9	46.8	30.4
Pericardial hydrated in H_2O	16.2	54.6	29.3
Pericardial hydrated in D_2O	0.49	53.0	46.6

Table 5.2: Summary of results for curve fitting of the amide III band for elastin and each of the lamprey matrix proteins, based on the method of Williams [12]. Values for β-sheet, unordered structures and α-helix are expressed as a percentage of the total amide I band area.

true for elastin, the opposite is true for the lamprey matrix proteins. We cannot be certain of the reason for this, but it is possible that the supramolecular assembly limits solvent interactions in ways that do not occur in proteins in solution. The effect of deuterium oxide exchange proved to be interesting although the outcome for elastin and the lamprey proteins differed. In all of the proteins there was a slight downward shift in the position of the amide I band. The change in line shape of the amide I band was attributed mainly to a decrease in β-structures, an increase in unordered structures and, in the case of lamprey matrix proteins, an increase in α-helix also. These changes in secondary structure were confirmed by our analysis of the amide III band. The changes in secondary structure in annular and piston cartilage may explain the loss of long-range elasticity observed for these proteins in deuterium oxide, but does not explain the mechanical properties of the other proteins. One concern raised from our Raman analysis was the increase in

contribution made by the 1630 cm^{-1} peak, previously attributed to hydration water, on exchange of water for deuterium oxide.

Again using Raman spectroscopy we investigated in some detail the interaction of water by analysis of the 3600-3100 cm^{-1} region. From these investigations we established that the lamprey proteins, like elastin, show a strong interaction with water. This was especially true for the annular and piston proteins, suggesting a greater role of hydrophobic interactions in their mechanical response compared to the other proteins.

A primary aim of this study was to investigate the effects of mechanical strain on elastic proteins at the molecular level. It was therefore disappointing to find that Raman spectroscopy was unable to detect any significant changes in peak positions or secondary structure compositions associated with applied strain, although this may in part be due to individual elastin fibres within a small bundle experiencing different levels of strain. Despite this, our polarization analysis of the elastin spectrum did show some structural changes with strain. A similar analysis of the lamprey proteins was not possible due to the complex architecture of these matrices.

It is well known that elastin exhibits autofluorescence, a characteristic that has also been detected in the lamprey branchial cartilage. This study has confirmed auto-fluorescence in these two proteins and also presented evidence for autofluorescence in pericardial, annular and piston cartilages, both by conventional light microscopy and two-photon fluorescence.

The complex architecture of the lamprey cartilages has previously been established by light microscopy and electron microscopy. This we confirmed using non-linear microscopy and dye injections to determine the connectivity of the network. The soft branchial and pericardial cartilages were shown to form open systems whilst the hard annular and piston matrices formed closed systems. These characteristics are likely to be important in realtion to their differing roles in vivo.

Supramolecular structure was also investigated by means of X-ray diffraction from which we have shown that, like elastin, the lamprey matrix proteins have limited structural order, corresponding to just two d-spacings of approximately 0.46 and 0.95 nm.

The key findings of this study are that proteins isolated from lamprey cartilages all display long-range elasticity comparable to that of elastin, the principle mammalian elastic protein. However, the annular and piston proteins have a 2-3 fold higher elastic modulus, higher breaking strains and larger hysteresis loss. All the proteins investigated have a strikingly similar secondary structure both to each other and to elastin, indicating that they too have the requisite conformational freedom for entropy elasticity. The mechanical behaviours of all the proteins are strongly influenced by levels of hydration and by hydrophobic interactions. The lamprey cartilages have very complex structures which contribute to their mechanical behaviour. This is further complicated by the existence of a closed structure in the annulus and piston, and an open system in the branchial and pericardial cartilages.

At various points we have located further work that needs to be done on elastin and lamprins. The methods we have employed could also be applied to almost completely unexplored elastic proteins, such as byssal threads, and abductin from the inner hinge ligament of bivalve molluscs.

Bibliography

[1] T.B.; Sandberg L. B. Soskel, N. T.; Wolt. Isolation and characterization of insoluble and soluble elastins. *Methods in Enzymology*, 7:196–, 1902.

[2] N. C. Maiti, M. M. Apetri, M. G. Zagorski, P. R. Carey, and V. E. Anderson. Raman spectroscopic characterization of secondary structure in natively unfolded proteins: alpha-synuclein. *Journal of the American Chemical Society*, 126(8):2399–2408, |2004|.

[3] S. U. Sane, S. M. Cramer, and T. M. Przybycien. A holistic approach to protein secondary structure characterization using amide i band raman spectroscopy. *Anal Biochem*, 269(2):255–72, |1999|. Journal Article.

[4] C. M. Kielty, S. Stephan, M. J. Sherratt, M. Williamson, and C. A. Shuttleworth. Applying elastic fibre biology in vascular tissue engineering. *Philosophical Transactions of the Royal Society B-Biological Sciences*, 362(1484):1293–1312, |2007|. Kielty, Cay M. Stephan, Simon Sherratt, Michael J. Williamson, Matthew Shuttleworth, C. Adrian.

[5] P. Robson, G. M. Wright, J. H. Youson, and F. W. Keeley. A family of non-collagen-based cartilages in the skeleton of the sea lamprey, petromyzon marinus. *Comparative Biochemistry and Physiology B-Biochemistry & Molecular Biology*, 118(1):71–78, |1997|.

[6] M. Berjot, J. Marx, and A. J. Alix. Determination of the secondary structure of proteins from the amide i band: The reference intensity profiles method. *Journal of Raman Spectroscopy*, 18:289–300, 1987.

[7] S. Leikin, V. A. Parsegian, W. H. Yang, and G. E. Walrafen. Raman spectral evidence for hydration forces between collagen triple helices. *Proceedings of the*

National Academy of Sciences of the United States of America, 94(21):11312–11317, |1997|.

[8] R. Ross and P. Bornstein. Elastic fiber.1. separation and partial characterization of its macromolecular components. *Journal of Cell Biology*, 40(2):366–&, |1969|.

[9] M. P. Jacob and L Robert. *Elastin and Elastase*, chapter 4, pages 49–64. CRC Press, Boca Raton, 1989.

[10] L.B. Sandberg and T.B. Wolt. Production and isolation of soluble elastin from copper-deficient swine. *Methods in Enzymology*, 82:657–665, 1982.

[11] G. M. Wright, F. W. Keeley, and J. H. Youson. Lamprin - a new vertebrate protein comprising the major structural protein of adult lamprey cartilage. *Experientia*, 39(5):495–497, |1983|.

[12] R. W. Williams. Protein secondary structure-analysis using raman amide-i and amide-iii spectra. *Methods in Enzymology*, 130:311–331, |1986|.

[13] B. Bochicchio, N. Floquet, A. Pepe, Alix., and A. Tamburro. Dissection of human tropoelastin: Solution structure, dynamics and self-assembly of the exon 5 peptide. *Chemical European Journal*, 10:3166–3176, 2004.

[14] L. Debelle, A. J. P. Alix, S. M. Wei, M. P. Jacob, J. P. Huvenne, M. Berjot, and P. Legrand. The secondary structure and architecture of human elastin. *European Journal of Biochemistry*, 258(2):533–539, |1998|. Article 145DA EUR J BIOCHEM.

[15] L. Debelle, A. J. P. Alix, M. P. Jacob, J. P. Huvenne, M. Berjot, B. Sombret, and P. Legrand. Bovine elastin and kappa-elastin secondary structure determination by optical spectroscopies. *Journal of Biological Chemistry*, 270(44):26099–26103, |1995|. Article TC978 J BIOL CHEM.

[16] W.L. Peticolas. Applications of raman spectroscopy to biological macromolecules. *Biochimie*, 57:417–428, 1975.

[17] J. T. Pelton and L. R. McLean. Spectroscopic methods for analysis of protein secondary structure. *Analytical Biochemistry*, 277(2):167–176, |2000|.

[18] G. Vendantham, H.G. Sparks, S. U. Sane, S. Tzannis, and T.M. Przybycien. A holistic approach for protein secondary structure estimation from infrared spectra in water solutions. *Analytical Biochemistry*, 285:33–49, 2000.

[19] A. Dong, P. Huang, and W.S. Caughey. Protein secondary structure in water from second-derivative amide i infrared spectra. *Biochemistry*, 29:3303–3308, 1990.

[20] A. Barth and C. Zscherp. What vibrations tell us about proteins. *Quarterly Reviews of Biophysics*, 35:369–430, 2002.

[21] B. G. Frushour and J. L. Koenig. Raman scattering of collagen, gelatin, and elastin. *Biopolymers*, 14(2):379–91, |1975|. Journal Article.

[22] H.G.M. Edwards and E.A. Carter. *Infrared and Raman Spectroscopy of Biological Materials*, chapter 11, pages 421–476. Marcel Dekker Inc, 2001.

[23] J. L. Haston, S. B. Engelsen, M. Roessle, J. Clarkson, E. W. Blanch, C. Baldock, C. M. Kielty, and T. J. Wess. Raman microscopy and x-ray diffraction, a combined study of fibrillin-rich microfibrillar elasticity. *Journal of Biological Chemistry*, 278(42):41189–41197, |2003|.

[24] J. M. Gosline. Structure and mechanical-properties of rubber-like proteins in animals. *Rubber Chemistry and Technology*, 60(3):417–438, |1987|.

[25] J. Gosline, M. Lillie, E. Carrington, P. Guerette, C. Ortlepp, and K. Savage. Elastic proteins: biological roles and mechanical properties. *Philosophical Transactions of the Royal Society of London Series B-Biological Sciences*, 357(1418):121–132, |2002|. Article 535NJ PHIL TRANS ROY SOC LONDON B.

[26] R. McNeil Alexander. *Elastic Mechanisms in Animal Movement*. Cambribge University Press, 1988.

[27] F.H. Silver. *Mechanosensing and Mechanochemical Transduction in Extracellular Matrix*, chapter 7, pages 181–198. Springer-Science+Buisness Media, New York, Inc, 2006.

[28] A. S. Tatham and P. R. Shewry. Comparative structures and properties of elastic proteins. *Philosophical Transactions of the Royal Society of London Series B-Biological Sciences*, 357(1418):229–234, |2002|.

[29] CP Winlove and KH Parker. Physiochemical properties of vascular elastin. In DWL Hukins, editor, *Connective Tissue Matrix II*, pages 167–198. Macmillan Press, London, |1990|.

[30] J. E. Scott. Extracellular-matrix, supramolecular organization and shape. In *Symposium on Carbohydrates in Cellular Interactions, at the Winter Meeting of the Anatomical-Society-of-Great-Britain-and-Ireland*, pages 259–269, Southampton, England, |1994|.

[31] W.D. Comper. Water: Dynamic aspects. In WD Comper, editor, *Extracellular Matrix: Molecular Components and Interactions*, volume 2, pages 1–21. Harwood Academic Publishers GmbH, Amsterdam, |1996|.

[32] J.E. Mark and B. Erman. *Rubberlike Elasticity: A Molecular Primer*. Cambridge University Press, Cambridge, 2nd edition, |2007|.

[33] N Boudreau and M.J.Bissell. Regulation of gene expression by the extracellular matrix. In W.D.Comper, editor, *Extracelluar Matrix: Molecular Components and Interactions*, volume 2, pages 246–261. Harwood Academic Publishers, Amsterdam, |1996|.

[34] E. D. Hay. Extracellular-matrix. *Journal of Cell Biology*, 91(3):S205–S223, |1981|.

[35] C. Knupp and J.M. Squire. Molecular packing in network-forming collagens. *The Scientific World Journal*, 3:558–577, 2003.

[36] D.J.S. Hulmes. Building collagen molecules, fibrils, and suprafibrillar structures. *Journal of Structural Biology*, 137:2–10, 2002.

[37] D. R. Eyre, M. A. Paz, and P. M. Gallop. Cross-linking in collagen and elastin. *Annual Review of Biochemistry*, 53:717–748, |1984|.

[38] AJ Bailey. Restraining cross-links in elastomeric proteins. In P. R. Shewry, A. S. Tatham, and A. J. Bailey, editors, *Elastomeric Proteins: Structures,*

Biomechanical Properties and Biological Roles, pages 321–351. Cambridge University Press, Cambridge, |2003|.

[39] A.J. Bailey. Collagen and elastin fibres. *Journal of Clinical Pathology*, 31:49–58, |1978|.

[40] S.L. Carney and H. Muir. The structure and function of cartilage proteioglycans. *Physiological Reviews*, 68:858–910, 1988.

[41] R. Raman, V. Sassisekharan, and R. Sasiseharan. Structural insights into biological roles of protein-glycosaminoglycan interactions. *Chemistry and Biology*, 12:267–277, 2005.

[42] R. Ellis, E. Green, and C. P. Winlove. Structural analysis of glycosaminoglycans and proteoglycans by means of raman microspectrometry. *Connective Tissue Research*, 50(1):29–36, |2009|. Ellis, Richard Green, Ellen Winlove, C. Peter.

[43] A. S. Tatham and P. R. Shewry. Elastomeric proteins: biological roles, structures and mechanisms. *Trends in Biochemical Sciences*, 25(11):567–571, |2000|. Review 373BD TRENDS BIOCHEM SCI.

[44] R McNeil Alexander. Rubber-like properties of the inner hinge-ligament of pectinidae. *J Exp Biol*, 44(1):119–30, |1966|. Journal Article.

[45] M. A. Bowie, J. D. Layes, and M. E. Demont. Damping in the hinge of the scallop placopecten-magellanicus. *Journal of Experimental Biology*, 175:311–315, |1993|.

[46] J. H. Waite, X. X. Qin, and K. J. Coyne. The peculiar collagens of mussel byssus. *Matrix Biology*, 17(2):93–106, |1998|.

[47] J. M. Gosline, M. E. Demont, and M. W. Denny. The structure and properties of spider silk. *Endeavour*, 10(1):37–43, |1986|.

[48] F. Vollrath and D.P. Knight. The nature of some spider silks. In A. S. Tatham, P. R. Shewry, and A. J. Bailey, editors, *Elastomeric Proteins: Structures, Biomechanical Properties and Biological Roles*, pages 152–174. Cambridge University Press, Cambribge, |2003|.

[49] F. Vollrath and D. Porter. Spider silk as archetypal protein elastomer. *Soft Matter*, 2(5):377–385, |2006|.

[50] E. C. Bell and J. M. Gosline. Mechanical design of mussel byssus: Material yield enhances attachment strength. *Journal of Experimental Biology*, 199(4):1005–1017, |1996|.

[51] E. Carrington and J.M. Gosline. Mechanical design of mussel byssus. load cycle and strain rate dependence. *American Malacological Bulletin*, 18:135–142, 2004.

[52] C. A. J. Hoeve and P. J. Flory. Elastic properties of elastin. *Biopolymers*, 13(4):677–686, |1974|.

[53] J. M. Gosline, M. E. Demont, and M. W. Denny. The structure and properties of spider silk. *Endeavour*, 10(1):37–43, |1986|.

[54] B.B. Aaron and J. Gosline. Elastin as a random-network elastomer: A mechanical and optical analysis of single elastin fibers. *Biopolymers*, 20:1247–1262, 1981.

[55] Y.C. Fung. *Biomechanics.Mechanical properties of LivingTissues.* Springer-Science+Buisness Media, New York, Inc, 1993.

[56] L. Debelle and A. M. Tamburro. Elastin: molecular description and function. *International Journal of Biochemistry & Cell Biology*, 31(2):261–272, |1999|. Review 175WR INT J BIOCHEM CELL BIOL.

[57] G. W. G. Chalmers, J. M. Gosline, and M. A. Lillie. The hydrophobicity of vertebrate elastins. *Journal of Experimental Biology*, 202(3):301–314, |1999|. Article 168RL J EXP BIOL.

[58] P. Robson, G. M. Wright, E. Sitarz, A. Maiti, M. Rawat, J. H. Youson, and F. W. Keeley. Characterization of lamprin, an unusual matrix protein from lamprey cartilage - implications for evolution, structure, and assembly of elastin and other fibrillar proteins. *Journal of Biological Chemistry*, 268(2):1440–1447, |1993|.

[59] B. Bochicchio, A. Pepe, and A. M. Tamburro. On (gglgy) synthetic repeating sequences of lamprin and analogous sequences. *Matrix Biology*, 20(4):243–250, |2001|.

[60] S. M.; Mithieux and A. S. Weiss. Elastin. *Advances in Protein Chemistry*, 70:437–461, 2006.

[61] L. D. Muiznieks, A. S. Weiss, and F. W. Keeley. Structural disorder and dynamics of elastin. *Biochemistry and Cell Biology-Biochimie Et Biologie Cellulaire*, 88(2):239–250, |2010|. Muiznieks, Lisa D. Weiss, Anthony S. Keeley, Fred W. 52nd Annual Meeting of the Canadian-Society-of-Biochemistry-Molecular-and-Cellular-Biology JUN 01-05, 2009 Niagara on the Lake, CANADA.

[62] R.P. Mecham and E.C. Davis. Elastic fibre structure and assembly. In *Extracellular Matrix Assembly and Structure*, pages 281–314. |1994|.

[63] B.A.; Kozel, R.P.; Mecham, and J. Rosenbloom. *The extracellular matrix: An overview*. Springer-Science+Buisness Media, New York, Inc, 2011.

[64] R.M. Brissie, S.S. Spicer, and N.T. Thompson. The variable fine structure of elastin visualized with verhoeff's iron haematoxylin. *The Anatomical Record*, 181:83–94, 1975.

[65] J. Weiss. The nature of the reaction between orcein and elastin. *Journal of Histochemistry and Cytochemistry*, 2:21–28, 1954.

[66] J.A. Eurell and B.L. Frappier. *Textbook of Veterinary Histology*. Blackwell Publishing, Oxford, 2006.

[67] A. Pepe and A. Bochicchio, B.and Tamburro. Supramolecular organization of elastin and elastin-related nanostructured biopolymers. *Nanomedicine*, 2:203–218, 2007.

[68] R.C. Cox and K Little. An electron microscopy study of elastic tissue. *Proceedings of the Royal Society of London. Series B, Biological Sciences*, 155:232–242, 1962.

[69] T. K. Greenlee, R. Ross, and J. L. Hartman. Fine structure of elastic fibers. *Journal of Cell Biology*, 30(1):59–&, |1966|.

[70] L Gotte, M Mammi, and G Pezzin. scanning electron microscope observations on elastin. *Connective Tissue Research*, 1:61–67, |1972|.

[71] L Gotte. Recent observations on the structure and composition of elastin. *Advanced experimental medical biology*, 79:105–117, |1977|.

[72] W.J. Cleary, E.G. Cliff. The substructure of elastin. *Experimental and Molecular Pathology*, 28:227–246, 1978.

[73] L. Gotte, D. F. Elsden, S. M. Partridge, and P. Stern. Chemistry of connective tissues .8. composition of elastin from 3 bovine tissues. *Biochemical Journal*, 87(2):344–&, |1963|.

[74] I. P. Ronchetti, A. Alessandrini, M. B. Contri, C. Fornieri, G. Mori, D. Quaglino, and U. Valdre. Study of elastic fiber organization by scanning force microscopy. *Matrix Biology*, 17(1):75–83, |1998|.

[75] L. Gotte, M.G. Giro, D. Volpin, and R.W. Horne. The ultrastructural organization of elastin. *Journal of Ultrastructure Research*, 46:23–33, 1974.

[76] L. Gotte, D. Volpin, R. W. Horne, and M. Mammi. Electron microscopy and optical diffraction of elastin. *Micron*, 7(2):95–102, |1976|.

[77] M. Serafini-Fracassini, A.; Spina. The macromolecular organization of the elastin fibril. *Journal of Molecular Biology*, 100:73–84, 1976.

[78] I. P. Ronchetti, A. Alessandrini, M. B. Contri, C. Fornieri, G. Mori, D. Quaglino, and U. Valdre. Study of elastic fiber organization by scanning force microscopy. *Matrix Biology*, 17(1):75–83, |1998|.

[79] D. Volpin, D. Urry, I. Pasquali-Ronchetti, and L Gotte. Studies by electron microscopy on the structure of coacervates of synthetic polypeptides of tropoelastin. *Micron*, 7:193–198, 1976.

[80] A. Ostuni, B. Bochicchio, M. F. Armentano, F. Bisaccia, and A. M. Tamburro. Molecular and supramolecular structural studies on human tropoelastin sequences. *Biophysical Journal*, 93(10):3640–3651, |2007|. Ostuni, Angela Bochicchio, Brigida Armentano, Maria F. Bisaccia, Faustino Tamburro, Antonio M.

[81] A Kadar. Scanning electron microscopy of purified elastin with and without exnzymic digestion. *Adv Exp Med Biol*, 79:71–95, 1976.

[82] B. A. Cox, B. C. Starcher, and D. W. Urry. Coacervation of tropoelastin results in fiber formation. *Journal of Biological Chemistry*, 249(3):997–998, |1974|.

[83] I.; Fornieri C.; Mattioli F.; Castellani I.; Volpin D. Bressan, G.M.; Pasquali-Ronchetti. Relevance of aggregation properties of tropoelastin to the assembly and structure of elastic fibres. *Journal of Ultrastructure and Molecular Structure Research*, 94:209–216, 1986.

[84] G. Quinterelli, M. Bellocci, and R. Zito. Structural features of insoluble elastin. *Histochemie*, 37(1):49–&, |1973|.

[85] Gotte.L., M. Mammi, and G. Pezzin. Some structural aspects of elastin revealed by x-ray diffraction and other physical methods. *Sympossium on Fibrous Proteins*, pages 236–245, |1968|.

[86] A Serafini-Fracassini. X ray analysis of enzymically purified elastin from bovine ligamentum nuchae. *Advances in Experimental medicine and Biology*, 79:679–683, |1977|.

[87] L. Ali, E. M. Green, R. E. Ellis, D. A. Bradley, J. G. Grossmann, and C. P. Winlove. Study of the molecular and supramolecular organisation of elastic tissue by x-ray diffraction. *Radiation Physics and Chemistry*, 71(3-4):951–952, |2004|.

[88] D.A. Torchia and K.A. Piez. Mobility of elastin chains as determined by 13c nuclear magnetic resonance. *Journal of Molecular Biology*, 76:419–424, 1973.

[89] W.W. Fleming, C.E. Sulivan, and D.A. Torchia. Characterization of molecular motions in 13c- labelled aortic elastin by 13c-1h magnetic double resonance. *Biopolymers*, 19:597–617, 1980.

[90] S. G. Wise and A. S. Weiss. Tropoelastin. *International Journal of Biochemistry & Cell Biology*, 41(3):494–497, |2009|. Wise, Steven G. Weiss, Anthony S.

[91] B. Vrhovski and A. S. Weiss. Biochemistry of tropoelastin. *European Journal of Biochemistry*, 258(1):1–18, |1998|.

[92] S.M. Partridge. Elastin. *Advances in Protein Chemistry*, 17:227–302, 1963.

[93] C. M. Kielty, M. J. Sherratt, and C. A. Shuttleworth. Elastic fibres. *Journal of Cell Science*, 115(14):2817–2828, |2002|.

[94] B. C. Starcher. Elastin and the lung. *Thorax*, 41:577–585, 1986.

[95] R Ross. The elastic fibre. *The Journal of Histochemistry and Cytochemistry*, 21 (3):199–208, 1972.

[96] B. C. Starcher. Lung elastin and matrix. *Chest*, 117:229–234, 2000.

[97] J.E Wagenseil and R.P Mecham. New insights into elastic fiber assembly. *Birth Defects Research*, 81:229–240, |2007|.

[98] C. M. Kielty, T. J. Wess, L. Haston, J. L. Ashworth, M. J. Sherratt, and C. A. Shuttleworth. Fibrillin-rich microfibrils: elastic biopolymers of the extracellular matrix. *Journal of Muscle Research and Cell Motility*, 23(5-6):581–596, |2002|.

[99] I. Sakai, D.R. Keene, R..W. Glanville, and H.P. Bachinger. Purification and partial characterization of fibrillin, a cystene-rich structural component of connective tissue microfibrils. *Journal of Biological Chemistry*, 22:14763–14770, 1991.

[100] D. Ramirez, F.; Rifkin. Extracellular microfibrils: contextual platforms for tgf beta and bmp signalling. *Current Opinion in Cell Biology*, 21:616–622, 2009.

[101] J. Uitto. Biochemistry of elastic fibers in normal connective tissue and its alteration in disease. *Journal of Investigative Dermatology*, 72(1):1–10, |1979|.

[102] C. M. Kielty, C. Baldock, D. Lee, M. J. Rock, J. L. Ashworth, and C. A. Shuttleworth. Fibrillin: from microfibril assembly to biomechanical function. *Philosophical Transactions of the Royal Society of London Series B-Biological Sciences*, 357(1418):207–217, |2002|.

[103] F. Ramirez. Pathophysiology of the microfibril/elastic fiber system: introduction. *Matrix Biology*, 19:455–456, 2000.

[104] E.G. Cleary. *Connective Tissue Disease: Molecular Pathology of the Extracellular Matrix.* Dekker, 1987.

[105] T. J. Wess, P. P. Purslow, and C. M. Kielty. X-ray diffraction studies of fibrillin-rich microfibrils: Effects of tissue extension on axial and lateral packing. *Journal of Structural Biology*, 122(1-2):123–127, |1998|.

[106] M. J. Sherratt, C. Baldock, J. L. Haston, D. F. Holmes, C. J. P. Jones, C. A. Shuttleworth, T. J. Wess, and C. M. Kielty. Fibrillin microfibrils are stiff reinforcing fibres in compliant tissues. *Journal of Molecular Biology*, 332(1):183–193, |2003|.

[107] M. J. Sherratt, T. J. Wess, C. Baldock, J. L. Ashworth, P. P. Purslow, A. Shuttleworth, and C. M. Kielty. Fibrillin-rich microfibrils of the extracellular matrix: ultrastructure and assembly. *Micron*, 32:185–200, 2001.

[108] M.A. Gibson and E.G. Cleary. The immunohistochemical localisation of microfibril-associated glycoprotein (magp) in elastic and non-elastic tissues. *Immunological Cell Biology*, 65:345–356, 1987.

[109] Broekelmann T. Brown-Augsburger, P., L. Mecham, R. Mercer, M.A. Gibson, E.G. Cleary, W.R. Abrams, J. Rosenbloom, and R.P. Mecham. Microfibril-associated gycoprotein bind to the carboxyl-terminal domain of tropoelastin and is a substrate for transglutaminase. *The Journal of Biological Chemistry*, 269:28443–28449, 1994.

[110] M. E. Demont and G. M. Wright. Elastic arteries in a primitive vertebrate - mechanics of the lamprey ventral aorta. *Experientia*, 49(1):43–46, |1993|.

[111] G.M.; DeMont M. E. McConnell, C.J.; Wright. The modulus of elasticity of lobster microfibrils. *Experimentia*, 52:918–921, 1996.

[112] C.J. McConnell, M. E. DeMont, and G. M. Wright. Microfibrils provide non-linear elastic behaviour in the abdominal artery of the lobster homarus americanus. *Journal of Physiology*, 499:513–526, 1997.

[113] F.A. Thurmond and J.A. Trotter. Morphology and biomechanics of the microfibrillar network of sea cucumber dermis. *The Journal of Experimental Biology*, 199:1817–1828, 1996.

[114] M. Spina, A. Friso, A. R. Ewins, K. H. Parker, and C. P. Winlove. Physicochemical properties of arterial elastin and its associated glycoproteins. *Biopolymers*, 49(3):255–265, |1999|. Article 162WX BIOPOLYMERS.

[115] D. M. Wright, V. C. Duance, T. J. Wess, C. M. Kielty, and P. P. Purslow. The supramolecular organisation of fibrillin-rich microfibrils determines the mechanical properties of bovine zonular filaments. *Journal of Experimental Biology*, 202(21):3011–3020, |1999|.

[116] M. J. Sherratt. Tissue elasticity and the ageing elastic fibre. *Age*, 31:305–325, 2009.

[117] N. Sandberg, L. B.; Weissman and D.W. Smith. The purification and partial characterization of a soluble elastin-like protein from copperdeficient porcine aorta. *Biochemistry*, 8:2940–2945, 1969.

[118] W. F. Daamen, J. H. Veerkamp, J. C. M. van Hest, and T. H. van Kuppevelt. Elastin as a biomaterial for tissue engineering. *Biomaterials*, 28(30):4378–4398, |2007|. Daamen, W. F. Veerkamp, J. H. van Hest, J. C. M. van Kuppevelt, T. H.

[119] A. M. Tamburro, V. Guantieri, L. Pandolfo, and A. Scopa. Synthetic fragments and analogs of elastin .2. conformational studies. *Biopolymers*, 29(4-5):855–870, |1990|.

[120] L. Debelle and A. J. P. Alix. The structures of elastins and their function. *Biochimie*, 81(10):981–994, |1999|. Article 256VD BIOCHIMIE.

[121] H.; Sheppard P.; Anderson N.; Rosenbloom J.; Peltonen L.; Rosenbloom J.C. Indik, Z.; Yeh. Alternative splicing of human elastin mrna indicated by sequence analysis of cloned genomic amnd complimentary dna. *Proceedings of National Academy of Science*, 84:5680–5684, 1987.

[122] W. R. Gray, L. B. Sandberg, and J. A. Foster. Molecular model for elastin structure and function. *Nature*, 246(5434):461–6, |1973|. Journal Article.

[123] A. S. Muiznieks, L. D. Weiss. Flexibility in the solution structure of human tropoelastin. *Biochemistry*, 46:8196–8205, 2007.

[124] M.M. Bashir, Z. Indik, H. Yeh, J. Rosenbloom, W. Abraham, M. Fazio, and J. Uitto. Characterization of the complete human elastin gene. *Journal of Biological Chemistry*, 264:8887–8891, 1989.

[125] M.I.S. Chung, M. Miao, R.J. Stahl, E. Chan, J. Parkinson, and F. W. Keeley. Sequence and domain structures of mammalian, avian, amphibian and teleost tropoelastins: Clues to the evolutionary history of elastins. *Matrix Biology*, 25:492–504, 2006.

[126] E. Hirano, R.H. Knutsen, H. Sugitani, C.H. Ciliberto, and R.P. Mecham. Functional rescue of elastin insufficiency in mice by the human elastin gene: Implications for mouse models of human disease. *Journal of the American Heart Association*, 107:523–534, 2007.

[127] Z. Szabo, S. Levi-Minzi, A.M. Christiano, C. Struminger, M. Stoneking, M.A. Batzer, and C.D. Boyd. Sequential loss of two neighbouring exons of the tropoelastin gene during primate evolution. *Journal of Molecular Evolution*, 49:664–671, 1999.

[128] K. K. Kumashiro, J. P. Ho, W. P. Niemczura, and F. W. Keeley. Cooperativity between the hydrophobic and cross-linking domains of elastin. *Journal of Biological Chemistry*, 281(33):23757–23765, |2006|. Kumashiro, Kristin K. Ho, Joanna P. Niemczura, Walter P. Keeley, Fred W.

[129] F. W. Keeley, C. M. Bellingham, and K. A. Woodhouse. Elastin as a self-organizing biomaterial: use of recombinantly expressed human elastin polypeptides as a model for investigations of structure and self-assembly of elastin. *Philosophical Transactions of the Royal Society of London Series B-Biological Sciences*, 357(1418):185–189, |2002|. Article 535NJ PHIL TRANS ROY SOC LONDON B.

[130] L. B. Sandberg, N. T. Soskel, and J. G. Leslie. Elastin structure, biosynthesis, and relation to disease states. *New England Journal of Medicine*, 304(10):566–579, |1981|.

[131] L. B. Sandberg, N. Weissman, and W. R. Gray. Structural features of tropoelastin related to sites of cross-links in aortic elastin. *Biochemistry*, 10(1):52–&, |1971|.

[132] D.A.D. Parry. Structural and functional implications of sequence repeats in fibrous proteins. *Advances in Protein Chemistry*, 70:11–35, 2005.

[133] M. Miao, C. M. Bellingham, R. Stahl, E. Sitarz, C.J. Lane, and F. W. Keeley. Sequence and structure determinants for the self-aggregation of reconmbinant polypeptides modeled after human elastin. *Journal of Biological Chemistry*, 278:48553–48562, 2003.

[134] H. Sage and W. R. Gray. Studies on the evolution of elastin .1. phylogenetic distribution. *Comparative Biochemistry and Physiology B-Biochemistry & Molecular Biology*, 64(4):313–327, |1979|.

[135] A. M. Tamburro, A. Pepe, and B. Bochicchio. Localizing alpha-helices in human tropoelastin: Assembly of the elastin "puzzle". *Biochemistry*, 45(31):9518–9530, |2006|.

[136] D. Urry, M. Long, T. Ohnishi, and M. P. Jacob. Circular dichroism and absorption of the polytetrapeptide of elastin: A polymer model for the beta-turn. *Biochemical and Biophysical Research Communications*, 61:1427–1433, 1974.

[137] A. M. Tamburro, B. Bochicchio, and A. Pepe. The dissection of human tropoelastin: from the molecular structure to the self-assembly to the elasticity mechanism. *Pathologie Biologie*, 53(7):383–389, |2005|.

[138] M. P. Williamson. The structure and function of proline-rich regions in proteins. *Biochemical Journal*, 297:249–260, |1994|. Part 2.

[139] B. Bochicchio and A. M. Tamburro. Polyproline ii structure in proteins:

Identification by chiroptical spectroscopies, stability, and functions. *Chirality*, 14(10):782–792, |2002|.

[140] B. Bochicchio, A. Ait-Ali, A. Tamburro, and A. J. Alix. Spectroscopic evidence revealing polyproline ii structure in hydrophobic, putatively elastomeric sequences encoded by specific exons of human tropoelastin. *Biopolymers*, 73:484–493, 2004.

[141] M. Martino, A. Bavoso, V. Guantieri, A. Coviello, and A. M. Tamburro. On the occurrence of polyproline ii structure in elastin. *Journal of Molecular Structure*, 519:173–189, |2000|.

[142] A.M. Tamburro, B. Bochicchio, and A. Pepe. Dissection of human tropoelastin: Exon-by exon chemical synthesis and related conformational studies. *Biochemistry*, 42:13347–13362, 2003.

[143] B. Vrhovski, S. Jensen, and A. S. Weiss. Coacervation characteristics of recombinant human tropoelastin. *European Journal of Biochemistry*, 250(1):92–98, |1997|.

[144] B. Prescott, V. Renugopalakrishnan, and G. J. Thomas. Raman spectrum and structure of elastin in relation to type ii beta turns. *Biopolymers*, 26:934–936, 1987.

[145] S. Rauscher, S. Baud, M. Miao, F. W. Keeley, and R Pomes. Proline and glycine control protein self-organization into elastomeric or amyloid fibrils. *Structure*, 14:1667–1676, 2006.

[146] A. M. Tamburro, V. Guantieri, D. Dagagordini, and G. Abatangelo. Conformational transitions of alpha-elastin. *Biochimica Et Biophysica Acta*, 492(2):370–376, |1977|.

[147] M Mammi, L Gotte, and G Pezzin. Evidence for order in the structure of alpha-elastin. *Nature*, 220:371–373, 1968.

[148] M Mammi, L Gotte, and G Pezzin. Comparison of soluble and native elastin conformations by far-ultraviolet circular dichroism. *Nature*, 225:379–380, 1970.

[149] N. Floquet, S.H. Here-Huynh, M. Dauchez, A. M. Tamburro, and A. J. Alix. Structural characterization of vgvapg, an elastin-derived peptide. *Biopolymers*, 96:266–280, 2004.

[150] A. Pepe, D. Guerra, B. Bochicchio, D. Quaglino, D. Gheduzzi, V. P. Ronchetti, and A. M. Tarnburro. Dissection of human tropoelastin: Supramolecular organization of polypeptide sequences coded by particular exons. *Matrix Biology*, 24(2):96–109, |2005|.

[151] P. Toonkool, S. A. Jensen, A. L. Maxwell, and A. S. Weiss. Hydrophobic domains of human tropoelastin interact in a context-dependent manner. *Journal of Biological Chemistry*, 276(48):44575–44580, |2001|.

[152] L. D. Toonkool P. Weiss A. S. Mackay, J.P. Muiznieks. The hydrophobic domain 26 of human tropoelastin is unstructured in solution. *Journal of Structural Biology*, 150:154–162, 2005.

[153] M. Miao, J. T. Cirulis, S. Lee, and F. W. Keeley. Structural determinants of cross-linking and hydrophobic domains for self-assembly of elastin-like polypeptides. *Biochemistry*, 44(43):14367–14375, |2005|.

[154] D. F. Partridge S. M. Thomas, J. Elsden. Degredation products from elastin. *Nature*, 200:651–652, 1963.

[155] B.C. Starcher. Determination of the elastin content of tissues by measuring desmosine and isodesmosine. *Analytical Biochemistry*, 79:11–15, 1977.

[156] S.R. Pinnell and G.R. Martin. The cross-linking of collagen and elastin: Enzymic conversion of lysine in peptide linkage to alpha-aminoadipic - semialdehyde (allysine) by an extract from bone. *Proceedings of National Academy of Science*, 61:3778–3782, 1968.

[157] J.A. Foster, L. Rubin, H.M. Kagan, and C. Franzblau. Isolation and characterization of cross-linked peptides from elastin. *Journal of Biological Chemistry*, 19:6191–6196, 1974.

[158] P. Brown-Augsburger, C. Tisdale, T. Broekmann, C. Sloan, and R.P. Mecham.

Identification of an elastin cross-linking domain that joins three peptide chains. *Journal of Biological Chemistry*, 270:17778–17783, 1995.

[159] N.R. Davis and R. Anwar. On the mechanism of formation of desmosine ans isodesmosine cross-links of elastin. *Journal of American Chemical Society*, 92:3778–3783, 1970.

[160] B. C. Starcher, S. M. Partridge, and D. F. Elsden. Isolation and partial characterization of a new amino acid from reduced elastin. *Biochemistry*, 6:2425–2432, 1967.

[161] R.W. Lent, B. Smith, B. Faris, and C. Franzblau. Studies on the reduction of elastin. ii. evidence for the presence of á-aminoadipic ä-semialdehyde and its aldol condensation products. *Biochemistry*, 8:2837–2845, 1969.

[162] S.G.; Wise, S. M.; Mithieux, M.J.; Raftery, and A. S. Weiss. Specificity inthe coacervation of tropoelastin: solvent exposed lysines. *Journal of Structural Biology*, 149:273–281, 2005.

[163] D. W. Urry. Entropic elastic processes in protein mechanisms .1. elastic structure due to an inverse temperature transition and elasticity due to internal chain dynamics. *Journal of Protein Chemistry*, 7(1):1–34, |1988|.

[164] F. W.; Weiss A. S. Yeo, G.C.; Keeley. Coacervation of tropoelastin. *Advances in Colloid and Interface Science*, 2010.

[165] B. C. Urry, D.W.; Starcher. Coacervation of solubilized elastin effects a notable conformational change. *Nature*, 222:795–796, 1969.

[166] S. M. Partridge, H. F. Davis, and G. S. Adair. Chemistry of connective tissues .2. soluble proteins derived from partial hydrolysis of elastin. *Biochemical Journal*, 61(1):11–21, |1955|.

[167] A. W. Clarke, E. C. Arnspang, S. M. Mithieux, E. Korkmaz, F. Braet, and A. S. Weiss. Tropoelastin massively associates during coacervation to form quantized protein spheres. *Biochemistry*, 45(33):9989–9996, |2006|. Clarke, Adam W. Arnspang, Eva C. Mithieux, Suzanne M. Korkmaz, Emine Braet, Filip Weiss, Anthony S.

[168] C. M. Bellingham, M. Lillie, J. Gosline, G.M. Wright, B. C. Starcher, A. Bailey, K. A. Woodhouse, and F. W. Keeley. Recombinant human elastin polypeptides self-assemble into biomaterials with elastin-like properties. *Biopolymers*, 70:445–455, 2003.

[169] I.; Giro M.G.; Volpin D.; Fornieri C.; Pasquali-Ronchetti I. Bressan, G.M.; Castellani. Banded fibres in tropoelastin at physiological temperatures. *Journal of Ultrastructure Research*, 82:335–340, 1983.

[170] C.M. Bellingham, K. A. Woodhouse, P. Robson, S.J. Rothstein, and F. W. Keeley. Self-aggregation characteristics of recombinantly expressed human elastin polypeptides. *Biochim Biophys Acta*, 1550:6–19, 2001.

[171] A. Pepe, R. Flamia, D. Guerra, D. Quaglino, B. Bochicchio, V. P. Ronchetti, and A. M. Tamburro. Exon 26-coded polypeptide: An isolated hydrophobic domain of human tropoelastin able to self-assemble in vitro. *Matrix Biology*, 27(5):441–450, |2008|. Pepe, Antonietta Flamia, Roberta Guerra, Deanna Quaglino, Daniela Bochicchio, Brigida Ronchetti, Vonne Pasquali Tamburro, Antonio M.

[172] A. M Tamburro, A. Pepe, B. Bochicchio, D. Quaglino, and I. P. Ronchetti. Supramolecular amyloid-like assembly of the polypeptide sequence coded by exon 30 of human tropoelastin. *The Journal of Biological Chemistry*, 280:2682–2690, 2005.

[173] D. Volpin, D.W. Urry, B. A. Cox, and L Gotte. Optical diffraction of tropoelastin and alpha-elastin coacervates. *Biochim Biophys Acta*, 439:253–258, 1976.

[174] D.W. Urry, M. Long, T. Ohnishi, L.W. Mitchell, and M. Jacobs. The synthetic polypentapeptide of elastin coacervates and forms filamentous aggregates. *Biochimica Et Biophysica Acta*, 371:597–602, 1974.

[175] D. Urry and M.M. Long. Conformations of the repeat peptides of elastin in solution: An application of proton and carbon-13 magnetic resonance and determination of polypeptide secondary structure. *Critical Reviews in Biochemistry and Molecular Biology*, 4:1–45, 1976.

[176] J.M. Gosline and J. Rosenbloom. *Extracellular Matrix Biochemistry.* Elsevier Science Publishing, 1984.

[177] J. Rosenbloom. *Connective Tissue and it's Herritable Disorders. Molecular, Genetis and Medical Aspects.* Wiley-Liss, Inc.New York, 1983.

[178] B.A.; Kozel, B.J.; Rongish, A.; Czirok, J.; Zach, C.D.; Little, E.C.; Davis, R.H.; Knutsen, J.E.; Wagenseil, M.A.; Levy, and R.P. Mecham. Elastic fiber formation: A dynamic view of extracellular matrix assembly using timer reporters. *Journal of Cellular Physiology*, 207:87–96, 2006.

[179] M. Gacko. Elastin: structure,properties and metabolism. *Cell and Molecular Biology Letters*, 5:327–348, 2000.

[180] M. Moczar, L. Labat-Robert, and L. Robert. *Elastin and Elastases.* CRC Press Inc, 1989.

[181] D.W. Urry. On the molecular mechanisms of elastin coacervation and coacervate calcification. *Faraday Discussions*, pages 205–213, 1975.

[182] L. D. Muiznieks, S. A. Jensen, and A. S. Weiss. Structural changes and facilitated association of tropoelastin. *Archives of Biochemistry and Biophysics*, 410(2):317–323, |2003|.

[183] Q. Xu and T.A. Keiderling. Trifluoroethanol-induced unfolding of concanavalin-a: Equilibrium and time-resolved optical spectroscopic studies. *Biochemistry*, 44:7976–7987, 2005.

[184] E. Scoffone, A.M. Tamburro, A. Scatturn, R. Rocchi, F. Marchiori, and G.; Borin. Conformational transitions of bovine pancreatic ribonucleases-peptide. *FEBS Letters*, 1(Anderson, N.;):298–300, 1968.

[185] J. M. Gosline. Hydrophobic interaction and a model for the elasticity of elastin. *Biopolymers*, 17(3):677–95, |1978|. Journal Article.

[186] A Kadar. *Elastin and Elastases.* CRC Press Inc, 1989.

[187] M. A. Lillie and J. M. Gosline. The effects of hydration on the dynamic mechanical-properties of elastin. *Biopolymers*, 29(8-9):1147–1160, |1990|.

[188] V. Samouillan, C. Andre, J. Dandurand, and C. Lacabanne. Effect of water on the molecular mobility of elastin. *Biomacromolecules*, 5(3):958–964, |2004|.

[189] M. A. Lillie and J. M. Gosline. The effects of polar solutes on the viscoelastic behaviour of elastin. In *8th International Congress of Biorheology*, pages 229–242, Yokohama City, Japan, |1992|.

[190] J. M. Gosline. Dynamic mechanical-properties of elastin. *Biorheology*, 15(5-6):485–485, |1978|.

[191] J. M. Gosline. The temperature-dependent swelling of elastin. *Biopolymers*, 17(3):697–707, |1978|. Journal Article.

[192] M. A. Lillie, G. J. David, and J. M. Gosline. Mechanical role of elastin-associated microfibrils in pig aortic elastic tissue. *Connective Tissue Research*, 37(1-2):121–141, |1998|. Article ZN773 CONNECT TISSUE RES.

[193] J.M. Aaron, B.B.; Gosline. Optical properties of single elastin fibres indicate random protein conformation. *Nature*, 287:865–867, 1980.

[194] Y.C. Fung. Biorheology of soft tissues. *Biorheology*, 10:139–55, 1973.

[195] C. Baldock, A.F. Oberhauser, L. Ma, D. Lammie, V. Siegler, S.M. Mithieux, Y. Tu, J.Y.H. Chow, M. Malfois, S. Rogers, L. Guo, T.C. Irving, T.J. Wess, and A.S. Weiss. Shape of tropoelastin, the highly extensible protein that controls human tissue elasticity. *Proceedings of National Academy of Science*, 108:4322–4327, 2011.

[196] J. Gosline. The physical properties of elastic tissue. *International Review of Connective Tissue Research*, 7:211–249, 1976.

[197] K.H. Meyer, G. von Susich, and E. Valko. The elastic properties of organic high polymers and their kinetic explanation. *Kolloid-Zeitschrift*, 59:208, 1932.

[198] P.J. Flory. Molecular theory of rubber elasticity. *Polymer*, 20:1317–1320, 1979.

[199] L.R.G. Treloar. *The Physics of Rubber Elasticity.* Clarendon Press; Oxford, 1975.

[200] K. L. Dorrington and N. G. McCrum. Elastin as a rubber. *Biopolymers*, 16(6):1201–1222, |1977|.

[201] A.L. Andrady and J.E. Mark. Thermoelasticity of swollen elastin networks at constant composition. *Biopolymers*, 19:849–855, 1980.

[202] E.Y.; Wittebort R.J. Pometum, M.S.; Chekmenev. Quantitative observation of backbone disorder in native elastin. *The Journal of Biological Chemistry*, 279:7982–7987, 2004.

[203] Rubin L.; Imberman M.; Kagan H.; Mecham R.; Franzblau C. Foster, J.A.; Bruenger. Circular dichroism studies of an elastin crosslinked peptide. *Biopolymers*, 15:833–841, 1976.

[204] L. Debelle, S. M. Wei, M. P. Jacob, W. Hornebeck, and A. J. P. Alix. Predictions of the secondary structure and antigenicity of human and bovine elastins. *European Biophysics Journal with Biophysics Letters*, 21(5):321–329, |1992|.

[205] D. W. Urry. Protein elasticity based on conformations of sequential polypeptides-the biological elastic fiber. *Journal of Protein Chemistry*, 3(5-6):403–436, |1984|.

[206] B. Li and V. Daggett. Molecular basis for the extensibility of elastin. *Journal of Muscle Research and Cell Motility*, 23(5-6):561–573, |2002|.

[207] T. Weisfogh and S. O. Andersen. New molecular model for long-range elasticity of elastin. *Nature*, 227(5259):718–&, |1970|.

[208] D.W. Urry. Characterization of soluble peptides of elastin by physical techniques. *Methods in Enzymology*, 82:673–716, 1982.

[209] B. Li, D. O. V. Alonso, and V. Daggett. The molecular basis for the inverse temperature transition of elastin. *Journal of Molecular Biology*, 305(3):581–592, |2001|.

[210] L. Partridge and D. Gems. Mechanisms of ageing: Public or private? *Nature Reviews Genetics*, 3:165–175, 2002.

[211] J. Vijg and J Campisi. Puzzles, promises and a cure for ageing. *Nature*, 454:1065–1071, 2008.

[212] L. Robert, A.M. Robert, and T Fiulop. Rapid increase in human life expectancy: will it soon be limited by the ageing of elastin? *Biogerontology*, 9:119–133, 2008.

[213] J. Uitto, M. Fazio, and D.R. Olsen. Molecular mechanisms of cutaneous aging. *Journal of the American Academy of Dermatology*, 21:614–622, 1989.

[214] D.R. Sell and V.M. Monnier. Molecular basis of arterial stiffening: Role of glycation-a mini review. *Gerontology*, 58:227–237, 2012.

[215] A.J. Bailey. Molecular mechanisms of ageing in connective tissues. *Mechanisms of Ageing and Development*, 122:735–755, 2001.

[216] C.P. Winlove, K.H. Parker, N.C. Avery, and A.J. Bailey. Interactions of elastin and aorta with sugars in vitro an their effects on biochemical and physical properties. *Diabetologia*, 39:1131–1139, 1996.

[217] L. Robert, A.M. Robert, and T Fiulop. Rapid increase in human life expectancy: willit soon be limited by the ageing of elastin? *Biogerontology*, 9:119–133, 2008.

[218] W. Hornebeck and S. M. Partridge. Conformational-changes in fibrous elastin due to calcium-ions. *European Journal of Biochemistry*, 51(1):73–78, |1975|.

[219] R.B. Rucker and K. Tom. Arterial elastin. *The American Journal of Clinical Nutrition*, 29:1021–1034, 1976.

[220] D. M. Milewicz, Z. Urban, and C. Boyd. Genetic disorders of the elastic fiber system. *Matrix Biology*, 19(6):471–480, |2000|.

[221] J Uitto. *Biochemistry of Disease*, volume 12 of *Connective Tissue Disease: Molecular Pathology of the Extracellular Matrix.* Marcel Dekker Inc, New York, |1987|.

[222] L. Rodriguez-Revenga, P. Iranzo, C. Badenas, S. Puig, A. Carrio, and M. Mila. A novel elastin gene mutation resulting in an autosomal dominant form of cutis laxa. *Archives of Dermatology*, 140:1135–1139, 2004.

[223] A.M. Tassabhji, M. Metcalfe, J. Hutst, C. M. Kielty, D. Wilmot, C. Donnai, A.P. Read, and C.J. Jones. An elastin gene mutation producing abnormal tropoelastin and abnormal elastic fibres in a patient with autosomal dominant cutis laxa. *Human Molecular Genetics*, 7:1021–1028, 1998.

[224] M. D. Boente, B. C. Winik, and R. A. Asial. Wrinkly skin syndrome: Ultrastructural alterations of the elastic fibers. *Pediatric Dermatology*, 16(2):113–117, |1999|.

[225] N. Chassaing, L. Martin, P. Calvas, M. LeBert, and A. Hovnanian. Pseudoanthoma elastica: a clinical, pathophysiological and genetic update including 11 novel abcc6 mutations. *Jpurnal of Medical Genetics*, 42:881–892, 2005.

[226] E. Arteaga-Solis, B. Gayraud, and F. Ramirez. Elastic and collagenous networks in vascular diseases. *Cell Structure and Function*, 25(2):69–72, |2000|.

[227] J. C. S. Dean. Management of marfan syndrome. *Heart*, 88(1):97–103, |2002|.

[228] D. P. Judge and H. C. Dietz. Marfan's syndrome. *Lancet*, 366(9501):1965–1976, |2005|.

[229] J. R. Gray and S. J. Davies. Marfan syndrome. *Journal of Medical Genetics*, 33(5):403–408, |1996|.

[230] H.C. Dietz, B. Loeys, L. Carta, and F. Ramirez. Recent progress towards a molecular understanding of marfan syndrome. *American Journal of Medical Genetics, Part C*, 139C:4–9, 2005.

[231] P. A. Abraham, A. J. Perejda, W. H. Carnes, and J. Uitto. Marfan syndrome-demonstration of abnormal elastin in aorta. *Journal of Clinical Investigation*, 70(6):1245–1252, |1982|.

[232] H. C. Dietz. Marfan syndrome: From molecules to medicines. *American Journal of Human Genetics*, 81(4):662–667, |2007|. Dietz, Harry C.

[233] F. Ramirez, I.Y. Sakai, D.B. Rifkin, and H.C. Dietz. Extracellular microfibrils in development and disease. *Cell and Molecular Life Sciences*, 64:2437–2446, 2007.

[234] R. J. Fernandes and D. R. Eyre. The elastin-like protein matrix of lamprey branchial cartilage is cross-linked by lysyl pyridinoline. *Biochemical and Biophysical Research Communications*, 261(3):635–640, |1999|.

[235] P. Robson, G. M. Wright, J. H. Youson, and F. W. Keeley. The structure and organization of lamprin genes: multiple-copy genes with alternative splicing and convergent evolution with insect structural proteins. *Mol Biol Evol*, 17(11):1739–52, |2000|. Journal Article.

[236] G. M. Wright and J. H. Youson. Ultrastructure of cartilage from young adult sea lamprey, petromyzon marinus. a new type of vertebrate cartilage. *American Journal of Anatomy*, 167(1):59–70, |1983|.

[237] P. Forey, P.; Janvier. Agnathans and the origin of jawed vertebrates. *Nature*, 361:129–134, 1993.

[238] J. Dawson. The breathing and feeding mechanism of the lampreys. *Biological Bulletin*, 9(1):1–21, |1905|.

[239] P.S. Maitland. Ecology of the river, brook and sea lamprey. *Conserving Natura 2000 Rivers Ecology Series No.5.*, pages 1–52, 2003.

[240] M. K. Richardson, J. Admiraal, and G. M. Wright. Developmental anatomy of lampreys. *Biological Reviews*, 85(1):1–33, |2010|. Richardson, Michael K. Admiraal, Jeroen Wright, Glenda M.

[241] R. Lund and P. Janvier. A second lamprey from the lower carboniferous (namurian) of bear gulch, montana (u.s.a.). *Geobios*, 19:647–652, 1986.

[242] M. Chang, J. Zhang, and D. Miao. A lamprey from the cretaceous jehol biota of china. *Nature*, 441:972–974, 2006.

[243] MW Hardisty. The skeleton. In *The Biology of Lampreys*, volume 3, pages 333–376. Academic Press, London, |1981|.

[244] W.K. Parker. On the skeleton of marsipobranch fishes.part ii. petromyzon. *Philosophical Transactions of the Royal Society B-Biological Sciences*, 174:411–457, 1883.

[245] G. M. Wright, F. W. Keeley, and P. Robson. The unusual cartilaginous tissues of jawless craniates, cephalochordates and invertebrates. *Cell Tissue Res*, 304(2):165–74, |2001|. Journal Article Review Review, Tutorial.

[246] J. Kelly, S. Tanaka, T. Hardt, E. F. Eikenberry, and B. Brodsky. Fibril-forming collagens in lamprey. *Journal of Biological Chemistry*, 263(2):980–987, |1988|.

[247] B. Brodsky, K. C. Belbruno, T. A. Hardt, and E. F. Eikenberry. Collagen fibril structure in lamprey. *Journal of Molecular Biology*, 243(1):38–47, |1994|.

[248] W.K. Parker. On the skeleton of marsipobranch fishes. ii. petromyzon. *Philosophical Transactions of the Royal Society B-Biological Sciences*, 174:411–457, 1883.

[249] M. W. Hardisty. The significance of lampreys for biological-research. *Endeavour*, 7(3):110–115, |1983|.

[250] G. Faury. Function-structure relationship of elastic arteries in evolution: from microfibrils to elastin and elastic fibres. *Pathologie Biologie*, 49(4):310–325, |2001|.

[251] I. G. Davison, G.M. Wright, and M. E. DeMont. The structure and physical properties of invertebrate and primitive vertebrate arteries. *Journal of Experimental Biology*, 198:2185–2196, 1995.

[252] G. M. Wright, L. A. Armstrong, A. M. Jacques, and J. H. Youson. Trabecular, nasal, branchial, and pericardial cartilages in the sea lamprey, petromyzon-marinus - fine-structure and immunohistochemical detection of elastin. *American Journal of Anatomy*, 182(1):1–15, |1988|.

[253] F.J. Cole. A monograph on the general morphology of the myxinoid fishes, based on a study of myxine 1. the anatomy of the skeleton. *Transactions of the Royal Society of Edinburgh*, 41:749–791, 1905.

[254] H. W. Courtland, G. M. Wright, R. G. Root, and M. E. DeMont. Comparative equilibrium mechanical properties of bovine and lamprey cartilaginous tissues. *J Exp Biol*, 206(Pt 8):1397–408, |2003|. Journal Article.

[255] M. W. Hardisty. The significance of lampreys for biological-research. *Endeavour*, 7(3):110–115, |1983|.

[256] R.E. Marsh, R.B. Corey, and L. Pauling. An investigation of the structure of silk fibroin. *Biochim Biophys Acta*, 16:1–24, 1955.

[257] P. Robson, G. M. Wright, and F. W. Keeley. Distinct non-collagen based cartilages comprising the endoskeleton of the atlantic hagfish, myxine glutinosa. *Anatomy and Embryology*, 202(4):281–290, |2000|.

[258] N.; Rodakis G.C.; Kafatos N.C. Jones, C.W.; Rosenthal. Evolution of two major chorion multigene families as inferred from cloned cdna and protein sequences. *Cell*, 18:1317–1332, 1979.

[259] K. J. Coyne, X. X. Qin, and J. H. Waite. Extensible collagen in mussel byssus: A natural block copolymer. *Science*, 277(5333):1830–1832, |1997|.

[260] T.J. Koob and D.R. Eyre. Molecular diversity of collagen cross-links in the lamprey skeleton. In *Proceedings of the 4th East Coast Connective Tissue Society Meeting*, 1984.

[261] M.A. Meyers, P-Y. Chen, A.Y-M. Lin, and Y. Seki. Biological materials: Structure and mechanical properties. *Progress in Materials Science*, 53:1–206, 2008.

[262] B.D. Ratner and S.J. Bryant. Biomaterials: Where have we been and where are we going. *Annual Review of Biomedical Engineering*, 6:41–75, 2004.

[263] M. Martino, T. Perri, and A. M. Tamburro. Biopolymers and biomaterials based on elastomeric proteins. *Macromolecular Bioscience*, 2(7):319–328, |2002|.

[264] D. Chow, M. L. Nunalee, D. W. Lim, A. J. Simnick, and A. Chilkoti. Peptide-based biopolymers in biomedicine and biotechnology. *Materials Science & Engineering R-Reports*, 62(4):125–155, |2008|. Chow, Dominic Nunalee, Michelle L. Lim, Dong Woo Simnick, Andrew J. Chilkoti, Ashutosh.

[265] L. Li, M.B. Charati, and K.L. Kiick. Elastiomeric polypeptide-based biomaterials. *Polymer Chemistry*, 1:1160–1170, 2010.

[266] L. Nivison-Smith and A.S. Weiss. *Regenerative Medicine and Tissue Engineering: Cells and Biomaterials*, chapter 15, pages 323–336. Tech Open, 2011.

[267] G. Goissis, S. Suzigan, D.R. Parreira, J.V. Maniglia, D.M. Braile, and R. Raymundo. Preparation and characterization of collagen-elastin matrices from blood vessels intended as small diameter vascular grafts. *Artificial Organs*, 24:217–223, 2000.

[268] D.W. Urry. Physical chemistry of biological free energy transduction as demonstrated by elastic protein-based polymers. *Journal of Physical Chemistry*, 101:11007–11028, 1997.

[269] D. W. Urry, A. Pattanaik, J. Xu, T. C. Woods, D. T. McPherson, and T. M. Parker. Elastic protein-based polymers in soft tissue augmentation and generation. *Journal of Biomaterials Science-Polymer Edition*, 9(10):1015–1048, |1998|.

[270] D.W.; Urry, R.D.; Harris, and M.M. Long. Irradiation crosslinking of the polypentapeptide of elastin and compounding to dacron to produce a potential prosthetic material with elasticity and strength. *Journal of Biomedical Materials Research*, 16:11–16, 1982.

[271] J.; Lee, C.W.; Macosko, and D.W. Urry. Mechanical properties of cross-linked synthetic elastomeric polypentapeptides. *Macromolecules*, 34:5968–5974, 2001.

[272] J. Cappello, J. Crissman, M. Dorman, M. Mikolajczak, G. Textor, M. Marquet, and F. Ferrari. Genetic engineering of structural protein polymers. *Biotechnology Progress*, 6:198–202, 1990.

[273] S.M. Mithieux, J.E.J. Rasko, and A.S. Weiss. Synthetic elastin hydrogels derived from massive elastic assemblies of self-organized human protein monomers. *Biomaterials*, 25:4921–4927, 2004.

[274] A.S. Hoffman. Hydrogels for biomedical applications. *Advanced Drug Delivery Reviews*, 43:3–12, 2002.

[275] D. Li and Y. Xia. Electrospinning of nanofibers:reinventing the wheel?**. *Advanced Materials*, 16:1151–1170, 2004.

[276] S.G. Wise, S.M. Mithieux, and A.S. Weiss. Engineered tropoelastin and elastin-based materials. *Advances in Protein Chemistry and Structural Biology*, 78:1–24, 2009.

[277] S. F. Badylak. The extracellular matrix as a biologic scaffold material. *Biomaterials*, 28(25):3587–3593, |2007|. Badylak, Stephen F.

[278] A.I.; Lansing, T.B.; Rosenthal, M.; Alex, and E.W. Dempsey. The structure and chemical characterization of elastic fibers as revealed by elastase and by electron microscopy. *The Anatomical Record*, 114:555–575, 1952.

[279] W. F. Daamen, T. Hafmans, J. H. Veerkamp, and T. H. van Kuppevelt. Comparison of five procedures for the purification of insoluble elastin. *Biomaterials*, 22(14):1997–2005, |2001|.

[280] R. P. Mecham. Methods in elastic tissue biology: Elastin isolation and purification. *Methods*, 45(1):32–41, |2008|. Mecham, Robert P.

[281] B. C. Starcher and M. J. Galione. Purification and comparison of elastins from different animal species. *Analytical Biochemistry*, 74(2):441–447, |1976|.

[282] Serafini-Fracassini. A., J.M. Field, G.W. Rodger, and M. Spina. Application of affinity chromatography to the purification of collagenase for the isolation of insoluble elastin. *Biochim Biophys Acta*, 386:80–86, 1975.

[283] M. Spina, A. Friso, A. R. Ewins, K. H. Parker, and C. P. Winlove. Physicochemical properties of arterial elastin and its associated glycoproteins. *Biopolymers*, 49(3):255–265, |1999|. Article 162WX BIOPOLYMERS.

[284] E. Smith and G. Dent. *Modern Raman Spectroscopy. A Practical Approach.*, chapter One, pages 1–20. John Wiley & Sons, 2004.

[285] R. Turma. Raman spectroscopy of proteins: from peptides to large assemblies. *Journal of Raman Spectroscopy*, 36:307–319, 2005.

[286] J. Bandekar. Amide modes and protein conformation. *Biochim Biophys Acta*, 1120(2):123–43, |1992|. Journal Article Review Review, Academic.

[287] I.N. Serdyuk, N.R. Zaccai, and J. Zaccai. *Methods in Molecular Biophysics: Structure, dynamics and function*, chapter E2, pages 562–572. Cambridge University Press, 2007.

[288] J. Darnell, H. Lodish, and D. Baltimore. *Molecular Cell Biology*. American Scientific Books, Inc, 1990.

[289] G. Turrell. *Raman Microscopy: Developments and Applications*, chapter One, pages 1–25. Elsevier Academic Press, 1990.

[290] E.B. Hanlon, R. Manoharan, T.W. Koo, K.E. Shafer, J.T. Motz, M. Fitzmaurice, J.R. Kramer, I. Itzkan, R. R. Dasari, and M. S. Feld. Topical review: Prospects for in vivo raman spectroscopy. *Physics in Medicine and Biology*, 45:R1–R59, 2000.

[291] J.W. Brauner, C.R. Flach, and R.J. Mendelsohn. A qualitative reconstruction of the amide i contour in the ir spectra of globular proteins: From structure to spectrum. *Journal of American Chemical Society*, 127:100–109, 2005.

[292] L. Debelle and A. J. Alix. Optical spectroscopic determination of bovine tropoelastin molecular model. *Journal of Molecular Structure*, 348:321–324, 1995.

[293] M. Siamwiza, C. Lord, M.C. Chen, T. Takamatsu, I. Harada, H. Matsuura, and T. Shimanouchi. Interpretation of the doublet at 850 and 830 cm-1 in the raman spectrum oftyrosyl residues in proteins and certain model compounds. *Biochemistry*, 14:4870–4876, 1975.

[294] M. Preghenella, G. Pezzotti, and C. Migliaresi. Comparative raman spectroscopic analysis of orientation in fibres and regenerated films of bombyx mori silk fibres. *Journal of Raman Spectroscopy*, 38:522–536, 2007.

[295] M. Rousseau, T. Lefevre, L. Beaulieu, T. Asakura, and M. Pezolet. Study of protein conformation and orientation in silkworm and spider silk fibers using raman microspectroscopy. *Biomacromolecules*, 5:2247–2257, 2004.

[296] and Buffeteau T. Lagugne Labarthet, F. and C. Sourisseau. A raman confocal microspectroscopic study on azopolymer holographic diffraction grat-

ings: Photo- and mass transport-induced effects on the molecular orientation. *Macromolecular Symposium*, 137:75–82, 1999.

[297] M. A. Lillie and J. M. Gosline. The viscoelastic behavior of elastin in aqueous ethylene-glycol. In *11th Meeting of the Polymer-Networks-Group*, pages 75–81, San Diego, Ca, |1992|.

[298] M. A. Lillie and J. M. Gosline. The viscoelastic basis for the tensile strength of elastin. *International Journal of Biological Macromolecules*, 30(2):119–127, |2002|. Article 543NJ INT J BIOL MACROMOL.

[299] M. A. Lillie and J. M. Gosline. Limits to the durability of arterial elastic tissue. *Biomaterials*, 28(11):2021–2031, |2007|.

[300] R.J. Young and P.A. Lovell. *Introduction to Polymers*. Chapman and Hall, New York, 1991.

[301] S. Cheng, E.C. Clarke, and L.E. Bilston. The effects of preconditioning strain on measured tisue properties. *Journal of Biomechanics*, 42:1360–1362, 2009.

[302] D.P. Mukherjee and A.S. Hoffman. The physical properties and molecular structure of ligamentum nuchae elastin. *Biopolymers*, 13:2447–2459, 1974.

[303] P. J. Flory, A. Ciferri, and C. A. J. Hoeve. The thermodynamic analysis of thermoelastic measurements on high elastic materials. *Journal of Polymer Science*, 45(145):235–236, |1960|.

[304] D.W. Urry. Physicochemical properties of elastin and constituent peptides. In R. Ladislas and W. Hornebeck, editors, *Elastin and Elastases*, volume 1, pages 141–174. CRC Press Inc, Florida, |1989|.

[305] A.I. Lansing, T.B. Rosenthal, M. Alex, and E.W. Dempsey. The structure and chemical composition of elastic fibers as revealed by elastase and by electron microscopy. *The Anatomical Record*, 114:555–575, 1952.

[306] H. Sage and W. R. Gray. Studies on the evolution of elastin .2. histology. *Comparative Biochemistry and Physiology B-Biochemistry & Molecular Biology*, 66(1):13–22, |1980|.

[307] R.A.B.. Drury and E.A. Wallington. *Carleton's Histological Technique*, chapter 10, pages 166–181. Oxford University Press, 1973.

[308] M.L. Jones, J.D. Bancroft, and M. Gamble. *Theory and Practice of Hoistological Technique*. Elsevier Science Publishing, 2008.

[309] N. Billinton and A.W.Knight. Seeing the woods through the trees: A review of techniques for distinguishing green fluorescent protein fron endogenous autofluorescence. *Analytical Biochemistry*, 291:175–197, 2001.

[310] Z. Deyl, K. Macek, and M.A. Vancikova. Studies on the chemical nature of elastin fluorescence. *Biochimica Et Biophysica Acta*, 625:248–254, 1980.

[311] D.P. Thornhill. Separation of a series of chromophores and fluorophores present in elastin. *Biochemical Journal*, 147:215–219, 1975.

[312] Z. Deyl, K. Macek, M. Adam, and VanCikova. Studies on the chemical nature of elastin fluorescence. *Biochimica et Biophysica Acta*, 625:248–254, 1980.

[313] N. White and R. Errington. Multi-photon microscopy: Seeing more by imaging less. *BioTechniques*, 33:298–303, 2002.

[314] W.R. Zipfel, R.M. Williams, R.M. Watt, and W. Webb. Nonlinear magic: multiphoton microscopy in the biosciences. *Nature*, 21:1369–1377, 2002.

[315] A. Ustione and D.W. Piston. A simple introduction to multiphoton microscopy. *Journal of Microscopy*, 243:221–226, 2011.

[316] P.J. Campagnola and L.M. Loew. Second-harmonic imaging microscopy for visualizing biomolecular arrays in cells, tissues and organisms. *Nature Biotechnology*, 11:1356–1360, 2003.

[317] A. Zambusch, G.R. Holtom, and X.S. Xie. Three-dimensional vibrational imaging by coherent anti-stokes raman scattering. *Physical Review Letters*, 82:4142–4145, 1999.

[318] J. Mansfield, J. Yu, J. Moger, U. Tirlapur, J. Urban, C. Zhanfeng, and P. Winlove. The elastin network: its relationship with collagen and cells in articular cartilage as visualized by multiphoton microscopy. *Journal of Anatomy*, 215:682–691, 2009.

[319] S.J. Wilkinson and D.W.L. Hukins. Determination of collagen fibril structure and orientation in connective tissues by x-ray diffraction. *Radiation Physics and Chemistry*, 56:197–204, 1999.

[320] V. Samouillan, F. Delaunay, J. Dandurand, N. Merbahi, J.P. Gardou, M. Yousfi, A. Gandaglia, M. Spina, and C. Lacabanne. The use of thermal techniques for the characterization and selection of natural biomaterials. *Journal of Functional Biomaterials*, 2:230–248, 2011.

[321] V. Samouillan, C. Andre, J. Dandurand, and C. Lacabanne. Effect of water on the molecular mobility of elastin. *Biomacromolecules*, 5(3):958–964, |2004|.

[322] V. Samouillan, J. Dandurand, C. Lacabanne, and W. Hornebeck. Molecular mobility of elastin: Effect of molecular architecture. *Biomacromolecules*, 3:531–537, 2002.

[323] V. Samouillan, A. Lamure, E. Maurel, C.and Ballarin F. Dandurand, J and; Lacabanne, and M. Spina. Characterisation of elastin and collagen in aortic bioprostheses. *Medical and Biological Engineering and Computing*, 38:226–231, 2000.

[324] Y.C. Fung. Biorheology of soft tissues. *Biorheology*, 10:139–155, 1973.

[325] D.W. Urry. Physicochemical properties of elastin and constituent peptides. In R. Ladislas and W. Hornebeck, editors, *Elastin and Elastases*, volume 1, pages 141–174. CRC Press Inc, Florida, |1989|.

[326] P. Cioni and G.B. Strambini. Effect of heavy water on protein flexibility. *Biophysical Journal*, 82:3246–3253, 2002.

[327] R. P. Mecham. Methods in elastic tissue biology: Elastin isolation and purification. *Methods*, 45(1):32–41, |2008|. Mecham, Robert P.

[328] K. Shiraki, K.; Nishikawa and Y. Goto. Trifluoroethanol-induced stabilization of the alpha-helical structure of beta-lactoglobulin: Implication for non-hierarchical protein folding. *Journal of Molecular Biology*, 245:180–194, 1995.

[329] Y. N. Wang, C. Galiotis, and D. L. Bader. Determination of molecular changes in soft tissues under strain using laser raman microscopy. *Journal of Biomechanics*, 33(4):483–486, |2000|.

[330] MD Morris. Bone tissue ultrastructural response to elastic deformation probed by raman spectroscopy. *Faraday Discussions*, 126:159–168, |2004|.

[331] J.S. Church, G.L. Corino, and A.L. Woodhaed. The effects of stretching on wool fibres as monitored by ft-raman spectroscopy. *Journal of Molecular Structure*, 440:15–23, 1998.

[332] M.E. Rousseau, L. Beaulieu, T. Lefevre, J. Paradis, T. Asakura, and M. Pezolet. Characterization by raman microspectrometry of the strain-induced conformational transition in fibroin fibres from the silkworm samia cynthia ricini. *Biomacromolecules*, 7:2512–2521, 2006.

[333] V. Samouillan, J. Dandurand-Lods, A. Lamure, E. Maurel, C. Lacabanne, G. Gerosa, A. Venturini, D. Casarotto, L. Gherardini, and M. Spina. Thermal analysis characterization of aortic tissues for cardial valve bioprostheses. *Journal of Biomedical Materials Research*, 46:531–538, 1999.

[334] H. Reiersen and A. R. Rees. Trifluoroethanol may form a solvent matrix for assisted hydrophobic interactions between peptide side chains. *Protein Engineering*, 13(11):739–743, |2000|.

[335] C.P. Winlove, K.H. Parker, N.C. Avery, and A.J. Bailey. Interactions of elastin and aorta with sugars in vitro an their effects on biochemical and physical properties. *Diabetologia*, 39:1131–1139, 1996.

[336] I Hesse. The occurance of elastic system fibers in the matrix of normal articular cartilage. *Cell and Tissue Research*, 248:589–593, 1987.

[337] A. Naumann, J.E. Dennis, A. Awadallah, D.A. Carrino, J.M. Mansour, E. Kastenbauer, and A.I. Caplan. Immunochemical and mechanical characterization of cartilage subtypes in rabbit. *Journal of Histochemistry and Cytochemistry*, 50:1049–1058, 2002.

[338] J. Yu. Elastic tissues of the intervertebral disc. *Biochemical Society Transactions*, 30:848–852, 2002.

[339] J. Yu, U. Tirlapur, J. Fairbank, P. Handford, S. Roberts, C. P. Winlove, Z. F. Cui, and J. Urban. Microfibrils, elastin fibres and collagen fibres in the human intervertebral disc and bovine tail disc. *Journal of Anatomy*, 210(4):460–471, |2007|. Yu, Jing Tirlapur, Uday Fairbank, Jeremy Handford, Penny Roberts, Sally Winlove, C. Peter Cui, Zhanfeng Urban, Jill.

[340] S. Navea, R. Tauler, and A. de Juan. Application of the local regression method interval partial least-squares to the elucidation of protein secondary structure. *Analytical Biochemistry*, 336(2):231–242, |2005|.

[341] M.N. Kinalwa, E.W. Blanch, and A.J. Doig. Accurate determination of protein secondary structure content from raman and raman optical activity spectra. *Analytical Chemistry*, 82:6347–6349, 2010.

[342] S.J. Eichhorn, J. Sirichaisit, and R. J. Young. Deformation mechanisms in cellulose fibres, paper and wood. *Journal of Materials Science*, 36:3129–3135, 2001.

[343] H-W. Wong, S-M. Choi, D.L. Phillips, and C-Y. Ma. Raman spectroscopic study of deaminated food proteins. *Food Chemistry*, 113:363–370, 2009.

[344] Y. Cho, L.B. Sagle, S. Limura, Y. Zhang, J. Kherb, A. Chilkoti, M. Scholtz, and P.S. Cremer. Hydrogen bonding of beta-turn structure is stabilized in deuterium oxide. *Journal of the American Chemical Society*, 131:15188–15193, 2009.

[345] M. Buck. Trifluoroethanol and colleagues: cosolvents come of age. recent studies with peptides. *Quarterly Reviews of Biophysics*, 31:297–355, 1998.

[346] K. Koenig and H. Schneckenburger. Laser-induced autofluorescence for medical diagnosis. *Journal of Fluorescence*, 4:17–40, 1994.

[347] L. Chunqiang, C. Pitsillides, J.M. Runnels, D. Cote, and C.P. Lin. Multiphoton microscopy of live tissues with ultraviolet autofluorescence. *IEEE Journal of Selected Topics in Quantum Electronics*, 16:516–523, 2010.

[348] S. Kimura, T. Kamimura, Y. Takema, and M. Kubota. Lower vertebrate collagen. evidence for type-i collagen in the skin of lamprey and shark. *Biochimica Et Biophysica Acta*, 669:251–257, 1981.

[349] S. Kimura and T. Kamimura. The characterization of lamprey notochord collagen with special reference to its skin collagen. *Comparative Biochemistry and Physiology B-Biochemistry & Molecular Biology*, 73B:335–339, 1982.

[350] D. Nettles, A. Chilkoti, and L. Selton. Applications of elastin-like polypeptides in tissue engineering. *Advanced Drug Delivery Reviews*, 62:1479–1485, 2010.

[351] N.H.; Lewis R.V. Hayashi, C. Y.Shipley. Hypotheses that correlate the sequence , structure and mechanical properties of spider silk proteins. *International Journal of Biological Macromolecules*, 24:271–275, 1999.

[352] Q. Cao, Y. Wang, and H. Bayley. Sequence of abductin the molluscan 'rubber' protein. *Current Biology*, 7:677–678, 1997.

[353] J.M. Gosline, P.A. Guerette, C.S. Ortlepp, and K.N. Savage. The mechanical design of spider silks: From fibroin sequence to mechanical function. *The Journal of Experimental Biology*, 202:3295–3303, 1999.

[354] E. Vaccaro and J. H. Waite. Yeild and post-yeild behaviour of mussel byssal thread:a self-healing biomolecular material. *Biomacromolecules*, 2:906–911, 2001.

[355] J.M. Gosline, M. Lillie, E. Carrington, P. Guerette, C. Ortlepp, and K. Savage. *Elastomeric Proteins:Structures, biomechanical properties and biological roles.*, chapter 2, pages 15–38. Cambridge University Press, 2003.